RĪGAS TEHNISKĀ UNIVERSITĀTE

Linards Lapčinskis

TRIBOELEKTRISKAIS EFEKTS POLIMĒRU SISTĒMĀS: VIRSMAS LĀDIŅA VEIDOŠANĀS UN ENERĢIJAS SAVĀKŠANA

Promocijas darbs

TRIBOELECTRIC EFFECT IN POLYMER-BASED SYSTEMS: SURFACE CHARGE FORMATION AND ENERGY HARVESTING

Doctoral Thesis

RTU Izdevniecība
RTU Press
Rīga 2022

RĪGAS TEHNISKĀ UNIVERSITĀTE
Materiālzinātnes un lietišķās ķīmijas fakultāte
Tehniskās fizikas institūts

RIGA TECHNICAL UNIVERSITY
Faculty of Materials Science and Applied Chemistry
Institute of Technical Physics

Linards Lapčinskis
Doktora studiju programmas "Materiālzinātne" doktorants
Doctoral Student of the Study Programme "Materials Science"

TRIBOELEKTRISKAIS EFEKTS POLIMĒRU SISTĒMĀS: VIRSMAS LĀDIŅA VEIDOŠANĀS UN ENERĢIJAS SAVĀKŠANA

Promocijas darbs

TRIBOELECTRIC EFFECT IN POLYMER-BASED SYSTEMS: SURFACE CHARGE FORMATION AND ENERGY HARVESTING

Doctoral Thesis

Zinātniskie vadītāji / Scientific supervisors:
profesors *Dr. sc. ing.* / Professor Dr. sc. ing.
ANDRIS ŠUTKA
profesors *Dr. habil. phys.* / Professor Dr. habil. phys.
MĀRIS KNITE

RTU Izdevniecība / RTU Press
Rīga 2022 / Riga 2022

Lapčinskis L. Triboelektriskais efekts polimēru sistēmās: virsmas lādiņa veidošanās un enerģijas savākšana. Promocijas darbs. – Rīga: RTU Izdevniecība, 2022. – 149 lpp.

Lapčinskis, L. Triboelectric Effect in Polymer-based Systems: Surface Charge Formation and Energy Harvesting. Doctoral Thesis. – Riga: RTU Press, 2022. – 149 p.

Iespiests saskaņā ar promocijas padomes "RTU P-02" 2022. gada 14. janvāra lēmumu, protokols Nr. 04030-9.2.1/2.

Published in accordance with the decision of the Promotion Council "RTU P-02" of 14 January 2022, Minutes No. 04030-9.2.1/2.

Promocijas darbs izstrādāts:

- ar Eiropas Reģionālās attīstības fonda daļēju atbalstu projektā "Hibrīdās enerģijas ieguves sistēmas" Nr. 1.1.1.1/16/A/013;
- ar Latvijas Zinātnes padomes daļēju atbalstu projektā "Starpmolekulāro H-saišu struktūras dizains polimēros spēcīgākai triboelektrifikācijai" Nr. lzp-2020/2-0382;
- daļēji ar RTU doktorantūras granta atbalstu Materiālzinātnes un lietišķās ķīmijas fakultātes doktorantiem.

The Doctoral Thesis has been developed with the support from

- the European Regional Development Fund within the project "Hybrid energy harvesting systems" No. 1.1.1.1/16/A/013;
- the Latvian Council of Science within project "A structural H-bond intermolecular design in polymers for strong triboelectrification" No. lzp-2020/2-0382; and

- RTU doctoral grant for doctoral students of the Faculty of Materials Science and Applied Chemistry.

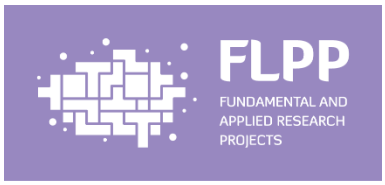

.

.

PATEICĪBAS

Sirsnīgs paldies abiem mana promocijas darba vadītājiem – *Dr. sc. ing.* Andrim Šutkam un *Dr. habil. phys.* Mārim Knitem – par vērtīgajām diskusijām, ierosinājumiem un vispārējo atbalstu visā darba izstrādes laikā! Esmu jums pateicīgs par dalīšanos savās zināšanās, prasmēs un, pats galvenais, aizrautību ar zinātni.

Vissirsnīgākā pateicība maniem komandas biedriem un padomdevējiem – *Dr. sc. ing.* Kasparam Mālniekam un *Dr. phys.* Artim Linartam – par palīdzību mērījumu veikšanā un datu analīzē! Esmu pateicīgs visiem lieliskajiem Tehniskās fizikas institūta un Materiālu un virsmas tehnoloģiju institūta kolēģiem par noderīgajiem padomiem un diskusijām. Es esmu pateicīgs arī kolēģiem no Cietvielu fizikas institūta un Tartu Universitātes par viņu ieguldījumu mūsu kopējo darbu tapšanā.

Vēlos pateikties manai mīļajai sievai Sindijai Lapčinskai par sniegto atbalstu, brīnišķīgajiem padomiem un iedvesmu, ko viņa man ir devusi.

Paldies Rīgas Tehniskajai universitātei par sniegto finansiālo atbalstu!

Linards Lapčinskis

ACKNOWLEDGEMENT

I would like to express my sincere gratitude to both my supervisors Dr. sc. ing. Andris Šutka and Dr. habil. phys. Māris Knite for all the valuable discussions, fruitful suggestions, and overall support throughout the Thesis. I am grateful to them for sharing their knowledge, skills and, most importantly, passion for science.

My most sincere gratitude goes to my teammates and mentors Dr. sc. ing. Kaspars Mālnieks and Dr. phys. Artis Linarts for all the help with the measurements and data analysis. I am grateful to all my dear colleagues in the Institute of Technical Physics and Institute of Materials and Surface Engineering for the useful advice and discussions. I am also thankful to the colleagues in Institute of Solid State Physics and University of Tartu for their contribution to our joint papers.

I would like to thank my dear wife Sindija Lapčinska for all the support, wonderful advice and the inspiration she has given me.

Financial support from Riga Technical University is gratefully acknowledged.

Linards Lapčinskis

PROMOCIJAS DARBS IZVIRZĪTS ZINĀTNES DOKTORA GRĀDA IEGŪŠANAI RĪGAS TEHNISKAJĀ UNIVERSITĀTĒ

Promocijas darbs zinātnes doktora (*Ph. D.*) grāda iegūšanai tiek publiski aizstāvēts 2022. gada 19. maijā plkst. 15 Rīgas Tehniskās universitātes Materiālzinātnes un lietišķās ķīmijas fakultātē, Paula Valdena ielā 3, 272. auditorijā.

OFICIĀLIE RECENZENTI

Profesors *Dr. sc. ing.* Remo Merijs-Meri,
Rīgas Tehniskā universitāte

Vadošais pētnieks *Dr. phys.* Raimonds Meija,
Latvijas Universitāte, Latvija

Profesors *Dr. Amir Fahmi*,
Reinas-Vālas Lietišķo zinātņu universitāte, Vācija

APSTIPRINĀJUMS

Apstiprinu, ka esmu izstrādājis šo promocijas darbu, kas iesniegts izskatīšanai Rīgas Tehniskajā universitātē zinātnes doktora (*Ph. D.*) grāda iegūšanai. Promocijas darbs zinātniskā grāda iegūšanai nav iesniegts nevienā citā universitātē.

Linards Lapčinskis ……. (paraksts)
Datums: ……

Promocijas darbs veidots kā zinātnisko publikāciju kopa, tas ietver kopsavilkumu latviešu un angļu valodā un septiņas *SCI* publikācijas. Publikācijas ir uzrakstītas angļu valodā, to kopējais lappušu skaits, iekļaujot elektroniski pieejamo informāciju, ir 132 lappuses. Kopsavilkumā ir 25 attēli, divas tabulas, kopējais lappušu skaits ir 50. Literatūras sarakstā ir 116 nosaukumu.

SATURS

AUTORA IEGULDĪJUMS

Zinātniskie raksti, kas veido šī promocijas darba pamatu, ir kopēja darba rezultāts, apvienojot būtisku visu līdzautoru ieguldījumu un zināšanas dažādās jomās. Autora ieguldījums rakstu sagatavošanā apkopots 1. tabulā.

1. tabula

Autora ieguldījums, sagatavojot katru promocijas darbā iekļauto zinātnisko rakstu

1. publikācija	Polimēra kontaktējamo kārtiņu izgatavošana, izmantojot uzklāšanu ar rotāciju un presēšanu paaugstinātā temperatūrā. Polimēru triboelektrisko īpašību mērījumi. PDMS cietības mērījumi un šķērssaistīšanās pakāpes aprēķini. Datu vizuālais attēlojums. Procentuālais ieguldījums – 50 %.
2. publikācija	Polimēra kārtiņu izgatavošana, izmantojot uzklāšanu ar rotāciju un triboelektrisko īpašību testēšana. Datu vizuālais attēlojums. TEĢ efektivitātes aprēķini un ieguldījums manuskripta rakstīšanā. Procentuālais ieguldījums – 75 %.
3. publikācija	Paraugu izgatavošana un triboelektrisko īpašību testēšana. Triboelektriskā efekta un lādiņa noturības paaugstinātā temperatūrā ilgtermiņa stabilitātes mērījumi. Procentuālais ieguldījums – 50 %.
4. publikācija	Paraugu izgatavošana un triboelektrisko īpašību testēšana. Skenējošās Kelvina zondes (SKZ) mērījumu analīze. Ieguldījums manuskripta rakstīšanā un datu vizualizācijā. Procentuālais ieguldījums – 60 %.
5. publikācija	Paraugu izgatavošana, izmantojot presēšanu paaugstinātā temperatūrā. Triboelektrisko īpašību izpēte. Skenējošās Kelvina zondes (SKZ) mērījumu analīze. Datu vizuālais attēlojums. Manuskripta sākotnējās versijas rakstīšana. Procentuālais ieguldījums – 80 %.
6. publikācija	Polimēru nanokompozītu izgatavošana un polarizācija. Triboelektrisko un pjezoelektrisko īpašību testēšana. Ieguldījums manuskripta rakstīšanā. Procentuālais ieguldījums – 75 %.
7. publikācija	Polimēru nanokompozītu izgatavošana un polarizācija. Triboelektrisko un pjezoelektrisko īpašību testēšana. SKZ mērījumu analīze. Ieguldījums manuskripta rakstīšanā. Procentuālais ieguldījums – 70 %.

SAĪSINĀJUMI

A	saskares laukums
AFM	atomspēku mikroskopija
Cel. Tr.	celulozes triacetāts
D	virsmas garuma izmaiņu atšķirības faktors
d_{33}	pjezoelektriskais koeficients
DMF	dimetilformamīds
DSK	diferenciālā skenējošā kalorimetrija
EOK	etilēna-oktēna kopolimērs
EPDM	etilēna propilēna diēna monomēra gumija
EVA	etilēna-vinilacetāta kopolimērs
GEA	galīgo elementu analīze
HDPE	augsta blīvuma polietilēns
I_{SC}	īsslēguma strāva
ITO	indija-alvas oksīds
KEB	kohēzijas enerģijas blīvums
KL	kontaktleņķis
KSM	Kelvina spēka mikroskopija
LDPE	zema blīvuma polietilēns
M_C	molekulas svars starp šķērssaitēm
ND	nanodaļiņas
P	polarizētība
PA 66	poliamīds 6,6
PC	polikarbonāts
PDMS	polidimetilsiloksāns
PET	polietilēna tereftalāts
PHC	heksāndiola-citronskābes kopolimērs
P_i	momentānais jaudas blīvums
PI	poliimīds
PMMA	poli(metilmetakrilāts)
PP	polipropilēns
PS	polistirols
PTFE	politetrafluoretilēns
PU	poliuretāns
PVAc	polivinilacetāts
PVC	polivinilhlorīds
PVDF	polivinilidēnfluorīds
Q	lādiņa blīvums
R	slodzes pretestība
RMS	vidējais kvadrātiskais laukuma raupjums
SEBS	stirola-etilēna-butilēna-stirola bloku kopolimērs

SEM	skenējošā elektronu mikroskopija
SKZ	skenējošā Kelvina zonde
TEĢ	triboelektriskais ģenerators
TEM	transmisijas elektronu mikroskopija
TENĢ	triboelektriskais nanoģenerators
T_g	stiklošanās temperatūra
UHMWPE	ultra augstas molekulmasas polietilēns
V_{OC}	atvērtas ķēdes potenciāls
XPS	rentgenstaru fotoelektronu spektroskopija
Δ_f	virsmas garuma izmaiņa
Φ	izejas darbs

DARBA VISPĀRĒJS RAKSTUROJUMS

Ievads

Mehāniskās enerģijas savākšana

Enerģijas savākšana nozīmē apkārtējā vidē esošās enerģijas pārveidi elektroenerģijā. Parasti savākšanu uzskata par neliela enerģijas daudzuma pārveidošanu autonomai mazjaudas iekārtu nodrošināšanai ar enerģiju (μW–mW).[1] Mehāniskās enerģijas ieguve šādu ierīču darbināšanai ir būtiska to plašākai pieejamībai un ļauj samazināt ierīču ietekmi uz vidi. Attiecīgi enerģijas ieguve ir lietderīga, ja savāktā enerģija sniedz ieguvumu, kas citādi nav sasniedzams ar baterijām vai elektrotīklu, piemēram, novērš nogurdinošu akumulatoru nomaiņu vai dārgu savienojumu ar elektrotīklu. 1. attēlā redzams dažu elektrisko ierīču enerģijas patēriņa uzskaitījums;[2–7] enerģijas savākšana varētu būt lietderīga ierīcēm ar enerģijas patēriņu, zemāku par 30–40 mW.

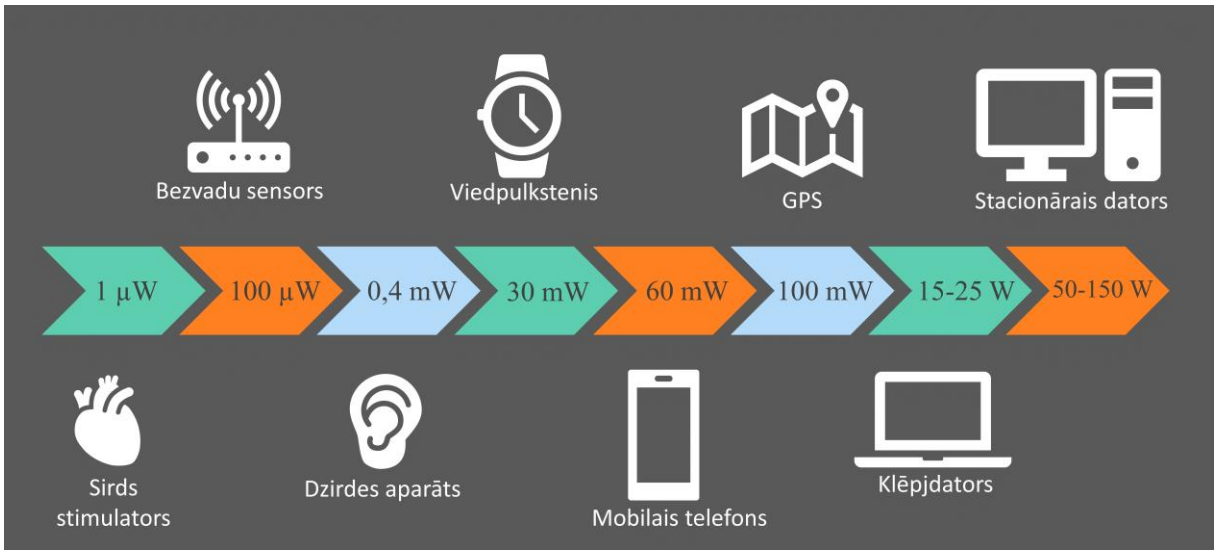

1. att. Ikdienā sastopamas elektriskās ierīces un to aptuvenais jaudas patēriņš.

Mehāniskā enerģija (kinētiskā enerģija) ir bagātīgi pieejama no tādiem avotiem kā vējš, ūdens viļņi, vibrācijas un cilvēku kustības. Vibrācijas nodrošina daudz enerģijas, tomēr savāktā enerģija bieži vien ir niecīga, salīdzinot ar vibrāciju enerģiju. Neskatoties uz relatīvi zemo efektivitāti, pēdējā laikā vibrāciju enerģijas savākšana, izmantojot TEĢ, ir aktualizējusies, jo samazinās elektroierīču izmērs un enerģijas patēriņš. Izmantojot TEĢ, var darbināt mikroierīces, piemēram, sensorus, detektorus un bezvadu tīkla pārraidītājus, tādējādi aizvietojot baterijas vai izvairoties no nepieciešamības pievienot nepārtrauktas strāvas avotu. Arī cilvēku kustības var izmantot kā mehāniskās enerģijas avotu, iestrādājot enerģijas savācējus apģērbā, apavos un aksesuāros (rokassprādzēs u. c.) vai arī izveidojot infrastruktūru (trotuāri, grīdas segumi), kurā iestrādāti enerģijas savācēji. Valkājami enerģijas savācēji kļūst aizvien aktuālāki, pateicoties pārnēsājamās elektronikas popularitātei, tomēr savācējam nevajadzētu ierobežot

valkāšanas ērtumu, tāpēc ļoti svarīgs aspekts ir ierīces dizains. Minēto mehāniskās enerģijas avotu savākšanai izmanto dažādus tehnoloģiskus risinājumus (2. tab.).

2. tabula

Mehāniskās enerģijas savākšanas tehnoloģiju, izmantoto materiālu, iegūstamā jaudas blīvuma un darbības principu kopsavilkums

Tehnoloģija	Materiāli	Jauda	Darbības principi
Elektro-magnētiskais ģenerators	Vadoša vada spole un magnēts	1–1000 $\mu W\ cm^{-3}$	Mehāniskā enerģija rada kustību starp ierīces daļām, un starp abiem spoles galiem tiek ierosināta potenciālu starpība.
Pjezo-elektriskais ģenerators	Dielektriķi ar iekšēju dipola momentu: kristāli, keramika, polimēri un kompozīti[8–15]	10–1000 $\mu W\ cm^{-3}$	Dipolu blīvums tilpumā izpaužas kā polarizētība uz materiāla virsmas. Dipoli inducē vienādus pretējas zīmes lādiņus elektrodos. Mehāniskā enerģija rada deformāciju, kas maina dipola momentu un tādējādi polarizētību. Izmaiņu rezultātā notiek lādiņa pārdale, nodrošinot elektronu plūsmu starp elektrodiem, kas savienoti ar ārējo ķēdi.
Kapacitīvais ģenerators	Elastīgs dielektriskais materiāls ar kustīgiem elektrodiem[16–20]	0,01–100 $mW\ cm^{-3}$	Ģeneratoriem nepieciešams sprieguma avots, lai nodrošinātu sākotnējo lādiņu uz elektrodiem. Mehāniskais spēks maina attālumu starp elektrodiem (vai elektrodu laukumu), tādējādi kondensatorā uzkrātā enerģija palielinās un pēc tam tiek izlādēta.
Ferroelektretu materiāli	Uzlādētas polimēru putas ar elektrodiem[21]	0,001–1 $mW\ cm^{-2}$	Augstsprieguma elektriskais lauks uzlādē poru sienas ar pretējas polaritātes lādiņiem, radot dipolus. Mehāniskais spēks izraisa polarizācijas izmaiņu un lādiņa pārdali starp elektrodiem, kas savienoti ar ārējo ķēdi.
Tribo-elektriskais ģenerators	Polimēra izolatora pārklāti elektrodi[22]	0,001–50 $mW\ cm^{-2}$	Elektrodi ir pārklāti ar polimēru slāņiem, kas savstarpēji saskaras. Lādiņš veidojas uz polimēra virsmas pēc saskares un atdalīšanas, un lādiņš tiek inducēts pievienotajos elektrodos. Elektrodi ir savienoti ar ārējo ķēdi, tajā novēro elektronu plūsmu, kas līdzsvaro potenciāla starpību, ko rada inducētie lādiņi.

Starp piedāvātajām tehnoloģijām triboelektriskie ģeneratori (TEĢ) ir kļuvuši par daudzsološiem mehāniskās enerģijas savācējiem. Profesors *Zhong Lin Wang* 2012. gadā tos pirmo reizi izmantoja, lai aprakstītu enerģijas ieguves ierīces, kas paredzētas, lai pārveidotu berzes radīto statisko lādiņu elektroenerģijā, izmantojot elektrostatisko indukciju.[22] Biežāk tiek lietots termins "triboelektriskie nanoģeneratori" (TENĢ), lai akcentētu nepieciešamību pēc

virsmas strukturēšanas nano izmēra mērogā, kas uzlabo veiktspēju, un norādītu, ka ģeneratora funkcionalitāti nodrošina procesi nano izmēra mērogā. *Scopus* datubāzē indeksēto dokumentu analīze, kas saistīti ar "*triboelectric nanogenerator*", liecina, ka dokumentu skaits katru gadu pastāvīgi pieaug, 2021. gadā sasniedzot 865 dokumentus (2. att.).

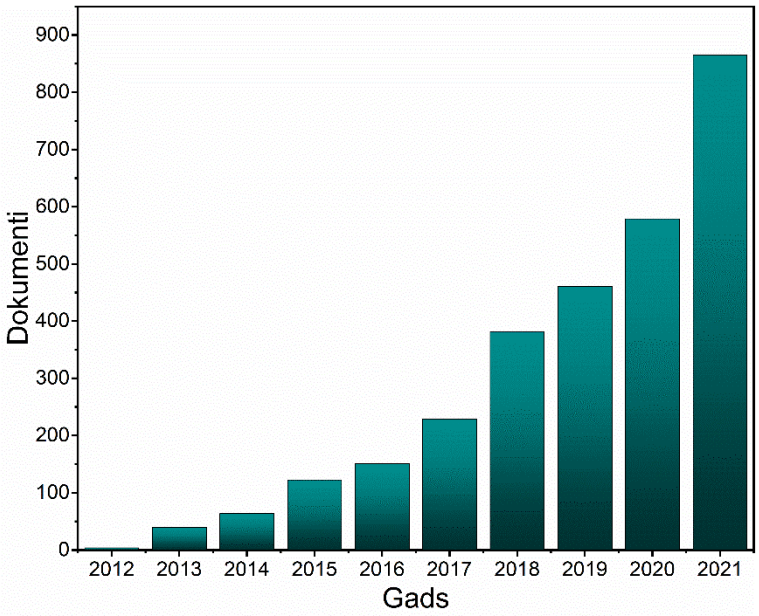

2. att. Dati par *Scopus* datubāzē indeksētiem dokumentiem, kas nosaukumā, aprakstā vai atslēgas vārdos satur "*triboelectric nanogenerator*".

TEĢ var veidot no lētiem, viegliem, elastīgiem, plaši pieejamiem polimēru materiāliem. Salīdzinot ar pjezoelektriskajiem un ferroelektretu materiāliem, TEĢ nav vajadzīga polarizēšana, lai nodrošinātu enerģijas savākšanas funkciju. TEĢ ierīces var darboties dažādos režīmos – atraušanas režīmā,[23] berzes,[24] rotācijas[25] vai viena elektroda.

TEĢ ir nodemonstrēts plašs lietojuma klāsts. Triboelektriskie *in vivo* enerģijas savācēji izmantoti, lai savāktu biomehānisko enerģiju, izmantojot žurku un cūku sirdspukstus un elpošanu.[26,27] Ir parādīts, ka implantējams triboelektriskais sensors, kas piestiprināts pie cūkas perikarda, spēj novērot sirdsdarbību un elpošanu, kā arī konstatēt dzīvībai bīstamu aritmiju.[28] Turklāt TEĢ var izmantot dzīvo šūnu, audu un orgānu stimulācijai, tādējādi nodrošinot iespējamu lietojumu cilmes šūnu diferenciācijas veicināšanā, neironu audu reģenerācijas veicināšanā un sirds stimulēšanā.[29,30]

Galvenie TEĢ ierīču veiktspējas raksturlielumi ir atvērtas ķēdes spriegums (V_{OC}) un īsslēguma strāva (I_{SC}). V_{OC} ir atkarīgs no slodzes pretestības R un pieaug, palielinot R. I_{SC} bieži ir nanoampēru mērogā, taču augstākās literatūrā minētās vērtības sasniedz 350 μA no 1 cm^2 liela parauga.[31] Precīzs polimēru triboelektrifikācijas spējas raksturlielums ir lādiņa blīvums Q, ko aprēķina no īsslēguma strāvas, izmantojot 1. vienādojumu:

$$Q = \frac{\int I_{SC} dt}{A}, \quad (1)$$

kur:

I_{SC} – īsslēguma strāva;

d*t* – laika diferenciālis;
A – kontakta virsmas laukums.

Lai novērtētu TEĢ enerģijas savākšanas potenciālu, ir noderīgi aprēķināt enerģijas un jaudas blīvumu (uz TEĢ laukuma vienību). Momentāno jaudas blīvumu P_i aprēķina no V_{OC} pie izvēlētā *R*, izmantojot 2. vienādojumu:

$$P_i = \frac{{V_{OC}}^2}{R \times A}, \quad (2)$$

kur:
V_{OC} – atvērtas ķēdes spriegums;
R – slodzes pretestība.

Pēc tam ar 2. vienādojumu iegūto P_i vērtību, attēlotu grafikā kā laika *t* funkciju, var izmantot, lai aprēķinātu enerģiju *E* pēc 3. vienādojuma:

$$E = \int P_i \mathrm{d}t. \quad (3)$$

Kondensatorā uzkrātā enerģija arī ir būtiska TEĢ raksturīpašība; dažos gadījumos tā, salīdzinot ar enerģiju, kas aprēķināta tieši kontaktatdalīšanas eksperimentos, var būt mazāka par 3–4 kārtām.[31] Zudumus galvenokārt rada taisngrieža slēgums, kas radīto maiņstrāvu pārvērš līdzstrāvā.[32] Šis ir viens no aspektiem, kas ierobežo lietojuma iespējas.

Trīs galvenie paņēmieni, ko izmanto, lai uzlabotu TEĢ ierīču veiktspēju, ir: i) virsmas topogrāfijas un morfoloģijas modifikācija; ii) polimēra virsmas ķīmiskā apstrāde un funkcionalizācija; iii) segnetoelektrisko materiālu izmantošana.

Triboelektriskā slāņa virsmas rakstam un ģeometrijai ir būtiska nozīme TEĢ darbībā. Ir pierādīts, ka lielāks īpatnējais virsmas laukums veicina augstāka *Q* veidošanos. Pētījumi liecina, ka asimetriska saskare (atšķirīgs katras kārtiņas saskares laukums) starp diviem identiskiem materiāliem rada augstu virsmas potenciālu.[33] Turklāt, jo vairāk abu virsmu topogrāfija un morfoloģija atšķiras, jo augstāka ir TEĢ veiktspēja.

Polimēru triboelektriskās īpašības var uzlabot, izmantojot ķīmisku virsmas modifikāciju.[34] Virsmas modifikācija paaugstina polimēru adhēziju pret kontaktēto virsmu, jo pastāv saistība starp virsmas adhēziju un triboelektrisko lādiņu. Process parasti ietver virsmas aktivāciju, izmantojot plazmas apstrādi, kam seko izvēlētās ķīmiskās vielas uzklāšana. Piemēram, pētnieki ir ierosinājuši ķīmiskus pārveidojumus, izmantojot apstrādi ar fluoroglekļu plazmu, lai uzlabotu triboelektriskās īpašības.[35] Viens no visbiežāk izmantotajiem polimēriem ķīmiskajām modifikācijām ir polidimetilsiloksāns (PDMS);[36] tā triboelektrisko virsmas lādiņu var palielināt ar dažādām virsmas apstrādes metodēm, piemēram, apstarošanu ar ultravioleto gaismu pēc apstrādes ar NaOH,[37] ķīmisku halogenizāciju[38] vai secīgu kodināšanu un ķīmisko modifikāciju, izmantojot O_2 un SF_6 plazmu.[39]

Viena no pieejām, lai panāktu augstāku TEĢ veiktspēju, ir segnetoelektriskā/pjezoelektriskā efekta izmantošana. Šo efektu ietverošos TEĢ parasti dēvē par hibrīdierīcēm, jo pjezoelektriskais efekts ir arī pjezoelektrisko ģeneratoru stūrakmens. Attiecīgi visi segnetoelektriskie materiāli varētu būt pjezoelektriski, tomēr ne visiem

pjezoelektriskajiem materiāliem piemīt segnetoelektriskais efekts (piemēram, ZnO un kvarcs). Segnetoelektrisko efektu parasti novēro materiālos ar perovskīta struktūru ($BaTiO_3$, $PbTiO_3$) un dažos polimēru materiālos (polivinilidēnfluorīds (PVDF), poliamīds-11 (PA-11)).[40] Segnetoelektriskie materiāli tilpumā satur spontāni orientētu dipolu momentu domēnus, kas savukārt orientēti haotiski, uzrādot kopējo polarizētību $P = 0$. Ārējais elektriskais lauks E spēj orientēt dipolus noteiktā virzienā, tādējādi izveidojot kopēju polarizētības vektoru. Mehāniskais spēks izraisa P izmaiņas, kas savukārt inducē virsmas lādiņu elektrodā. Hibrīdās TEĢ ierīces ir uzrādījušas vienus no labākajiem rezultātiem, sasniedzot visaugstāko jaudas blīvumu – 50 mW cm^{-2}.[31]

Kā redzams, TEĢ piemīt augsts potenciāls veicināt enerģijas savākšanas jomu. Promocijas darbā ziņots par enerģijas savākšanas rezultātiem, izmantojot polimēru materiālos balstītus TEĢ. Enerģijas savākšanas uzlabošana tiks panākta, izveidojot TEĢ ierīces, kurās iestrādāti segnetoelektriskie materiāli. Jaunās zināšanas, kas ir atklātas promocijas darbā par lādiņu veidošanos, iespējams izmantot, lai uzlabotu TEĢ ierīču enerģijas savākšanas potenciālu.

Triboelektrifikācija un materiāli TEĢ ierīcēm

Triboelektrifikācija (saukta arī par kontaktelektrifikāciju) ir elektriskā lādiņa veidošanās uz divu materiālu virsmām pēc to savstarpējas saskares. Triboelektrifikācijas fenomens ir TEĢ darbības pamatā. Procesā abi materiāli iegūst elektriskos lādiņus – vienādus pēc lieluma, bet ar pretējām zīmēm. Triboelektrifikāciju novēro dažādiem materiālu veidiem, tomēr lādiņa lielums un novērojuma laika skala ievērojami atšķiras. Divu atšķirīgu metālu triboelektrifikācija rada samērā nelielu lādiņu (0,1–10 pC uz cm^2), kas ātri pazūd (mazāk par sekundi), taču polimēru gadījumā iegūtais lādiņš ir lielāks (0,1–100 nC uz cm^2) un stabilāks (līdz pat 24 stundām).

Dažos gadījumos triboelektriskajam efektam ir būtisks lietojums, savukārt ir gadījumi, kad tas ir traucējošs. Piemēram, elektrostatiskajā krāsošanā krāsas daļiņu berze pret krāsošanas pistoles stobru piešķir daļiņām virsmas lādiņu.[41] Uzlādētās krāsas daļiņas nosedz virsmu vienmērīgāk, piepildot spraugas un tukšumus. Triboelektriskais efekts tiek izmantots arī kserogrāfijā – tehnikā, ko izmanto fotokopiju radīšanai bez šķidrām ķimikālijām.[42] Dažu printeru toneros šis efekts nodrošina tonera polimēra daļiņu piesaisti dzelzs nesējdaļiņām, lai magnētiskais lauks tās varētu sakārtot. Elektrostatisko lādiņu, ko rada triboelektriskais efekts, var izmantot arī filtrācijas sistēmās. Par triboelektriskās iedarbības graujošo dabu – nejauša virsmas lādiņu izlāde var aizdegt viegli uzliesmojošus materiālus vai putekļu mākoņus.[43,44] Izlāde var sabojāt arī mikroelektronikas sastāvdaļas.[45,46] Triboelektrifikācija spēj radīt arī problēmas ražošanā – tā var traucēt vielu plūsmu un samaisīšanos,[47–51] un tā rezultātā palielinās berze un rodas enerģijas zudumi.[52,53]

Metālu un pusvadītāju gadījumā (kontakts starp metālu un metālu, metālu un pusvadītāju vai pusvadītāju un pusvadītāju) ir panākta zinātnieku vienprātība, ka par kopējā lādiņa veidošanos atbildīga ir elektronu pārnese starp iesaistītajiem materiāliem, jo šie materiāli var saturēt delokalizētus elektronus. Elektronu pārnese starp diviem metāliem ir samērā vienkārša: tās pamatā ir izejas darba Φ atšķirības. Pēc kontakta elektroni plūst no metāla ar zemāko Φ uz metālu ar augstāko Φ. Līdzsvars tiek sasniegts, kad metālā ar augstāko Φ uzkrātie elektroni kompensē sākotnējo Φ starpību un abos metālos izlīdzinās Fermi līmeņi. Tālāk materiālu

atdalīšana izraisa elektronu plūsmu atpakaļ uz sākotnējo materiālu, jo tie cenšas atgriezties sākotnējā stāvoklī, tomēr, palielinoties attālumam starp virsmām līdz punktam, kad nav iespējama elektronu tunelēšanās starp virsmām, šis process tiek ievērojami ierobežots. Rezultātā uz metāla ar augstāko Φ paliek atlikušie pārnestie elektroni.

Vispiemērotākos materiālus (metālus, pusvadītājus vai polimērus) izmantošanai virsmu kontaktēšanai TEĢ ierīcēs var izvēlēties, izmantojot triboelektriskās rindas. Tas ir empīriski sastādīts saraksts, kas sarindo materiālus pēc to tieksmes uzlādēties pozitīvi vai negatīvi. Bieži tās parāda arī paredzamo triboelektrifikācijas lielumu, izteiktu kā lādiņa blīvumu. Ierasti ir pieņemts materiālus uzskaitīt noteiktā secībā, kā parādīts 3. attēlā, pēc to tendences uzlādēties pozitīvi vai negatīvi, saskaroties citam ar citu vai arī pēc kontakta ar kādu konkrētu materiālu.[54] Tomēr ir atrodamas variācijas materiālu secībā, dažkārt – ar pretrunīgiem rezultātiem.[55–58]

Izolatora nosaukums	Lādiņa afinitāte (nC/J)		Izolatora nosaukums	Lādiņa afinitāte (nC/J)
Poliuretāna putas	+60		Sorbotāns	+58
Mati, taukaina āda	+45		Ciets poliuretāns	+40
Magnija fluorīds	+35		Neilons, sausa āda	+30
Mašīneļļa	+29		Nylatron	+28
Stikls	+25		Papīrs	+10
Koks (priede)	+7		Kokvilna	+5
Nitrilagumija	+3		Vilna	0
Polikarbonāts	−5		Akrils	−10
Epoksīdsveķi	−32		Stirola-butadiēna gumija	−35
PET (Mylar)	−40		EVA gumija	−55
Košļājamā gumija	−60		Polistirols	−70
Poliimīds	−70		Silikoni	−72
Vinils, lokans	−75		LDPE	−90
Polipropilēns	−90		HDPE	−90
Celulozes nitrāts	−93		UHMWPE	−95
Polihloroprēns	−98		PVC, stingrs vinils	−100
Lateksa gumija	−105		Viton gumija, pildīts	−117
Epihlorhidrīna gumija	−118		Santoprene gumija	−120
Hypalon gumija, pildīta	−130		Butilgumija, pildīta	−135
EPDM gumija, pildīta	−140		PTFE, (Teflons)	−190

3. att. Kvantificētas triboelektriskās rindas piemērs.[54]

Novērotās atšķirības triboelektriskajās sērijās ir viens no iemesliem ilgstošām diskusijām par mehānismiem, kas nosaka lādiņu veidošanos un pārnesi polimēru triboelektrifikācijā. Galvenie mehānismi, kas tiek piedāvāti polimēru triboelektrifikācijas skaidrojumam, ir elektronu pārnese, makromolekulu lādētu fragmentu pārnese vai jonu pārnese. Mehānisma noteikšana ir sarežģīta, jo pastāv vairāki faktori, kas ietekmē lādiņa veidošanos polimēru triboelektrifikācijas laikā: (i) vide (temperatūra un mitrums);[59–62] (ii) saskares laiks un spēks;[63] (iii) morfoloģija (virsmas raupjums, raksts); (iv) tilpuma īpašības (makromolekulu sakārtotība, šķērssaistīšanās pakāpe);[64] (v) virsmas ķīmiskais sastāvs (funkcionālās grupas).[65]

Elektronu pārnese pienācīgi raksturo lādiņa pārnesi starp metāliem,[66] tāpēc to pašu loģiku sākotnēji piemēroja arī izolatoriem – gan neorganiskiem, gan organiskiem. Izolatoram raksturīga ar elektroniem pildīta valences zona un tukša vadītspējas zona, kas atdalītas ar platu

aizliegto zonu, tāpēc, lai nodrošinātu elektronu pārnesi, jāpievada ievērojams enerģijas daudzums. Šāds endotermisks process enerģētiski patērē aptuveni 10 eV, ņemot vērā elektrona atraušanu no pirmā polimēra materiāla, tā pārvietošanu noteiktā attālumā un pievienošanu otrajam polimēru materiālam.[67] Acīmredzams, ka elektronu pārnese starp izolatoriem ir enerģētiski mazāk iespējama nekā starp metāliem, tomēr polimēri uzlādējas spēcīgāk nekā metāli. Vairākos veidos ir mēģināts izskaidrot elektronu pārneses modeļa nepilnības izolatoru triboelektriskās uzlādes gadījumā. Viens no ierosinājumiem ir tāds, ka aizliegtajā zonā pastāv elektronu aizpildīti starpstāvokļi, kurus izraisa dažādi defekti, piemēram, nospriegotas ķīmiskās saites vai virsmas īpašības.[68] Termoluminiscences eksperimenti ir pierādījuši šādu starpstāvokļu esamību, tomēr šo elektronu daudzums nav pietiekams, lai radītu novēroto triboelektrisko lādiņu.[69] Kā virzītājspēks elektronu pārnesei ir ieteikta arī elektronu viļņu funkciju delokalizācija, ko izraisa materiāla deformācija kontakta laikā.[70–73] Attiecīgi abu virsmu kontakts ļauj to elektronu orbitālēm savstarpēji pārklāties tādā veidā, ka daži elektroni tiek delokalizēti un kļūst pieejami pārnesei.

Pateicoties tādām virsmas analīzes metodēm kā rentgenstaru fotoelektronu spektroskopija (*X-ray photoelectron spectroscopy – XPS*), atomspēku mikroskopija (*atomic force microscopy – AFM*) un *Raman* spektroskopija, ir savākti pierādījumi, kas atbalsta jonu pārneses mehānisma skaidrojumu.[74–76] Bez šaubām, jonu pārnese ir galvenais mehānisms, kad tiek kontaktēti jonomēri, jo "mobilus" jonus var viegli pārnest.[77–79] Tomēr rodas jautājums, vai joni var būt atbildīgi par spēcīgo triboelektrifikāciju, ko novēro ierasto polimēru kontaktēšanā. Tradicionālajos polimēru izolatoros nav "mobilu" jonu, tāpēc ir tieksme uzskatīt, ka centrālā nozīme varētu būt hidroksīdjoni (OH^-), jo pat hidrofobi polimēri satur plānu ūdens slāni uz to virsmas apkārtējās vides apstākļos.[80] Saskaroties divu polimēru virsmām, starp virsmām veidojas ūdens "tilts", kas ļauj OH^- joniem pāriet uz polimēru, kas uzrāda spēcīgāku noteiktā jona adsorbcijas spēju. Kad materiāli tiek atdalīti, līdzsvara trūkums jonu daudzumā ūdens adorbāta slāņos uz atsevišķām virsmām veido nekompensētu lādiņu. Hidroksīdjonu adsorbcijas tieksme ir saistīta ar polimēru zeta potenciālu (elektrisko potenciālu stacionārajā ūdens slānī).[81,82] Tomēr jonu pārneses skaidrojumam ir trūkumi: polimēru triboelektrifikācija ir novērota arī vidē bez ūdens klātbūtnes[83] un arī vakuumā starp virsmām, kas nav tikušas pakļautas atmosfēras iedarbībai.[84,85] Turklāt jonu pārnese neizskaidro polimēru triboelektrifikāciju, kad tiek kontaktēti ķīmiski identiski materiāli, jo abiem piemīt vienāda OH^- jonu adsorbcijas tieksme.[59,86]

Makromolekulu lādēto fragmentu pārnese kā triboelektrifikācijas mehānisms izriet no fakta, ka polimēru kovalentās saites var tikt heterolītiski šķeltas mehāniskas ietekmes rezultātā, ko pierāda plaši pētījumi mehanoķīmijā un triboloģijā.[87,88] Kovalento saišu enerģija polimēros svārstās robežās 3,7–4,5 eV atkarībā no heteroatomu (N, Si, O, S, F utt.) klātbūtnes galvenajā virknē un sānu ķēdēs.[89] Kovalentas saites disociācija var būt homolītiska (homolīze) vai heterolītiska šķelšana (heterolīze).[90] Pēc homolītiskās šķelšanas katras pārrautās makromolekulas virknes galā izveidojas identiski radikāļi.[91] Tomēr par lādiņa veidošanos atbildīga ir tikai heterolītiskā šķelšanās, jo iznākums ir katjona un anjona pāris (mehanojoni, organojoni). Kā novērojams Kelvina spēka mikroskopijā (*Kelvin force microscopy – KFM*), kontaktatdalītas virsmas pēc nejaušības principa veido pozitīvi un negatīvi lādētus nano mēroga

izmēra domēnus (4. att.).[76] Attiecīgi kopējais lādiņa blīvums, ko nomēra uz katras kontaktētās virsmas, ir šo nano mēroga izmēra domēnu ieguldījumu summa, un virsmas polaritāti nosaka dominējošie mehanojoni. Kad virsmas tiek atdalītas, materiāla pārnesē starp virsmām tiek pārnesti arī elektriski lādētie jonu fragmenti.[75,76]

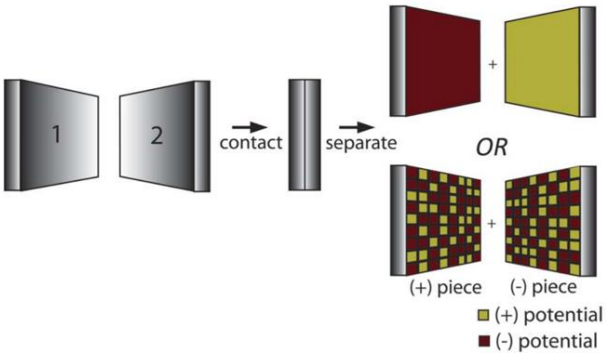

4. att. Lādiņa veidošanās attēlojums materiāla pārneses gadījumā.[76]

Pārpublicēts ar AAAS atļauju no "Baytekin, H. T.; Patashinski, A. Z.; Branicki, M.; Baytekin, B.; Soh, S.; Grzybowski, B. A. *Science* **2011**, *333*, 308".

Materiālu pārnesi rada virsmu adhēzija, jo veidojas lokāli koncentrētas adhēzijas saites, kuru iedarbības spēku summa ir lielāka par polimēra molekulu kovalento saišu spēku.[91,92] Virsmas adhēzija palielinās, kad polimēru virknes spēj brīvi mijiedarboties un savīties ar pretējām virsmām. Papildus tam elastomēri nodrošina pilnīgāku saskares laukumu, un kontaktēšanas laikā palielinās starpmolekulāro adhēzijas saišu blīvums. Berze veicina kovalento saišu šķelšanos, veidojot bīdes spriegumus kontaktēšanas laikā, tādējādi lielāki berzes spēki rada lielāku saišu šķelšanas varbūtību. Parasti berze ir atkarīga no polimēra molekulmasas un šķērssaistīšanās blīvuma, piemēram, ir pierādīts, ka šķērssaistītu polimēru virsmu berze ir par vairākām kārtām mazāka nekā nešķērssaistītu.[91]

Lai gan homolīze nerada lādiņu saturošus fragmentus, tā tomēr ir noderīga polimēru kontaktelektrifikācijai. Ir parādīts, ka radikāļu fragmenti spēj lokalizēties kopā ar jonu fragmentiem un stabilizēt tos uz kontaktētajām polimēru virsmām. Radikāļu ķērāju pievienošana (piemēram, E vitamīns) strauji samazina sākotnēji stabilo lādiņu.[45] Saskaņā ar teorētiskajiem pētījumiem radikāļa-lādiņa stabilizācijas mehānisms balstās uz starpmolekulāras nepāra elektronu (viens vai trīs) saites izveidošanos.[93]

No trīs literatūrā apspriestajiem lādiņa pārneses mehānismiem visvarbūtīgākā šķiet materiāla pārnese. Promocijas darbā pētīta lādiņa veidošanās un meklētas iespējas apstiprināt materiāla pārneses lomu polimēru triboelektrifikācijā, izmantojot pārnestā materiāla noteikšanu ar *XPS, AFM* un kontaktatdalīšanas eksperimentiem. Liela nozīme lādiņa veidošanās procesā starp virsmām ir adhēzijai, tāpēc tiks izstrādāti un pētīti materiāli ar paaugstinātu adhēziju. Darbā tiks apskatīta arī fizikāli ķīmisko īpašību ietekme uz triboelektrisko efektu, tāpēc tiks pētīta tādu parametru kā kohēzijas enerģijas blīvums, kompozīta cietība vai virsmas morfoloģija, pielāgošana augstāka virsmas lādiņa iegūšanai. Promocijas darbs arī veicinās izpratni par aspektiem, kas ietekmē lādiņa veidošanos, pētot ķīmiski identisku materiālu triboelektrifikāciju.

Promocijas darba mērķi

1. Noteikt polimēru fizikāli ķīmisko īpašību ietekmi uz virsmas lādiņa veidošanos.
2. Pierādīt, ka heterolītiska kovalento saišu šķelšana ar tai sekojošu materiāla pārnesi ir noteicošais polimēru triboelektrifikācijas mehānisms.
3. Izpētīt veidus, kā paaugstināt polimēru tieksmi triboelektrificēties.

Aizstāvamās tēzes

1. Lādiņa blīvums polimēru triboelektrifikācijā korelē ar materiāla mehāniskajām īpašībām (piemēram, elastības modulis, cietība) un virsmas raupjumu, kas ļauj paredzēt polimēra triboelektriskās īpašības.
2. Kovalento saišu heterolītiska šķelšana un tai sekojoša materiālu pārnese ir apstiprināts kā polimēru triboelektrifikācijas mehānisms.
3. Hibrīdās segnetoelektriskās-triboelektriskās ģeneratoru ierīces uzrāda lielāku veiktspēju, ja triboelektriskie dipoli (dipola moments, kas radīts triboelektrifikācijas laikā) sakrīt ar segnetoelektrisko dipolu virzienu (dipols, kas eksistē segnetoelektriskajā fāzē).

Zinātniskā novitāte

Ir radīts būtisks ieguldījums polimēru materiālu triboelektrifikācijas mehānismu skaidrošanā, parādot dažādu parametru ietekmi: cietība; elastības modulis; virsmas raupjums; makromolekulārā sakārtotība un šķērssaistīšanās pakāpe. Ieskicēta jauna pieeja augstas veiktspējas TEĢ ierīču konstruēšanai, izmantojot segnetoelektriskā/pjezoelektriskā efekta sinerģiju ar triboelektrisko efektu.

Praktiskā nozīme

Izmantojot zināšanas par polimēru fizikāli ķīmisko īpašību ietekmi uz triboelektrifikāciju, izveidotas hibrīdās triboelektrisko ģeneratoru ierīces, kas spēj pārvērst mehānisko enerģiju elektriskajā ar uzlabotu efektivitāti. Triboelektriskie ģeneratori nodrošina enerģiju mikroierīcēm vai bezvadu sensoriem, tādējādi ļaujot izvairīties no bateriju izmantošanas.

Darba struktūra un apjoms

Promocijas darbs ir zinātnisko rakstu kopa, kas veltīta kontaktelektrifikācijas efekta izpētei un triboelektrisko nanoģeneratoru izstrādei. Darba kopsavilkums ir uzrakstīts latviešu un angļu valodā. Promocijas darba rezultāti ir publicēti septiņās zinātniskajās publikācijās, kas ir indeksētas gan *Scopus*, gan *Web of Science* (*WOS*) datubāzēs. Promocijas darba kopsavilkumā ir 25 attēli un divas tabulas. Promocijas darbā iekļauto publikāciju kopējais ietekmes faktors 2020. gadam ir 84,055, to kopējais apjoms, iekļaujot elektroniski pieejamo papildu informāciju, ir 132 lapaspuses. Rezultāti ir prezentēti deviņās starptautiskajās konferencēs.

Publikācijas un darba aprobācija

Publikācijas, kurās publicēti promocijas darba rezultāti

1. A. Šutka, K. Malnieks, **L. Lapčinskis**, P. Kaufelde, A. Linarts, A. Berziņa, R. Zabels, V. Jurķans, I. Gorņevs, J. Blums, M. Knite, The role of intermolecular forces in contact electrification on polymer surfaces and triboelectric nanogenerators, *Energy Environ. Sci.* **2019**, *12 (8)*, 2417–2421. (*Scopus, WOS, IF(2020)=38.532*).
2. **L. Lapčinskis**, K. Mālnieks, J. Blūms, M. Knite, S. Oras, T. Käämbre, S. Vlassov, M. Antsov, M. Timusk, A. Šutka, The Adhesion-Enhanced Contact Electrification and Efficiency of Triboelectric Nanogenerators, *Macromol. Mater. Eng.* **2020**, *305 (1)*, 1900638. (*Scopus, WOS, IF(2020)=4.367*).
3. A. Šutka, A. Linarts, K. Malnieks, K. Stiprais, **L. Lapčinskis**, Dramatic increase in polymer triboelectrification by transition from a glassy to rubbery state, *Mater. Horiz.* **2020**, *7 (2)*, 520-523. (*Scopus, WOS, IF(2020)=13.266*).
4. A. Šutka, K. Mālnieks, **L. Lapčinskis,** M. Timusk, K. Kalniņš, A. Kovaļovs, J. Bitenieks, M. Knite, D. Stevens, J. Grunlan, Contact electrification between identical polymers as the basis for triboelectric/flexoelectric materials, *Phys. Chem. Chem. Phys.* **2020**, *22 (23)*, 13299-13305. (*Scopus, WOS, IF(2020)=3.676*).
5. **L. Lapčinskis**, A. Linarts, K. Mālnieks, H. Kim, K. Rubenis, K. Pudzs, K. Smits, A. Kovaļovs, K. Kalniņš, A. Tamm, C.K. Jeong, and A. Šutka, Triboelectrification of nanocomposites using identical polymer matrixes with different concentrations of nanoparticle fillers, *J. Mater. Chem. A* **2021**, *9 (14)*, 8984-8990. (*Scopus, WOS, IF(2020)=12.732*).
6. **L. Lapčinskis**, K. Mālnieks, A. Linarts, J. Blūms, K. Šmits, M. Järvekülg, M. Knite, A. Šutka, Hybrid Tribo-Piezo-Electric Nanogenerator with Unprecedented Performance Based on Ferroelectric Composite Contacting Layers, *ACS Appl. Energy Mater.* **2019**, *2 (6)*, 4027-4032. (*Scopus, WOS, IF(2020)=6.024*).
7. A. Šutka, K. Mālnieks, **L. Lapčinskis**, M. Timusk, K. Pudzs, M. Rutkis, Matching the Directions of Electric Fields from Triboelectric and Ferroelectric Charges in Nanogenerator Devices for Boosted Performance, *iScience* **2020**, *23 (4)*, 101011. (*Scopus, WOS, IF(2020)=5.458*).

Citas promocijas darba izstrādes laikā publicētas zinātniskās publikācijas

1. M. Knite, A. Linarts, K. Ozols, V. Tupureina, I. Stalte, **L. Lapcinskis**, A study of electric field-induced conductive aligned network formation in high structure carbon black/silicone oil fluids, *Colloids Surf., A* **2017**, *526*, 8–13. (*Scopus, WOS, IF(2020)=4.539*).
2. **L. Lapčinskis**, A. Linarts, M. Knite, I. Gorņevs, J. Blūms, A. Šutka. Solid-state supercapacitor application for pressure sensing. *Appl. Surf. Sci.* **2019**, *474*, 91–96. (*Scopus, WOS, IF(2020)=6.707*).
3. **L. Lapčinskis**, I. Cīrulis, P. Lesničenoks, A. Ābele, A. Šutka, M. Knite. PVA hydrogel electrolyte and porous polyisoprene carbon nanostructure composite based pressure

sensitive supercapacitor. *IOP Conf. Ser.: Mater. Sci. Eng.*, **2019**, *500 (1)*, 012018. (*Scopus, WOS, IF=0.53*).

4. A. Šutka, P. C. Sherrell, N. A. Shepelin, **L. Lapčinskis**, K. Mālnieks, and A. V. Ellis, Measuring Piezoelectric Output – Fact or Friction?, *Adv. Mater.* **2020**, *32 (32)*, 2002979. (*Scopus, WOS, IF(2020)=30.849*).
5. A. Šutka, K. Mālnieks, A. Linarts, **L. Lapčinskis**, O. Verners, M. Timusk, Triboelectric Laminates with Volumetric Electromechanical Response for Mechanical Energy Harvesting, *Adv. Mater. Technol.* **2021**, *6 (8)*, 2100163. (*Scopus, WOS, IF(2020)=7.848*).
6. A. Šutka, M. Zubkins, A. Linarts, **L. Lapčinskis**, K. Mālnieks, O. Verners, A. Sarakovskis, R. Grzibovskis, J. Gabrusenoks, E. Strods, K. Smits, V. Vibornijs, L. Bikse, J. Purans, Tribovoltaic Device Based on the W/WO_3 Schottky Junction Operating through Hot Carrier Extraction, *J. Phys. Chem. C* **2021**, *125 (26)*, 14212–14220. (*Scopus, WOS, IF(2020)=4.126*).
7. S. Lapcinska, P. Dimitrijevs, **L. Lapcinskis**, P. Arsenyan, Visible Light-Mediated Functionalization of Selenocystine-Containing Peptides, *Adv. Synth. Catal.* **2021**, *363 (13)*, 3318-3328. *(Scopus, WOS, IF(2020)=5.837)*.
8. P. C. Sherrell, A. Sutka, N. A. Shepelin, **L. Lapcinskis**, O. Verners, L. Germane, M. Timusk, R. A. Fenati, K. Malnieks, A. V. Ellis, Probing Contact Electrification: A Cohesively Sticky Problem, *ACS Appl. Mater. Interfaces* **2021**, *13 (37)*, 44935–44947. (*Scopus, WOS, IF(2020)=9.229*).

Konferences

1. Stenda referāts starptautiskajā konferencē "6th Nano Today International Conference": **L. Lapčinskis**, J. Blūms, M. Jarvekulg, M. Knite, A. Šutka, "Ferroelectric PVDF and $BaTiO_3$ nanocomposites for enhanced energy harvesting devices", Lisabona, Portugāle, 16.–20. jūnijs, 2019. gads.
2. Stenda referāts starptautiskajā konferencē "2019 MRS Fall Meeting": **L. Lapčinskis**, K. Mālnieks, J. Blūms, M. Jarvekulg, M. Knite, A. Šutka, "Hybrid Tribo Piezo Electric Nanogenerator with Unprecedented Performance Based on Ferroelectric Composite Contacting Layers", Bostona, ASV, 1.–6. decembris, 2019. gads.
3. Stenda referāts starptautiskajā konferencē "2019 MRS Fall Meeting": K. Mālnieks, A. Šutka, A. Linarts, **L. Lapčinskis**, "The Role of Intermolecular Forces in Contact Electrification on Polymer Surfaces", Bostona, ASV, 1.–6. decembris, 2019. gads.
4. Stenda referāts starptautiskajā konferencē "2019 MRS Fall Meeting": A. Linarts, K. Malnieks, **L. Lapčinskis**, M. Knite, J. Blums, A. Šutka, "Inversely Polarized Ferroelectric Polymer Contact Electrodes for Triboelectric Generators from Identical Materials", Bostona, ASV, 1.–6. decembris, 2019. gads.
5. Tiešsaistes referāts starptautiskajā konferencē "RTU MSAC conference": **L. Lapčinskis**, K. Mālnieks, L. Ģērmane, M. Knite, A. Šutka, "Polymer Based Triboelectric Nanogenerators: how to choose the right materials?", Rīga, Latvija, 23. oktobris, 2020. gads.

6. Tiešsaistes stenda referāts starptautiskajā konferencē "FMNT 2020": L. Ģērmane, **L. Lapčinskis**, M. Knite, A. Šutka, "Prediction of triboelectric series based on polymer physico-chemical properties", Viļņa, Lietuva, 23. novembris, 2020. gads.
7. Tiešsaistes stenda referāts starptautiskajā konferencē "2020 MRS Fall Meeting": **L. Lapčinskis**, K. Mālnieks, M. Knite, A. Šutka, "Strategy to Choose Best Building Blocks for Efficient Triboelectric Generator Devices", Bostona, ASV, 27. novembris–4. decembris, 2020. gads.
8. Tiešsaistes stenda referāts starptautiskajā konferencē "2020 MRS Fall Meeting": A. Linarts, A. Šutka, K. Malnieks, **L. Lapčinskis**, "Dramatic Increase in Polymer Triboelectrification by Transition from a Glassy to Rubbery State", Bostona, ASV, 27. novembris–4. decembris, 2020. gads.
9. Tiešsaistes stenda referāts starptautiskajā konferencē "2020 MRS Fall Meeting": K. Malnieks, A. Šutka, **L. Lapčinskis**, A. Linarts, "Matching the Directions of Electric Fields from Triboelectric and Ferroelectric Charges in Nanogenerator Devices for Boosted Performance", Bostona, ASV, 27. novembris–4. decembris, 2020. gads.

PROMOCIJAS DARBA GALVENIE REZULTĀTI

Starpmolekulāro spēku loma kontaktelektrifikācijā (1. publikācija)

1. publikācija izceļ fizikāli ķīmisko īpašību korelāciju ar virsmas lādiņa lielumu, kas veidojas pēc kontaktatdalīšanas. Polimēru virsmu triboelektrifikācija nodrošina enerģijas ieguves funkciju triboelektriskajos ģeneratoros (TEĢ). Elektronu pārnesi starp kontaktatdalītajām virsmām bieži uzskata par galveno polimēru elektrifikācijas mehānismu. Saskaņā ar elektronu pārneses mehānismu nepieciešams kontakts starp ķīmiski atšķirīgiem polimēru materiāliem, kā arī kontakta īpatnējā virsmas laukuma palielināšana, ko parasti paveic ar nanostrukturēšanas palīdzību. Tomēr 1. publikācijā mēs parādījām, ka kontaktelektrifikāciju var kontrolēt, modificējot polimēra starpmolekulāros spēkus un adhēzijas spēkus kontaktatdalīšanā.

Galvenais 1. publikācijā noteiktais mērķis bija izpētīt polimēru fizikāli ķīmisko īpašību izmaiņu ietekmi uz lādiņa veidošanos kontakta atdalīšanas laikā. Šīs ietekmes izpētei noteiktie uzdevumi bija:

- pētīt saistību starp polimēra elastības moduli un triboelektriskā lādiņa blīvumu, kontaktējot ar vadošu metāla oksīdu materiālu;
- noteikt, kā divu savstarpēji kontaktatdalītu polimēru cietību atšķirība ietekmē ģenerēto *Q*;
- pārbaudīt polimēra termiskās apstrādes parametru (termiskās vēstures) ietekmi uz ģenerēto *Q* pēc identiska ķīmiskā sastāva polimēru kontaktatdalīšanas;
- noteikt korelāciju starp elastomēra PDMS šķērssaistīšanās pakāpi, ģenerēto *Q* un arī atraušanai nepieciešamo (adhēzijas) spēku.

Triboelektrisko mērījumu galvenie rezultāti redzami 5.–7. attēlā.

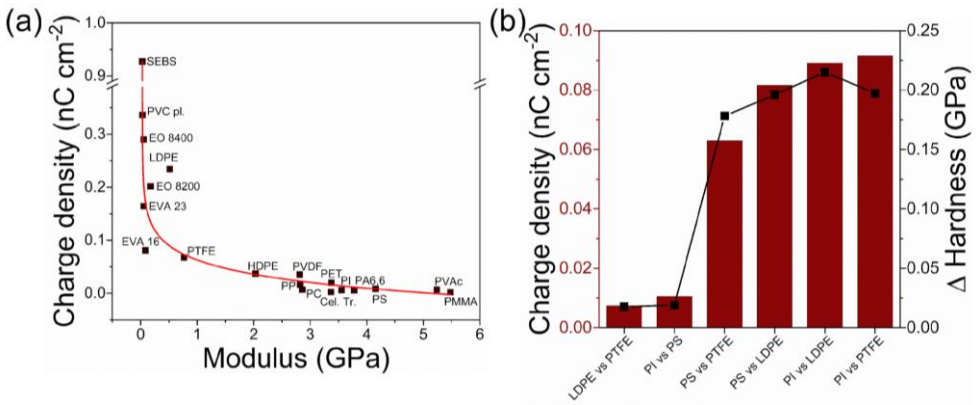

5. att. Termoplastisku polimēru triboelektrifikācijas lādiņa saistība ar to mehāniskajām īpašībām: (a) korelācija starp polimēra materiālu elastības moduli un virsmas lādiņu 20 dažādiem polimēriem, tos kontaktējot ar *ITO*; (b) kontaktelektrifikācijas lādiņa blīvums un cietības starpība dažādām polimēru kombinācijām.[94]

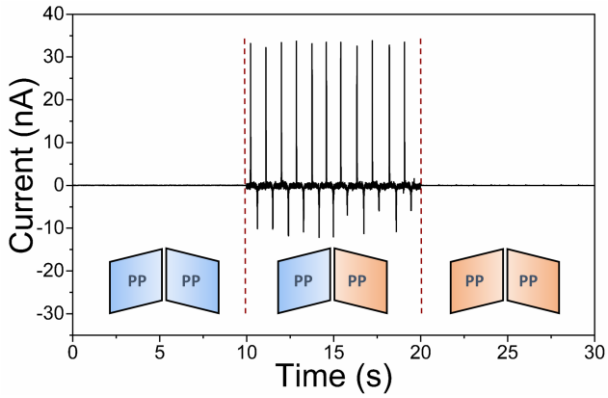

6. att. Īsslēguma strāvas maksimumi, kas veidojas, kontaktējot un atdalot divus PP ar līdzīgu un atšķirīgu termisko vēsturi. Zilās figūras atveido oriģinālās polimēra plēves, sarkanās figūras – izotermiskai kristalizācijai pakļautas polimēra kārtiņas (130 °C, 60 min).[94]

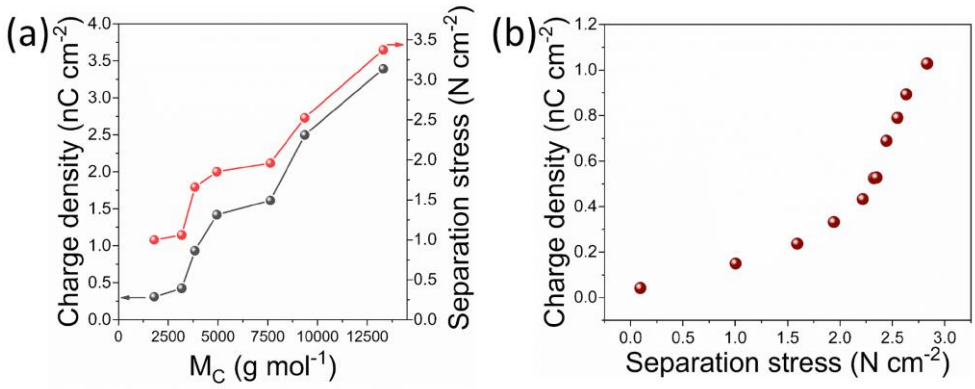

7. att. (a) Virsmas lādiņa blīvums un atdalīšanas spriegums atkarībā no molekulmasas posmam starp PDMS šķērssaistīšanās punktiem M_C; (b) sakarība starp PDMS lādiņu un nepieciešamo atdalīšanas spriegumu.[94]

1. publikācijas galvenie rezultāti un secinājumi

- Polimēriem ar zemāku elastības moduli ir augstākas virsmas lādiņa blīvuma vērtības nekā tiem, kuru modulis ir augstāks, kā redzams 5. (a) attēlā. Polimēri ar augstāko moduli: polimetilmetakrilāts (PMMA), poliamīds 6,6 (PA-66) un polivinilacetāts (PVAc) pēc saskares ar *ITO* uzrāda lādiņa blīvumu ar kārtu 10 pC cm^{-2}, savukārt mīkstiem elastomēru polimēriem, tādiem kā stirola-etilēna-butilēna-stirola bloka kopolimērs (SEBS), virsmas lādiņš ir divas kārtas augstāks (0,92 nC cm^{-2}). Modulis ir proporcionāls materiāla kohēzijas enerģijas blīvumam (KEB),[95] tātad 5. (a) attēls liecina arī par korelāciju starp virsmas lādiņu un polimēra KEB. Triboelektrifikācijas pastiprināšanos dažādu kontakta īpatnējo virsmas laukumu dēļ var izslēgt, jo visi paraugi ir plakani (sagatavoti ar vienādu presēšanas pieeju paaugstinātā temperatūrā) un tiem ir līdzīgas virsmas raupjuma vērtības, kā parādīts AFM augstuma mērījumos (59,76 ± 21,78 nm). Salīdzinājumam, paraugiem, kuriem ar nolūku tika paaugstināts virsmas raupjums, RMS virsmas raupjums sasniedza 654 nm.
- Savstarpēja kontaktatdalīšana tika veikta, izmantojot ķīmiski atšķirīgus polimērus ar līdzīgām vai atšķirīgām cietības vērtībām (5. (b) att.). Polimēru cietība tika noteikta,

izmantojot nanoindentatora adatu – Berkoviča trīsstūra piramīdu. Lai gan tie bija ķīmiski atšķirīgi, divi cietie polimēri, piemēram, poliimīds (PI, 230 MPa) un polistirols (PS, 210 MPa), radīja niecīgu virsmas lādiņa blīvuma vērtību (0,011 nC cm^{-2}). Zems lādiņa blīvums tika novērots arī, savstarpēji kontaktējot divus salīdzinoši mīkstus polimērus ar līdzīgām cietības vērtībām: LDPE (15 MPa) un PTFE (33 MPa). Cieta un mīksta polimēra savstarpēja kontaktatdalīšana sniedza par kārtu augstākus virsmas lādiņa vērtības. Šis eksperiments skaidri norāda, ka elektronu pārnese, visticamāk, nenosaka lādiņa veidošanos polimēru triboelektrifikācijas laikā.

- Pretēji vispārēji pieņemtajai izpratnei[54] mēs nodemonstrējām, ka nav nepieciešams kontaktēt ķīmiski atšķirīgus polimērus, lai notiktu triboelektrifikācija, par ko liecina no ķīmiski identiskām PP plēvītēm izgatavotās TEĢ ierīces I_{SC} (6. att.). Kontaktējot un atdalot PP plēvītes, ar identisku termisko vēsturi netika novērota īsslēguma strāva. Tomēr, kad tika kontaktatdalītas PP plēvītes ar atšķirīgām termiskajām vēsturēm, tika nomērīta 35 nA liela I_{SC} un 0,071 nC cm^{-2} liels Q. Dažāda termiskā vēsture maina makromolekulāro sakārtotību, ko apstiprina zemāka fāžu pārejas temperatūra un virsmas cietības izmaiņa no 107,6 MPa uz 96,2 MPa.
- PDMS triboelektrifikāciju pret *ITO* pētīja, mainot PDMS šķērssaistīšanās pakāpi; tā tika izmainīta, mainot attiecību starp bāzes prepolimēru un šķērssaistīšanas aģentu.[96] Virsmas lādinš, kontaktējot ar *ITO*, pieauga no 0,31 nC cm^{-2} līdz 3,39 nC cm^{-2}, palielinot molekulmasu starp šķērssaitēm (M_C) PDMS paraugā no 1800 g mol^{-1} līdz 13 300 g mol^{-1} (7. (a) att.).
- Divu ķīmiski identisku PDMS savstarpējā triboelektrifikācija tika pētīta, kontaktējot un atdalot divus PDMS gan ar identiskām, gan atšķirīgām M_C vērtībām. Kad kontaktēto PDMS kārtiņu M_C bija identisks, kontaktelektrifikāciju gandrīz nenovēroja. Pēc divu vienādu slāņu, kuru M_C bija 7600 g mol^{-1}, kontaktatdalīšanas Q bija 0,00143 nC cm^{-2}, savukārt, kontaktatdalot divus slāņus, kuru M_C bija 1800 g mol^{-1}, tas bija 0,00161 nC cm^{-2}. Kontaktējot PDMS kārtiņas ar dažādiem M_C (7600 vs. 1800 g mol^{-1}), tika iegūts vismaz par kārtu augstāks virsmas lādiņa blīvums (0,0168 nC cm^{-2}), V_{OC} (20 V) un I_{SC} (120 nA).
- Augstāks lādiņa blīvums, samazinoties šķērssaistīšanās pakāpei, ir saistīts ne tikai ar mazāku šķērssaišu daudzumu un mazāku kohēzijas enerģiju, bet arī ar augstāku adhēziju starp PDMS un *ITO*. Kā redzams 7. (a) attēlā, atdalīšanas spriegums, kas nepieciešams, lai atdalītu abas kontaktētās kārtiņas, ir lielāks, ja šķērssaistīšanās pakāpe samazinās (pieaug M_C). Novērotā sakarība starp atdalīšanas mehānisko spriegumu un lādiņa blīvumu saglabājas arī tad, ja atdalīšanas spriegumu palielina PDMS kārtiņai ar konkrētu M_C (3840 g mol^{-1}) – augstāks atdalīšanas spriegums korelē ar paaugstinātu lādiņa blīvumu (7. (b) att.). Atdalīšanas spriegums ir palielināts, pakāpeniski paaugstinot kontaktēšanai izmantoto spēku no 1 N uz 50 N ar 5 N soli. Šie rezultāti apstiprina, ka polimērā var iegūt augstu virsmas lādiņa blīvumu, ja polimēram piemīt spēcīga virsmas adhēzija un zema kohēzijas enerģija. Šādā gadījumā blakus esošo adhēzijas (fizikālo) saišu, kas veidojas starp saskares virsmām, kopējā enerģija ir lielāka nekā ķīmisko vai/un fizikālo saišu enerģija tilpumā. Tas izraisa kovalento saišu šķelšanos un materiāla pārnesi starp abām kontaktētajām virsmām.[64]

Adhēzijas uzlabota kontaktelektrifikācija un TEĢ efektivitāte (2. publikācija)

2. publikācijā tika ziņots par polimēru, kam atšķiras virsmas adhēzija, kontaktelektrifikāciju. TEĢ ierīces tika izgatavotas, izmantojot polidimetilsiloksānu (PDMS), etilēna-oktēna kopolimēru (EOK), stirola–etilēna–butilēna–stirola kopolimēru (SEBS) un etilēna-vinilacetāta kopolimēru (EVA). Papildus šiem izvēlētajiem polimēriem tika sintezēts heksāndiola-citronskābes kopolimērs (*PHC*), kas literatūrā zināms kā elastomēra veida līme.[97] Elektriskie mērījumi tika veikti kopā ar adhēzijas mērījumiem makro izmēra kontaktatdalīšanas eksperimentos. Papildus tam lokālā adhēzija un virsmas raupjums tika pētīts ar *AFM*, lai iegūtu dziļāku ieskatu sakarībās starp virsmas īpašībām un elektrifikāciju. Rezultāti rāda, ka lielāks virsmas lādiņš veidojas uz polimēru kārtiņām ar specīgāku adhēziju. Kopā ar *XPS* mērījumiem tas apstiprina, ka par polimēru kontaktelektrifikāciju atbildīgs ir kovalentās saites šķelšanas mehānisms. Pētītajiem materiāliem piemīt uzlabota kontaktelektrifikācija, kas padara tos pievilcīgus izmantošanai triboelektrisko nanoģeneratoru ierīcēs, lai pārveidotu mehānisko enerģiju elektriskajā.

2. publikācijā noteiktie mērķi bija šādi:

- tālāk izpētīt korelāciju starp virsmas lādiņa blīvumu un adhēziju;
- pārbaudīt materiāla pārnesi PDMS polimēra gadījumā;
- ierosināt metodi, kā aprēķināt triboelektrisko ģeneratoru efektivitāti, iekļaujot iepriekš vērā neņemtos adhēzijas spēkus.

Mērījumu galvenie rezultāti redzami 8.–10. attēlā.

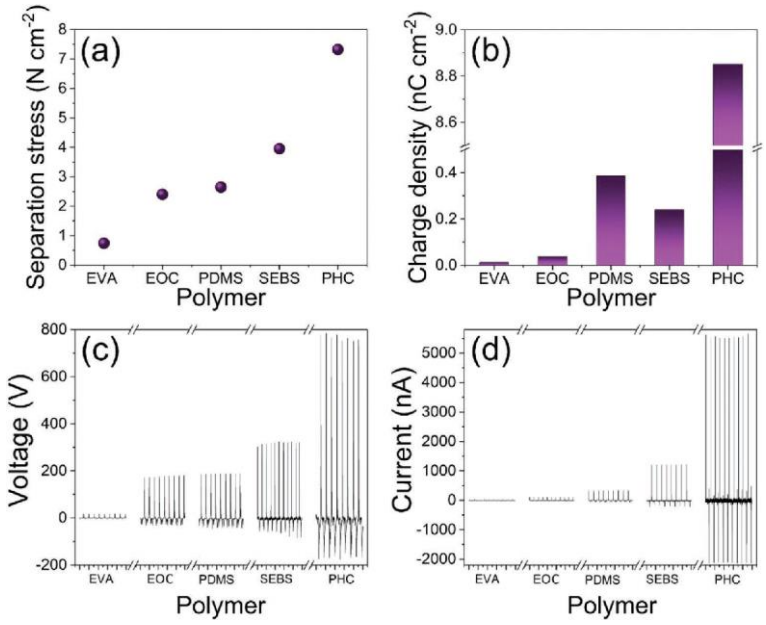

8. att. (a) Atdalīšanas spriegums abām kontaktētajām TEĢ kārtiņām dažādiem polimēru materiāliem; (b) atbilstošais lādiņš šīm TEĢ ierīcēm; (c) V_{OC} maksimumi dažādu polimēru TEĢ; (d) I_{SC} maksimumi dažādu polimēru TEĢ.[98]

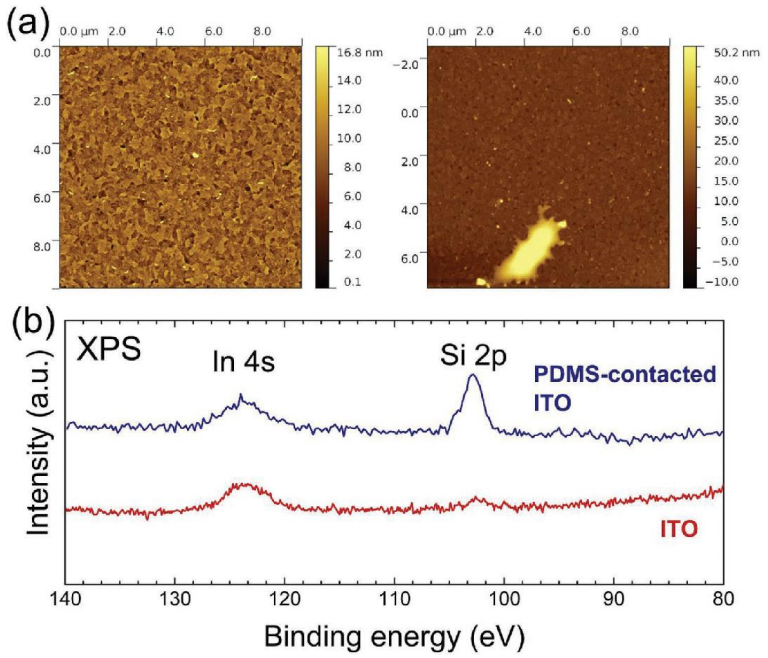

9. att. Materiāla masas pārnese: (a) *ITO* virsma pirms (pa kreisi) un pēc (pa labi) 10 000 kontaktēšanas cikliem ar PDMS (masas attiecība starp prepolimēru un šķērssaistīšanas aģentu – 10 : 1); (b) *XPS* rezultāti, salīdzinot neizmantota *ITO* virsmu un *ITO* virsmu pēc 10 000 kontaktēšanas cikliem ar PDMS (masas attiecība starp prepolimēru un šķērssaistīšanas aģentu – 10 : 1), kas parāda Si 2p maksimumus uz *ITO* virsmas.[98]

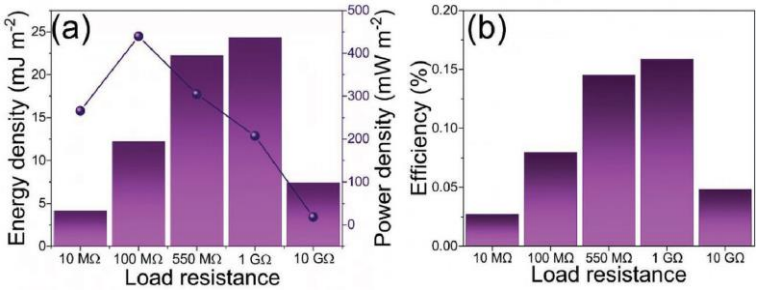

10. att. PHC polimēra TEĢ ierīces raksturlielumi: (a) enerģijas blīvums un jaudas blīvums kā funkcija no slodzes pretestības; (b) efektivitāte.[98]

2. publikācijas galvenie rezultāti un secinājumi

- Testēto materiālu atdalīšanas spēks palielinājās šādā secībā: EVA < EOK < PDMS < SEBS < *PHC* (8. (a) att.). Polimēri, kas uzrāda lielāku atdalīšanas spriegumu pret kontaktēto *ITO* virsmu, uzrāda augstāku lādiņa blīvumu, V_{OC} un I_{SC} (8. (b–d) attēls). Vislielākais atdalīšanas spriegums vērojams TEĢ ierīcei, kas veidota no *PHC* (7,32 N cm^{-2}), un *Q* sasniedz 8,853 nC cm^{-2}. Novērotā korelācija starp atdalīšanas spēku un virsmas lādiņu saskan ar iepriekš veiktiem pētījumiem,[75,76] kuros lādiņa veidošanās ir skaidrota ar heterolītisku kovalento saišu šķelšanu un materiāla pārnesi. Augstāks atdalīšanas spēks varētu veicināt materiāla pārnesi un kovalentu saišu šķelšanas varbūtību.
- Jāņem vērā, ka var izslēgt polimēru kontaktam pieejamā īpatnējā virsmas laukuma izmaiņas ietekmi uz lādiņa blīvumu, jo polimēriem *AFM* mērījumos bija līdzīgas virsmas raupjuma

vērtības (gan 3 × 3 μm, gan 50 × 50 μm izmēros). Izmēram 3 × 3 μm *RMS* virsmas raupjuma vērtības bija diapazonā 9–59 nm, savukārt 50 × 50 μm izmēram tās bija 9–209 nm. *PHC* virsma bija pārāk lipīga virsmas raupjuma noteikšanai.

- *AFM* koloidālās zondes metode sniedza dziļāku ieskatu sakarībā starp virsmas īpašībām un TEĢ veiktspēju, jo tā ļauj veikt adhēzijas mērījumus nano izmēra mērogā. Vidējās adhēzijas vērtības bija 13,4 mJ m^{-2} EVA polimēram, 37,9 mJ m^{-2} PDMS polimēram, 49,1 mJ m^{-2} SEBS polimēram un 66,9 mJ m^{-2} EOK. Tieši tāpat kā raupjuma mērījumos, *PHC* bija ārpus izmērāmajām robežām.
- Izmērītās nano izmēra mēroga adhēzijas vērtības galvenokārt sakrīt ar makro izmēra mēroga atdalīšanas spēka mērījumiem ar EOK kā izņēmumu, jo makro izmēra mērogā tas uzrādīja salīdzinoši nelielu atdalīšanas spēku. Tas skaidrojams ar dažādām raupjuma vērtībām dažādos mērogos. Izmērā 50 × 50 μm, kas attiecas uz makro izmēra mēroga adhēzijas testiem, EOK ir relatīvi liels raupjums (175 nm), savukārt 3 × 3 μm izmērā, kas ir salīdzināms ar sfēriskās *AFM* zondes rādiusu, EOK raupjums ir mazāks (17 nm). Nelīdzenām makroskopiskām virsmām pilns kontakts visas virsmas laukumā ir grūtāk sasniedzams, jo virsmas tukšumi novērš pilnu abu virsmu kontaktēšanos pretstatā mērījumiem ar mazo *AFM* zondi, kas var sasniegt pilnu kontaktu ar gandrīz visu virsmu.
- Heterolītisko saišu šķelšanas mehānisms iepriekš ir parādīts materiālu pārneses mērījumos, izmantojot *AFM, XPS* un *Raman* spektroskopiju.[64,75,76] Šajā publikācijā materiālu pārnese tika noteikta, izmantojot *AFM* un *XPS*. *ITO* virsmas raupjums pēc 10 000 kontaktatdalīšanas cikliem pret PDMS palielinājās no 5,15 nm uz 21,51 nm un saturēja polimēra daļas, kā redzams *AFM* attēlos (9. (a) att.). *XPS* apstiprināja PDMS klātbūtni uz kontaktatdalītā *ITO* virsmas, kad fotoelektronu spektrā (9. (b) att.) tika novēroti Si 2s (153,9 eV) un Si 2p (102,7 eV) signāla maksimumi. Tādus pašus signāla maksimumus novēroja PDMS spektrā pirms kontaktatdalīšanas, savukārt uz *ITO* virsmas pirms kontaktatdalīšanas netika manīti iepriekš minētie signāli.
- TEĢ, kas balstīts uz *PHC*, tika pētīts detalizētāk, jo iepriekš aprakstītajos mērījumos tika novērots augstāks lādiņa blīvums. Augstākā enerģija (24,36 mJ m^{-2}) tika novērota pie *R* 1 GΩ, visaugstākais vidējais jaudas blīvums (439,86 mW m^{-2}) kontaktatdalīšanā tika sasniegts pie 100 MΩ (10. (a) att.). Skatoties perspektīvā, aprēķinātā enerģija norāda, ka TEĢ ierīcei ar 1 m^2 lielu laukumu būtu nepieciešamas aptuveni 9,3 dienas (223,7 h) pie 1 Hz kontaktatdalīšanas frekvences, lai pilnībā uzlādētu tipiska mobilā tālruņa akumulatoru (5,45 Wh). TEĢ ierīce, kuras virsmas laukums ir 20 cm^2 un kas darbojas ar kontaktatdalīšanas frekvenci 1 Hz, tomēr varētu darbināt bezvadu sensoru mezglu ar jaudas patēriņu 100 μW,[99] tādējādi apstiprinot TEĢ iespējamo izmantošanu sensoros.
- Tika pētīta *PHC* TEĢ ierīces efektivitāte. Aprēķinam mēs dalījām saražoto enerģiju ar darbu, kas tika veikts kontaktēšanas un atdalīšanas laikā. Parasti, aprēķinot darbu, ņem vērā tikai saspiešanas spēku, pārvietojumu vai kustību kinētisko enerģiju, bet neņem vērā atdalīšanas spēku.[100–105] Ja šīs ziņotās metodoloģijas izmanto *PHC* balstītam TEĢ, tad efektivitāte pārsniegtu 300 %, tādējādi liecinot par iespējamiem trūkumiem metodoloģijā. Ja aprēķinā tiek iekļauts saspiešanas spēks, kustības kinētiskā enerģija un atdalīšanas spēks, efektivitāte samazinās zem 1 % (10. (b) att.), parādot, ka ir pietiekami daudz brīvas vietas

uzlabojumiem attiecībā uz TEĢ dizainu. Rezumējot – adhēzija veicina lādiņa veidošanos, taču ierobežo TEĢ praktisko lietojamību.

Fāžu pārejas ietekme uz triboelektrisko lādiņu (3. publikācija)

Iedvesmojoties no 1. publikācijā izdarītajiem atklājumiem, ka mīkstāki materiāli uzrāda lielāku triboelektrifikāciju, mēs paredzējām, ka arī stiklveida stāvoklī esošu polimēru uzsildīšanai virs stiklošanās temperatūras (T_g) vajadzētu palielināt virsmas lādiņu, neskatoties uz to, ka ķīmiskais sastāvs paliek nemainīgs. 3. publikācija parāda, ka, pārejot no stiklveida stāvokļa superelastīgajā stāvoklī, virs T_g polimēriem PS, *PC* un PMMA triboelektriskā lādiņa blīvums pieaug par kārtu. Polimēri pāriet superelastīgajā stāvoklī, tāpēc palielinās arī atdalīšanai nepieciešamais adhēzijas spēks.

3. publikācijas mērķis bija pārbaudīt polimēra struktūras stāvokļa (stiklveida vai superelastīgais) ietekmi uz lādiņa blīvumu, tāpēc tika veikti kontaktatdalīšanas eksperimenti temperatūras diapazonā no istabas temperatūras līdz temperatūrai, kas pārsniedz polimēru T_g. Veikto mērījumu galvenie rezultāti redzami 11. un 12. attēlā.

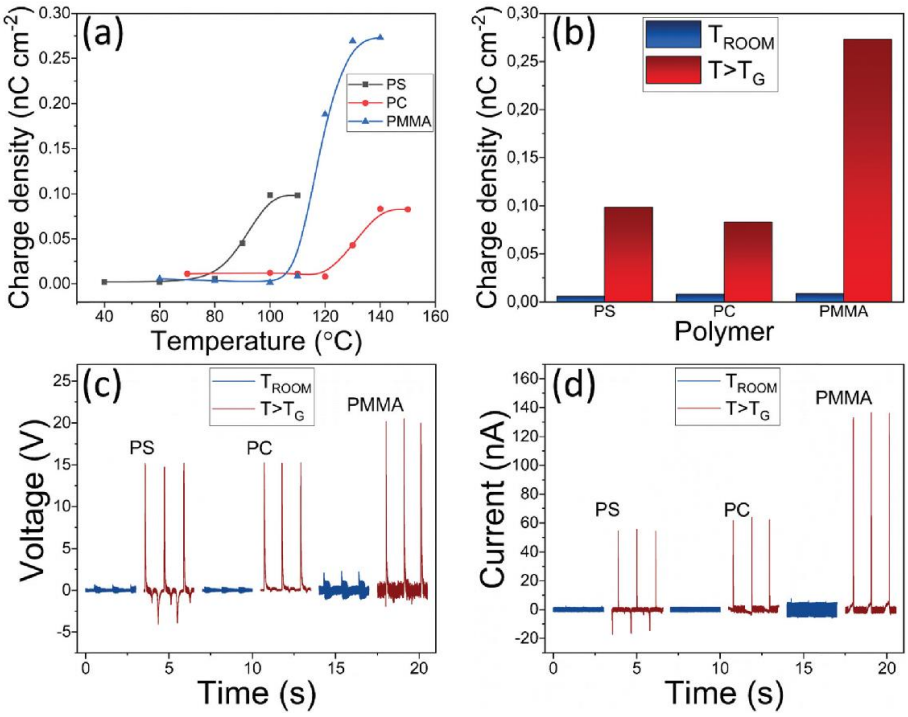

11. att. (a) Lādiņa blīvuma strauja paaugstināšanās, TEĢ ierīces temperatūrai sasniedzot polimēra T_g; (b) lādiņa blīvums uz polimēra virsmas pie temperatūras, kas pārsniedz T_g, un istabas temperatūrā; (c) V_{OC} maksimumi polimēram istabas temperatūrā un temperatūrā virs T_g; (d) I_{SC} maksimumi polimēram istabas temperatūrā un temperatūrā virs T_g.[106]

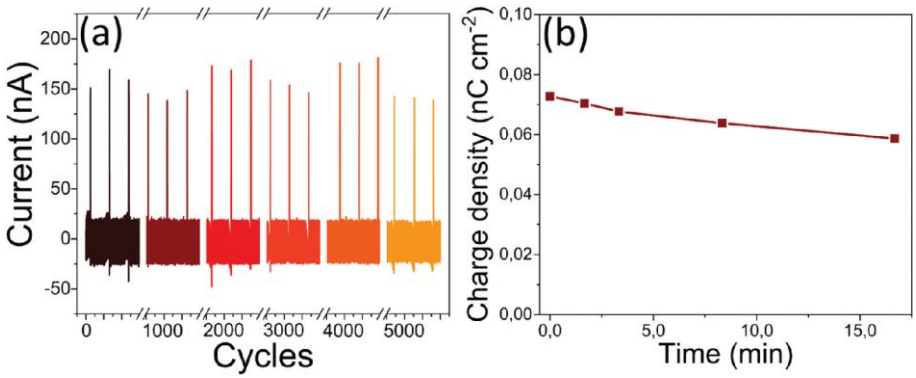

12. att. (a) PMMA balstītas TEĢ ierīces strāvas mērījumi 5000 kontaktēšanas ciklu laikā; (b) PS balstītas TEĢ ierīces virsmas lādiņa blīvums kustībās bez kontaktēšanas temperatūrā, kas pārsniedz T_g.[106]

3. publikācijas galvenie rezultāti un secinājumi

- Trīs stiklveida stāvoklī esošu polimēru ar atšķirīgu ķīmisko struktūru (PMMA, *PC* un PS) temperatūras palielināšana no istabas temperatūras līdz punktam, kas ir tieši zem T_g, radīja nelielu virsmas lādiņa blīvuma pieaugumu. Tomēr, kad temperatūru palielināja virs T_g, virsmas lādiņa blīvums, V_{OC} un I_{SC} strauji palielinājās par vairāk nekā kārtu visiem pētītajiem polimēriem (11. att. (a)–(d)).
- Virs T_g, superelastīgajā stāvoklī polimēri uzvedas kā elastomēri – tiem piemīt liela atgriezeniskā deformācija, tādēļ tika novērota arī adhēzijas īpašību palielināšanās. Attiecīgi tika novērots, ka, polimēru karsējot virs T_g, atdalīšanas spēks kontaktatdalīšanā strauji pieaug. PS atdalīšanas spēks palielinājās no 0,25 N līdz 31 N, savukārt *PC* un PMMA tas mainījās no 0,15 N līdz 3 N un no 0,2 N līdz 4,8 N.
- Ņemot vērā 1. un 2. publikācijā uzrādītos rezultātus, ka iespējamais lādiņa veidošanās mehānisms ir saistīts ar polimēra kovalento saišu heterolīzi, tika secināts, ka novērotais lādiņa blīvuma pieaugums ir saistīts ar uzlabotu materiālu pārnesi, kas notiek vienlaikus ar heterolītisku saites šķelšanu, kad polimērs ir pārgājis superelastīgajā stāvoklī. Elastomēru polimēri vairāk tiek pakļauti mehāniskiem bojājumiem, un deformācija ļauj izveidot lielāku saskares laukumu, savukārt adhēzija uzlabo materiāla pārnesi. Materiālu pārnese ir nepārtraukts divvirzienu process,[75] tāpēc tika novērota arī ilgtermiņa darbība. PMMA TEĢ ierīces, kas darbojas temperatūrā virs polimēra T_g, rādītāji bija stabili vairāk nekā 5000 ciklu garumā (12. (a) att.).
- Netika atrasti pierādījumi, kas liecinātu par saistību starp *RMS* virsmas raupjumu (mērīts ar *AFM*) un virsmas lādiņa blīvumu kontaktatdalīšanas eksperimentos zem un virs T_g. Viskozi tekošajā stāvoklī materiāla pārnese ir pastiprināta, tāpēc tika sagaidāmas virsmas raupjuma izmaiņas. Attiecībā uz *PC RMS* virsmas raupjums saglabājās gandrīz vienāds – pirms testēšanas tas bija 38,4 nm, pēc kontaktatdalīšanas temperatūrā virs T_g – 33,9 nm. PS raupjums palielinājās no 9,9 nm uz 59,6 nm, PMMA tas samazinājās no 162,0 nm uz 78,1 nm. Lai pierādītu, ka virsmas raupjums lādiņa blīvumu ietekmē mazāk nekā polimēra uzsildīšana virs T_g, PMMA virsmas raupjums tika palielināts virs 1000 nm, to iegremdējot šķīdinātājā un pēc tam iegremdējot izgulsnētājā. Lādiņa blīvuma pieaugums

kontaktatdalīšanas testos temperatūrā zem T_g bija niecīgs – no 0,008 nC cm^{-2} uz 0,037 nC cm^{-2}.

- Virsmas lādiņu stabilitāti pētīja, oscilējot TEĢ ierīci bezkontakta režīmā, kad PS tika uzsildīts virs T_g. Bezkontakta režīmā iepriekš kontaktatdalītās kārtiņas tika kustinātas bez fiziskas kontaktēšanas. Virsmas lādiņš ir salīdzinoši stabils, uzrādot mazāk nekā 15 % samazinājumu pirmo 15 minūšu laikā (12. (b) att.), tādējādi apliecinot, ka elektronu pārnese nevar būt par iemeslu paaugstinātam lādiņa blīvumam, jo, kā parādīts literatūrā,[59] šādā temperatūrā būtu jānotiek intensīvai termoelektronu emisijai no polimēra virsmas. Lēno izlādi var skaidrot ar polimēra virsmas mijiedarbību ar molekulām, joniem un daļiņām no apkārtējās atmosfēras.[76]

Kontaktelektrifikācija starp identiskiem polimēriem (4. publikācija)

1. publikācijā tika parādīts, ka ir iespējama kontaktelektrifikācija starp ķīmiski identiskiem polimēriem, ja tiem ir atšķirīga makromolekulārā sakārtotība vai šķērssaistīšanās pakāpe. Šeit, 4. publikācijā, mēs izpētījām, kā mainās triboelektrifikācija, kontaktējot pēc ķīmiskā sastāva identiskus polimērus ar atšķirīgu virsmas morfoloģiju. Attiecīgi mēs ierosinājām, ka virsmas lādiņa veidošanās iemesls, kontaktējot divus identiskus polimērus, ir atšķirības virsmas nelīdzenumos. Turklāt, ja kontaktētajiem materiāliem ir lielāka porainības vai virsmas nelīdzenuma starpība, rezultātā tiks iegūts lielāks virsmas lādiņš. To apstiprināja gan eksperimentālie rezultāti, gan galīgo elementu analīzes (GEA) simulācijas. Porainība un virsmas raupjums uz virsmas rada nospriegotus un saspiestus apgabalus, tādējādi ietekmējot savstarpējo materiāla pārnesi starp abām virsmām. Jaunais ieskats padziļināja polimēru kontaktelektrifikācijas izpratni un ieskicēja nākotnes virzienus virsmu inženierijā, lai paaugstinātu triboelektrifikāciju.

Galvenais 4. publikācijas mērķis bija izpētīt polimēra virsmas morfoloģijas ietekmi uz lādiņa veidošanos ķīmiski identisku polimēru kontaktatdalīšanas laikā.
Triboelektrisko mērījumu galvenie rezultāti redzami 13.–16. attēlā.

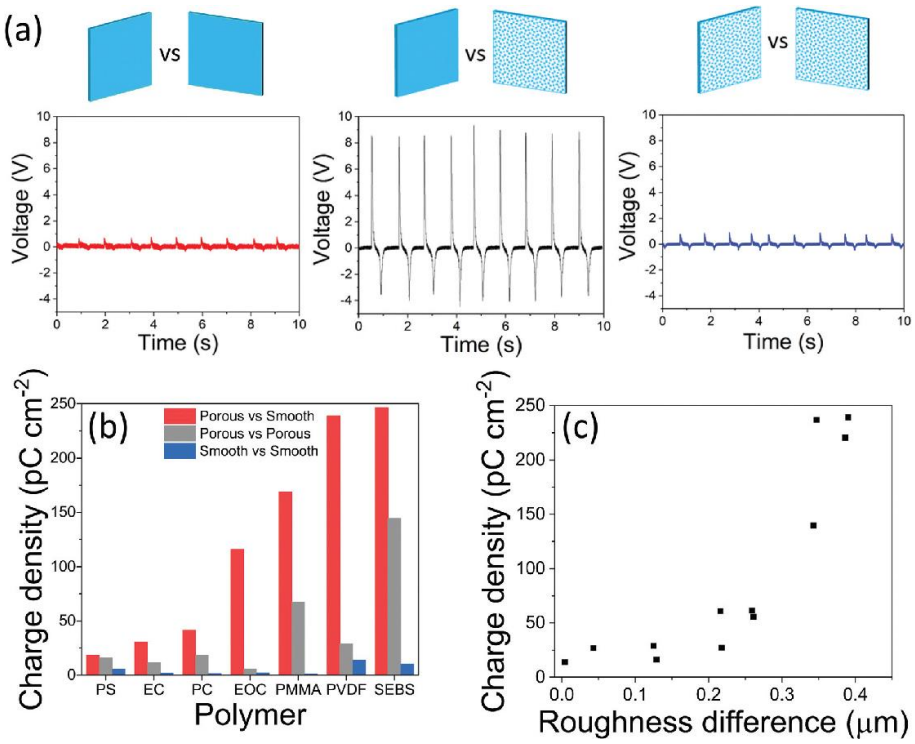

13. att. (a) V_{OC}, ko ģenerē gluds–gluds, gluds–raupjš un raupjš–raupjš EOC kārtiņu kombinācijas kontaktatdalīšanā (no kreisās uz labo pusi); (b) virsmas lādiņa blīvums, ko veido divu identisku polimēru plēvju ar atšķirīgu virsmas raupjumu kontaktatdalīšana; (c) sakarība starp virsmas lādiņa blīvumu, kas rodas kontaktatdalīšanā, un starpību virsmas raupjumos izmantotajām PVDF kārtiņām.[107]

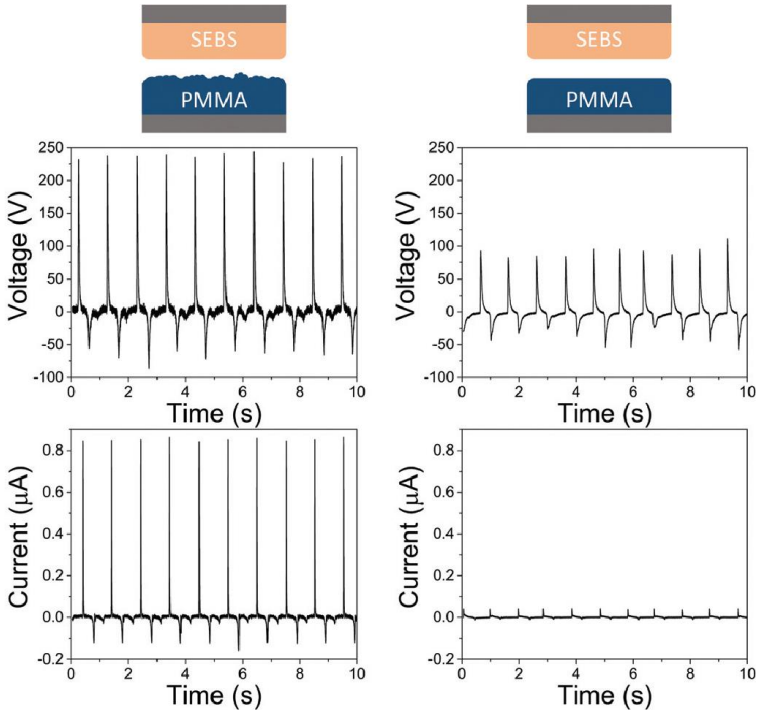

14. att. Izmērītās V_{OC} un I_{SC} vērtības, kad elastomērs SEBS tiek kontaktēts ar raupju (pa kreisi) un salīdzinoši gludāku (pa labi) PMMA plēvi TEĢ ierīcē.[107]

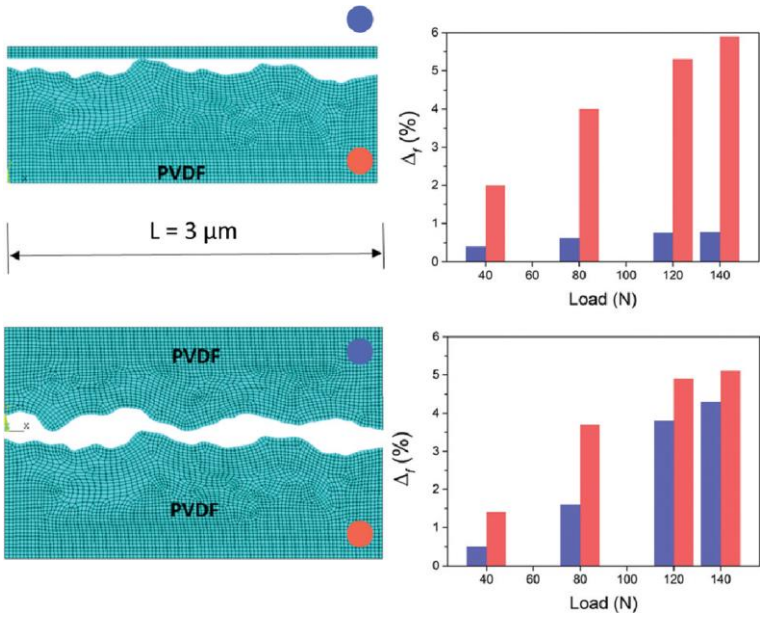

15. att. Virsmas garuma procentuālās izmaiņas (Δ_f) katrai virsmai: kontaktējot raupju un gludu virsmu (augšējais) vai raupju un raupju virsmu (apakšējais).[107]

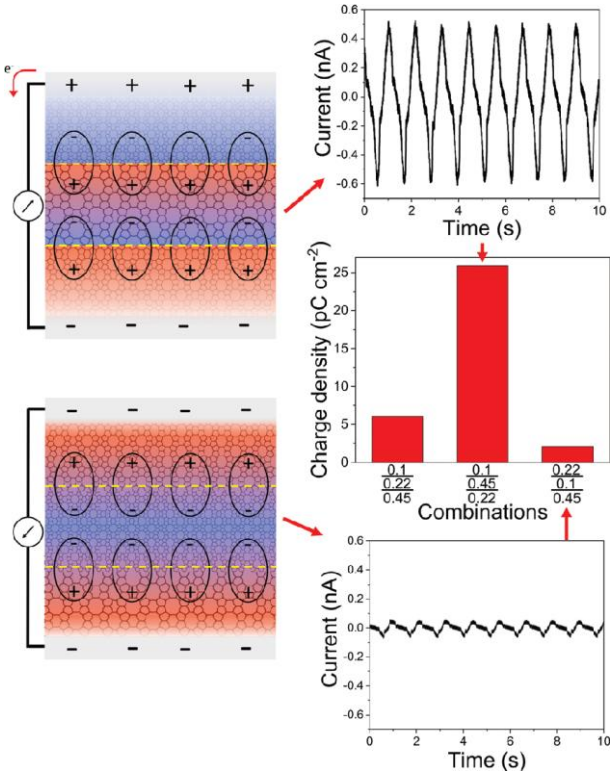

16. att. Dipolu un fleksoelektrisko lādiņu veidošanās daudzslāņu membrānu paraugos ar dažādu membrānu secību.[107]

4. publikācijas galvenie rezultāti un secinājumi

- TEĢ ierīces tika izgatavotas no diviem identiskiem polimēriem, kam bija vienāds (gluds–gluds vai raupjš–raupjš) vai atšķirīgs (gluds–raupjš) virsmas raupjums. Izraudzītie polimēri bija: polietilēna-oktēna kopolimērs (EOK), polistirols (PS), etilceluloze (EC), polikarbonāts

(PK), poli(metilmetakrilāts) (PMMA), stirola–etilēna–butilēna–stirola kopolimērs (SEBS) un poli(vinilidēnfluorīds) (PVDF). TEĢ ierīces, kas tika izgatavotas no slāņiem ar atšķirīgu raupjumu (13. (a), (b) att.), parādīja augstāku Q, V_{OC} un I_{SC} kā ierīces, kas tika pagatavotas no divām vienādām kārtiņām.

- Novērotās atšķirības Q lielumā starp izmantotajiem polimēriem ir izskaidrojamas ar to, ka starp kontaktēto kārtiņu virsmas raupjuma vērtībām ir dažādas starpības. Virsmas raupjuma veidošanās un viendabīgums tika noteikts: i) vizuāli; ii) mērot ūdens piliena kontaktleņķi; iii) veicot AFM virsmas topogrāfijas mērījumus. Iegūtajām kārtiņām bija vizuāli novērojama izkliedējoša gaismas atstarošanās, kas liecina par raupjas virsmas veidošanos. Raupjajai polimēra kārtiņai bija novērojams lielāks ūdens piliena kontakleņķis nekā salīdzinoši gludajai kārtiņai, kas liecina par virsmas hidrofobitāti. Kārtiņām ar raupju virsmu ierasti piemīt hidrofobas īpašības. AFM topogrāfijas mērījumus izmantoja, lai noteiktu RMS virsmas raupjumu, un lielākajai daļai polimēru bija ievērojamas atšķirības gludo un raupjo kārtiņu virsmas raupjumā. PMMA un SEBS ir novērojamas līdzīgas RMS raupjuma vērtības raupjajiem un gludajiem paraugiem, savukārt dažādās virsmas morfoloģijas liecina, ka tā var ietekmēt virsmas lādiņa veidošanos.
- PVDF kārtiņas ar atšķirīgu virsmas raupjumu tika sagatavotas, izgulsnējot polimēru metanola izgulsnētājā no dimetilformamīda (DMF) šķīdumiem dažādās koncentrācijās. Kontaktēto PVDF polimēra kārtiņu Q tika mērīts kā funkcija no virsmas raupjuma starpības (13. (c) att.). Paraugu virsmas raupjums bija robežās 0,2–1 μm. Kā tika paredzēts, Q pieauga, palielinoties raupjumu starpībai.
- Skenējošā Kelvina zonde (SKZ) tika izmantota, lai noteiktu gludā PVDF virsmas potenciālu pirms un pēc kontaktēšanas ar citu gludu vai raupju PVDF. Kontaktatdalīšana pret citu gludu paraugu palielināja vidējo virsmas potenciālu par 20 mV. Pēc kontakta ar raupju PVDF virsmas potenciāls palielinājās par 243 mV.
- Virsmas raupjuma ietekme uz Q tika novērota arī tad, kad raupjo un gludo kontaktējamo slāņu izgatavošanai tika izmantoti polimēri ar atšķirīgām fizikāli ķīmiskajām īpašībām. Tika salīdzinātas divas TEĢ ierīces: gluds elastomēra SEBS slānis pret salīdzinoši cietāko PMMA gan kā gludo, gan raupjo slāni. Augstākas vērtības (240 V V_{OC}; 0,85 mA I_{SC}; 9,6 nC cm^{-2} Q un 2,5 mJ m^{-2} E) tika iegūtas, kad relatīvi gludie SEBS tika kontaktēti ar raupjo PMMA (14. att.). Salīdzinājumam, gludais SEBS kopā ar gludu PMMA sasniedza 100 V V_{OC}; 0,05 mA I_{SC}; 1,2 nC cm^{-2} Q un 0,6 mJ m^{-2} E.
- Novērotā triboelektrifikācija, atdalot vienādus polimērus ar atšķirīgiem raupjumiem, ir saistīta ar katra slāņa nevienmērīgu deformāciju saskares laukumā. Relaksācijas laikā tas izmaina lādiņa blīvumu uz virsmas.[108] Nevienmērīgā deformācija tika apstiprināta ar 2D plaknes GEA modeli makro mēroga simulācijai. Raupjo paraugu virsmas konfigurācijas 2D modelis ir ņemts no PVDF virsmas AFM mērījumiem. Kad raupjais modelis tika piespiests pie gludās virsmas, abām virsmām virsmas garuma procentuālās izmaiņas (Δ_f) sānu virzienā bija atšķirīgas (pie 140 N atšķīrās 7,4 reizes). Turpretim, kad tika kontaktēti divi raupjie modeļi ar līdzīgiem raupjumiem, novērotais Δ_f abām virsmām bija gandrīz vienāds (pie 140 N atšķīrās tikai 1,2 reizes) (15. att.). Novērotās nevienmērīgās deformācijas rezultātā

noris heterolītiska saišu šķelšanās, kas rada mehanojonus saturošus polimēru virknes fragmentus, kas palielina kopējo virsmas lādiņu.

- *Q* veidošanās tika novērota, arī noslogojot un atslogojot bez atdalīšanas divas sakontaktētas polimēru plēvītes. Tika izgatavotas slāņainās struktūras, izmantojot komerciāli pieejamas PVDF membrānas ar atšķirīgām porainībām (0,10 μm, 0,22 μm un 0,45 μm poras). Abas plēvītes tika noslogotas un atslogotas bez atdalīšanas ar spēku, kas mainījās no 5 N uz 100 N. Kā tika paredzēts, I_{SC} un *Q* palielinājās, pieaugot porainības starpībai starp membrānām.
- Elektromehāniskā atbildes reakcija vēl vairāk palielinājās, izgatavojot daudzslāņu paraugus no visām trim iepriekšminētajām PVDF membrānām. Lielākais *Q* (26 pC cm^{-2}) tika nomērīts daudzslāņu paraugam ar 0,45 μm poru izmēra membrānu vidū (membrānas ar poru izmēriem 0,10 μm un 0,22 μm attiecīgi katrā pusē). Kad membrāna ar poru izmēru 0,10 μm tika novietota vidū, tika nomērīts ievērojami zemāks *Q* (16. att.). To var izskaidrot ar triboelektrisku dipolu veidošanos divu membrānu saskares virsmā. Membrāna ar 0,45 μm poru izmēru uzlādējas pozitīvi pret 10 μm poru izmēra membrānu, negatīvi pret 0,22 μm poru izmēra membrānu. Sakombinējot tās daudzslāņainā struktūrā, tiek izveidotas divas saskares virsmas; katrai no tām ir raksturīgs dipola virziens. Pirmajā gadījumā abi dipolu virzieni bija salāgoti, un tie pastiprināja viens otru, tādējādi palielinot nomērīto *Q*. Tomēr, kad vidū tika ievietota membrāna ar 0,1 μm poru izmēru, saskares virsmās izveidotajiem dipoliem bija pretēji virzieni, un tā rezultātā *Q* bija daudz mazāks.

Triboelektrifikācija starp polimēru kompozītiem ar identiskām polimēru matricām (5. publikācija)

1. un 4. publikācijā tika parādīts, ka kontaktelektrifikācija starp ķīmiski identiskiem polimēriem var radīt ievērojamu *Q*, ja pastāv atšķirības tādās īpašībās kā makromolekulu sakārtotība, šķērssaistīšanās pakāpe vai virsmas raupjums. Līdzīgi, triboelektriskais lādiņš pieauga arī tad, kad palielinājās nanodaļiņu (ND) pildvielas koncentrācijas starpība starp diviem slāņiem ar identiskām polimēru matricām. Šo ietekmi novēroja eksperimentos, izmantojot dažādus polimērus (etilēna un vinilacetāta kopolimēru (EVA), polidimetilsiloksānu (PDMS), polivinilacetātu (PVAc) un poliuretānu (PU)) un dažādas ND pildvielas (TiO_2, FeO(OH), WO_3 un MnO_2). GEA simulācijas apstiprināja, ka polimēru triboelektrifikācija ir saistīta ar virsmas viskoelastīgo deformāciju, kas rodas mehāniskas saskares un atdalīšanas laikā. Tas liecina par iespējamību, ka kovalentu saišu heterolītiska šķelšanās polimēru virknēs ir skaidrojums triboelektriskajam efektam.

Galvenais 5. publikācijas mērķis bija izpētīt triboelektrifikāciju starp ķīmiski identiskiem polimēru kompozītiem ar dažādu ND saturu. Šā mērķa sasniegšanai tika izvirzīti šādi uzdevumi:

- izpētīt polimēru kompozītmateriālu kontaktelektrifikāciju, izmantojot TiO_2 kā pildvielu dažādās koncentrācijās;
- izpētīt EVA kompozītmateriālu kontaktelektrifikāciju, izmantojot dažādu veidu pildvielas;
- izpētīt mehāniskos procesus kontaktatdalīšanas procesā, izmantojot GEA.

Triboelektrisko mērījumu galvenie rezultāti redzami 17.–19. attēlā.

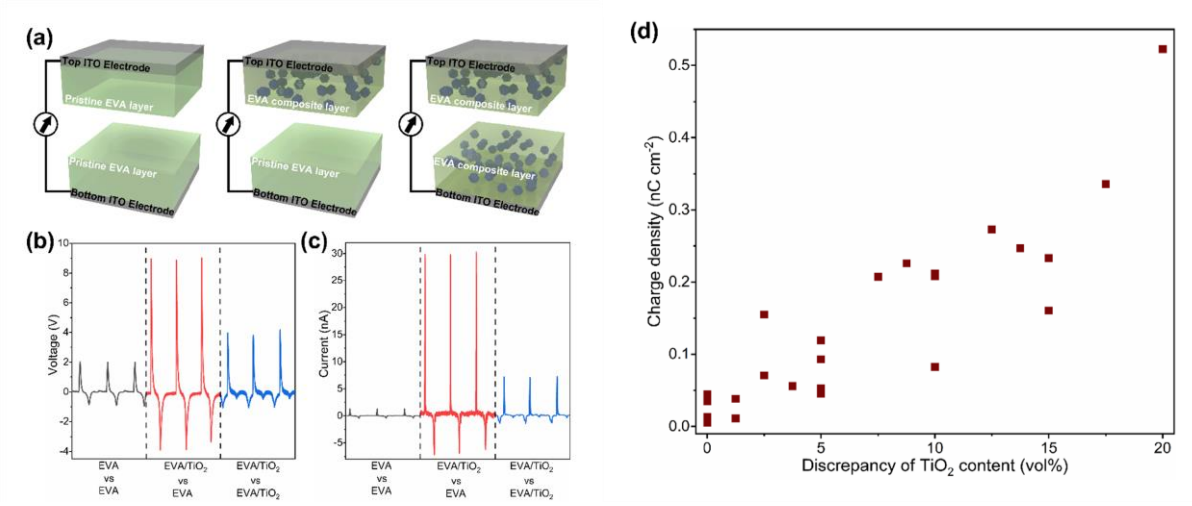

17. att. (a) Trīs veidu TEĢ ierīču shēmas, kurās izmanto tīru EVA polimēru un/vai EVA kompozītmateriālus; (b) trīs TEĢ ierīču ģenerētie V_{OC} maksimumi; (c) trīs TEĢ ierīču ģenerētie I_{SC} maksimumi; (d) palielinot starpību TiO_2 saturā EVA slāņiem, ko izmantoja TEĢ ierīcēs, iegūst paaugstinātu triboelektrisko virsmas lādiņa blīvumu.[109]

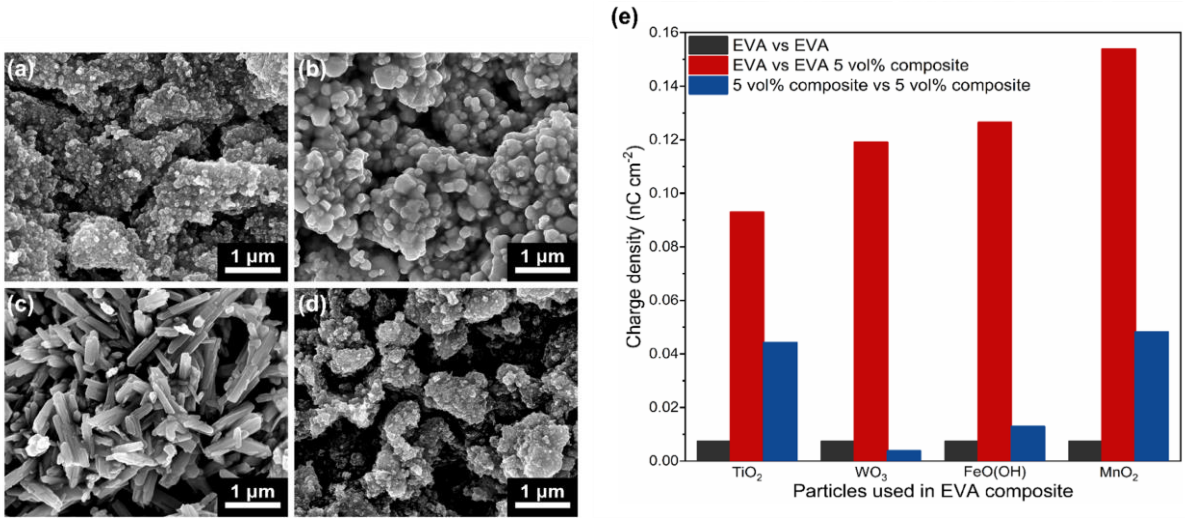

18. att. (a) TiO_2 ND SEM attēli; (b) WO_3 ND SEM attēli; (c) FeO(OH) ND SEM attēli; (d) MnO_2 ND SEM attēli; (e) trīs veidu TEĢ ierīču, kuru pamatā ir tīrs EVA polimērs un EVA kompozīti ar 5 tilp. % ND, ģenerētais virsmas lādiņa blīvums, kā pildvielas izmantojot dažādas ND.[109]

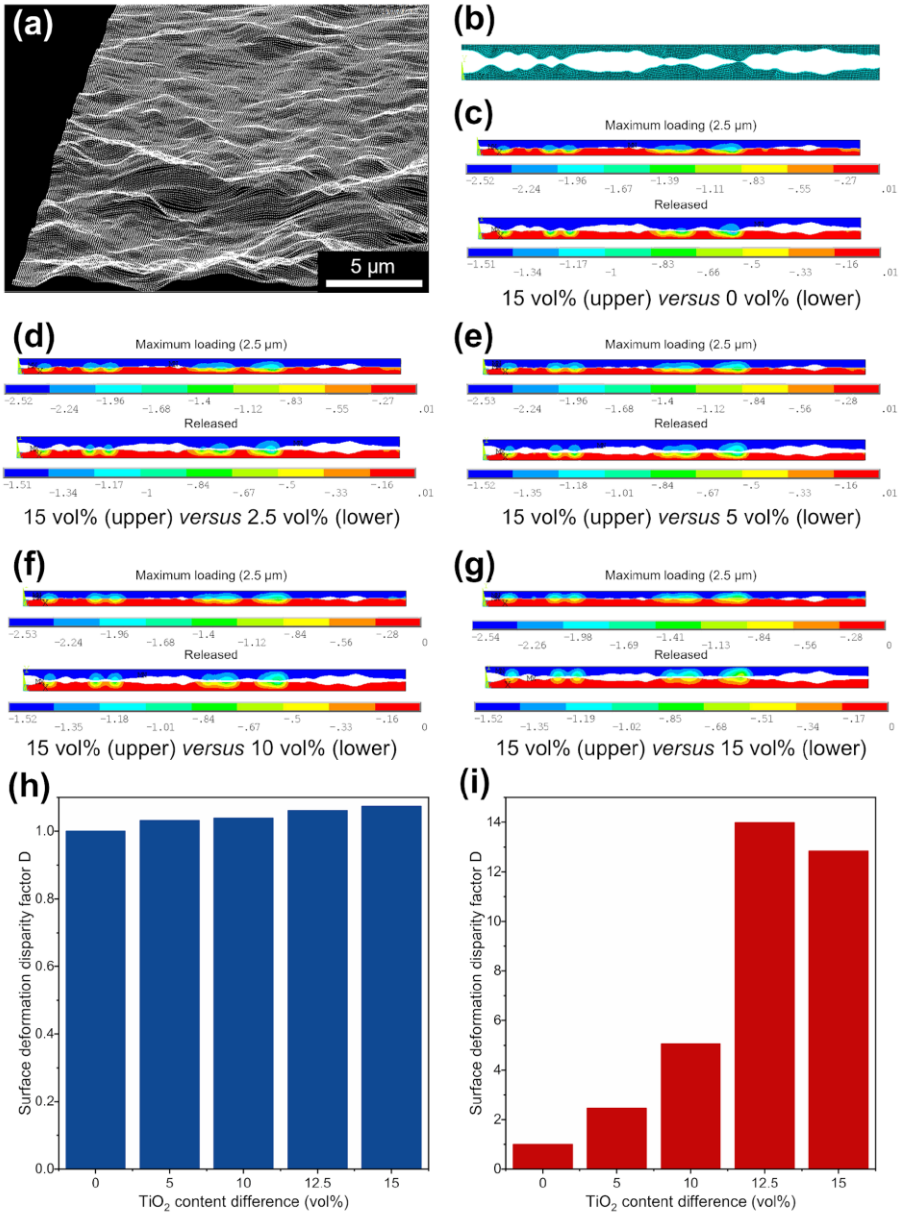

19. att. (a) AFM noteikta virsmas topoloģija kompozītmateriālam, kas satur 15 tilp. % TiO_2 ND; (b) 2D tīkla simulāciju modelis aprēķinu veikšanai; (c) 15 tilp.% (augšējais) un 0 tilp.% (apakšējais) kompozītu deformācijas simulācijas modelis; (d) 15 tilp.% un 2,5 tilp.% kompozītu deformācijas simulācijas modelis; (e) 15 tilp.% un 5 tilp.% kompozītu deformācijas simulācijas modelis; (f) 15 tilp.% un 10 tilp.% kompozītu deformācijas simulācijas modelis; (g) abi 15 tilp.% kompozītu deformācijas simulācijas modeļi; (h) *D* kā funkcija no starpības TiO_2 koncentrācijā modeļos maksimālās slogošanas laikā; (i) *D* kā funkcija no starpības TiO_2 koncentrācijā modeļos pēc atslogošanas. Krāsu joslai izmantota μm skala.[109]

5. publikācijas galvenie rezultāti un secinājumi

- Kontaktējot identiskus triboelektriskos slāņus ar vienādām daļiņām vienādā koncentrācijā, ieguva nelielus I_{SC} un V_{OC} maksimumos (17. (a) att. kreisās un labās puses paneļi). Turpretim daudz augstāki I_{SC} un V_{OC} maksimumi tika radīti, ja polimēra matricas bija vienādas, bet

abiem triboelektriskajiem slāņiem bija atšķirīga pildvielu nanodaļiņu (ND) koncentrācija (17. (a) att. vidējais panelis). Šī tendence īpaši skaidri izpaužas EVA polimēra un tā matricas kompozītiem ar TiO_2 ND pildvielu 5 tilp.% sastāvā (17. (b), (c) att.). Triboelektriskais *Q* palielinājās no 0,007 nC cm^{-2} uz 0,093 nC cm^{-2}. Šī parādība tika novērota arī citu polimēru un to matricas kompozītu, tostarp PVAc, PU un PDMS, testos ar TiO_2 ND kā pildvielu. Rezultāti parāda, ka augstākus virsmas lādiņus visu veidu polimēri vienmēr uzrāda, kad tīrs polimērs kontaktējas ar kompozītmateriāla slāni.

- Virsmas lādinš palielinājās, kad palielinājās TiO_2 ND koncentrācijas starpība kompozītos. 17. (d) attēlā parādīts, kādu triboelektrisko *Q* ģenerē TEĢ, kas sastāv no EVA/TiO_2 kompozītiem ar dažādām TiO_2 ND koncentrācijām triboelektriskajos slāņos. Rezultāti liecina, ka polimēru kompozītu triboelektrisko lādiņu nosaka kontaktēto kompozītu ND koncentrācijas starpība, nevis koncentrācijas absolūtās vērtības. Tas norāda, ka kompozīta mehāniskās īpašības, kas saistītas ar masas pārneses mehānismu, ir svarīgākas par dielektriskajām īpašībām, kas tiek saistītas ar elektronu vai jonu pārneses mehānismiem.
- Lai gan triboelektrifikācija ir atkarīga no pildvielas daļiņu koncentrācijas, tā nav atkarīga no daļiņu sastāva vai formas. EVA kompozīti, kuru pamatā ir dažādu veidu ND pildvielas (TiO_2, FeO(OH), WO_3 un MnO_2) (18. (a) – (d) att.), tika izgatavoti, lai pierādītu, ka pildvielas ķīmiskā struktūra neietekmē triboelektriskā lādiņa veidošanos. SEM attēli apstiprina, ka WO_3 ND ir salīdzinoši lielākas par TiO_2 ND, savukārt FeO(OH) ND piemīt adatveida forma, nevis lodveida kā pārējām ND. Iepriekš minēto kompozītu ūdens kontaktleņķis (KL) tika noteikts, lai novērtētu ND ietekmi uz kompozītu virsmas enerģiju. Tika noteikts, ka kompozītiem ar TiO_2, MnO_2, WO_3 un FeO(OH) pildvielām KL ir attiecīgi 96,9 ± 0,4°; 92,9 ± 1,6°; 89,2 ± 2,4° un 98,1 ± 1,0°. Kā bija paredzams, ietekme ir niecīga, kas liecina, ka pildviela galvenokārt ietekmē mehāniskās īpašības. Lai gan ģenerētā triboelektriskā *Q* absolūtās vērtības var atšķirties atkarībā no pildvielas dispersijas viendabīguma un citu sekundāro efektu dēļ, tendence visos gadījumos bija nemainīga; triboelektriskie lādiņi vienmēr bija visaugstākie starp dažāda sastāva kompozītmateriāliem (18. (e) att.). Novērotā korelācija vēlreiz apstiprina, ka elektronu pārnese nav atbildīga par polimēru triboelektrifikāciju.
- Iemesls spēcīgākai triboelektrifikācijai mehāniska kontakta laikā starp identiskām polimēru matricām ar dažādām pildvielas daļiņu koncentrācijām ir saistīts ar atšķirībām virsmas deformācijā un saistītajām atšķirībām mehāniskajās īpašībās, kā aprakstīts 4. publikācijā.[107] Lielākā daļa no ND ir iekapsulētas polimēra matricā, tādējādi neietekmējot virsmas morfoloģiju, tomēr tās ietekmē kompozītmateriāla Junga moduli. Junga modulis pieaug no 2,20 MPa kompozītam ar 0 tilp.% TiO_2 ND līdz 7,10 MPa kompozītam ar 15 tilp.% TiO_2 ND. Mehāniski kontaktējot kompozītu slāņus ar dažādu pildvielas saturu, katrā slānī rodas atšķirīga deformācija. Tas rada dažādus spriegumus uz katras no triboelektriskajām virsmām un izraisa atšķirības masas pārnesē katrai no virsmām. Toties gadījumos, ja polimēru virsmas ir pakļautas vienādām deformācijam, masas pārnese starp virsmām notiek ar vienādu varbūtību, kas ir novērojams kā neliels kopējais triboelektriskais lādiņš.
- Nevienmērīgu triboelektrisko virsmu deformāciju apstiprināja ar tīra EVA polimēra (0 tilp.%) un EVA kompozītu (TiO_2 ND pildvielu koncentrācija 2,5; 5; 10 un 15 tilp.%)

GEA simulācijām, izmantojot programmatūru *ANSYS R17.1*. 2D modeļu virsmas konfigurācija tika ņemta no atomspēku mikroskopijas (AFM) mērījumiem (19. (a), (b) att.). Kā redzams 19. (c)–(f) attēlos, viena virsma tika noteikta kā 15 tilp.% kompozīta virsma, savukārt pretējās virsmas sastāvs tika mainītas robežās 0–15 tilp.%. Makro mēroga simulācijas raksturo virsmas deformāciju mehāniskas slogošanas laikā un pēc atslogošanas. Gadījumā, kad divu deformējamu ķermeņu ar identiskām mehāniskajām īpašībām saskare izraisīja identiskas virsmas deformācijas, virsmas deformācijas atšķirība *D* bija 1 (19. (h) un (i) att.). Ja aprēķinos saskārās virsmas ar atšķirīgu TiO_2 saturu (15 tilp.% atšķirība), tad *D* maksimālās slogošanas laikā palielinājās no 1 līdz ~ 1,07 (19. (h) att.). Tomēr pēc triboelektrisko virsmu mehāniskas atslogošanas virsmas deformācijas atšķirība *D* palielinājās līdz ~ 14 (19. (i) att.). Turpretim triboelektriskās virsmas ar nelielām koncentrācijas starpībām parādīja nelielu deformācijas atšķirību. Simulācijas rezultāti liecina par tendenci, ka augstāka TiO_2 ND saturu starpība rada lielākas nevienmērības virsmu deformācijā un relaksācijā. Šie rezultāti atbilst mūsu kontaktelektrifikācijas mērījumiem un pamato mūsu secinājumu, ka nevienmērīga deformācija un tam sekojoša virsmas relaksācija ir atbildīga par masas pārneses mehānisma vadītu virsmas triboelektriskā lādiņa veidošanos.

Hibrīdais tribo-pjezo-elektriskais nanoģenerators (6. publikācija)

Hibrīdās TEĢ ierīces, kas izmanto segnetooelektriskos materiālus kā triboelektriskos kontaktēšanas materiālus, ievadā tika minētas saistībā ar vienu no pieejām, lai panāktu augstu enerģijas savākšanas veiktspēju. 6. publikācijā šī stratēģija tika lietota, lai izveidotu triboelektriskos slāņus no segnetoelektriskajiem PVDF/$BaTiO_3$ kompozītiem. Abas kompozītu kārtiņas bija identiskas un polarizētas, izmantojot elektrisko lauku, bet apgrieztos virzienos, tā, lai kontaktatdalīšanas laikā polarizācijas virziens sakristu. Tika demonstrēta nepārprotama korelācija starp PVDF/$BaTiO_3$ nanokompozītu kārtiņu pjezoelektrisko atbildes reakciju un no šīm kārtiņām izveidoto TEĢ ierīču veiktspēju. Novērojums tika skaidrots ar palielinātu elektrostatisko indukciju, ko izraisa šo kārtiņu segnetoelektriskās īpašības. Tika piedāvāts dubulta kondensatora modelis, lai attēlotu mijiedarbību starp segnetoelektriskajiem slāņiem kontaktatdalīšanas laikā un sekojošo lādiņa pārdali ārējā ķēdē. Tas ļāva sasniegt visaugstāko ziņoto TEĢ V_{OC} ar 2,7 kV.

6. publikācijas galvenais mērķis bija izpētīt segnetoelektriskā efekta ietekmi uz TEĢ ierīces veikstspēju.

Triboelektrisko mērījumu galvenie rezultāti redzami 20. un 21. attēlā.

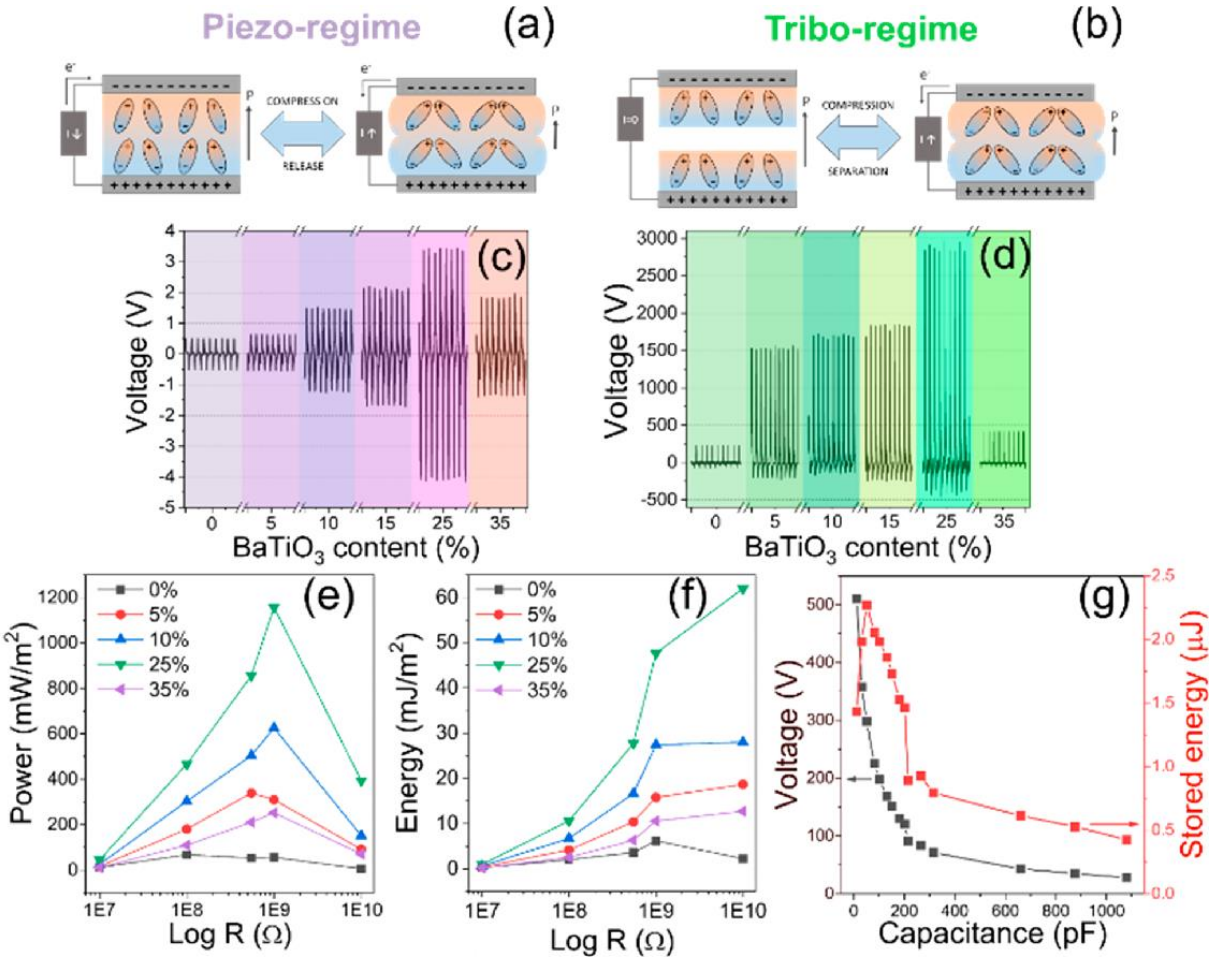

20. att. (a) Pjezo un (b) TEĢ testēšanas režīmu shematisks attēlojums. Atvērtās ķēdes spriegums, ko mēra pie 1×10^{10} Ω slodzes pretestības (c) pjezo un (d) TEĢ režīmiem. Grafiki apakšējā rindā parāda (e) jaudu un (f) enerģiju dažādām kompozīcijām, kas testētas TEĢ režīmā. Kondensatorā uzkrātā enerģija (g) tika noteikta nanokompozītam, kas uzrādīja augstāko veiktspēju (PVDF/$BaTiO_3$ 25 tilp.%).[110]

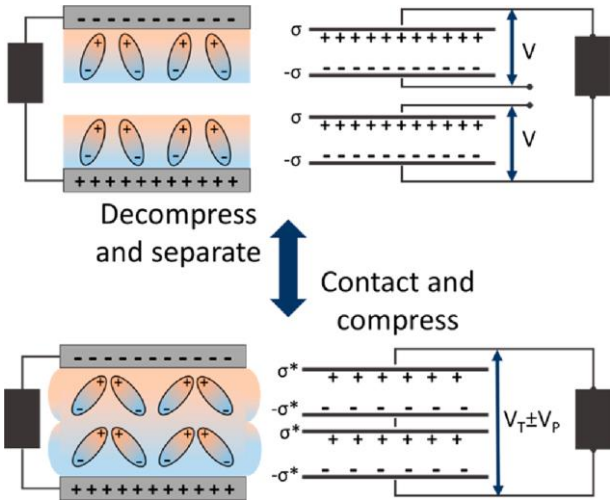

21. att. Dubultā kondensatora modelis un atbilstošās kontaktatdalīšanas stadijas. Shematiskā attēla dipoli apzīmē gan PVDF, gan $BaTiO_3$ dipolus segnetoelektriskajos slāņos.[110]

6. publikācijas galvenie rezultāti un secinājumi

- Sagatavotās segnetoelektriskās PVDF/$BaTiO_3$ kārtiņas testēja pjezoelektriskajā režīmā (20. (a) att.), kā arī tās izmantoja kā kontaktslāņus TEĢ ierīcē (20. (b) att.). Kā novērojams 20. (c) un (d) attēlos, PVDF kompozīts, kas satur 25 tilp.% $BaTiO_3$, uzrāda augstāko V_{OC} gan piezoelektriskajā, gan kontaktatdalīšanas režīmā, liecinot par korelāciju starp pjezoelektrisko signālu un atbilstošo nanokompozīta kārtiņu TEĢ ierīces darbību. TEĢ no polarizētiem, PVDF polimēra slāņiem radīja 250 V V_{OC} vērtību, ģenerators no PVDF/$BaTiO_3$ (25 tilp.%) nanokompozītiem ģenerēja 2700 V. Novērotā V_{OC} vērtība bija viena no augstākajām ziņotajām vērtībām TEĢ ierīcēm. Segnetoelektrisko nanokompozītu TEĢ ierīču uzlabotā veiktspēja, salīdzinot ar tām, ko izmanto tīru PVDF polimēru, ir saistīta ar augstāku segnetoelektrisko kontaktslāņu polarizāciju, kas izpaužas kā paaugstināts piezoelektriskais signāls.
- TEĢ ierīces, kuras pamatā ir PVDF/$BaTiO_3$ (25 tilp.%) nanokompozīts, jaudas blīvums sasniedza 1,157 W m^{-2} pie 10^9 Ω optimālās slodzes pretestības (20. (e) att.), enerģijas blīvums sasniedza 65,95 mJ m^{-2} (20. (f) att.). Tā pati TEĢ ierīce tika izmantota, lai uzlādētu mainīgu kondensatoru slēgumu. 20. (g) attēlā parādīta enerģija, kas tiek glabāta kondensatorā (un attiecīgais spriegums uzlādētā stāvoklī) katrai kondensatora vērtībai pēc kontakta starp abiem segnetoelektriskajiem slāņiem. Lielākā enerģija, kas tika uzkrāta kondensatorā pēc viena kontaktatdalīšanas soļa (2,27 μJ), tika sasniegta, kad kondensatora kapacitāte tika iestatīta uz 50 pF.
- Pjezoelektriskais signāls ļāva aprēķināt pjezoelektrisko koeficientu d_{33}, kas 25 tilp.% $BaTiO_3$ kompozītiem sasniedza 47,9 pC N^{-1}. Līdzīgu nanokompozītu vērtības ir robežās 2,7–25 pC N^{-1}.[111, 112] Lielāks d_{33} var būt saistīts ar ievērojami augstāku deformējamību paraugu augstās porainības pakāpes dēļ (ap 70 %). Porainība nodrošina deformācijas materiāla tilpumā, kas ir svarīgas piezoelektriskā lādiņa radīšanai, un veicina segnetoelektriskās β-PVDF fāzes veidošanos izgatavošanas laikā.[113] Blīvam kompozītmateriālam d_{33} tika noteikts tikai 9,11 pC N^{-1}.
- Lai izskaidrotu uzlaboto TEĢ ierīces veiktspēju un potenciāla starpības izmaiņu elektrodos, tika piedāvāts dubultā kondensatora modelis (21. att.). Attiecīgi katrs segnetoelektriskais slānis tika uzskatīts par individuālu kondensatoru ar *Q*, ko izveido polarizācijas laikā. Kad slāņi saskaras, tie izveido divu vienādu kondensatoru ķēdi virknē, abu slāņu kopējā kapacitāte samazinās, savukārt spriegums palielinās. Pēc tam saspiešana izraisa pjezoelektrisko lādiņu veidošanos, jo dipoli deformējas un slāņa kopējā polarizācija samazinās. Rezultātā samazinās *Q*, bet, ņemot vērā to, ka seko strauja saspiesto segnetoelektrisko slāņu atdalīšana, kopējā polarizācija strauji pieaug, savukārt *Q* atgriežas sākotnējā vērtībā. Atdalīšanas laikā potenciāla starpība samazinās, kas izraisa papildu inducēto lādiņu pārdali starp elektrodiem ārējā virknē.

Triboelektrisko un segnetoelektrisko lādiņu dipolu salāgošana TEĢ (7. publikācija)

6. publikācija pierādīja, ka segnetoelektrisko dipolu iestrāde kontaktējamo polimēru slāņos uzlabo TEĢ ierīču darbību, tomēr, kā minēts 4. publikācijā, kontaktatdalīšanas laikā starp abām kontaktvirsmām veidojas arī triboelektriskais dipols. Visos saistošajos pētījumos dipolu, ko veido triboelektriskie virsmas lādiņi starp atšķirīgajiem triboelektriskajiem materiāliem, un dipolu, kas atrodas abās kontaktētajās segnetoelektriskajās kārtiņās, kombinētā ietekme ir tikusi ignorēta. Tāpēc 7. publikācijā mēs nodemonstrējām, ka pienācīga uzmanība abu dipolu veidu salāgošanai var radīt četras reizes lielāku enerģijas un jaudas blīvumu, salīdzinot ar nesalāgotu dipolu izkārtojumu. Piedāvātā stratēģija un izpratne par spēcīgāku elektrostatisko indukciju kontaktējamajos slāņos ļauj attīstīt TEĢ ierīces ar ievērojami uzlabotām īpašībām.

Galvenais 7. publikācijas mērķis bija izpētīt triboelektrisko un segnetooelektrisko dipolu salāgošanas ietekmi, ja TEĢ ierīču izgatavošanai izmanto divus dažādus segnetoelektriskos polimēru kompozītus.

Triboelektrisko mērījumu galvenie rezultāti redzami 22.–25. attēlā.

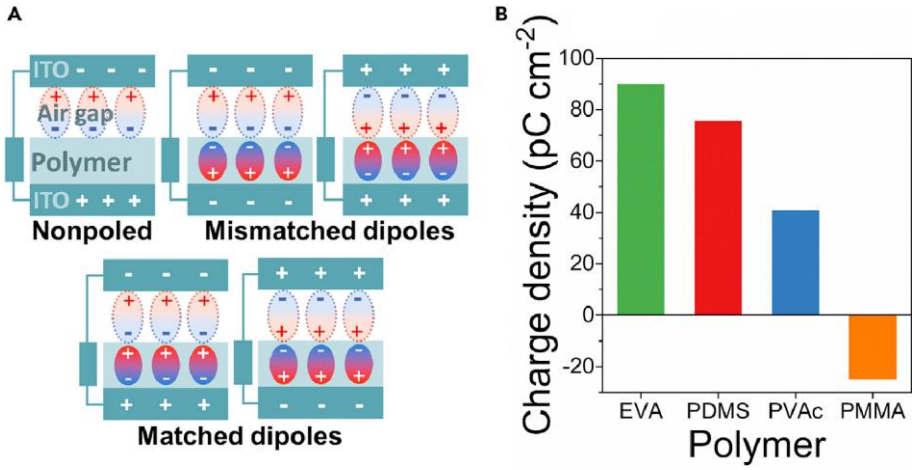

22. att. (a) Shematiskais attēlojums iespējamajām mijiedarbībām starp virsmas lādiņa dipoliem gaisa spraugā un segnetoelektriskajiem dipoliem TEĢ ierīcē; (b) aprēķinātais virsmas lādiņa blīvums polimēriem bez segnetoelektriskajām īpašībām.[114]

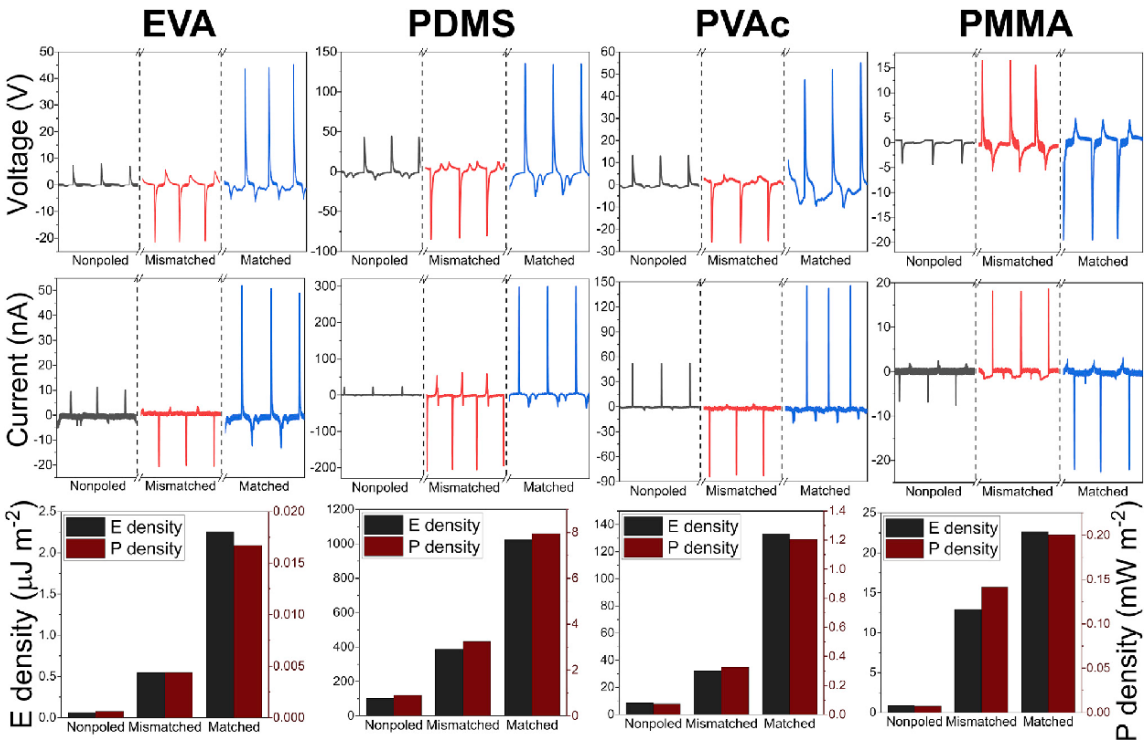

23. att. Trīs iespējamo dipolu salāgošanas konfigurāciju (nepolarizēts, nesalāgots un salāgots) salīdzinājums, parādot V_{OC}, I_{SC}, enerģijas un jaudas blīvumu katram $BaTiO_3$/polimēra kompozītam.[114]

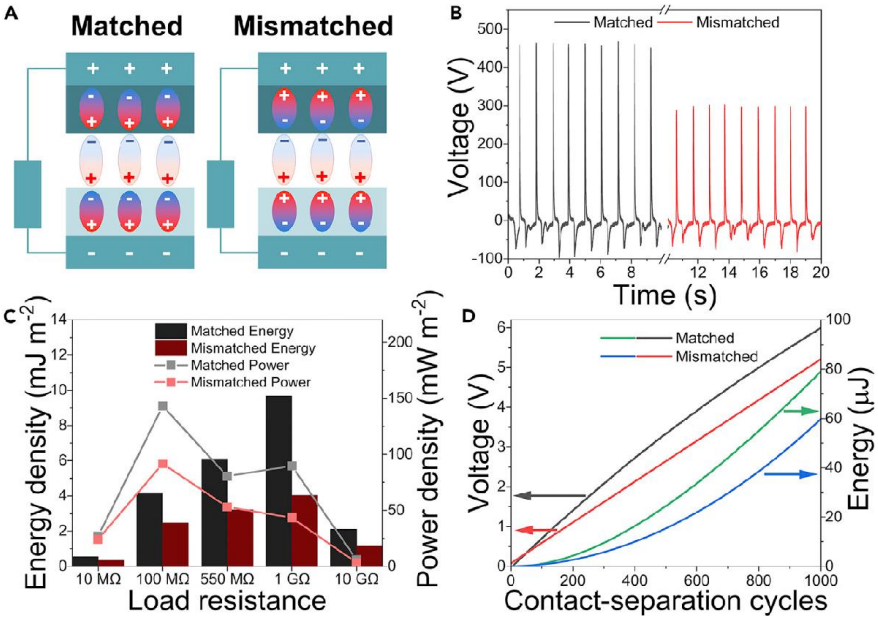

24. att. (a) Apgriezti polarizētu $BaTiO_3$/PDMS (augšējā slānī) un $BaTiO_3$/PMMA (apakšējā slānī) TEĢ ierīce, kas konstruēta tā, lai segnetoelektriskais polarizācijas virziens būtu salāgots (kreisajā pusē) un nesalāgots (labajā pusē) ar kontaktelektrifikācijas ģenerētā virsmas lādiņa dipola virzienu; (b) V_{OC} (pie 1 GΩ slodzes pretestības) salāgotai un nesalāgotai TEĢ ierīcei; (c) enerģijas un jaudas blīvumu salīdzinājums salāgotai un nesalāgotai TEĢ ierīcei viena kontaktatdalīšanas cikla laikā; (d) spriegums 4,4 μF kondensatorā uzlādes laikā no salāgotas un nesalāgotas TEĢ ierīces kopā ar attiecīgo uzkrāto enerģiju.[114]

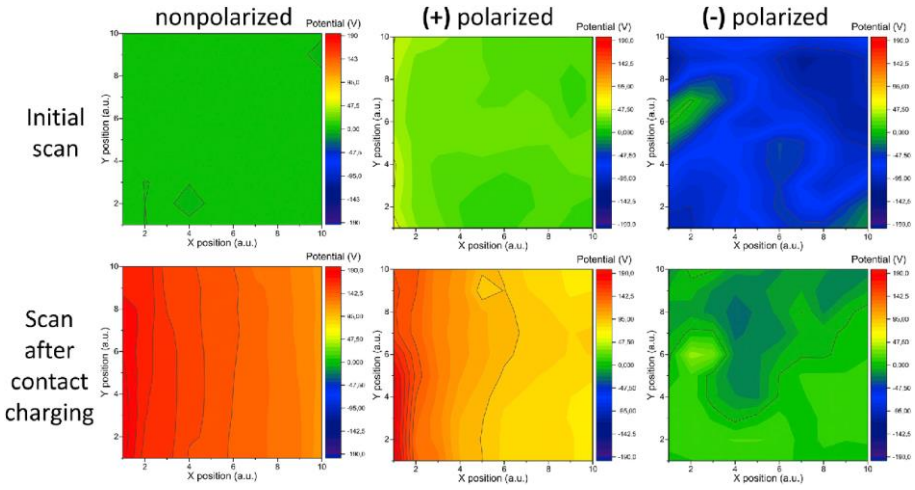

25. att. Virsmas potenciāla kartes trim $BaTiO_3$/PDMS kompozītiem (nepolarizēts, pozitīvi un negatīvi polarizēti), potenciālu mērot pirms (augšējā rinda) un pēc (apakšējā rinda) kontaktēšanas ar PMMA.[114]

7. publikācijas galvenie rezultāti un secinājumi

- Lai panāktu augstu TEĢ ierīces enerģijas savākšanas darbību, segnetoelektrisko dipolu virzienam ir jāsakrīt ar dipolu virzienu, kas veidojas starp triboelektriskajiem lādiņiem uz pretējām kontaktvirsmām, kā parādīts 22. (a) attēlā. Triboelektriskā lādiņa polaritāte, kas veidojas uz tīriem polimēriem pēc saskares ar *ITO*, tika noteikta, mērot strāvu starp elektrodu un zemi Faradeja kausa režīmā. Polimēri PDMS, PVAc un EVA uz virsmas ieguva negatīvu lādiņu, savukārt PMMA gadījumā tika novērots pozitīvs lādiņš (22. (b) att.). Polaritāte nemainījās, ja polimēros tika iejauktas nepolarizētas $BaTiO_3$ nanodaļiņas.
- Pēc polarizācijas visiem $BaTiO_3$/polimēru kompozītiem piemita pjezoelektriskās īpašības, un 2,9 pC cm^{-2}; 10,9 pC cm^{-2}; 3,7 pC cm^{-2} un 2,4 pC cm^{-2} lieli pjezoelektriskie lādiņi tika nomērīti attiecīgi $BaTiO_3$/EVA, $BaTiO_3$/PDMS, $BaTiO_3$/PVAc un $BaTiO_3$/PMMA kompozītiem.
- 23. attēls parāda I_{SC} un V_{OC} pie 1 GΩ slodzes pretestības TEĢ ierīcēm, kas veidotas, izmantojot kompozītmateriāla un *ITO* slāņus. Kompozītmateriāla slānis katrā TEĢ ierīcē tika testēts ne tikai kā nepolarizēts, bet arī pozitīvi un negatīvi polarizēts, tā, lai segnetoelektriskais dipols būtu salāgots un nesalāgots ar iepriekš noteikto triboelektrisko *Q*. Neatkarīgi no izmantotā polimēra TEĢ ierīces augstākās vērtības parādīja salāgotā stāvoklī. Kopējo dipola virzienu starp triboelektriskajiem *Q* apstiprināja arī COMSOL GEA simulācija. Eksperimenti rāda, ka augstāka veiktspēja (I_{SC}, V_{OC}, enerģijas un jaudas blīvums) TEĢ ierīcei piemīt, ja ir salāgots triboelektrisko un segnetoelektrisko dipolu virziens.
- Tālākā darba gaitā tika izgatavotas TEĢ ierīces ar divām $BaTiO_3$/polimēru kompozītu kārtiņām, ko izmantot kā kontaktēšanas slāņus. Augstākajai veiktspējai abas kārtiņas tika polarizētas pretēji,[110] savukārt polimēru matricas materiāls katrai pusei tika izvēlēts tā, lai triboelektriskā un segnetoelektriskā lādiņa dipolu momenta virzieni būtu salāgoti vai nesalāgoti. Attiecīgi TEĢ ierīce tika veidota no PMMA un PDMS, jo PMMA uzlādējas pozitīvi, PDMS – negatīvi. Ierīču shematiskais attēlojums redzams 24. (a) attēlā. Ierīces ar salāgotiem dipoliem V_{OC} sasniedza 460 V, kā redzams 24. (b) attēlā, un šīs TEĢ ierīces

enerģijas un jaudas blīvums sasniedza attiecīgi 9,7 mJ m^{-2} un 143,2 mW m^{-2} (melnie stabiņi un pelēkā līnija 24. (c) att.). Nesalāgotā TEĢ ierīce uzrādīja ievērojami mazākas vērtības – V_{OC} 300 V (sarkanā līnija 24. (b) att.) un enerģijas un jaudas blīvumu 4,0 mJ m^{-2} un 91,6 mW m^{-2} (sarkanie stabiņi un sarkanā līnija 24. (c) att.). Salīdzinājumam, TEĢ ierīce no tiem pašiem polimēriem, kuriem nav $BaTiO_3$ ND, uzrādīja 16 V V_{OC} un trīs kārtas mazāku enerģijas un jaudas blīvumu 0,012 mJ m^{-2} un 0,104 mW m^{-2}.

- Ar SKZ tika noteikts, ka nepolarizēta $BaTiO_3$/PDMS vidējais virsmas potenciāls ir 0,06 V. Pēc kontakta ar PMMA vidējais potenciāls palielinājās līdz 146,4 V (25. att.). Virsmas potenciāla skenēšana tika veikta arī gan pozitīvi, gan negatīvi polarizētiem $BaTiO_3$/PDMS paraugiem pirms un pēc kontaktēšanas ar PMMA. Pozitīvi polarizētā $BaTiO_3$/PDMS vidējā potenciāla vērtība pieauga no 24,3 V uz 107,2 V un negatīvi polarizētā $BaTiO_3$/PDMS gadījumā no –70,5 V uz –1,1 V. Visām virsmām ir tendence uzlādēties pozitīvi pēc saskares ar PMMA, par ko liecina pozitīvāks virsmas potenciāls. Ir novērojama pakāpeniska potenciāla samazināšanās virzienā no kreisās uz labo pusi, jo, virsmu skenējot šajā virzienā, triboelektriskais lādiņš samazinās laikā. Eksperimentālie rezultāti apstiprina piedāvāto mehānismu augstākai TEĢ ierīču veiktspējai, kurā ir divi elektriskā lauka avoti – triboelektriskie lādiņi un segnetoelektriskie dipoli.
- 4,4 μF kondensatora uzlādēšanai tika izmantota gan salāgota, gan nesalāgota TEĢ ierīce, kas veidota no polarizētām $BaTiO_3$/PDMS un $BaTiO_3$/PMMA kompozītu kārtiņām. Salāgotajam TEĢ pēc 1000 kontaktatdalīšanas cikliem spriegums kondensatorā palielinājās par 6,0 V, kas atbilst 79 μJ uzkrātajai enerģijai (24. (d) att.). Tikmēr TEĢ ierīce ar nesalāgotiem dipoliem kondensatorā spriegumu palielināja tikai par 5,2 V un uzkrāja 60 μJ enerģijas tādos pašos darbības apstākļos. Šeit parādīto konceptu var izmantot turpmāk, lai izveidotu TEĢ ierīces ar rekordaugstu veiktspēju, jo literatūrā ir ziņots par polimēriem ar daudz augstāku triboelektrifikāciju[98] un polimēru kompozītmateriāliem ar augstu pjezoelektrisko efektu.[14, 115, 116] Metodoloģija, kas parādīta šajā publikācijā, apvienojumā ar augstas veiktspējas segnetoelektriskajiem materiāliem varētu tuvināt TEĢ pētnieku kopienu jauniem, progresīviem atklājumiem.

SECINĀJUMI

1. Polimēri ar zemāku elastības moduli un kohēzijas enerģiju iegūst lielāku triboelektriskā lādiņa blīvumu, ja kontaktē ar cietu materiālu. Gadījumos, kad tiek kontaktēti divi polimēri, lielāks triboelektriskais lādiņš veidojas, ja polimēriem ir pēc iespējas atšķirīgāks elastības modulis un cietība. Eksperimenti liecina, ka polimēru triboelektrifikāciju nosaka to mehāniskās, nevis ķīmiskās vai dielektriskās īpašības.
2. Triboelektrifikāciju var novērot arī gadījumos, kad kontaktē ķīmiski identiskus polimērus, ja tiem ir atšķirīgas īpašības, piemēram, makromolekulārā sakārtotības pakāpe, šķērssaistīšanās pakāpe vai virsmas raupjums. Jo intensīvāka ir konkrētā parametra atšķirība starp kontaktējamiem polimēriem, jo lielāks būs triboelektriskā lādiņa blīvums.
3. Lielāka virsmas adhēzija var uzlabot materiāla pārnesi un tādējādi palielināt triboelektrisko lādiņu uz polimēra virsmas. Tomēr augsta adhēzija samazina TEĢ ierīču efektivitāti, jo ir nepieciešams lielāks mehāniskās enerģijas ieguldījums virsmu atdalīšanai.
4. Virsmu, kas kontaktatdalītas ar heteroatomu saturošiem polimēriem (piemēram, Si, F vai Cl), analīze ar *AFM* un *XPS* ļauj secināt, ka polimēru triboelektrifikācija notiek līdztekus polimēru makromolekulu fragmentu pārnesei.
5. Segnetoelektrisko materiālu izmantošana TEĢ kontaktslāņos ir efektīva metode enerģijas savākšanas veiktspējas paaugstināšanai. Nozīmīgi, ka to var papildus uzlabot, ja segnetoelektriskā dipola virzienu salāgo ar triboelektriskā dipola, kas veidojas starp kontaktēto polimēru negatīvajiem un pozitīvajiem lādiņiem, virzienu.

LITERATŪRAS SARAKSTS

(1) ONiO. What is energy harvesting? https://www.onio.com/article/what-is-energy-harvesting.html.

(2) Karami, M. A.; Inman, D. J. *Appl. Phys. Lett.* **2012**, *100*, 042901.

(3) Temp. And Humidity Sensor With A CR2032 For Over 1 Year! https://create.arduino.cc/projecthub/musskopf/temp-and-humidity-sensor-with-a-cr2032-for-over-1-year-580114.

(4) Liu, X.; Chen, T.; Qian, F.; Guo, Z.; Lin, F. X.; Wang, X.; Chen, K. Characterizing Smartwatch Usage in the Wild. *MobiSys 2017* - Proceedings of the 15th Annual International Conference on Mobile Systems, Applications, and Services, 2017, 385.

(5) Culman, C.; Aminikhanghahi, S.; Cook, D. J. *Sensors* **2020**, *20*, 310.

(6) Gray, C. Energy Consumption of Internet of Things Applications and Services. PhD Thesis, University of Melbourne, Melbourne, 2018.

(7) Smart home spot. My Xiaomi Bluetooth Temperature Humidity Sensor Review https://medium.com/@smarthomespot/my-xiaomi-bluetooth-temperature-humidity-sensor-review-d37b32ab1d0.

(8) Curie, J.; Curie, P. *Bull. Minéralogie* **1880**, 90.

(9) Bhalla, A. S.; Guo, R.; Roy, R. *Mater. Res. Innov.* **2000**, *4*, 3.

(10) Park, D. Y.; Joe, D. J.; Kim, D. H.; Park, H.; Han, J. H.; Jeong, C. K.; Park, H.; Park, J. G.; Joung, B.; Lee, K. J. *Adv. Mater.* **2017**, *29*, 1702308.

(11) Soin, N.; Shah, T. H.; Anand, S. C.; Geng, J.; Pornwannachai, W.; Mandal, P.; Reid, D.; Sharma, S.; Hadimani, R. L.; Bayramol, D. V.; Siores, E. *Energy Environ. Sci.* **2014**, *7*, 1670.

(12) Lund, A.; Rundqvist, K.; Nilsson, E.; Yu, L.; Hagström, B.; Müller, C. *npj Flex. Electron.* **2018**, *2*, 9.

(13) Singh, D.; Choudhary, A.; Garg, A. *ACS Appl. Mater. Interfaces* **2018**, *10*, 2793.

(14) Jeong, C. K.; Baek, C.; Kingon, A. I.; Park, K. Il; Kim, S. H. *Small* **2018**, *14*, 1.

(15) Bodkhe, S.; Turcot, G.; Gosselin, F. P.; Therriault, D. *ACS Appl. Mater. Interfaces* **2017**, *9*, 20833.

(16) Suzuki, Y.; Miki, D.; Edamoto, M.; Honzumi, M. *J. Micromechanics Microengineering* **2010**, *20*, 104002.

(17) Mitcheson, P. D.; Miao, P.; Stark, B. H.; Yeatman, E. M.; Holmes, A. S.; Green, T. C. *Sensors Actuators, A Phys.* **2004**, *115*, 523.

(18) Chiu, Y.; Kuo, C.-T.; Chu, Y.-S. *Symp. Des. Test Integr. Packag. MEMS/MOEMS* **2007**.

(19) Moretti, G.; Rosset, S.; Vertechy, R.; Anderson, I.; Fontana, M. *Adv. Intell. Syst.* **2020**, *2*, 2000125.

(20) Opris, D. M. *Adv. Mater.* **2018**, *30*, 1.

(21) Hillenbrand, J.; Sessler, G. M. *IEEE Trans. Dielectr. Electr. Insul.* **2004**, *11*, 72.

(22) Fan, F.-R.; Tian, Z.-Q.; Lin Wang, Z. *Nano Energy* **2012**, *1*, 328.

(23) Wang, S.; Lin, L.; Wang, Z. L. *Nano Lett.* **2012**, *12*, 6339.

(24) Wang, S.; Lin, L.; Xie, Y.; Jing, Q.; Niu, S.; Wang, Z. L. *Nano Lett.* **2013**, *13*, 2226.

(25) Lin, Z.; Zhang, B.; Zou, H.; Wu, Z.; Guo, H.; Zhang, Y.; Yang, J.; Wang, Z. L. *Nano Energy* **2020**, *68*, 104378.
(26) Zheng, Q.; Zhang, H.; Shi, B.; Xue, X.; Liu, Z.; Jin, Y.; Ma, Y.; Zou, Y.; Wang, X.; An, Z.; Tang, W.; Zhang, W.; Yang, F.; Liu, Y.; Lang, X.; Xu, Z.; Li, Z.; Wang, Z. L. *ACS Nano* **2016**, *10*, 6510.
(27) Zheng, Q.; Shi, B.; Fan, F.; Wang, X.; Yan, L.; Yuan, W. **2014**, 5851.
(28) Ma, Y.; Zheng, Q.; Liu, Y.; Shi, B.; Xue, X.; Ji, W.; Liu, Z.; Jin, Y.; Zou, Y.; An, Z.; Zhang, W.; Wang, X.; Jiang, W.; Xu, Z.; Wang, Z. L.; Li, Z.; Zhang, H. *Nano Lett*. **2016**, *16*, 6042.
(29) Zheng, Q.; Zou, Y.; Zhang, Y.; Liu, Z.; Shi, B.; Wang, X.; Jin, Y.; Ouyang, H.; Li, Z.; Wang, Z. L. *Sci. Adv*. **2016**, 1–10.
(30) Tang, W.; Tian, J.; Zheng, Q.; Yan, L.; Wang, J.; Li, Z.; Wang, Z. L. *ACS Nano* **2015**, *9*, 7867.
(31) Kim, M.; Park, D.; Alam, M. M.; Lee, S.; Park, P.; Nah, J. *ACS Nano* **2019**, *13*, *4640.*
(32) Fang, C.; Tong, T.; Bu, T.; Cao, Y.; Xu, S.; Qi, Y.; Zhang, C. *Adv. Intell. Syst*. **2020**, *2*, 1900129.
(33) Pham, R.; Virnelson, R. C.; Sankaran, R. M.; Lacks, D. J. *J. Electrostat*. **2011**, *69*, 456.
(34) Dzhardimalieva, G. I.; Yadav, B. C.; Lifintseva, T. V.; Uflyand, I. E. *Eur. Polym. J*. **2021**, *142*, 110163.
(35) Zhang, X.; Han, M.; Wang, R.; Meng, B.; Zhu, F.; Sun, X.; Hu, W.; Wang, W.; Li, Z. *Nano Energy* **2014**, *4*, 123.
(36) Li, J.; Shepelin, N. A.; Sherrell, P. C.; Ellis, A. V. *Chem. Mater*. **2021**, *33*, 4304.
(37) Kil, B.; Woong, J.; Soo, H.; Hoon, J. *Nano Energy* 2015, 15, 523.
(38) Song, G.; Kim, Y.; Yu, S.; Kim, M. O.; Park, S. H.; Cho, S. M.; Velusamy, D. B.; Cho, S. H.; Kim, K. L.; Kim, J.; Kim, E.; Park, C. *Chem. Mater.* **2015**, *27*, 4749.
(39) Chu, H.; Jang, H.; Lee, Y.; Chae, Y.; Ahn, J. *Nano Energy* **2016**, *27*, 298.
(40) Newman, B. A.; Chen, P.; Pae, K. D.; Scheinbeim, J. I. *J. Appl. Phys.* **1980**, *51*, 5161.
(41) Haller, C. B.; Knobbe, A. J.; Crum, G. W. Tribo-Electric Powder Spray Gun. EP0592137A1, 1994.
(42) Williams, M. W. *Am. Scientist* **2012**, *100*, 316.
(43) Ohsawa, A. *J. Electrostat*. **2017**, *88*, 171.
(44) Faraday, M. *Mag. J. Sci*. **1845**, *26*, 16.
(45) Baytekin, H. T.; Baytekin, B.; Hermans, T. M.; Kowalczyk, B.; Grzybowski, B. A. *Science* **2013**, *341*, 1368.
(46) Tamminen, P.; Ukkonen, L.; Sydänheimo, L. *J. Electrostat*. **2016**, *79*, 38.
(47) Salama, F.; Sowinski, A.; Atieh, K.; Mehrani, P. *J. Electrostat*. **2013**, *71*, 21.
(48) Pingali, K. C.; Hammond, S. V.; Muzzio, F. J.; Shinbrot, T. *Int. J. Pharm*. **2009**, *369*, 2.
(49) Pu, Y.; Mazumder, M.; Cooney, C. *J. Pharm. Sci*. **2009**, *98*, 2412.
(50) Fotovat, F.; Bi, X. T.; Grace, J. R. *Chem. Eng. Sci*. **2017**, *173*, 303.
(51) Mehrani, P.; Murtomaa, M.; Lacks, D. J. *J. Electrostat*. **2017**, *87*, 64.
(52) Burgo, T. A. L.; Silva, C. A.; Balestrin, L. B. S.; Galembeck, F. *Sci. Rep*. **2013**, *3*, 1.

(53) Sayfidinov, K.; Cezan, S. D.; Baytekin, B.; Baytekin, H. T. *Sci. Adv.* **2018**, *4*, 1. https://doi.org/10.1126/sciadv.aau3808.
(54) Chen, J.; Wang, Z. L. *Joule* **2017**, *1*, 480.
(55) Sherrell, P. C.; Sutka, A.; Shepelin, N. A.; Lapcinskis, L.; Verners, O.; Germane, L.; Timusk, M.; Fenati, R. A.; Malnieks, K.; Ellis, A. V. *ACS Appl. Mater. Interfaces* **2021**. *13*, 44935.
(56) Gooding, D. M.; Kaufman, G. K. Tribocharging and the Triboelectric Series. Encyclopedia of Inorganic and Bioinorganic Chemistry, Wiley, 2019.
(57) Diaz, A. F.; Felix-Navarro, R. M. *J. Electrostat*. **2004**, *62*, 277.
(58) Henniker, J. *Nature* **1962**, *196*, 474.
(59) Xu, C.; Zhang, B.; Wang, A. C.; Zou, H.; Liu, G.; Ding, W.; Wu, C.; Ma, M.; Feng, P.; Lin, Z.; Wang, Z. L. *ACS Nano* **2019**, *13*, 2034.
(60) Wen, X.; Su, Y.; Yang, Y.; Zhang, H.; Wang, Z. L. *Nano Energy* **2014**, *4*, 150.
(61) Lu, C. X.; Han, C. B.; Gu, G. Q.; Chen, J.; Yang, Z. W.; Jiang, T.; He, C.; Wang, Z. L. *Adv. Eng. Mater*. **2017**, *19*, 1700275.
(62) Wang, J.; Wu, C.; Dai, Y.; Zhao, Z.; Wang, A.; Zhang, T.; Wang, Z. L. *Nat. Commun*. **2017**, *8*, 1.
(63) Vasandani, P.; Mao, Z. H.; Jia, W.; Sun, M. *J. Electrostat*. **2017**, *90*, 147.
(64) Pandey, R. K.; Kakehashi, H.; Nakanishi, H.; Soh, S. *J. Phys. Chem. C* **2018**, *122*, 16154.
(65) Hamdi, M.; Saleh, M. N.; Poulis, J. A. *J. Adhes. Sci. Technol*. **2020**, *34*, 1853.
(66) Harper, W. R. Contact and Frictional Electrification, Oxford, Clarendon Press, 1967.
(67) McCarty, L. S.; Whitesides, G. M. *Angew. Chem. Int. Ed*. **2008**, *47*, 2188.
(68) Lowell, J.; Rose-Innes, A. C. *Adv. Phys*. **1980**, *29*, 947.
(69) Waitukaitis, S. R.; Lee, V.; Pierson, J. M.; Forman, S. L.; Jaeger, H. M. *Phys. Rev. Lett*. **2014**, *112*, 1.
(70) Lin, S.; Shao, T. *Phys. Chem. Chem. Phys*. **2017**, *19*, 29418.
(71) Shen, X.; Wang, A. E.; Sankaran, R. M.; Lacks, D. J. *J. Electrostat*. **2016**, *82*, 11.
(72) Zhang, Y.; Shao, T. *J. Phys. D. Appl. Phys*. **2013**, *46*, 235304.
(73) Xu, C.; Zi, Y.; Wang, A. C.; Zou, H.; Dai, Y.; He, X.; Wang, P.; Wang, Y. C.; Feng, P.; Li, D.; Wang, Z. L. *Adv. Mater*. **2018**, *30*, 1.
(74) Burgo, T. A. L.; Ducati, T. R. D.; Francisco, K. R.; Clinckspoor, K. J.; Galembeck, F.; Galembeck, S. E. *Langmuir* **2012**, *28*, 7407.
(75) Baytekin, H. T.; Baytekin, B.; Incorvati, J. T.; Grzybowski, B. A. *Angew. Chem. Int. Ed*. **2012**, *51*, 4843.
(76) Baytekin, H. T.; Patashinski, A. Z.; Branicki, M.; Baytekin, B.; Soh, S.; Grzybowski, B. A. *Science* **2011**, *333*, 308.
(77) Diaz, A. F. *J. Adhes.* **1998**, *67*, 111.
(78) Diaz, A. F.; Wollmann, D.; Dreblow, D. *Chem. Mater.* **1991**, *3*, 997.
(79) Medley, J. A. *Nature* **1953**, *171*, 1077.
(80) Sumner, A. L.; Menke, E. J.; Dubowski, Y.; Newberg, J. T.; Penner, R. M.; Hemminger, J. C.; Wingen, L. M.; Finlayson-pitts, B. J. *Phys. Chem. Chem. Phys.* **2004**, *6*, 604.
(81) Kuehn, N.; Jacobasch, H.-J.; Lunkenheimer, K. *Acta Polym*. **1986**, *37*, 394.

(82) Kirby, B. J.; Hasselbrink Jr., E. F. *Electrophoresis* **2004**, *25*, 203.
(83) Baytekin, H. T.; Baytekin, B.; Soh, S.; Grzybowski, B. A. *Angew. Chem. Int. Ed.* **2011**, *50*, 6766.
(84) Fabish, T. J.; Saltsburg, H. M.; Hair, M. L. *J. Appl. Phys*. **1976**, *47*, 940.
(85) Lowell, J. *J. Phys. D. Appl. Phys.* **1984**, *17*, 1859.
(86) Sow, M.; Widenor, R.; Kumar, A.; Lee, S. W.; Lacks, D. J.; Sankaran, R. M. *Angew. Chem. Int. Ed.* **2012**, *51*, 2695.
(87) Li, J.; Nagamani, C.; Moore, J. S. *Acc. Chem. Res*. **2015**, *48*, 2181.
(88) Beyer, M. K.; Clausen-Schaumann, H. *Chem. Rev*. **2005**, *105*, 2921.
(89) Giannetti, E. *J. Fluor. Chem*. **2005**, *126*, 623.
(90) Kalniņš, M. Physical Chemistry of Polymers [in Latvian]; Zvaigzne: Riga, 1988.
(91) Maeda, N.; Chen, N.; Tirrell, M.; Israelachvili, J. N. *Science* **2002**, *297*, 379.
(92) Beraldo da Silveira Balestrin, L.; Del Duque, D.; Soares da Silva, D.; Galembeck, F. **2014**, *170*, 369.
(93) Mazur, T.; Grzybowski, B. A. *Chem. Sci*. **2017**, *8*, 2025.
(94) Šutka, A.; Malnieks, K.; Lapčinskis, L.; Kaufelde, P.; Linarts, A.; Berziņa, A.; Zabels, R.; Jurķans, V.; Gorņevs, I.; Blums, J.; Knite, M. *Energy Environ. Sci.* **2019**, *12*, 2417.
(95) Lee, C. J. *Polym. Eng. Sci*. **1987**, *27*, 1015.
(96) Lamberti, A.; Di Donato, M.; Chiappone, A.; Giorgis, F.; Canavese, G. *Smart Mater. Struct.* **2014**, *23*, 105001.
(97) Yang, J.; Webb, A. R.; Ameer, G. A. *Adv. Mater*. **2004**, *16*, 511.
(98) Lapčinskis, L.; Mālnieks, K.; Blūms, J.; Knite, M.; Oras, S.; Käämbre, T.; Vlassov, S.; Antsov, M.; Timusk, M.; Šutka, A. *Macromol. Mater. Eng*. **2020**, *305*, 1.
(99) Mathúna, C. Ó.; O'Donnell, T.; Martinez-Catala, R. V.; Rohan, J.; O'Flynn, B. *Talanta* **2008**, *75*, 613.
(100) Chun, J.; Ye, B. U.; Lee, J. W.; Choi, D.; Kang, C. Y.; Kim, S. W.; Wang, Z. L.; Baik, J. M. *Nat. Commun*. **2016**, *7*, 1.
(101) He, S.; Yu, Z.; Zhou, H.; Huang, Z.; Zhang, Y.; Li, Y.; Li, J.; Wang, Y.; Li, D. *Nano Energy* **2018**, *52*, 134.
(102) Qiao, H.; Zhang, Y.; Huang, Z.; Wang, Y.; Li, D.; Zhou, H. *Nano Energy* **2018**, *50*, 126.
(103) Xu, G.; Li, X.; Xia, X.; Fu, J.; Ding, W.; Zi, Y. *Nano Energy* **2019**, *59*, 154.
(104) Yang, U. J.; Lee, J. W.; Lee, J. P.; Baik, J. M. *Nano Energy* **2019**, *57*, 293.
(105) Xie, Y.; Wang, S.; Niu, S.; Lin, L.; Jing, Q.; Yang, J.; Wu, Z.; Wang, Z. L. *Adv. Mater*. **2014**, *26*, 6599.
(106) Šutka, A.; Linarts, A.; Malnieks, K.; Stiprais, K.; Lapčinskis, L. *Mater. Horizons* **2020**, *7*, 520.
(107) Šutka, A.; Mālnieks, K.; Lapčinskis, L.; Timusk, M.; Kalniņš, K.; Kovaļovs, A.; Bitenieks, J.; Knite, M.; Stevens, D.; Grunlan, J. *Phys. Chem. Chem. Phys.* **2020**, *22*, 13299.
(108) Yi, F.; Lin, L.; Niu, S.; Yang, P. K.; Wang, Z.; Chen, J.; Zhou, Y.; Zi, Y.; Wang, J.; Liao, Q.; Zhang, Y.; Wang, Z. L. *Adv. Funct. Mater*. **2015**, *25*, 3688.

(109) Lapčinskis, L.; Linarts, A.; Mālnieks, K.; Kim, H.; Rubenis, K.; Pudzs, K.; Smits, K.; Kovaļovs, A.; Kalniņš, K.; Tamm, A.; Jeong, C. K.; Šutka, A. *J. Mater. Chem. A* **2021**, *9*, 8984.
(110) Lapčinskis, L.; Mālnieks, K.; Linarts, A.; Blūms, J.; Šmits, K.; Järvekülg, M.; Knite, M.; Šutka, A. *ACS Appl. Energy Mater*. **2019**, *2*, 4027.
(111) Li, R.; Zhao, Z.; Chen, Z.; Pei, J. *Mater. Express* **2017**, *7*, 536.
(112) Olszowy, M. *Proc. SPIE* **1997**, 3181.
(113) Chang, C.; Tran, V. H.; Wang, J.; Fuh, Y.-K.; Lin, L. *Nano Lett*. **2010**, *10*, 726.
(114) Šutka, A.; Mālnieks, K.; Lapčinskis, L.; Timusk, M.; Pudzs, K.; Rutkis, M. *iScience* **2020**, *23*, 101011.
(115) Zhang, Y.; Sun, H.; Jeong, C. K. *ACS Appl. Mater. Interfaces* **2018**, *10*, 35539.
(116) Han, J. H.; Park, K.-I.; Jeong, C. K. *Sensors* **2019**, *19*, 1444.

DOCTORAL THESIS PROPOSED TO RIGA TECHNICAL UNIVERSITY FOR THE PROMOTION TO THE SCIENTIFIC DEGREE OF DOCTOR OF SCIENCE

To be granted the scientific degree of Doctor of Science (Ph. D.), the present Doctoral Thesis has been submitted for the defence at the open meeting of RTU Promotion Council on May 19, 2022 at 15.00 at the Faculty of Materials Science and Applied Chemistry of Riga Technical University, 3 Paula Valdena Street, Room 272.

OFFICIAL REVIEWERS

Professor Dr. sc. ing. Remo Merijs-Meri
Riga Technical University

Senior Researcher Dr. phys. Raimonds Meija
University of Latvia, Latvia

Professor Dr. Amir Fahmi
Rhine-Waal University of Applied Sciences, Germany

DECLARATION OF ACADEMIC INTEGRITY

I hereby declare that the Doctoral Thesis submitted for the review to Riga Technical University for the promotion to the scientific degree of Doctor of Science (Ph. D.) is my own. I confirm that this Doctoral Thesis had not been submitted to any other university for the promotion to a scientific degree.

Linards Lapčinskis ……. (signature)
Date: ……

The Doctoral Thesis has been written as collection of articles. It consists of a summary in Latvian and English and 7 SCI publications. The publications have been written in English; the total volume is 132 pages, including electronically available supplementary information. The summary contains 25 figures and 2 tables; the total number of pages is 50. The Bibliography contains 116 titles.

TABLE OF CONTENTS

AUTHOR'S CONTRIBUTION

The papers that form the basis of this Thesis are the result of collective work with important input and contribution from all of the co-authors with complementary expertise in different fields. The author's contribution to the papers is described in Table 1.

Table 1

Author's Contribution to Preparation of Each Paper Included in the Thesis

Paper I	Polymer contact film preparation by spin-coating and hot-pressing. Measurements of polymer triboelectric properties. Measurements of polydimethylsiloxane (PDMS) hardness and calculation of crosslinking degree. Visualization of data. Contribution percentage – 50 %.
Paper II	Polymer film preparation using spin-coating method and testing of triboelectric properties. Visualization of data. Calculations of triboelectric generator (TEG) efficiency and contribution in writing of the manuscript. Contribution percentage – 75 %.
Paper III	Sample preparation and testing of triboelectric properties. The long-term stability measurements of triboelectric effect and charge durability at elevated temperatures. Contribution percentage – 50 %.
Paper IV	Sample preparation and testing of triboelectric properties. Analysis of Scanning Kelvin probe (SKP) measurements. Contribution to writing of the manuscript and data visualization. Contribution percentage – 60 %.
Paper V	Sample preparation using hot pressing approach. Investigation of triboelectric properties. Analysis of Scanning Kelvin probe (SKP) measurements. Visualization of data. Writing of the original draft. Contribution percentage – 80 %.
Paper VI	Polymer nanocomposite preparation and polarization. Measurements of triboelectric and piezoelectric properties. Contribution to writing of the manuscript. Contribution percentage – 75 %.
Paper VII	Polymer nanocomposite preparation and polarization. Measurements of triboelectric and piezoelectric properties. Analysis of Scanning Kelvin probe (SKP) measurements. Contribution to writing of the manuscript. Contribution percentage – 70 %.

ABBREVIATIONS

A	contact area
AFM	atomic force microscopy
CA	contact angle
CED	cohesive energy density
Cel. Tr.	cellulose triacetate
d_{33}	piezoelectric coefficient
D	surface length change disparity factor
DMF	dimethylformamide
DSC	differential scanning calorimetry
EPDM	ethylene propylene diene monomer rubber
EOC	ethylene-octene copolymer
EVA	ethylene-vinyl acetate copolymer
FEA	finite element analysis
HDPE	high density polyethylene
IoT	Internet of Things
I_{SC}	short-circuit current
ITO	Iidium-tin oxide
KFM	Kelvin force microscopy
LDPE	low density polyethylene
M_C	molecular weight between crosslinks
NP	nanoparticles
PA 66	polyamide 6,6
PC	polycarbonate
PDMS	polydimethylsiloxane
PET	polyethylene terephthalate
PHC	poly(hexanediol–co-citric acid)
P_i	instantaneous power density
PI	polyimide
PMMA	polymethyl methacrylate
PP	polypropylene
PS	polystyrene
PTFE	polytetrafluoroethylene
PU	polyurethane
PVAc	polyvinyl acetate
PVC	polyvinyl chloride
PVDF	polyvinylidene fluoride
Q	charge density
R	load resistance
RMS	root mean square
SEBS	styrene-ethylene-butylene-styrene block copolymer

SEM	scanning electron microscopy
SKP	scanning Kelvin probe
TEG	tiboelectric generator
TEM	transmission electron microscopy
TENG	triboelectric nanogenerator
T_g	glass transition temperature
UHMWPE	ultra-high molecular weight polyethylene
V_{OC}	open-circuit voltage
XPS	X-ray photoelectron spectroscopy
Δ_f	surface length change
Φ	work function

GENERAL OVERWIEV OF THE THESIS

Introduction

Mechanical energy harvesting

Energy harvesting means the conversion of ambient energy into electrical energy. Generally, harvesting is regarded as conversion of small amounts of energy to autonomously power low-energy devices (μW–mW).[1] Harvesting of mechanical energy for powering of such devices is essential to their wider accessibility and allows to lower the impact of devices on environment. Accordingly, energy harvesting is useful when the harvested energy matches the necessary energy and when it provides a benefit otherwise not achievable by batteries or grid electricity, e.g., due to tedious battery replacement and costly connection to grid. Figure 1 lists energy consumption of some electrical devices;[2-7] the energy harvesting might be useful for devices with power consumption below 30–40 mW.

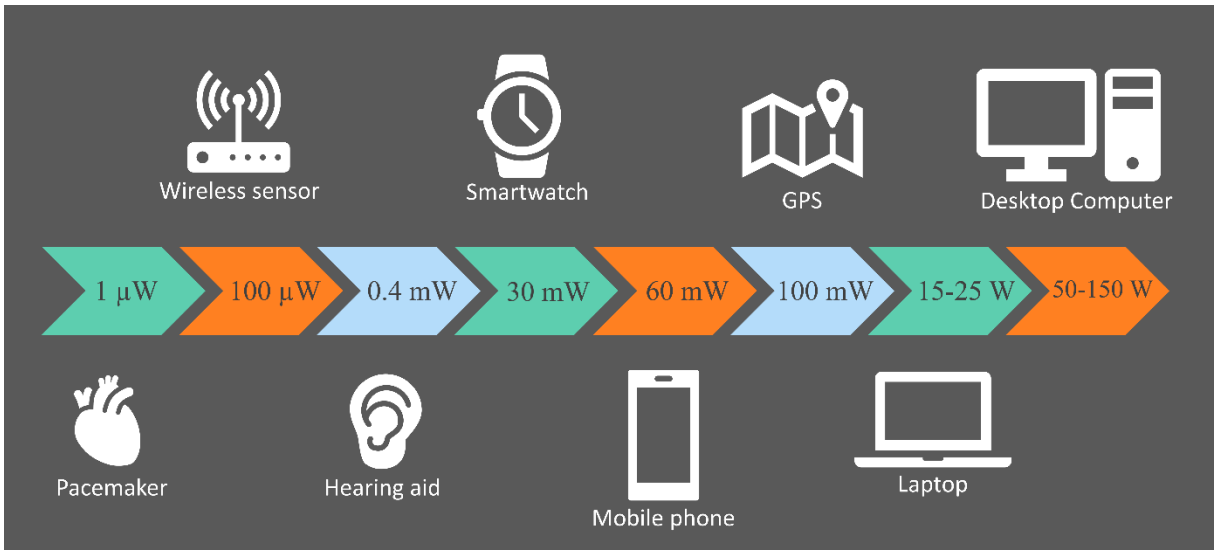

Fig. 1. Common electrical devices and their approximate power consumption.

Mechanical energy is abundantly accessible from sources like wind, water waves, vibrations and human motions. Vibrations provide plenty of energy, however, the harvested energy is often negligible in comparison to vibration energy. Despite the relatively low efficiency, recently vibration energy harvesting has seen a rise in popularity, since the size and energy consumption of electric devices reduces. Microdevices, for example, sensors, detectors and wireless transmitters can be powered by TEG, therefore replacing batteries or avoiding the need for connection of permanent power source. Human motions can be used as a source of mechanical energy by incorporating energy harvesters in clothes, shoes and other wearables (bracelets etc.) or creating infrastructure that incorporate energy harvesters. Wearable energy harvesters are on the rise due to popularity of portable electronics; however, harvester should not impair the wearing comfortability, therefore, design is a crucial aspect. A variety of

technological solutions (Table 2) are employed to harvest the aforementioned sources of mechanical energy.

Table 2

Summary of Mechanical Energy Harvesting Technologies, Employed Materials, and Range of Power Density that can be Harvested and Working Principles

Technology	Materials	Power	Working principle
Electro-magnetic generator	Conductive wire coil and magnet	1–1000 $\mu W\ cm^{-3}$	Mechanical forces create a relative motion between parts, and potential difference is induced between both ends of the coil.
Piezoelectric generators	Dielectrics with intrinsic dipole moment: crystals, ceramics, polymers and composites[8-15]	10–1000 $\mu W\ cm^{-3}$	The density of dipoles in the volume manifests as polarization density on the surface of material. Polarization induces opposite sign equal charge in the electrodes. Mechanical forces create a strain that changes the magnitude of the dipole moment and thus the polarization density. Changes result in charge redistribution providing an electron flow between electrodes connected by outer circuit.
Capacitive generators	Elastic dielectric with moveable electrodes[16-20]	0.01–100 $mW\ cm^{-3}$	Generators require a voltage source to provide the initial charge on electrodes. Mechanical force changes the distance between electrodes (or changes electrode area) so the energy stored in the capacitor increases and can be discharged.
Ferroelectret materials	Charged polymer foams with electrodes[21]	0.001–1 $mW\ cm^{-2}$	High voltage electric field charges pore walls with opposite polarities to create internal polarization. Mechanical force causes changes in polarization and charge redistribution between the electrodes connected by outer circuit.
Triboelectric generator	Electrodes covered with polymer insulator[22]	0.001–50 $mW\ cm^{-2}$	Electrodes are coated with polymer layers that are mutually contacted. Charge forms on the polymer surface after contact separation and charge is induced in the underlying electrodes. Electrodes are connected by outer circuit, and upon movement electrons flow to balance the potential difference created by induced charges.

Triboelectric generators (TEGs) have emerged as promising kinetic energy harvesters among the proposed technologies. They were first coined in 2012 by Professor Zhong Lin Wang

to describe energy harvesting devices for conversion of friction generated static charge into electrical energy through electrostatic induction.[22] More frequently the term "triboelectric nanogenerators" (TENG) is used, to imply the necessity for surface nanostructuring that enhances the performance and to point out that functionality of generator is provided by processes at nanoscale. Analysis of documents associated with "triboelectric nanogenerators" indexed in the SCOPUS database reveal that number of documents steadily increases each year, in 2021 reaching 865 (Fig. 2).

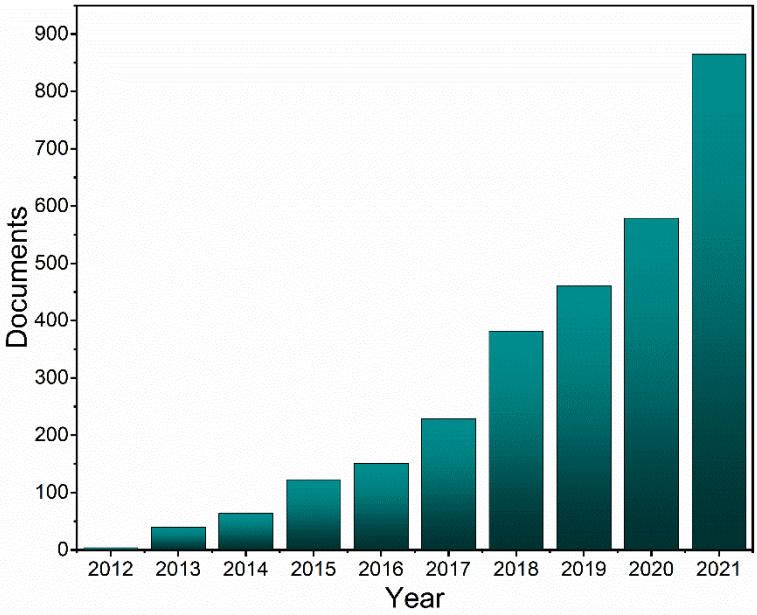

Fig. 2. Data on documents indexed in SCOPUS database containing "triboelectric nanogenerator" in the title, abstract or keywords.

TEG can be produced from cheap, lightweight, flexible, abundantly available polymer materials. In comparison to piezoelectric and ferroelectret materials, TEGs do not require costly poling procedures to enable the harvesting function. TEG devices can be operated in different modes – vertical separation mode,[23] sliding,[24] rotation,[25] or single electrode.

TEGs have been demonstrated for a wide range of applications. Triboelectric *in vivo* energy harvesters have been used to collect biomechanical energy from the heartbeat and respiration of rats and pigs.[26,27] Implantable triboelectric sensor fixed to the pericardium of a pig has been demonstrated for monitoring of heart and respiratory rates as well as detection of life-threatening arrhythmia.[28] Furthermore, TEG can be used for stimulation of living cell, tissue and organs, therefore providing potential applications in promotion of stem cell neuronal differentiation, facilitation of neuronal tissue regeneration, and heart stimulation.[29,30]

Main performance characteristics of TEG devices are the open-circuit voltage (V_{OC}) and short-circuit current (I_{SC}). V_{OC} depends on load resistance R and grows as R is increased. I_{SC} often is on the scale of nanoamperes with state-of-the-art values reaching 350 μA from 1 cm^2 sample.[31] An accurate characteristic of the polymers triboelectrification capability is charge density Q, calculated from the short-circuit current by Equation (1):

$$Q = \frac{\int I_{SC} \mathrm{d}t}{A}, \quad (1)$$

where I_{SC} is short-circuit current; dt is time differential; and A is contact surface area.

To evaluate the energy harvesting potential of TEGs, it is useful to calculate energy and power density (per area of TEG). Instantaneous power density P_i is calculated from V_{OC} at the chosen R by Equation (2):

$$P_i = \frac{{V_{OC}}^2}{R \times A}, \quad (2)$$

where V_{OC} is open circuit voltage and R is load resistance.

Next, plot of the P_i values obtained by Equation (2) as a function of time t allows the calculation of energy E by Equation (3):

$$E = \int P_i \mathrm{d}t. \quad (3)$$

The energy stored in the capacitor also is a crucial characteristic of TEG; it can be lower by 3–4 orders of magnitude than the energy calculated directly from the contact-separation experiments.[31] Losses are mostly caused by rectification circuit[32] that converts the generated alternating current to direct current. This is one of the aspects that limits the range of applications.

Three main routes used to enhance the performance of TEG devices are: i) modification of surface topography and morphology; ii) chemical treatment and functionalization of polymer surface; and iii) incorporation of ferroelectric materials.

Pattern and geometry of the triboelectric layer play a vital role in the performance of TEG. Greater specific surface area has been shown to contribute to enhanced Q generation. Research has shown that asymmetric contact (differences in contact area of films) between two identical materials results in high surface potential.[33] Accordingly, the more both surfaces differ in their topography and morphology, the higher the performance of TEG can be expected.

Triboelectric properties of polymers can be enhanced through chemical surface modification.[34] Surface modification increases the adhesion of polymer against the contacted surface, since there is a relationship between the surface adhesion and triboelectric charge. The process usually involves surface activation by plasma treatment followed by coating of the chosen chemical. For example, chemical modification by fluorocarbon plasma treatment has been proposed by researchers to enhance triboelectric properties.[35] One of the most commonly used polymers for chemical modification is polydimethylsiloxane (PDMS);[36] its triboelectric surface charge can be increased by various surface treatment methods, like ultraviolet light illumination after NaOH treatment,[37] chemical halogenation[38] or sequential etching and chemical modification by O_2 and SF_6 plasma.[39]

One of the approaches to achieve greater TEG performance involves the use of ferroelectric/piezoelectric effect. TEGs incorporating this effect are commonly referred as hybrid devices, since piezoelectricity is the cornerstone of piezoelectric generators. Accordingly, all ferroelectric materials could be piezoelectric, however, not all piezoelectric materials exhibit ferroelectricity (e.g., ZnO and quartz). Ferroelectricity is commonly observed

in perovskites ($BaTiO_3$, $PbTiO_3$) and some polymer materials (polyvinylidene fluoride (PVDF), polyamide-11 (PA-11)).[40] Ferroelectric materials in the volume possess dipole moments that are oriented randomly to give net polarization density $P = 0$. Electrical field E aligns dipoles in a specific direction, thus creating a net polarization vector. Applied stress causes change in P, which induces surface charge in electrode. Hybrid TEG devices have shown the greatest output performance among all, reaching state-of-the-art power density – 50 mW cm^{-2}.[31]

In summary, TEGs possess a great potential to boost the field of energy harvesting. The Thesis will report on energy harvesting results using polymer based TEG. Enhancement of energy harvesting will be achieved by creating TEG devices incorporating ferroelectric materials. The new insights discovered regarding charge formation will be utilized to improve the energy harvesting potential of TEG devices.

Triboelectrification and materials for TEG devices

Triboelectrification (also known as contact electrification) is the formation of electric charge on the surface of one material after contact-separation with another material and provides the basis for functionality of TEG. In the process both materials gain electric charge; equal in magnitude but opposite in polarity. Triboelectrification is observed for different types of materials, however, the magnitude of charge and the temporal resolution differ significantly. Accordingly, triboelectrification of two metals yields a rather small charge (0.1–10 pC per cm^2) that is quickly dissipated (less than a second), while for polymers the obtained charge is higher (0.1–100 nC per cm^2) and more stable (up to 24 hours).

Triboelectric effect can be crucial for some applications or totally disruptive for other. For example, in electrostatic spray-painting the friction of paint particles against the paint gun's barrel grants them the surface charge.[41] The charged paint particles cover the surface more evenly by filling crevices and voids. Triboelectric effect is also used in xerography – a technique used to create photocopies without liquid chemicals.[42] In some printer toners this effect provides the attraction of toner's polymer particles to iron carrier particles so that magnetic field can arrange them. Electrostatic charge generated by triboelectric effect can also be used in filtration systems. Regarding the disruptive side of triboelectric effect – accidental discharge of surface charges can ignite flammable materials or dust clouds.[43,44] Discharge can also destroy microelectronics components.[45,46] Triboelectrification can also cause a handful of problems in production – it can disrupt flow and blending,[47-51] which leads to increased friction and loss of energy.[52,53]

In the case of metals and semiconductors (contact between metal and metal, metal and semiconductor or semiconductor and semiconductor) a consensus has been reached that electron transfer between the involved materials is responsible for net charge formation, because these materials possess delocalized electrons. Electron transfer between two metals is relatively straightforward: it is based on differences in work function Φ. Upon contact, electrons flow from the metal with the lowest Φ to the metal with the highest Φ. Equilibrium is reached when the accumulated electrons in the metal with higher Φ cancel out the initial Φ difference. Next, separation induces electron backflow as they tend to return to the original state, however,

a sharp increase in distance limits this process to the point when tunnelling between surfaces is improbable. As a result, residual electrons remain on the high Φ metal.

The most suitable materials (metals, semiconductors or polymers) for contacting surfaces in TEG devices can be chosen by triboelectric series. It is a guide, that shows which material will gain a positive and which a negative charge in the mutual contact of these materials. Often, they also show the expected magnitude of the triboelectrification as charge density. Commonly materials are listed in the order shown in Fig. 3, according to their tendency to charge positively or negatively after the contact with each other or after a contact with one specific material.[54] However, variations in the order of materials can be found, sometimes with contradictory results.[55-58]

Insulator Name	Charge Affinity (nC/J)		Insulator Name	Charge Affinity (nC/J)
Polyurethane foam	+60		Sorbothane	+58
Hair, oily skin	+45		solid polyurethane	+40
Magnesium fluoride	+35		nylon, dry skin	+30
Machine oil	+29		Nylatron	+28
Glass (soda)	+25		paper	+10
Wood (pine)	+7		cotton	+5
Nitrile rubber	+3		wool	0
Polycarbonate	−5		acrylic	−10
Epoxy	−32		styrene-butadiene rubber	−35
PET (mylar) solid	−40		EVA rubber	−55
Gum rubber	−60		polystyrene	−70
Polyimide	−70		silicones	−72
Vinyl: flexible	−75		LDPE	−90
Polypropylene	−90		HDPE	−90
Cellulose nitrate	−93		UHMWPE	−95
Polychloroprene	−98		PVC (rigid vinyl)	−100
Latex (natural) rubber	−105		Viton, filled	−117
Epichlorohydrin rubber	−118		Santoprene rubber	−120
Hypalon rubber, filled	−130		butyl rubber, filled	−135
EDPM rubber, filled	−140		PTFE (Teflon)	−190

Fig. 3. Example of quantified triboelectric series.[54]

The observed variations in triboelectric series is one of the causes for a long-standing discussion about the mechanisms governing the charge formation and transfer in triboelectrification of polymers. Main mechanisms that are proposed for polymer triboelectrification are electron transfer, transfer of charged fragments from macromolecules or transfer of ions. Determination of mechanism is complex due to a range of factors that influence the charge formation in polymer triboelectrification: (i) environment (temperature and humidity);[59-62] (ii) contact time and force;[63] (iii) morphology (surface roughness, pattern); (iv) bulk properties (macromolecule ordering, crosslinking degree);[64] and (v) chemical composition of surface (functional groups).[65]

Electron transfer adequately describes the charge transfer between metals,[66] therefore, the same logic was initially applied to insulators, both inorganic and organic. Insulator is characterized by a filled valence band and an empty conduction band separated by a large band

gap; therefore, a significant amount of energy must be supplied to allow electron transfer. The cost of this endothermic process is close to 10 eV, when considering electron removal from the first polymer material, charge separation over distance and addition to the second polymer material.[67] Evidently, direct electron transfer between insulators is energetically more improbable than between metals, however, polymers charge more strongly than metals. Several attempts have been made to address the flaws of electron transfer model for insulator triboelectric charging. One proposes existence of intermediate states for electrons in the bandgap, which are provided by defects like highly strained bonds or surface states.[68] Thermoluminescence experiments have shown the existence of such states, however, the amount of these electrons is insufficient to account for the developed charge.[69] Delocalization of electron-wave functions due to material strain during contact also has been suggested as the driving force for electron transfer.[70-73] Accordingly, the contact of both surfaces allows hybridization of their electron states so that some electrons are delocalized and become available for transfer.

Thanks to surface analysis methods like X-ray photoelectron spectroscopy (XPS), atomic force microscopy (AFM) and Raman spectroscopy, evidence has been collected to support ion exchange mechanism.[74-76] Without doubt, ion transfer is the main mechanism when ionomers are contacted, since the "mobile" ions can be easily transferred.[77-79] However, can ions be responsible for the strong triboelectrification when conventional polymers are contacted? As there are no "mobile" ions in conventional polymer insulators, the hydroxide ions (OH^-) are thought to play the central role, because even hydrophobic polymers adsorb a thin layer of water on their surface in ambient conditions.[80] When polymer surfaces are contacted, a water "bridge" forms on the surfaces enabling the transfer of OH^- ions to the polymer, which exhibits the strongest affinity. When materials are separated, a net charge is formed on the surface due to ion imbalance in the layers of adsorbed water. The affinity to attract OH^- ions is linked to the zeta potentials of polymers (electrical potential on the stationary water layer).[81,82] However, ion transfer explanation has its flaws: polymer triboelectrification has been observed in the absence of water[83] and also in vacuum between surfaces that have not been exposed to the atmosphere.[84,85] Furthermore, it does not explain the polymer triboelectrification when chemically identical materials are contacted where both exhibit the same affinity towards OH^- ions.[59,86]

The triboelectrification mechanism from transfer of charged fragments of macromolecules arises from the fact that the polymer covalent bonds undergo scission due to mechanical impact, as evident from extensive studies in mechanochemistry and tribology.[87,88] The energy of covalent bonds in polymers are in range 3.7–4.5 eV depending on the presence of heteroatoms (N, Si, O, S, F, etc.) in the main chain and side moieties.[89] Dissociation of covalent bond can be either a homolytic (homolysis) or heterolytic scission (heterolysis).[90] After homolytic scission, identical radicals are formed on the ends of each chain of the ruptured macromolecule.[91] However, only heterolytic scission is responsible for the charge formation, since the outcome is a pair of cation and anion (mechano-ions). As observed by Kelvin force microscopy (KFM), after contact-separation surfaces develop random patterns of positively and negatively charged nanoscale domains (Fig. 4).[76] Accordingly, the net charge density measured

on each contacted surface is the sum of contributions from these nanoscale domains, with the dominant mechano-ions determining the polarity. As surfaces are separated, a material transfer happens along with the charged ionic fragments.[75,76]

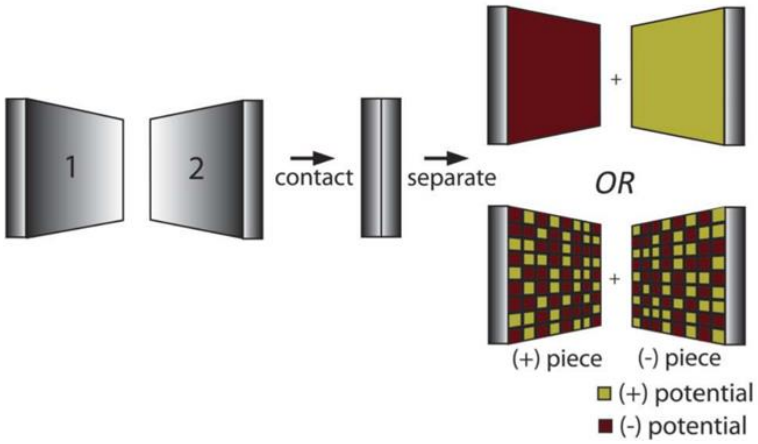

Fig. 4. Demonstration of charge generation in the case of material transfer.[76] From "Baytekin, H. T.; Patashinski, A. Z.; Branicki, M.; Baytekin, B.; Soh, S.; Grzybowski, B. A. The Mosaic of Surface Charge in Contact Electrification. *Science* **2011**, *333* (6040), 308–312". Reprinted with permission from AAAS.

Material transfer is caused by adhesion between surfaces due to formation of locally concentrated adhesive bonds for which the sum of interaction forces overcomes the strength of covalent bond.[91,92] Adhesiveness increases when polymer chains are free to interact and entangle with the opposed surfaces. Additionally, elastomers provide a fuller contact area and increase the density of intermolecular adhesion bonds during contact. Friction contributes to bond scission by creating shear force during contact, thus higher friction forces lead to higher bond scission probability. Generally, friction depends on the molecular weight and crosslinking density; for example, it has been shown that crosslinked polymer surfaces exhibit a several orders of magnitude lower friction than non-crosslinked.[91]

While homolysis does not yield charge species, it is still beneficial to contact-electrification of polymers. It has been shown that radicals colocalize with the ions and stabilize them on the contacted polymer surfaces. Addition of radical-scavenging molecules (e.g., E-vitamin) rapidly decreases the previously stable charge density.[45] According to theoretical studies, the radical-charge stabilization mechanism is based on the formation of intermolecular odd-electron (one or three) bond.[93]

Material transfer among the three charge transfer mechanism discussed in literature seems the most probable. The Thesis will investigate the charge formation and search to verify the role of material transfer in polymer triboelectrification through detection of transferred material by XPS and AFM and contact-separation tests. Since adhesion between surfaces plays an important role in charge formation, TEG devices with increased adhesion will be developed and investigated. The impact of physico-chemical properties on the triboelectric effect will also be investigated in the Thesis, that is why tuning of parameters such as cohesive energy density, composite hardness or surface morphology for higher surface charge generation will be studied.

The Thesis will also contribute to understanding of aspects that influence the charge formation by investigating triboelectrification of chemically identical materials.

Aims of the Thesis

1. To determine the influence of physico-chemical characteristics of polymer on the surface charge formation.
2. To prove that heterolytic covalent bond scission with material transfer is the principal mechanism responsible for polymer triboelectrification.
3. To investigate the ways to increase polymer triboelectrification tendency.

Statements to be defended

1. Charge density generated in polymer triboelectrification corelates with the mechanical properties (e.g., elastic modulus, hardness) and surface roughness of the material allowing the prediction of polymer's triboelectric properties.
2. Heterolytic scission of covalent bonds is confirmed as a mechanism to explain charge formation in polymer insulator materials.
3. Hybrid ferroelectric-triboelectric nanogenerator devices achieve greater performance when triboelectric dipoles (dipole moment created during triboelectrification) match the direction of the ferroelectric dipoles (dipole present in the ferroelectric phase).

Scientific novelty

An essential contribution to explanation of polymer material triboelectrification mechanisms has been made by showing the influence of parameters like hardness, elastic modulus, surface roughness, macromolecular ordering, and crosslinking degree. A novel approach to construct high-performance TEG devices utilizing ferroelectric effect synergy with triboelectricity is outlined.

Practical significance

Using knowledge about the effects of the polymer's physicochemical properties on triboelectrification, hybrid triboelectric generator devices capable to transform mechanical energy into electrical with improved efficiency are developed. Triboelectric generators provide energy for microdevices or wireless sensors, therefore avoiding the use of batteries.

Structure of the Thesis

The Doctoral Thesis is a collection of scientific articles dedicated to examination of contact-electrification effect and development of triboelectric nanogenerator devices. Summary of the Thesis is written in Latvian and English. The results of the Thesis have been published in 7

original research papers indexed in Scopus and in Web of Science (WOS). Summary of the Thesis contains 25 figures and 2 tables. The papers included in the Thesis have a cumulative impact factor of 84.055 for year 2020, and their total volume is 132 pages, including electronically available supplementary information. The results have been presented in 9 international conferences.

Publications and approbation of the Thesis

Original papers in which Thesis results are published

1. A. Šutka, K. Malnieks, **L. Lapčinskis, P.** Kaufelde, A. Linarts, A. Berziņa, R. Zabels, V. Jurķans, I. Gorņevs, J. Blums, M. Knite. The role of intermolecular forces in contact electrification on polymer surfaces and triboelectric nanogenerators, *Energy Environ. Sci.* **2019**, *12(8)*, 2417–2421. (*Scopus, WOS, IF(2020) = 38.532*).
2. **L. Lapčinskis,** K. Mālnieks, J. Blūms, M. Knite, S. Oras, T. Käämbre, S. Vlassov, M. Antsov, M. Timusk, A. Šutka. The Adhesion-Enhanced Contact Electrification and Efficiency of Triboelectric Nanogenerators, *Macromol. Mater. Eng.* **2020**, *305(1)*, 1900638. (*Scopus, WOS, IF(2020) = 4.367*).
3. A. Šutka, A. Linarts, K. Malnieks, K. Stiprais, **L. Lapčinskis.** Dramatic increase in polymer triboelectrification by transition from a glassy to rubbery state, *Mater. Horiz.* **2020**, *7(2)*, 520–523. (*Scopus, WOS, IF(2020) = 13.266*).
4. A. Šutka, K. Mālnieks, **L. Lapčinskis,** M. Timusk, K. Kalniņš, A. Kovaļovs, J. Bitenieks, M. Knite, D. Stevens, J. Grunlan, Contact electrification between identical polymers as the basis for triboelectric/flexoelectric materials, *Phys. Chem. Chem. Phys.* **2020**, *22(23)*, 13299–13305. (*Scopus, WOS, IF(2020) = 3.676*).
5. **L. Lapčinskis**, A. Linarts, K. Mālnieks, H. Kim, K. Rubenis, K. Pudzs, K. Smits, A. Kovaļovs, K. Kalniņš, A. Tamm, C.K. Jeong, and A. Šutka. Triboelectrification of nanocomposites using identical polymer matrixes with different concentrations of nanoparticle fillers, *J. Mater. Chem. A* **2021**, *9(14)*, 8984–8990. (*Scopus, WOS, IF(2020) = 12.732*).
6. **L. Lapčinskis, K.** Mālnieks, A. Linarts, J. Blūms, K. Šmits, M. Järvekülg, M. Knite, A. Šutka. Hybrid Tribo-Piezo-Electric Nanogenerator with Unprecedented Performance Based on Ferroelectric Composite Contacting Layers, *ACS Appl. Energy Mater.* **2019**, *2(6)*, 4027–4032. (*Scopus, WOS, IF(2020) = 6.024*).
7. A. Šutka, K. Mālnieks, **L. Lapčinskis**, M. Timusk, K. Pudzs, M. Rutkis. Matching the Directions of Electric Fields from Triboelectric and Ferroelectric Charges in Nanogenerator Devices for Boosted Performance, *iScience* **2020**, *23(4)*, 101011. (*Scopus, WOS, IF(2020) = 5.458*).

Other papers published during development of the Thesis

1. M. Knite, A. Linarts, K. Ozols, V. Tupureina, I. Stalte, **L. Lapcinskis**. A study of electric field-induced conductive aligned network formation in high structure carbon black/silicone oil fluids, *Colloids Surf., A* **2017**, *526*, 8–13. (*Scopus, WOS, IF(2020) = 4.539*).

2. **L. Lapčinskis**, A. Linarts, M. Knite, I. Gorņevs, J. Blūms, A. Šutka. Solid-state supercapacitor application for pressure sensing. *Appl. Surf. Sci.* **2019**, *474*, 91–96. (*Scopus, WOS, IF(2020) = 6.707*).
3. **L. Lapčinskis**, I. Cīrulis, P. Lesničenoks, A. Ābele, A. Šutka, M. Knite. PVA hydrogel electrolyte and porous polyisoprene carbon nanostructure composite based pressure sensitive supercapacitor. *IOP Conf. Ser.: Mater. Sci. Eng.*, **2019**, *500(1)*, 012018. (*Scopus, WOS, IF = 0.53*).
4. A. Šutka, P.C. Sherrell, N.A. Shepelin, **L. Lapčinskis**, K. Mālnieks, and A.V. Ellis. Measuring Piezoelectric Output – Fact or Friction?, *Adv. Mater.* **2020**, *32(32)*, 2002979. (*Scopus, WOS, IF(2020) = 30.849*).
5. A. Šutka, K. Mālnieks, A. Linarts, **L. Lapčinskis**, O. Verners, M. Timusk. Triboelectric Laminates with Volumetric Electromechanical Response for Mechanical Energy Harvesting, *Adv. Mater. Technol.* **2021**, *6(8)*, 2100163. (*Scopus, WOS, IF(2020) = 7.848*).
6. A. Šutka, M. Zubkins, A. Linarts, **L. Lapčinskis**, K. Mālnieks, O. Verners, A. Sarakovskis, R. Grzibovskis, J. Gabrusenoks, E. Strods, K. Smits, V. Vibornijs, L. Bikse, J. Purans. Tribovoltaic Device Based on the W/WO_3 Schottky Junction Operating through Hot Carrier Extraction, *J. Phys. Chem. C* **2021**, *125(26)*, 14212–14220. (*Scopus, WOS, IF(2020) = 4.126*).
7. S. Lapcinska, P. Dimitrijevs, **L. Lapcinskis**, P. Arsenyan. Visible Light-Mediated Functionalization of Selenocystine-Containing Peptides, *Adv. Synth. Catal.* **2021**, *363(13)*, 3318–3328. *(Scopus, WOS, IF(2020) = 5.837).*
8. P. C. Sherrell, A. Sutka, N. A. Shepelin, **L. Lapcinskis**, O. Verners, L. Germane, M. Timusk, R. A. Fenati, K. Malnieks, A. V. Ellis. Probing Contact Electrification: A Cohesively Sticky Problem, *ACS Appl. Mater. Interfaces* **2021**, *13(37)*, 44935–44947. (*Scopus, WOS, IF(2020) = 9.229*).

Participation in Conferences

1. Poster presentation in the 6th Nano Today International Conference: **L. Lapčinskis**, J. Blūms, M. Jarvekulg, M. Knite, A. Šutka, "Ferroelectric PVDF and $BaTiO_3$ nanocomposites for enhanced energy harvesting devices", Lisbon, Portugal, June 16–20, 2019.
2. Poster presentation in international conference "2019 MRS Fall Meeting": **L. Lapčinskis**, K. Mālnieks, J. Blūms, M. Jarvekulg, M. Knite, A. Šutka, "Hybrid Tribo Piezo Electric Nanogenerator with Unprecedented Performance Based on Ferroelectric Composite Contacting Layers", Boston, USA, December 1–6, 2019.
3. Poster presentation in international conference "2019 MRS Fall Meeting": K. Mālnieks, A. Šutka, A. Linarts, **L. Lapčinskis**, "The Role of Intermolecular Forces in Contact Electrification on Polymer Surfaces", Boston, USA, December 1–6, 2019.
4. Poster presentation in international conference "2019 MRS Fall Meeting": A. Linarts, K. Malnieks, **L. Lapčinskis**, M. Knite, J. Blums, A. Šutka, "Inversely Polarized Ferroelectric Polymer Contact Electrodes for Triboelectric Generators from Identical Materials", Boston, USA, December 1–6, 2019.

5. Online presentation at international conference “RTU MSAC conference”: **L. Lapčinskis**, K. Mālnieks, L. Ģērmane, M. Knite, A. Šutka, “Polymer Based Triboelectric Nanogenerators: how to choose the right materials?”, Riga, Latvia, October 23, 2020.
6. Online poster presentation at international conference “FMNT 2020”: L. Ģērmane, **L. Lapčinskis**, M. Knite, A. Šutka, “Prediction of triboelectric series based on polymer physico-chemical properties”, Vilnius, Lithuania, November 23, 2020.
7. Online poster presentation at international conference “2020 MRS Fall Meeting”: **L. Lapčinskis**, K. Mālnieks, M. Knite, A. Šutka, “Strategy to Choose Best Building Blocks for Efficient Triboelectric Generator Devices”, Boston, USA, November 27 – December 4, 2020.
8. Online poster presentation at international conference “2020 MRS Fall Meeting”: A. Linarts, A. Šutka, K. Malnieks, **L. Lapčinskis**, “Dramatic Increase in Polymer Triboelectrification by Transition from a Glassy to Rubbery State”, Boston, USA, November 27 – December 4, 2020.
9. Online poster presentation at international conference “2020 MRS Fall Meeting”: K. Malnieks, A. Šutka, **L. Lapčinskis**, A. Linarts, “Matching the Directions of Electric Fields from Triboelectric and Ferroelectric Charges in Nanogenerator Devices for Boosted Performance”, Boston, USA, November 27 – December 4, 2020.

MAIN RESULTS OF THE THESIS

The role of intermolecular forces in contact electrification (Paper I)

Paper I showcases the correlation of intrinsic physico-chemical properties with the magnitude of surface charge formed after contact-separation. The contact electrification of polymer interfaces provides an energy harvesting function of triboelectric generators (TEGs). Often electron transfer between contact-separated surfaces is considered as the main electrification mechanism for polymers. The electron transfer mechanism requires a contact between chemically different polymer materials, as well as subsequent increase of the specific contact area, which is commonly accomplished via nanostructuring. However, in Paper I we showed that contact electrification can be controlled by modifying the intermolecular forces in the polymer and adhesive forces at the contact interface.

The main goal set by Paper I was to investigate the influence of changes in physico-chemical properties of polymers on the charge formation during contact-separation. Accordingly, the tasks established for studying this influence were:

- To study triboelectrification of polymers with different cohesive energy. Since experimental determination of cohesive energy is challenging, to establish a relationship between the elastic modulus of the polymer and the charge density after contact-separation against indium-tin oxide (ITO) electrode.
- To determine how the hardness difference of two mutually contact-separated polymers influence the generated *Q*.
- To examine the influence of polymer's macromolecular ordering on the generated *Q* upon contact-separation of identical polymers.
- to determine the correlation between the crosslinking density of elastomer PDMS, the generated *Q*, and also the adhesive forces upon contact-separation.

Main results of the triboelectric measurements are demonstrated in Figs. 5–7.

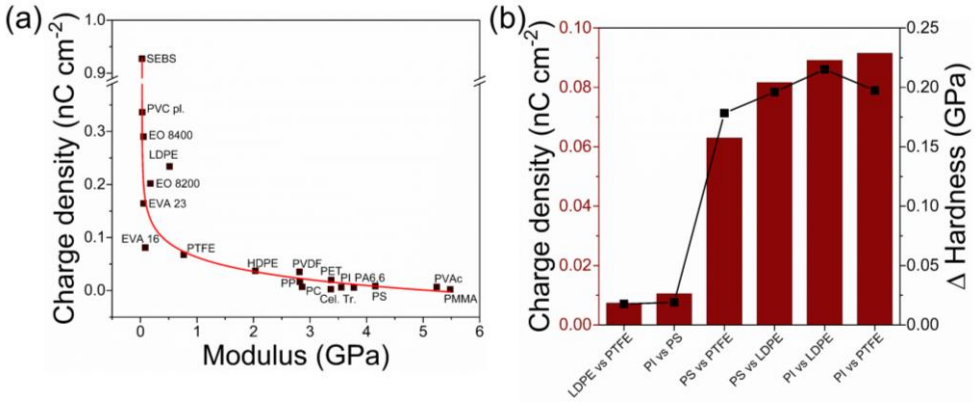

Fig. 5. Contact-electrification charge of thermoplastic polymers related to their mechanical properties: (a) correlation between the modulus of polymer material and surface charge; (b) contact-electrification charge density and hardness gap for different polymer combinations.[94]

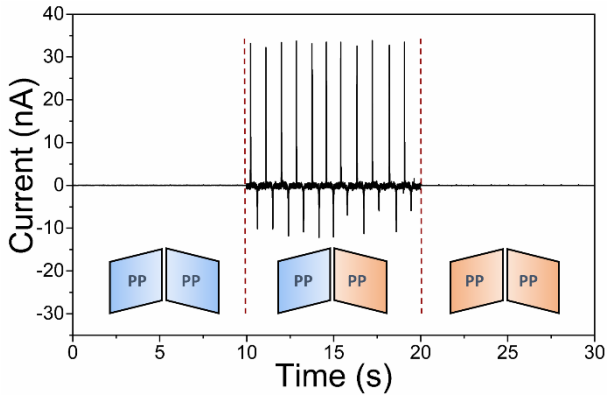

Fig. 6. Short-circuit current peaks generated by the contact-electrification of (PP) with similar and different thermal histories. Blue figures represent original polymer films, and red figures represent polymer films subjected to isothermal crystallization (130 °C, 60 min).[94]

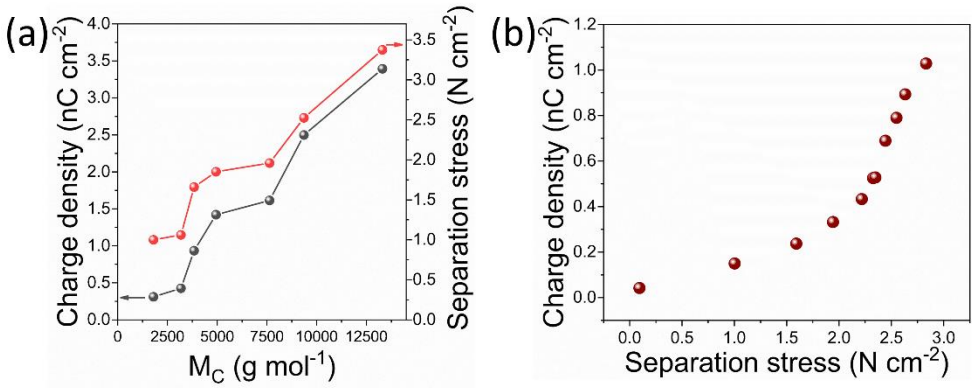

Fig. 7. (a) Surface charge density and separation stress dependency on the molecular weight between PDMS crosslinking points M_C; (b) relationship between the PDMS charge and the required separation stress.[94]

The main results and conclusions of Paper I:

- Polymers having a lower elastic modulus exhibit higher surface charge density values than those with higher modulus, as shown in Fig. 5 (a). Polymers with the highest modulus: polymethyl methacrylate (PMMA); polyamide 6,6 (PA-66); and polyvinyl acetate (PVAc) after contact-separation with ITO show charge density on the order of 10 pC cm^{-2}, while for soft elastomeric polymers like styrene-ethylene-butylene-styrene block copolymer (SEBS) the surface charge is two orders of magnitude higher (0.92 nC cm^{-2}). Modulus is proportional to the cohesive energy density (CED) of the material[95], thus Fig. 5 (a) also hints at correlation between the surface charge and polymers CED. Enhanced triboelectrification due to different specific surface contact areas can be excluded because all samples are flat (prepared with the same hot-pressing approach) and have similar surface roughness values, as shown by AFM height measurements (59.76 ± 21.78 nm). In comparison, for the samples with intentionally increased surface roughness, the RMS surface roughness reached 654 nm.
- Mutual contact-separation was performed with chemically different polymers with similar or different hardness values (Fig. 5 (b)). Polymer hardness was determined using

nanoindenter tip – Berkovich three-sided pyramid. Although being chemically different, two hard polymers like polyimide (PI, 230 MPa) and polystyrene (PS, 210 MPa) produced a surface charge density of only 0.011 nC cm^{-2}. Low charge density was observed also when contacting two soft polymers with similar hardness values: contact-separating low-density polyethylene (LDPE, 15 MPa) and polytetrafluoroethylene (PTFE, 33 MPa). However, contact-separation between hard and soft polymers yielded surface charges higher by an order of magnitude. This experiment clearly indicates that the electron transfer is not likely to govern the charge formation in polymer triboelectrification.

- Contrary to general understanding,[54] we demonstrated that there is no need to contact chemically different polymers for triboelectrification to occur, as shown by I_{SC} generated by the TEG device constructed from chemically identical polypropylene (PP) films (Fig. 6). For PP films with identical thermal histories no current was observed; however, when PP films with different thermal histories were contact-separated, the I_{SC} of 35 nA and Q of 0.071 nC cm^{-2} were generated. Different thermal histories change macromolecular ordering, as confirmed by lower phase transition temperature and surface hardness change from 107.6 MPa to 96.2 MPa, respectively.
- Triboelectrification of PDMS against ITO was studied by changing the cross-linking degree of PDMS; it was varied by changing the ratio between pre-polymer and the curing agent.[96] The surface charge after contact with ITO increased from 0.31 nC cm^{-2} to 3.39 nC cm^{-2}, with an increase in the molecular weight between crosslinks (M_C) of PDMS from 1800 g mol^{-1} to 13300 g mol^{-1} (Fig. 7 (a)).
- Triboelectrification of two chemically identical PDMS was studied by contact-separating two PDMS with identical and different M_C values. When the M_C of the contacting PDMS films was identical, almost no contact electrification was observed. The Q upon contact-separation of two identical layers with M_C of 7600 g mol^{-1} was 0.00143 nC cm^{-2}, while for two layers with M_C of 1800 g mol^{-1} it was 0.00161 nC cm^{-2}. When PDMS films with different M_C were contacted (7600 vs. 1800 g mol^{-1}), surface charge density of 0.0168 nC cm^{-2}, V_{OC} of 20 V, and I_{SC} of 120 nA higher by at least an order of magnitude were obtained.
- The higher charge density upon the decrease of crosslinking degree is connected not only to less crosslinks and smaller cohesive energy but also to higher adhesion between PDMS and the ITO. As shown in Fig. 7 (a), the separation stress necessary to separate both contacted films is higher when the cross-linking degree reduces (M_C increases). The observed relationship between the separation stress and charge density stands also when the separation stress is increased for a PDMS with a specific M_C (3840 g mol^{-1}) – higher separation stress correlates with increased charge density (Fig. 7 (b)). Separation stress is increased by gradually raising the contacting force from 1 N to 50 N with 5 N step. These results confirm that high surface charge density on the polymer can be obtained if the polymer shows a strong surface adhesion and low cohesion energy in the bulk. In such a case, the net energy of the neighbouring adhesive (physical) bonds formed between contacting surfaces is larger than the energy of the chemical or/and physical bonds in bulk. This results in covalent bond scission and material transfer between two contacting surfaces.[64]

The adhesion-enhanced contact electrification and efficiency of TEG (Paper II)

In Paper II, the contact electrification of polymers that differ in surface adhesion was reported. TEG devices were prepared from polydimethylsiloxane (PDMS), ethylene-octene copolymer (EOC), styrene-ethylene-butylene-styrene copolymer (SEBS) and polyethylene-co-vinyl acetate copolymer (EVA). In addition, poly(hexanediol-co-citric acid) (PHC), known in the literature as an elastomeric adhesive, was synthesized.[97] Electrical measurements were conducted along the adhesion measurements in macroscale contact-separation experiments. Additionally, local adhesion and roughness were studied with AFM to get a deeper insight into relationship between the surface properties and electrification. Results show that a higher surface charge is formed on more adhesive surfaces, and in combination with XPS measurements they confirm that covalent bond scission is the mechanism responsible for contact electrification of polymers. The investigated materials possess an enhanced contact electrification, making them attractive candidates for the conversion of mechanical energy to electrical in triboelectric nanogenerator devices.

The goals set in Paper II were:

- to further investigate the correlation between the surface charge density and adhesiveness;
- to examine the material transfer of PDMS polymer;
- to propose a method for calculation of triboelectric generator efficiency that considers the previously neglected adhesive forces.

Main results of measurements are demonstrated in Figs. 8–10.

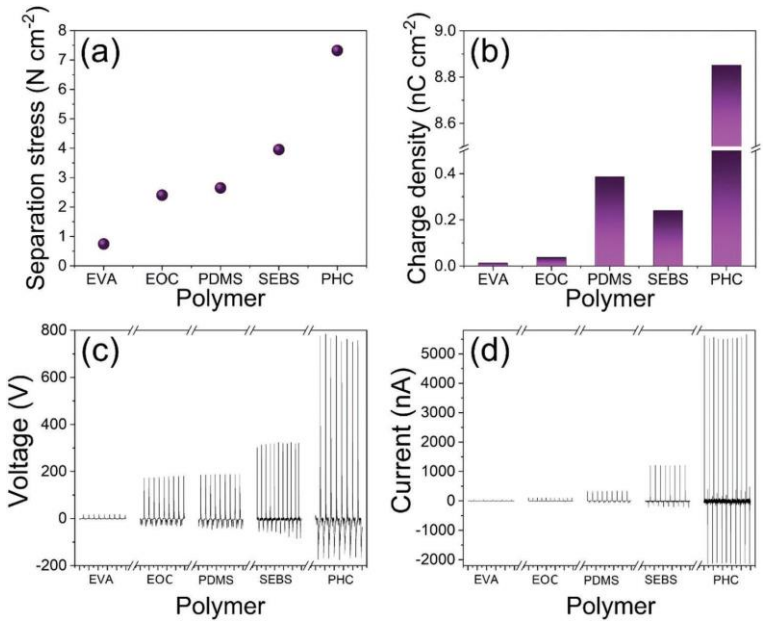

Fig. 8. (a) The separation stress for two contacted sides in TEG based on different polymer materials; (b) corresponding Q for these TEG devices; (c) V_{OC} peaks for TEG based on different polymers; (d) I_{SC} peaks for TEG based on different polymers.[98]

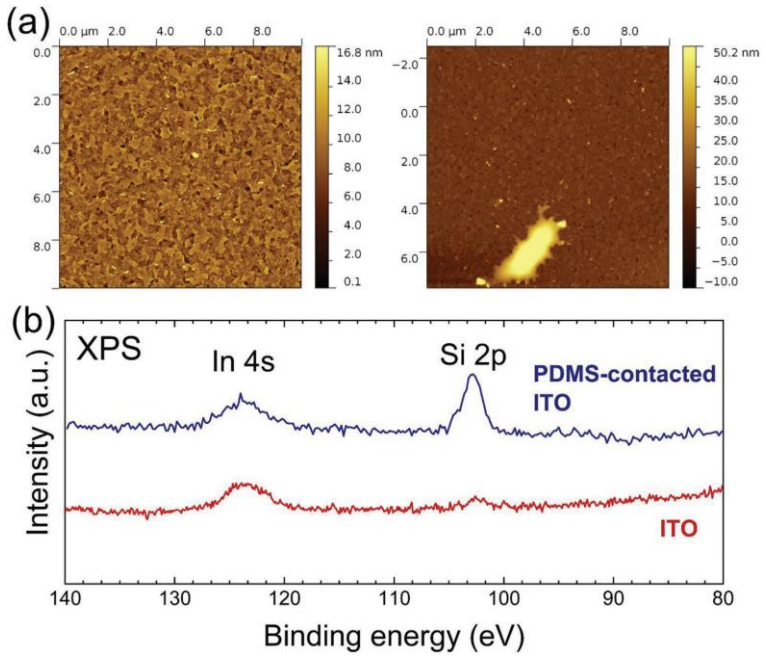

Fig. 9. Material mass transfer: (a) ITO surface before (left) and after (right) contacting with PDMS (weight ratio of components – 10 : 1) for 10 000 cycles; (b) XPS results comparing pristine ITO and ITO surface after contacting against PDMS (weight ratio of components – 10 : 1) for 10 000 cycles showing Si 2p peaks on the surface of ITO.[98]

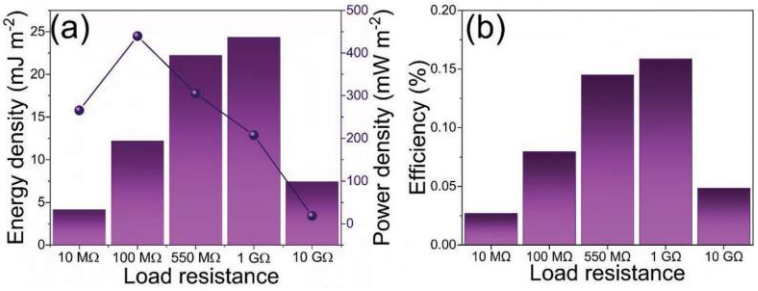

Fig. 10. Characteristics of TEG device based on PHC polymer: (a) energy density and power density as a function of load resistance; (b) efficiency.[98]

The main results and conclusions of Paper II:

- The separation force of tested materials increased in the following order: EVA < EOC < PDMS < SEBS < PHC (Fig. 8 (a)). Accordingly, polymers exhibiting higher separation stress against the contacted ITO surface show higher charge density, V_{OC} and I_{SC} (Fig. 8 (b)–(d)). The highest separation stress is observed for the TEG device constructed of PHC (7.32 N cm^{-2}) with Q reaching 8.853 nC cm^{-2}. The observed correlation between separation force and surface charge is in agreement with previous studies[75,76], where heterolysis and material transfer is presented as an explanation for charge formation. Greater separation force might contribute to a higher probability of material transfer and covalent bond scission.
- Notably, influence of changes in polymer specific surface area on charge density can be excluded, since polymers showed comparable surface roughness values in AFM measurements (both on areas of 3 × 3 µm and 50 × 50 µm). For an area of 3 × 3 µm the RMS

surface roughness values were in the range 9–59 nm, while for 50 × 50 μm area the range was 9–209 nm. Exclusion is PHC, which was found to be too adhesive for surface roughness determination.

- AFM colloidal probe technique offered a deeper insight into relationship between the surface properties and TEG performance as it allows to perform the adhesion measurements at the nanoscale. Median adhesion values were 13.4 mJ m^{-2} for EVA, 37.9 mJ m^{-2} for PDMS, 49.1 mJ m^{-2} for SEBS, and 66.9 mJ m^{-2} for EOC. Just like in roughness measurements the PHC was outside measurable limits.
- The measured nanoscale adhesion values mostly coincide with the macroscale separation force measurements with EOC as exception because in macroscale it showed a relatively small separation force. It is due to different roughness values at different scales. On the scale of 50 × 50 μm, relevant for macroscale adhesion tests, EOC has a relatively high roughness (175 nm), while on 3 × 3 μm scale, that is comparable to spherical AFM probe radius, EOC roughness is lower (17 nm). For rougher macroscopic surfaces full contact over the entire surface is harder achievable, as surface asperities prevent full contact of both surfaces in contrast to the small AFM probe that can achieve almost full contact with the whole surface.
- The heterolytic bond scission mechanism has been previously shown by material transfer measurements using AFM, XPS, and Raman spectroscopy.[64,75,76] Similarly, in this paper material transfer was determined using AFM and XPS. The surface roughness of ITO after 10 000 contact-separation cycles against PDMS increased from 5.15 to 21.51 nm and contained polymer pieces as demonstrated by AFM images in Fig. 9 (a). XPS confirmed the presence of PDMS on the contact-separated ITO surface after Si 2s (153.9 eV) and Si 2p (102.7 eV) signal peaks were observed in the photoelectron spectrum of ITO (Fig. 9 (b)). The same signal peaks were observed in the spectrum of PDMS before contact-separation, and no presence of aforementioned signals was seen on the surface of ITO before contact-separation.
- TEG based on PHC was investigated in detail due to the high charge density demonstrated in the above described tests. The highest energy (24.36 mJ m^{-2}) was observed at R of 1 GΩ, while the highest average power density (439.86 mW m^{-2}) for a contact-separation was reached at 100 MΩ (Fig. 10 (a)). In perspective, the calculated energy indicates that 1 m^2 large TEG device would require approximately 9.3 days (223.7 h) at 1 Hz contact-separation frequency to fully charge a typical mobile phone battery (5.45 Wh). However, a TEG device with a surface area of 20 cm^2 operating at 1 Hz contact-separation frequency could power a wireless sensor node with power consumption of 100 μW,[99] thus confirming the potential use of TEG in sensor applications.
- The efficiency of the PHC TEG device was investigated. For calculation we divided the generated energy with the work done during contact-separation. Typically, the work calculations consider only the pressing force, displacement or the kinetic energy of motions but neglect the separation force.[100-105] When applied for PHC based TEG, these reported methodologies demonstrate that efficiency can surpass 300 %, therefore, indicating potential flaws. When compression force, kinetic energy of motions, and separation force is included in the calculation, the efficiency drops below 1 % (Fig. 10 (b)), showing that there is ample

room for improvements regarding the TEG design. In conclusion, adhesiveness promotes charge formation but limits the practical application of TEG.

Effects of phase transition on triboelectric charge (Paper III)

Inspired by discoveries made in Paper I, where softer materials exhibit higher triboelectrification, we envisioned that heating of glassy polymers above glass transition temperature (T_g) should also yield increase in surface charge. Paper III reports an order of magnitude increase in triboelectric charge density of polymers PS, PC, and PMMA when they transition from glassy to rubbery state above T_g. Since polymers transition to rubbery state, the adhesive force required for separation is also increased.

The goal of Paper III was to examine the influence of individual polymer's structural state (glassy or rubbery) on charge density, therefore, contact separation tests were performed in a range of temperature from room temperature to temperatures exceeding T_g of polymers.

Main results of the conducted measurements are demonstrated in Figs. 11 and 12.

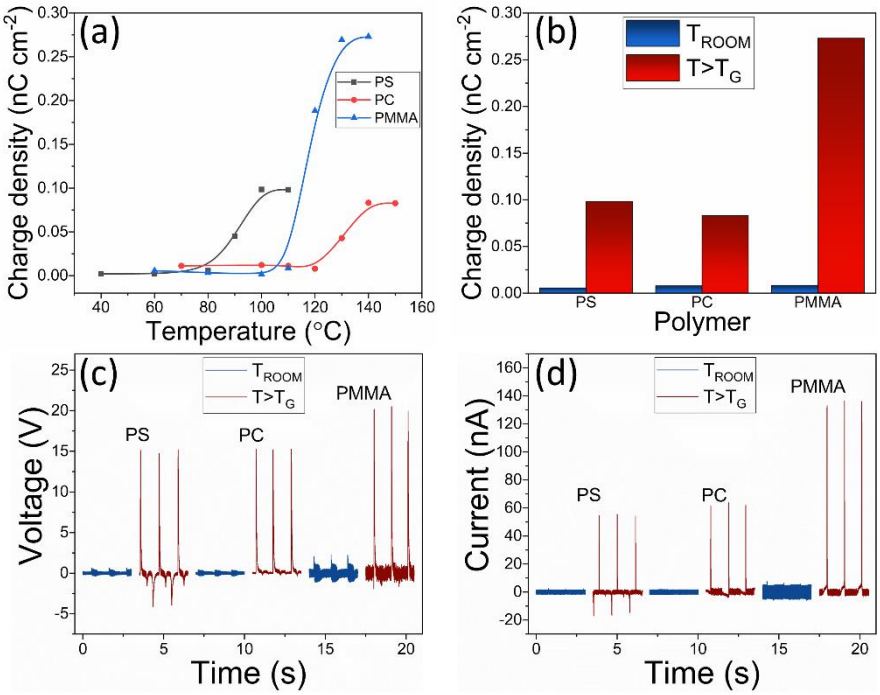

Figure. 11. (a) Steep rise in charge density as the temperature of the TEG device reaches the T_g of the polymer; (b) charge density on polymer surface at a temperature exceeding T_g and at room temperature; (c) V_{OC} peaks of polymers at room temperature and at temperature above T_g; (d) I_{SC} peaks of polymers at room temperature and at temperature above T_g.[106]

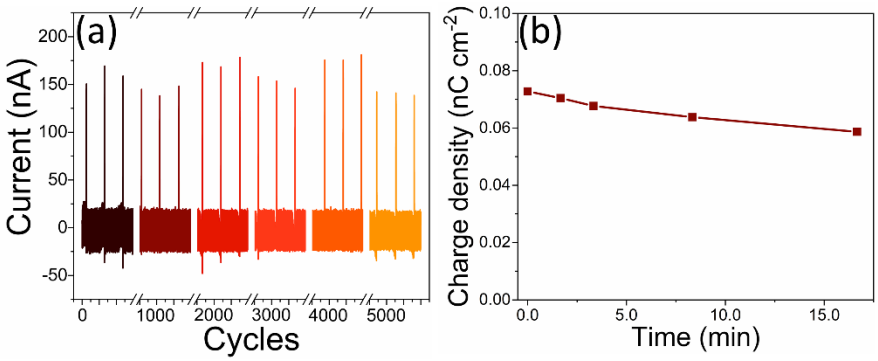

Fig. 12. (a) Current measurements of a PMMA based TENG device over 5000 contacting cycles; (b) surface charge density of a PS based TENG device in non-contact motions at temperature exceeding T_g.[106]

The main results and conclusions of Paper III are:

- Increasing the temperature of three glassy polymers with different chemical structure (PMMA, PC and PS) from the room temperature to the point just below T_g yielded a small increase in surface charge density. However, when these polymers were heated above T_g, the surface charge density, V_{OC} and I_{SC} rapidly increased by more than an order of magnitude for all polymers under study (Fig. 11 (a)–(d)).
- Above T_g, in the rubbery state, polymers behave like elastomers – they can undergo high reversible deformations, therefore, increase in the adhesive properties was also observed. Correspondingly, it was observed that separation force in contact-separation suddenly increases when polymer is heated above T_g. For PS the separation force increased from 0.25 N to 31 N, while for PC and PMMA it changed from 0.15 N to 3 N and from 0.2 N to 4.8 N, respectively.
- Considering the results shown in Papers I and II that the possible mechanism for charge formation is connected to heterolysis of polymer covalent bonds, it was concluded that the observed increase in charge density is due to enhanced covalent bond scission when polymer has entered the "rubbery" state. Elastomeric polymers are more prone to mechanical damage, and deformation will allow to achieve a larger contact area, while adhesion will enhance the material transfer. As material transfer is continuously bidirectional,[75] the long-term performance was also observed. The output of a PMMA TEG device operating at a temperature above the polymer T_g was stable for over 5000 cycles (Fig. 12 (a)).
- There was found no evidence for relationship between the RMS surface roughness (measured by AFM) and the surface charge density in contact-separation tests below and above T_g. In the rubbery state material, transfer is enhanced, therefore, changes in surface roughness were expected. However, for PC the RMS surface roughness remained almost the same – before testing it was 38.4 nm while after contact-separation, above T_g – 33.9 nm. For PS the roughness increased from 9.9 nm to 59.6 nm, but for PMMA it decreased from 162.0 nm to 78.1 nm. To demonstrate that surface roughness has less impact on the charge density than the polymer crossing T_g the RMS surface roughness of PMMA was increased

above 1000 nm by immersion in solvent and subsequent immersion in antisolvent for precipitation. The increase in charge density from contact-separation tests below T_g was negligible – from 0.008 nC cm^{-2} to 0.037 nC cm^{-2}.

- The stability of surface charges was studied by running the vertical separation TEG device in the non-contact regime heating PS above T_g. In non-contact regime the previously contact-separated films were oscillated without physical contact. The surface charges were relatively stable showing less than a 15 % decrease during the first 15 minutes of oscillation (Fig. 12 (b)), thus suggesting that the electron transfer and thermionic emission must not be the cause of increased charge density, as shown in literature.[59] The slow discharge can be attributed to the interaction of the polymer surface with the molecules, ions, and particles from the surrounding atmosphere.[76]

Contact electrification between identical polymers (Paper IV)

In Paper I it was shown that contact electrification between chemically identical polymers is possible if they have different degree of macromolecular ordering or crosslinking density. Here, in Paper IV, we explored how the contact electrification changes if there is difference in surface morphology keeping all other relevant parameters unchanged. Accordingly, we proposed that the reason for the formation of surface charge by contacting two identical polymers is a result of fluctuations in the surface irregularities. Additionally, if contacted materials have a greater porosity or surface roughness difference, the result will be a greater surface charge. It was confirmed by both experimental and finite element analysis (FEA) simulations. Porosity and surface roughness produce strained and compressed regions on the surface, thus affecting the extent of mutual material transfer between two surfaces. The new insight and deepened understanding of polymer contact electrification highlights the future directions in engineering pathways for surfaces with increased triboelectrification.

The main goal of Paper IV was to investigate the influence of polymer's surface morphology on the charge formation during contact-separation of chemically identical polymers.

Main results of the triboelectric measurements are demonstrated in Figs. 13–16.

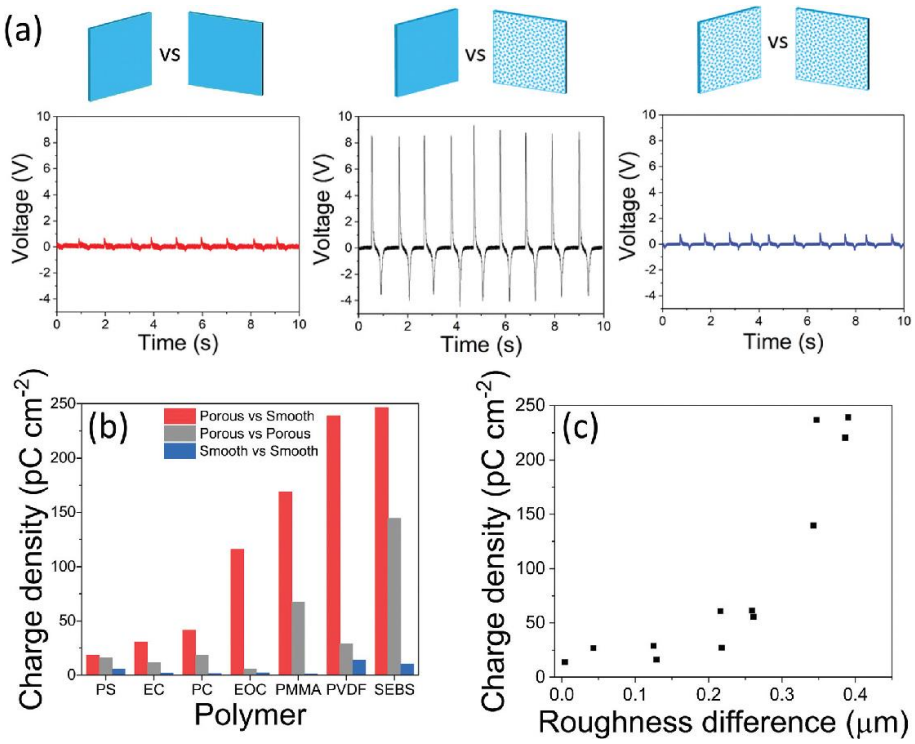

Fig. 13. (a) V_{OC} generated by contact-separating smooth-smooth, smooth-rough and rough-rough EOC film combinations (from left to right); (b) surface charge density formed in contact-separation of two identical polymer films with different surface roughness; (c) relationship between the surface charge density generated in contact-separation and surface roughness disparity of employed PVDF films.[107]

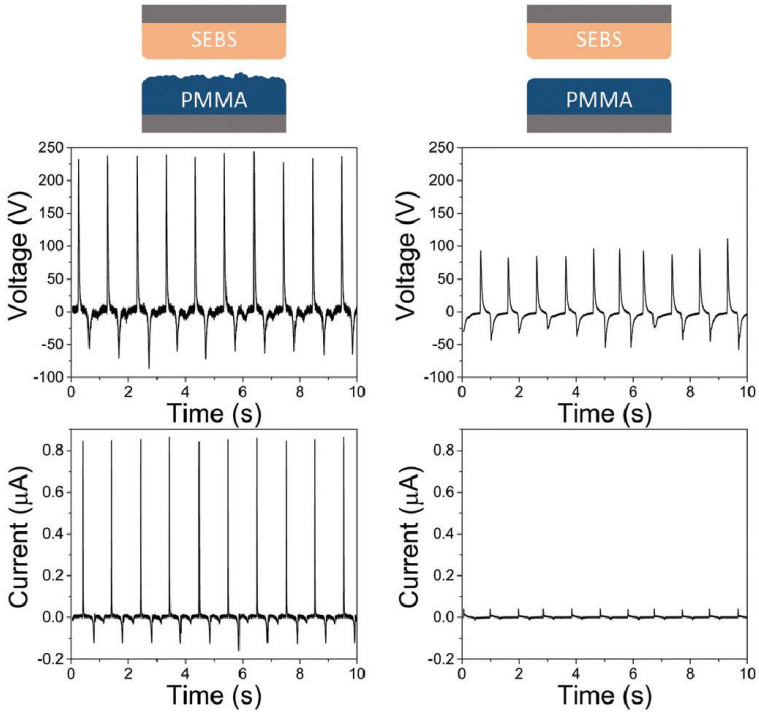

Fig. 14. Measured V_{OC} and I_{SC} values when elastomer SEBS is contacted against rough (left) and much smoother (right) PMMA film in TENG device.[107]

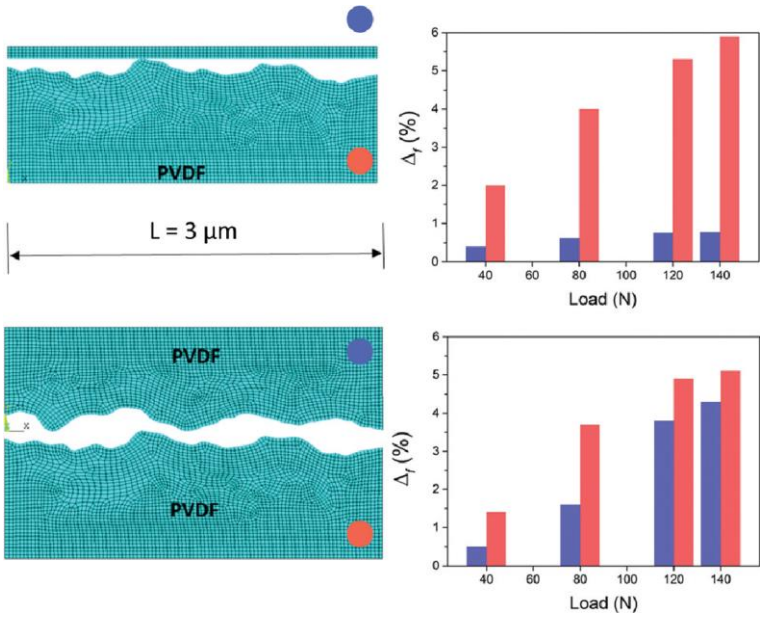

Fig. 15. Surface length percentage change (Δ_f) for each surface: in rough-smooth (top) or rough-rough (bottom) contacts.[107]

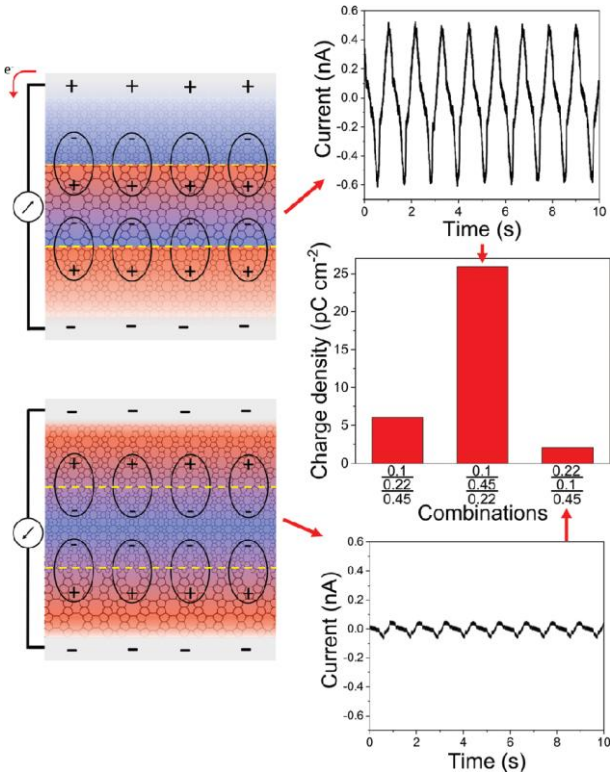

Fig. 16. Dipole and flexoelectric charge formation in multi-layered membrane samples with different membrane order.[107]

The main results and conclusions presented in Paper IV:

- TEG devices were prepared from two identical polymers that had the same (smooth-smooth or rough-rough) or different (smooth-rough) surface roughness. The selected polymers were: polyethylene-octene copolymer (EOC), polystyrene (PS), ethyl cellulose (EC),

polycarbonate (PC), poly(methyl methacrylate) (PMMA), styrene-ethylene-butylene-styrene copolymer (SEBS) and poly(vinylidene fluoride) (PVDF). TEGs with differing roughness generated greater V_{OC}, I_{SC}, and Q than the devices prepared from two alike films (Fig. 13 (a) and (b)).

- The differences in Q magnitude among polymers are due to the varying differences in surface roughness between the contacted films. The formation and uniformity of a rough polymer surface was observed: i) visually; ii) by measuring water droplet contact angle; and iii) by AFM surface topography measurements. A diffusive light reflection behaviour was visually observable for the obtained polymer films, which indicates the formation of rough surface. The contact angle of water droplet for the rough polymer film was observed higher than for the relatively smooth film, which points to hydrophobicity. Films with rough surface often possess hydrophobic properties. AFM topography measurements were used to determine the RMS surface roughness, and most of the polymers have notable differences in surface roughness of the smooth and rough films. PMMA and SEBS show similar RMS roughness values for the rough and smooth samples but different surface morphologies suggesting that the different morphology may affect surface charge formation.
- PVDF films with different surface roughness were prepared by precipitation from solutions in dimethylformamide (DMF) at different concentrations, using methanol as the non-solvent. The Q of contacted PVDF polymer films was measured as a function of the difference in surface roughness (Fig. 13 (c)). Surface roughness of samples was in a range 0.2–1 μm. As expected, the Q increased with higher difference in roughness.
- Scanning Kelvin Probe (SKP) was used to determine surface potential on smooth PVDF before and after contacting with another smooth or rough PVDF. Contact-separation against another smooth sample increased the average surface potential by 20 mV. However, after contact with rough PVDF, the surface potential increased by 243 mV.
- The influence of surface roughness on Q was also observed when polymers with distinctive physicochemical properties were used as the rough and smooth contact layers. Two TEG devices were compared: smooth elastomer SEBS layer against the relatively more rigid PMMA as smooth and rough layer. Higher values (V_{OC} of 240 V, I_{SC} of 0.85 mA, Q of 9.6 nC cm^{-2} and E of 2.5 mJ m^{-2}) were obtained when the relatively smooth SEBS was contacted against the rough PMMA (Fig. 14). In comparison, smooth SEBS combined with smooth PMMA yielded V_{OC} of 100 V, I_{SC} of 0.05 mA, Q of 1.2 nC cm^{-2} and E of 0.6 mJ m^{-2}.
- The observed triboelectrification from contact-separation of the same polymer but with different roughness is due to uneven deformation of each layer at the contacted area. It changes the charge density across the surface during relaxation.[108] The uneven deformation was confirmed by the 2D plane FEA model for a macro-scale simulation. The 2D model of surface configuration of rough samples was taken from PVDF surface AFM measurements. When the rough model was pressed against a smooth surface, the surface length percentage change (Δ_f) in lateral direction for two surfaces was different (at 140 N – 7.4 times). In contrast, when two rough models with similar roughness were contacted, the observed Δ_f on both was almost the same (at 140 N it differed only 1.2 times) (Fig. 15). The observed uneven

deformations result in heterolytic bond scission that creates mechano-ion polymer chain fragments, which contribute to net surface charge.

- The charge formation was also observed when loading and unloading two contacted polymer films without separation. Layered structures were prepared from commercially available PVDF membranes with different porosity (0.10 μm, 0.22 μm, and 0.45 μm). Both samples were loaded and unloaded without separation with forces ranging 5–100 N. As expected, I_{SC} and Q increased with higher difference in porosity between the membranes.
- Electromechanical response was further increased by constructing multi-layered films from all three aforementioned PVDF membranes. The largest Q of 26 pC cm^{-2} was measured from the multilayer film with a 0.45 μm pore size membrane in the middle (membranes with a pore size of 0.10 μm and 0.22 μm on each side, respectively). When the membrane with a pore size of 0.10 μm was placed in the middle, the measured order of magnitude Q was lower (Fig. 16). It can be explained by triboelectric dipole formation at the interface of two membranes. The membrane with a 0.45 μm pore size charged positively against the 10 μm pore size membrane but negatively charged against a 0.22 μm pore size membrane. Combined in a multi-layered structure they created two interfaces; each having a characteristic dipole direction. In this case both dipole directions matched and they intensified each other, thus magnifying the measured Q. However, when the membrane with a 0.1 μm pore size was placed in the middle, the dipoles formed at interface had opposite direction resulting in a much smaller Q.

Triboelectrification between polymer composites with identical polymer matrixes (Paper V)

It was previously shown in Papers I and IV that contact electrification between chemically identical polymers can yield a significant Q if there are differences in properties like macromolecule ordering, crosslinking degree or surface roughness. Similarly, triboelectric charge grew when difference in nanoparticle (NP) filler concentration between the two identical polymer matrix layers increased. This effect was observed in tests using different polymers (ethylene-vinyl acetate copolymer (EVA), polydimethylsiloxane (PDMS), polyvinyl acetate (PVAc) and polyurethane (PU)) and different filler NPs (TiO_2, FeO(OH), WO_3 and MnO_2). FEA simulations confirmed that polymer triboelectrification is related to the surface viscoelastic deformation that occurs during mechanical contact and separation. This points to the probability that heterolytic scission of covalent bonds in polymer chains is the explanation for the triboelectricity.

The main goal of Paper V was to explore triboelectrification between chemically identical polymer composites with different NP contents. The tasks set to achieve this goal were:

- to explore contact-electrification between polymer composites using TiO_2 as the filler in different concentrations;
- to explore contact-electrification between EVA polymer composites with different types of fillers;
- to investigate the mechanical processes during contact-separation process using FEA.

The main results of triboelectric measurements are demonstrated in Figs. 17–19.

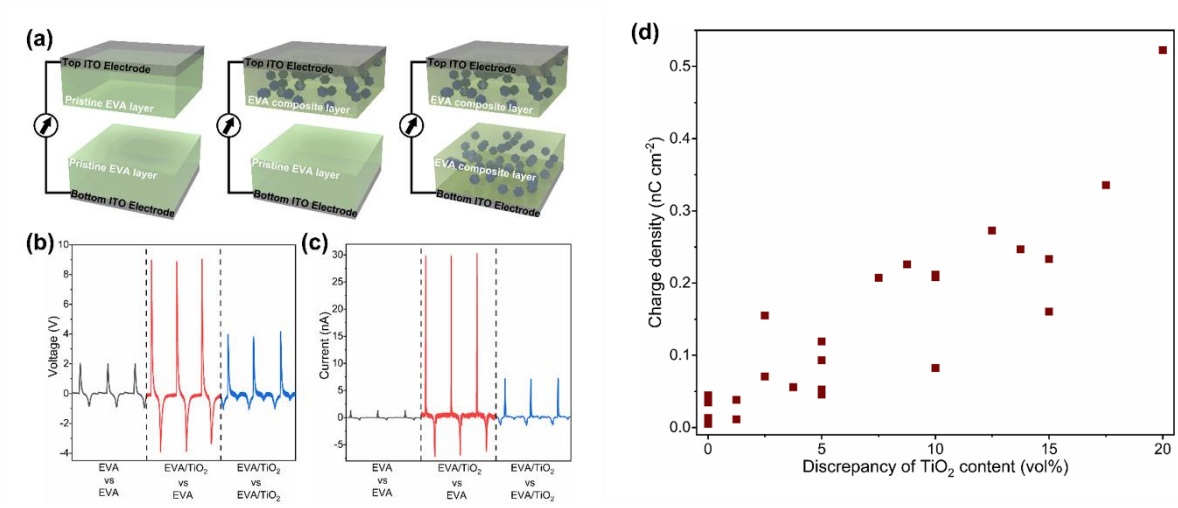

Fig. 17. (a) Schematics of three types of TEG devices using pristine EVA polymer and/or EVA-based composites; (b) V_{OC} peaks generated by the three TEG devices; (c) I_{SC} peaks generated by the three TEG devices; (d) increased difference between the TiO_2 content in EVA layers used for TEG devices leads to increased triboelectric surface charge density.[109]

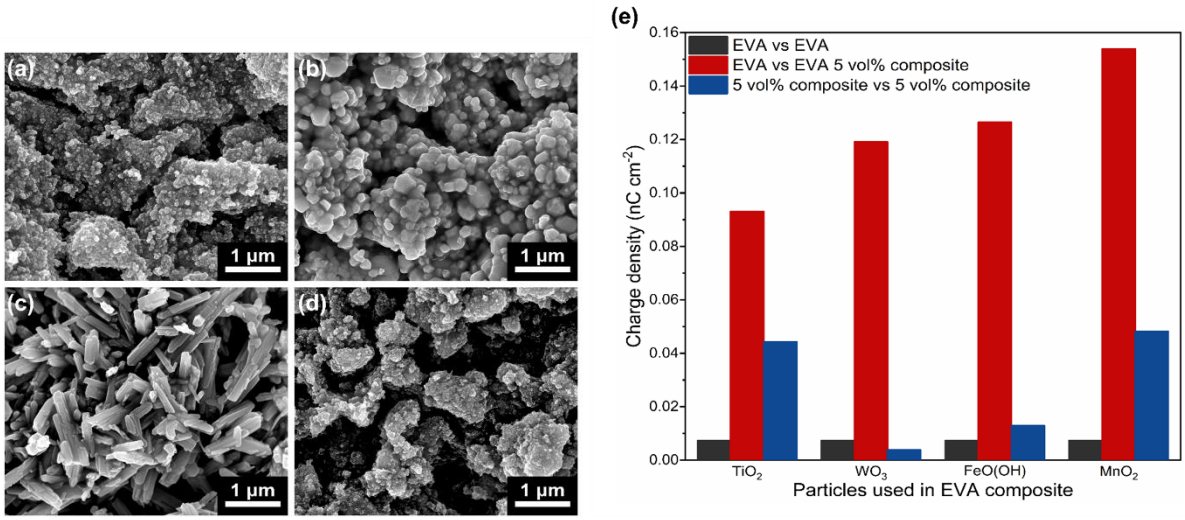

Fig. 18. (a) TiO_2 NP SEM images; (b) WO_3 NP SEM images; (c) FeO(OH) NP SEM images; (d) MnO_2 NP SEM images; (e) the generated surface charge density of three types of TEG devices based on pristine EVA polymer and EVA/5 vol% NPs composites using various NPs as fillers.[109]

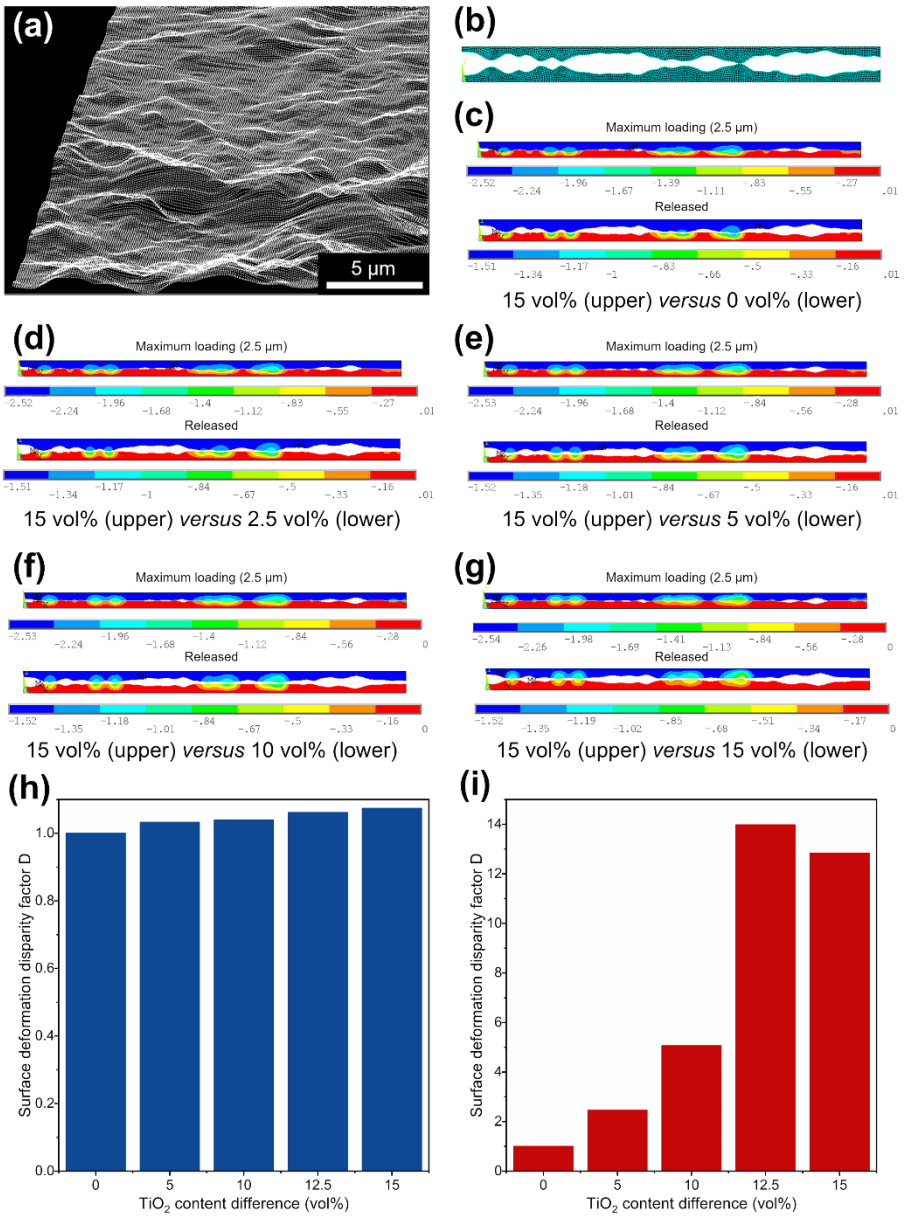

Fig. 19. (a) AFM surface topology of 15 vol% TiO_2 NPs-containing composite; (b) 2D-mesh simulation model for calculations; (c) 15 vol% (upper) and 0 vol% (lower) composite deformation simulation model, (d) 15 vol% and 2.5 vol% composite deformation simulation model; (e) 15 vol% and 5 vol% composite deformation simulation model; (f) 15 vol% and 10 vol% composite deformation simulation model; (g) both 15 vol% composite deformation simulation models; (h) *D* as a function of differences in TiO_2 concentration in the simulations during maximum loading; (i) *D* as a function of differences in TiO_2 concentration in the simulations after release. Colour bar uses μm-scale.[109]

The main results and conclusions presented in Paper V:

- Contact between identical triboelectric layers with the same particles in the same concentrations resulted in small I_{SC} and V_{OC} peaks (Fig. 17 (a), leftmost and rightmost panels). In contrast, much higher I_{SC} and V_{OC} peaks were produced when the polymer matrix was the same but both triboelectric layers had different concentrations of filler particles (Fig.

17 (a), middle panel). This tendency particularly clearly manifested in the case of pristine EVA polymer and its matrix-based composites with 5 vol% TiO_2 NP filler (Figs. 17 (b) and (c)). Triboelectric *Q* increased by an order of magnitude from 0.007 nC cm^{-2} to 0.093 nC cm^{-2}. This phenomenon was consistently observed during the tests of other pristine polymers and their matrix-based composites, including PVAc, PU, and PDMS matrixes with the TiO_2 NPs filler. The results illustrate that higher surface charges are consistently induced across all types of polymers when a pristine polymer contacts a composite layer.

- Surface charge increased as the difference in concentration of TiO_2 NPs in the composite increased. Figure 17 (d) shows the triboelectric *Q* generated on the TEGs comprised of EVA/TiO_2 composites with different concentrations of TiO_2 NPs in triboelectric layers. The results strongly suggest that the difference in composite NP concentration determines the triboelectric charges of polymer-based composites and not the absolute value of concentration. This points out that the mechanical properties of a composite related to the mass transfer mechanism are more important for triboelectricity than the dielectric properties associated with the electronic or ionic transfer mechanisms.
- While triboelectrification is dependent on the particle filler concentration, it is not a function of particle composition or shape. EVA composites based on different NPs filler types (TiO_2, FeO(OH), WO_3 and MnO_2) (Figs. 18 (a)–(d)) were created to demonstrate that the chemical structure of filler does not influence the triboelectric charge generation. SEM images confirm that WO_3 NPs are larger than TiO_2 NPs, while FeO(OH) NPs are needle-shaped rather than sphere-shaped. The water contact angle (CA) of the aforementioned composites was determined to evaluate their impact on the surface energy of composites. For the composites with TiO_2, MnO_2, WO_3, and FeO(OH) fillers, CA was determined to be 96.9 ± 0.4°, 92.9 ± 1.6°, 89.2 ± 2.4°, and 98.1 ± 1.0°, respectively. As expected, the impact is negligible, indicating that the filler mainly influences the mechanical properties. Although the absolute values of generated triboelectric *Q* may vary according to the filler type due to dispersion homogeneity and other secondary effects, the trend was consistent across all cases; triboelectric charges between different composition composites were always the highest (Fig. 18 (e)). The observed correlations once more confirm that electron transfer is not responsible for polymer triboelectrification.
- The reason for stronger triboelectrification during mechanical contact between identical polymer matrixes with different filler particle concentrations relates to the differences in the surface deformation and the associated differences in mechanical properties as described in Paper IV.[107] Majority of NPs is encapsulated inside the polymer matrix, thus not influencing surface morphology, however, it affects the Young's modulus of the composite. The Young's modulus of 2.20 MPa for 0 vol% TiO_2 NPs rises to 7.10 MPa for 15 vol% TiO_2 NPs. Mechanical contact-separation of composite layers with different filler contents causes unequal deformation of each layer. This induces different stress on each of the triboelectric surfaces and yields differences in mass transfer for each surface. But when polymer surfaces are under equal deformation, the bi-directional mass transfer between surfaces occurs with the same probability, resulting in a small net triboelectric charge.

- Uneven deformation at the triboelectric surfaces was also confirmed by the FEA simulations of the pristine EVA (0 vol%) and the EVA composites (TiO_2 NPs filler concentrations of 2.5, 5, 10, and 15 vol%) using ANSYS R17.1 software. The surface configuration of the 2D models was taken from atomic force microscopy (AFM) measurements (Figs. 19 (a) and (b)). As presented in Figs. 19 (c)–(f), one surface was fixed as a 15 vol% composite surface, while the counterpart surfaces were changed from 0 vol% to 15 vol%. Macroscale simulations describe the surface deformation during mechanical loading and after unloading. In the situation where mechanical contact between two deformable bodies with identical mechanical properties resulted in equal surface deformation *D* was 1 (Figs. 19 (h) and (i)). When surfaces with different TiO_2 contents (difference of 15 vol%) contacted each other, the surface deformation disparity ratio increased from 1 to ~1.07 during the maximum contact loading (Fig. 19 (h)). However, after the mechanical release of the triboelectric surfaces, the surface deformation disparity increased to as high as ~14 (Fig. 19 (i)). In contrast, the triboelectric surfaces of small concentration differences continued to show low deformation disparity. The simulation results illustrate a trend of higher differences in TiO_2 NPs content leading to elevated levels of uneven deformation and relaxation of surfaces. These results are consistent with the contact electrification measurements and support the conclusion that uneven deformation and subsequent surface relaxation are responsible for mass transfer mechanism-based surface triboelectric charge generation, as they encourage heterolytic bond scission of polymer chains.

Hybrid tribo-piezo-electric nanogenerator (Paper VI)

Hybrid TEG devices utilizing ferroelectric materials as triboelectric contacting materials were mentioned in Introduction as one of approaches to achieve high energy harvesting performance. In Paper VI, this strategy was applied by creating triboelectric layers from ferroelectric PVDF/$BaTiO_3$ composites. Both composite films were identical and polarized using electric field but in inverse directions, so that during contact-separation polarization would coincide. A clear correlation between the piezoelectric response of PVDF/$BaTiO_3$ nanocomposite films and the performance of the TEG devices based on these films was demonstrated. The observation is explained by magnified electrostatic induction driven by the ferroelectric properties of these films. A double capacitor model was proposed to portray the interactions between ferroelectric layers during contact-separation and subsequent charge redistributions in the external circuit. This allowed to reach state-of-the-art TEG V_{OC} of 2.7 kV.

The main goal of Paper VI was to investigate the influence of ferroelectricity on the performance of TEG device.

The main results of the triboelectric measurements are demonstrated in Figs. 20 and 21.

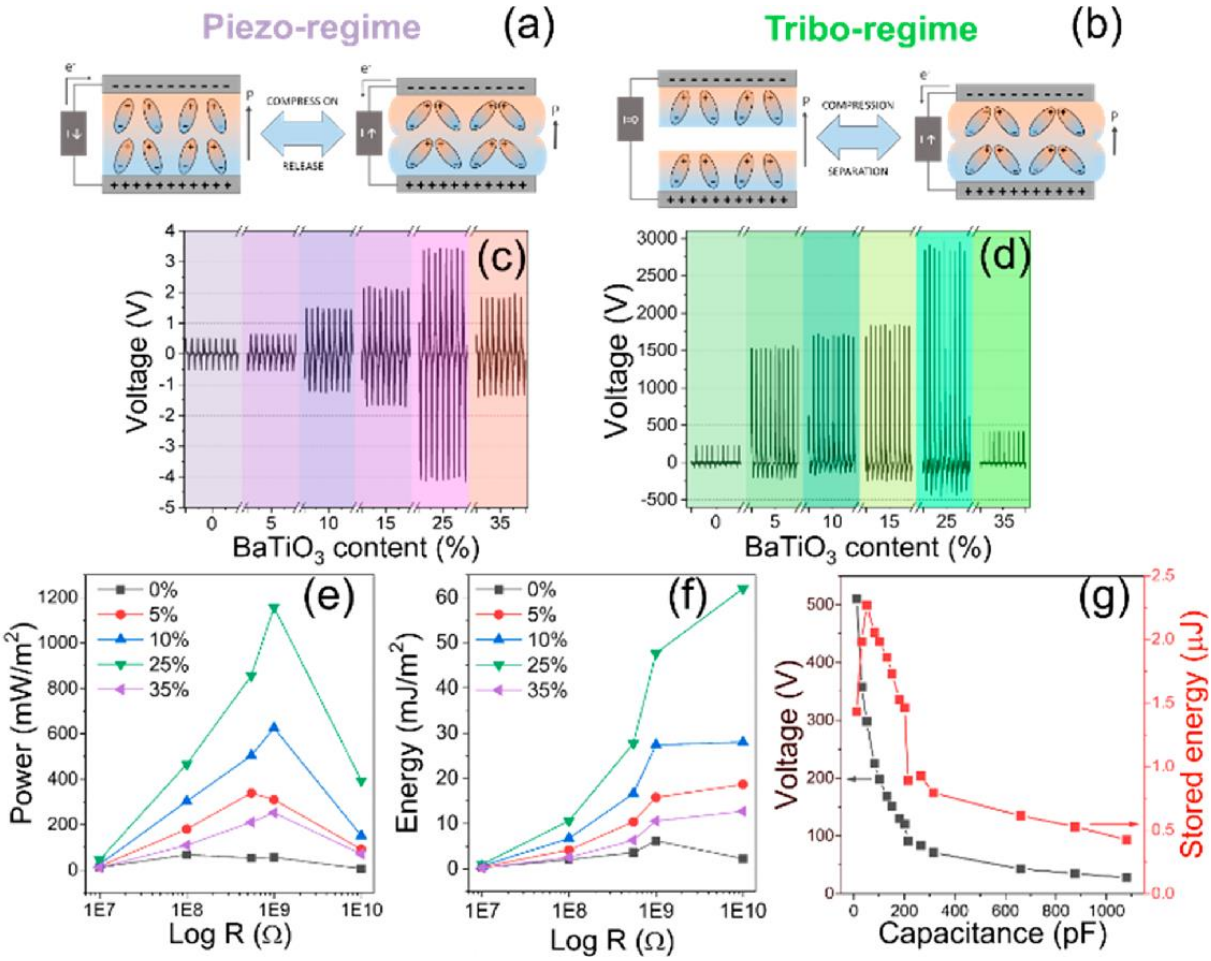

Fig. 20. Schematic representation of piezo (a) and TEG (b) testing regimes. The open circuit output voltage measured at load resistance 1×10^{10} Ω in piezo (c) and TEG (d) regimes. Graphs at the bottom show power (e) and energy (f) for different compositions tested in the TEG regime. Energy stored in the capacitor (g) was determined for the nanocomposite showing the highest performance (PVDF/$BaTiO_3$ 25 vol %).[110]

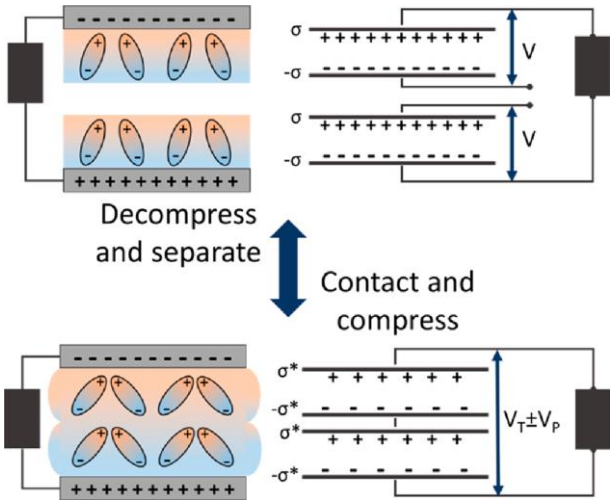

Fig. 21. Double capacitor model and corresponding contact-separation stages. Dipoles in the schematic here represent both PVDF and $BaTiO_3$ dipoles in ferroelectric layers.[110]

The main results and conclusions presented in Paper VI:

- Prepared ferroelectric PVDF/$BaTiO_3$ films were tested in piezoelectric mode (Fig. 20 (a)) and also used as contacting layers in a TENG device (Fig. 20 (b)). As observed in Figs. 20 (c) and (d), the PVDF containing 25 vol% of $BaTiO_3$ shows the highest V_{OC} both in piezoelectric and contact-separation mode, indicating a correlation between piezoelectric response and the corresponding performance of a nanocomposite film TEG device. The TEG from polarized pure PVDF layers produced a V_{OC} value of 250 V, while the generator from the PVDF/$BaTiO_3$ (25 vol%) nanocomposite generated 2700 V. The observed V_{OC} was state-of-the-art value for TEG devices. Boosted performance of ferroelectric nanocomposite TEG devices in comparison to the ones using pure PVDF relates to a higher ferroelectric polarization of contact layers, evident as improved piezoelectric response.
- The power density of PVDF/$BaTiO_3$ (25 vol% content) based TEG reached 1.157 W m^{-2} under an optimized load resistance of 10^9 Ω (Fig. 20 (e)), whereas energy density reached 65.95 mJ m^{-2} (Fig. 20 (f)). The same TEG device was used to charge a variable capacitor circuit. Figure 20 (g) depicts energy stored in the capacitor (and the corresponding voltage of the charged state) for each capacitor value after contact between the two ferroelectric layers. The highest energy stored in a capacitor after a single contact-separation step (2.27 μJ) was reached when the capacitance of the capacitor circuit was set to 50 pF.
- The piezoelectric response allowed calculation of the piezoelectric coefficient d_{33}, which for the 25 vol% $BaTiO_3$ composites reached 47.9 pC N^{-1}. The reported values of similar nanocomposites are in the range from 2.7 to 25 pC N^{-1}.[111,112] A greater d_{33} can be related to a significantly larger deformability due to high porosity (around 70 %) of the samples. Porosity provides space for local deformations in the material that are important for piezoelectric charge generation and boost the formation of ferroelectric β-PVDF during fabrication.[113] The d_{33} of a dense composite was determined to be only 9.11 pC N^{-1}.
- A double capacitor model was proposed to explain the enhanced TEG device output and change of potential difference between electrodes (Fig. 21). Accordingly, each ferroelectric layer was considered as an individual capacitor with a *Q*, which is induced during polarization. As layers come together and contact, they form a circuit of two identical capacitors in series, and the total capacitance of two layers decreases; however, the voltage increases. Next, compression of both layers induces piezoelectric charge formation as intrinsic dipoles deform and the net polarization of layers drops. As a result, *Q* decreases but since it is followed by fast separation of the compressed ferroelectric layers the net polarization quickly rises and *Q* returns to the initial value. During separation, the potential difference decreases, which induces additional redistribution of induced charges between electrodes in the external circuit.

Matching dipoles from the triboelectric and ferroelectric charges in TEG (Paper VII)

Paper VI demonstrated that incorporation of ferroelectric dipoles in the contacting polymer layers enhances the performance of TEG devices, however, as mentioned in Paper IV, a triboelectric dipole is also formed between the two contacting surfaces during contact-separation. The combined influence of dipoles formed by the triboelectric surface charges between the distinct triboelectric materials and the dipoles in the two contacting ferroelectric films previously had been ignored in all relevant studies. Therefore, in Paper VII we demonstrated that proper attention to the alignment of both dipole types can lead to four times higher energy and power density output in comparison to mismatched dipole arrangement. The presented strategy and understanding of stronger electrostatic induction in the contacting layers enable the development of TEG devices with greatly enhanced properties.

The main goal set forward by Paper VII was to investigate the influence of triboelectric and ferroelectric dipole matching when two distinct ferroelectric polymer composites are used to prepare TEG devices.

The main results of the triboelectric measurements are demonstrated in Figs. 22–25.

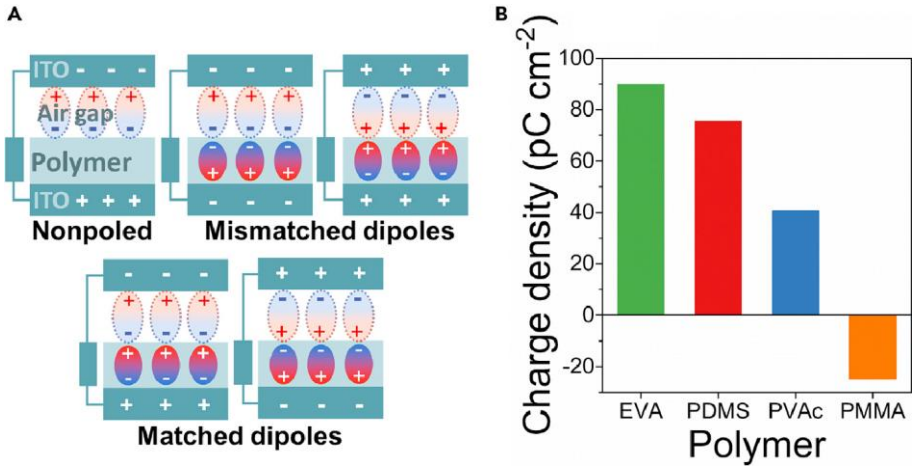

Fig. 22. A) Schematic representation of possible interactions between surface charge dipoles in the air gap and ferroelectric dipoles in TEG device; B) the calculated surface charge density of non-ferroelectric polymers.[114]

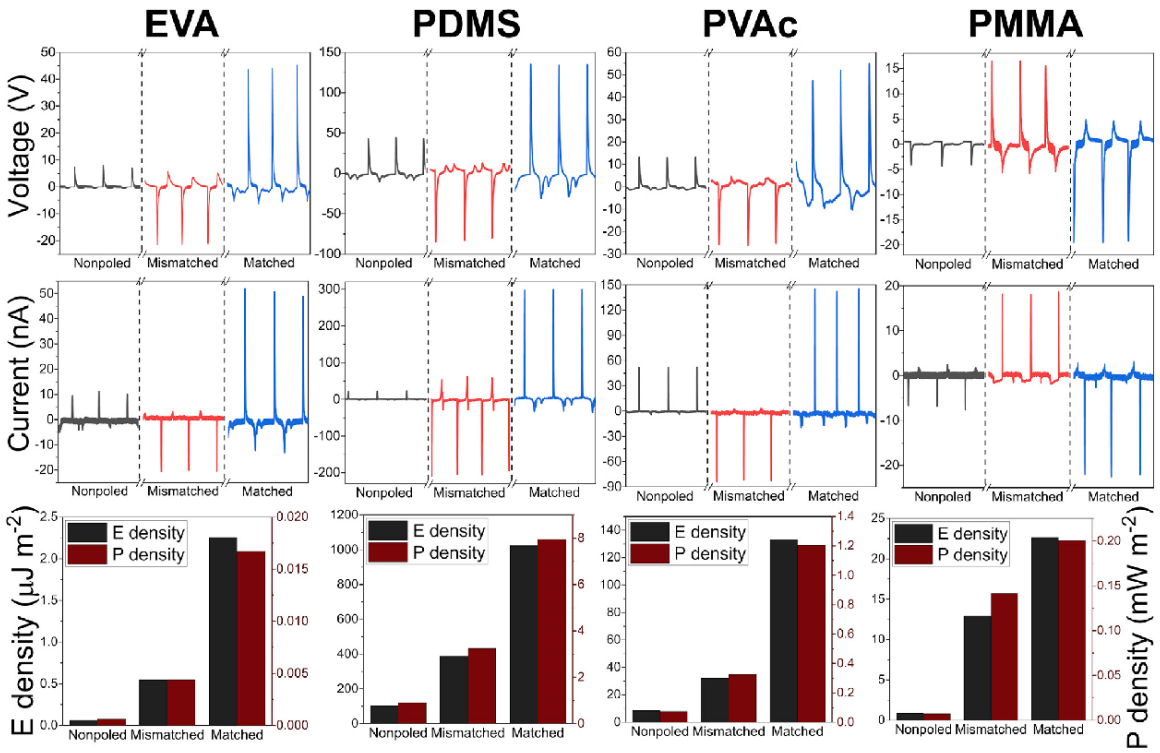

Fig. 23. Comparison of three possible dipole alignment configurations (non-poled, mismatched and matched) shown by V_{OC}, I_{SC}, energy and power density for each $BaTiO_3$/polymer composite.[114]

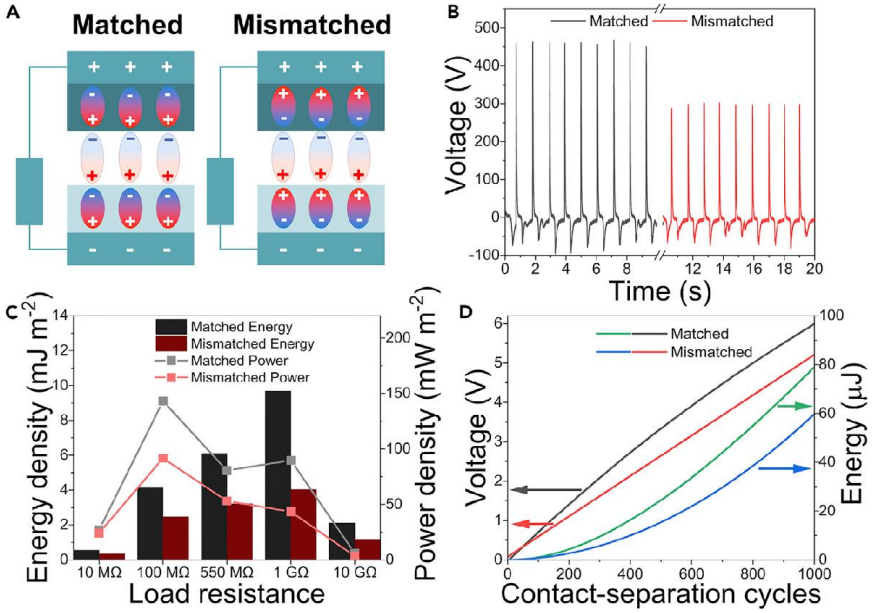

Fig. 24. A) inversely polarized $BaTiO_3$/PDMS (top layer) and $BaTiO_3$/PMMA (bottom layer) TEG device constructed in a way that ferroelectric polarization direction is matched (left) and mismatched (right) with contact-electrification-generated surface charge dipole direction; B) V_{OC} (at 1 GΩ) for matched and mismatched TEG device; C) comparison of energy and power density for matched and mismatched TEG device during one contact-separation cycle; D) voltage across the 4.4 μF capacitor during charging from a matched and mismatched TEG device with the corresponding stored energy.[114]

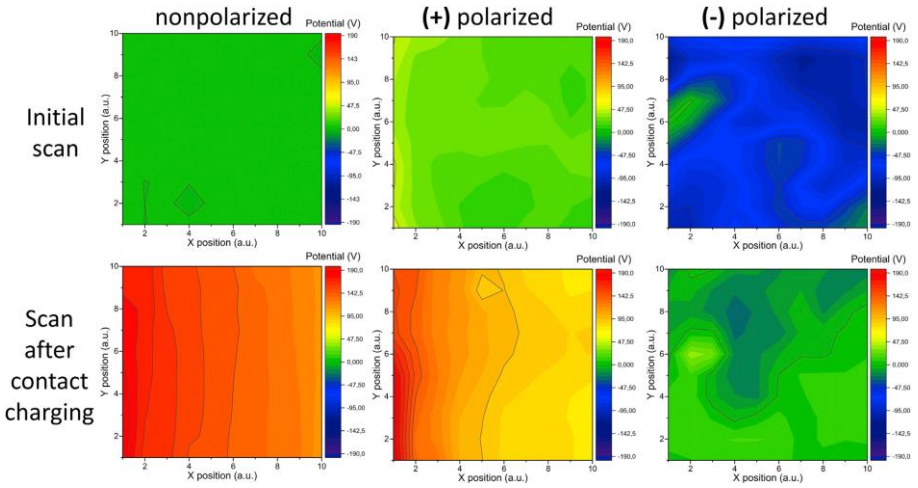

Fig. 25. Surface potential maps of three $BaTiO_3$/PDMS composites (nonpolarized, positively and negatively polarized) by measuring the potential before (to row) and after (bottom row) after contact with PMMA.[114]

The main results and conclusions presented in Paper VII:

- To achieve a high energy harvesting performance of TEG device, the alignment direction of ferroelectric dipoles has to coincide with the direction of dipoles forming between the triboelectric charges on opposite contacting surfaces as demonstrated in Fig. 22 (a). The polarity of triboelectric charge formed on pure polymers after the contact against ITO was determined by measuring the current between the underlying electrode and the ground in Faraday cup mode. Polymers PDMS, PVAc and EVA obtained a negative charge on their surface, while for PMMA a positive charge was observed (Fig. 22 (b)). The polarity did not change when nonpolarized $BaTiO_3$ nanoparticles were incorporated into the polymers.
- After polarization all $BaTiO_3$/polymer composites exhibited piezoelectric properties and piezoelectric charges of 2.9 pC cm^{-2}, 10.9 pC cm^{-2}, 3.7 pC cm^{-2}, and 2.4 pC cm^{-2} were measured for $BaTiO_3$/EVA, $BaTiO_3$/PDMS, $BaTiO_3$/PVAc and $BaTiO_3$/PMMA composites, respectively.
- Figure 23 shows I_{SC} and V_{OC} at 1 GΩ load resistance for TEG devices based on composite and ITO layers. The composite layer in each TEG device was tested not only as non-poled but also positively and negatively poled, so that ferroelectric dipole is matched and mismatched with the previously determined triboelectric Q. Regardless of the polymer, TEG devices showed higher values at matched condition. Net dipole direction between triboelectric Q was also confirmed by COMSOL finite element simulation. The experiments show that the TEG device has higher performance (I_{SC}, V_{OC}, energy and power density) when the direction of triboelectric dipoles and ferroelectric dipoles are matched.
- Further, we constructed TEG devices with two $BaTiO_3$/polymer composite films used as contact layers. For the highest performance, both films were polarized inversely,[110] while the polymer matrix material for each side was chosen so that the dipole moment direction of triboelectric and ferroelectric charges are matched or mismatched. Accordingly, a TEG device was constructed from PMMA and PDMS since PMMA charges positively and PDMS negatively. A schematic representation of devices is shown in Fig. 24 (a). The V_{OC} of device

with matched dipoles reached 460 V as shown in Fig. 24 (b), but the energy and power densities of this TEG device reached 9.7 mJ m^{-2} and 143.2 mW m^{-2}, respectively (black bars and grey line in Fig. 24 (c)). The mismatched TEG device exhibited a significantly lower output – V_{OC} of 300 V (red line in Fig. 24 (b)) and instant energy and power densities of 4.0 mJ m^{-2} and 91.6 mW m^{-2} (red bars and red line in Figure 24 (c)). For comparison, a TEG device from the same polymers without $BaTiO_3$ NPs showed V_{OC} as small as 16 V and three orders of magnitude smaller energy and power densities of 0.012 mJ m^{-2} and 0.104 mW m^{-2}.

- The average surface potential for non-polarized $BaTiO_3$/PDMS was determined to be 0.06 V by SKP. After contact with PMMA, the average potential had increased to 146.4 V (Fig. 25). Surface potential scanning was also performed on both positively and negatively polarized $BaTiO_3$/PDMS samples before and after contacting with PMMA. For the positively polarized $BaTiO_3$/PDMS the average potential value grew from 24.3 V to 107.2 V and from –70.5 V to –1.1 V in the case of the negatively polarized $BaTiO_3$/PDMS. All surfaces show tendency to charge positively after contact with PMMA, as evidenced by more positive surface potential. A gradual decrease of potential in the direction from left to right is observed because the triboelectric charge decreases as the surface is being scanned in this direction. Experimental results confirm the proposed mechanism for higher output of TEG devices where two sources of the electric field are present – triboelectric charges and ferroelectric dipoles.
- Both matched and mismatched TEG device constructed from inversely polarized $BaTiO_3$/PDMS and $BaTiO_3$/PMMA composite films were used to charge a 4.4 μF capacitor. For the matched TEG, after 1000 contact-separation cycles the voltage across the capacitor increased by 6.0 V corresponding to stored energy of 79 μJ (Fig. 24 (d)). In the meantime, the TEG device with mismatched dipoles increased the voltage across the capacitor only by 5.2 V and accumulated 60 μJ energy under the same operating conditions. The proof-of-concept demonstrated here can be further used to construct TEG devices with record-high performance, since polymers with far more superior tendency for triboelectrification[98] and polymer composite materials with high intrinsic piezoelectric responses have been reported in literature widely.[14,115,116] A combination of methodology shown in this paper with high-performance ferroelectric materials could bring the TENG research community closer to new cutting-edge discoveries.

CONCLUSIONS

1. Polymers with lower elastic modulus and cohesive energy density obtain higher triboelectric charge density if contacted with hard material. In cases when two polymers are contacted, higher triboelectric charge is created when polymers show the most distinct elastic modulus and hardness. It is evident from tests that polymer triboelectrification is governed by its mechanical properties not chemical or dielectric properties.
2. Triboelectrification can be also observed in contact-separation of chemically identical polymers when contacted polymers have differences in properties such as macromolecular ordering degree, crosslinking degree or surface roughness. The more intense is the difference in particular parameter between contacted polymers, the higher is the generated triboelectric charge density.
3. Higher surface adhesiveness can improve the material transfer and, therefore, enhance the surface charge on polymer. However, high adhesiveness is detrimental to efficiency of TEG devices, since it demands higher mechanical energy input for separation.
4. AFM and XPS analysis of surfaces contact-separated with polymers containing a heteroatom (e.g., Si, F or Cl) allows to conclude that polymer triboelectrification occurs alongside the transfer of polymer macromolecule fragments.
5. Incorporation of ferroelectric materials in TEG contact layers is an efficient method to raise the energy harvesting performance. More importantly, it can be further enhanced if the direction of ferroelectric dipole is matched with the direction of the triboelectric dipole that forms between the negative and positive charges on contacted polymers.

REFERENCES

(1) ONiO. What is energy harvesting? https://www.onio.com/article/what-is-energy-harvesting.html.

(2) Karami, M. A.; Inman, D. J. *Appl. Phys. Lett.* **2012**, *100*, 042901.

(3) Temp. And Humidity Sensor With A CR2032 For Over 1 Year! https://create.arduino.cc/projecthub/musskopf/temp-and-humidity-sensor-with-a-cr2032-for-over-1-year-580114.

(4) Liu, X.; Chen, T.; Qian, F.; Guo, Z.; Lin, F. X.; Wang, X.; Chen, K. Characterizing Smartwatch Usage in the Wild. *MobiSys 2017* – Proceedings of the 15th Annual International Conference on Mobile Systems, Applications, and Services, 2017, 385.

(5) Culman, C.; Aminikhanghahi, S.; Cook, D. J. *Sensors* **2020**, *20*, 310.

(6) Gray, C. Energy Consumption of Internet of Things Applications and Services. PhD Thesis, University of Melbourne, Melbourne, 2018.

(7) Smart home spot. My Xiaomi Bluetooth Temperature Humidity Sensor Review https://medium.com/@smarthomespot/my-xiaomi-bluetooth-temperature-humidity-sensor-review-d37b32ab1d0.

(8) Curie, J.; Curie, P. *Bull. Minéralogie* **1880**, 90.

(9) Bhalla, A. S.; Guo, R.; Roy, R. *Mater. Res. Innov.* **2000**, *4*, 3.

(10) Park, D. Y.; Joe, D. J.; Kim, D. H.; Park, H.; Han, J. H.; Jeong, C. K.; Park, H.; Park, J. G.; Joung, B.; Lee, K. J. *Adv. Mater.* **2017**, *29*, 1702308.

(11) Soin, N.; Shah, T. H.; Anand, S. C.; Geng, J.; Pornwannachai, W.; Mandal, P.; Reid, D.; Sharma, S.; Hadimani, R. L.; Bayramol, D. V.; Siores, E. *Energy Environ. Sci.* **2014**, *7*, 1670.

(12) Lund, A.; Rundqvist, K.; Nilsson, E.; Yu, L.; Hagström, B.; Müller, C. *npj Flex. Electron.* **2018**, *2*, 9.

(13) Singh, D.; Choudhary, A.; Garg, A. *ACS Appl. Mater. Interfaces* **2018**, *10*, 2793.

(14) Jeong, C. K.; Baek, C.; Kingon, A. I.; Park, K. Il; Kim, S. H. *Small* **2018**, *14*, 1.

(15) Bodkhe, S.; Turcot, G.; Gosselin, F. P.; Therriault, D. *ACS Appl. Mater. Interfaces* **2017**, *9*, 20833.

(16) Suzuki, Y.; Miki, D.; Edamoto, M.; Honzumi, M. *J. Micromechanics Microengineering* **2010**, *20*, 104002.

(17) Mitcheson, P. D.; Miao, P.; Stark, B. H.; Yeatman, E. M.; Holmes, A. S.; Green, T. C. *Sensors Actuators, A Phys.* **2004**, *115*, 523.

(18) Chiu, Y.; Kuo, C.-T.; Chu, Y.-S. *Symp. Des. Test Integr. Packag. MEMS/MOEMS* **2007**.

(19) Moretti, G.; Rosset, S.; Vertechy, R.; Anderson, I.; Fontana, M. *Adv. Intell. Syst.* **2020**, *2*, 2000125.

(20) Opris, D. M. *Adv. Mater.* **2018**, *30*, 1.

(21) Hillenbrand, J.; Sessler, G. M. *IEEE Trans. Dielectr. Electr. Insul.* **2004**, *11*, 72.

(22) Fan, F.-R.; Tian, Z.-Q.; Lin Wang, Z. *Nano Energy* **2012**, *1*, 328.

(23) Wang, S.; Lin, L.; Wang, Z. L. *Nano Lett.* **2012**, *12*, 6339.

(24) Wang, S.; Lin, L.; Xie, Y.; Jing, Q.; Niu, S.; Wang, Z. L. *Nano Lett.* **2013**, *13*, 2226.

(25) Lin, Z.; Zhang, B.; Zou, H.; Wu, Z.; Guo, H.; Zhang, Y.; Yang, J.; Wang, Z. L. *Nano Energy* **2020**, *68*, 104378.
(26) Zheng, Q.; Zhang, H.; Shi, B.; Xue, X.; Liu, Z.; Jin, Y.; Ma, Y.; Zou, Y.; Wang, X.; An, Z.; Tang, W.; Zhang, W.; Yang, F.; Liu, Y.; Lang, X.; Xu, Z.; Li, Z.; Wang, Z. L. *ACS Nano* **2016**, *10*, 6510.
(27) Zheng, Q.; Shi, B.; Fan, F.; Wang, X.; Yan, L.; Yuan, W. **2014**, 5851.
(28) Ma, Y.; Zheng, Q.; Liu, Y.; Shi, B.; Xue, X.; Ji, W.; Liu, Z.; Jin, Y.; Zou, Y.; An, Z.; Zhang, W.; Wang, X.; Jiang, W.; Xu, Z.; Wang, Z. L.; Li, Z.; Zhang, H. *Nano Lett*. **2016**, *16*, 6042.
(29) Zheng, Q.; Zou, Y.; Zhang, Y.; Liu, Z.; Shi, B.; Wang, X.; Jin, Y.; Ouyang, H.; Li, Z.; Wang, Z. L. *Sci. Adv*. **2016**, 1–10.
(30) Tang, W.; Tian, J.; Zheng, Q.; Yan, L.; Wang, J.; Li, Z.; Wang, Z. L. *ACS Nano* **2015**, *9*, 7867.
(31) Kim, M.; Park, D.; Alam, M. M.; Lee, S.; Park, P.; Nah, J. *ACS Nano* **2019**, *13*, *4640.*
(32) Fang, C.; Tong, T.; Bu, T.; Cao, Y.; Xu, S.; Qi, Y.; Zhang, C. *Adv. Intell. Syst*. **2020**, *2*, 1900129.
(33) Pham, R.; Virnelson, R. C.; Sankaran, R. M.; Lacks, D. J. *J. Electrostat*. **2011**, *69*, 456.
(34) Dzhardimalieva, G. I.; Yadav, B. C.; Lifintseva, T. V.; Uflyand, I. E. *Eur. Polym. J*. **2021**, *142*, 110163.
(35) Zhang, X.; Han, M.; Wang, R.; Meng, B.; Zhu, F.; Sun, X.; Hu, W.; Wang, W.; Li, Z. *Nano Energy* **2014**, *4*, 123.
(36) Li, J.; Shepelin, N. A.; Sherrell, P. C.; Ellis, A. V. *Chem. Mater*. **2021**, *33*, 4304.
(37) Kil, B.; Woong, J.; Soo, H.; Hoon, J. *Nano Energy* 2015, 15, 523.
(38) Song, G.; Kim, Y.; Yu, S.; Kim, M. O.; Park, S. H.; Cho, S. M.; Velusamy, D. B.; Cho, S. H.; Kim, K. L.; Kim, J.; Kim, E.; Park, C. *Chem. Mater.* **2015**, *27*, 4749.
(39) Chu, H.; Jang, H.; Lee, Y.; Chae, Y.; Ahn, J. *Nano Energy* **2016**, *27*, 298.
(40) Newman, B. A.; Chen, P.; Pae, K. D.; Scheinbeim, J. I. *J. Appl. Phys.* **1980**, *51*, 5161.
(41) Haller, C. B.; Knobbe, A. J.; Crum, G. W. Tribo-Electric Powder Spray Gun. EP0592137A1, 1994.
(42) Williams, M. W. *Am. Scientist* **2012**, *100*, 316.
(43) Ohsawa, A. *J. Electrostat*. **2017**, *88*, 171.
(44) Faraday, M. *Mag. J. Sci*. **1845**, *26*, 16.
(45) Baytekin, H. T.; Baytekin, B.; Hermans, T. M.; Kowalczyk, B.; Grzybowski, B. A. *Science* **2013**, *341*, 1368.
(46) Tamminen, P.; Ukkonen, L.; Sydänheimo, L. *J. Electrostat*. **2016**, *79*, 38.
(47) Salama, F.; Sowinski, A.; Atieh, K.; Mehrani, P. *J. Electrostat*. **2013**, *71*, 21.
(48) Pingali, K. C.; Hammond, S. V.; Muzzio, F. J.; Shinbrot, T. *Int. J. Pharm*. **2009**, *369*, 2.
(49) Pu, Y.; Mazumder, M.; Cooney, C. *J. Pharm. Sci*. **2009**, *98*, 2412.
(50) Fotovat, F.; Bi, X. T.; Grace, J. R. *Chem. Eng. Sci*. **2017**, *173*, 303.
(51) Mehrani, P.; Murtomaa, M.; Lacks, D. J. *J. Electrostat*. **2017**, *87*, 64.
(52) Burgo, T. A. L.; Silva, C. A.; Balestrin, L. B. S.; Galembeck, F. *Sci. Rep*. **2013**, *3*, 1.

(53) Sayfidinov, K.; Cezan, S. D.; Baytekin, B.; Baytekin, H. T. *Sci. Adv.* **2018**, *4*, 1. https://doi.org/10.1126/sciadv.aau3808.
(54) Chen, J.; Wang, Z. L. *Joule* **2017**, *1*, 480.
(55) Sherrell, P. C.; Sutka, A.; Shepelin, N. A.; Lapcinskis, L.; Verners, O.; Germane, L.; Timusk, M.; Fenati, R. A.; Malnieks, K.; Ellis, A. V. *ACS Appl. Mater. Interfaces* **2021**. *13*, 44935.
(56) Gooding, D. M.; Kaufman, G. K. Tribocharging and the Triboelectric Series. Encyclopedia of Inorganic and Bioinorganic Chemistry, Wiley, 2019.
(57) Diaz, A. F.; Felix-Navarro, R. M. *J. Electrostat*. **2004**, *62*, 277.
(58) Henniker, J. *Nature* **1962**, *196*, 474.
(59) Xu, C.; Zhang, B.; Wang, A. C.; Zou, H.; Liu, G.; Ding, W.; Wu, C.; Ma, M.; Feng, P.; Lin, Z.; Wang, Z. L. *ACS Nano* **2019**, *13*, 2034.
(60) Wen, X.; Su, Y.; Yang, Y.; Zhang, H.; Wang, Z. L. *Nano Energy* **2014**, *4*, 150.
(61) Lu, C. X.; Han, C. B.; Gu, G. Q.; Chen, J.; Yang, Z. W.; Jiang, T.; He, C.; Wang, Z. L. *Adv. Eng. Mater*. **2017**, *19*, 1700275.
(62) Wang, J.; Wu, C.; Dai, Y.; Zhao, Z.; Wang, A.; Zhang, T.; Wang, Z. L. *Nat. Commun*. **2017**, *8*, 1.
(63) Vasandani, P.; Mao, Z. H.; Jia, W.; Sun, M. *J. Electrostat*. **2017**, *90*, 147.
(64) Pandey, R. K.; Kakehashi, H.; Nakanishi, H.; Soh, S. *J. Phys. Chem. C* **2018**, *122*, 16154.
(65) Hamdi, M.; Saleh, M. N.; Poulis, J. A. *J. Adhes. Sci. Technol*. **2020**, *34*, 1853.
(66) Harper, W. R. Contact and Frictional Electrification, Oxford, Clarendon Press, 1967.
(67) McCarty, L. S.; Whitesides, G. M. *Angew. Chem. Int. Ed*. **2008**, *47*, 2188.
(68) Lowell, J.; Rose-Innes, A. C. *Adv. Phys*. **1980**, *29*, 947.
(69) Waitukaitis, S. R.; Lee, V.; Pierson, J. M.; Forman, S. L.; Jaeger, H. M. *Phys. Rev. Lett*. **2014**, *112*, 1.
(70) Lin, S.; Shao, T. *Phys. Chem. Chem. Phys*. **2017**, *19*, 29418.
(71) Shen, X.; Wang, A. E.; Sankaran, R. M.; Lacks, D. J. *J. Electrostat*. **2016**, *82*, 11.
(72) Zhang, Y.; Shao, T. *J. Phys. D. Appl. Phys*. **2013**, *46*, 235304.
(73) Xu, C.; Zi, Y.; Wang, A. C.; Zou, H.; Dai, Y.; He, X.; Wang, P.; Wang, Y. C.; Feng, P.; Li, D.; Wang, Z. L. *Adv. Mater*. **2018**, *30*, 1.
(74) Burgo, T. A. L.; Ducati, T. R. D.; Francisco, K. R.; Clinckspoor, K. J.; Galembeck, F.; Galembeck, S. E. *Langmuir* **2012**, *28*, 7407.
(75) Baytekin, H. T.; Baytekin, B.; Incorvati, J. T.; Grzybowski, B. A. *Angew. Chem. Int. Ed*. **2012**, *51*, 4843.
(76) Baytekin, H. T.; Patashinski, A. Z.; Branicki, M.; Baytekin, B.; Soh, S.; Grzybowski, B. A. *Science* **2011**, *333*, 308.
(77) Diaz, A. F. *J. Adhes.* **1998**, *67*, 111.
(78) Diaz, A. F.; Wollmann, D.; Dreblow, D. *Chem. Mater.* **1991**, *3*, 997.
(79) Medley, J. A. *Nature* **1953**, *171*, 1077.
(80) Sumner, A. L.; Menke, E. J.; Dubowski, Y.; Newberg, J. T.; Penner, R. M.; Hemminger, J. C.; Wingen, L. M.; Finlayson-pitts, B. J. *Phys. Chem. Chem. Phys.* **2004**, *6*, 604.
(81) Kuehn, N.; Jacobasch, H.-J.; Lunkenheimer, K. *Acta Polym*. **1986**, *37*, 394.

(82) Kirby, B. J.; Hasselbrink Jr., E. F. *Electrophoresis* **2004**, *25*, 203.
(83) Baytekin, H. T.; Baytekin, B.; Soh, S.; Grzybowski, B. A. *Angew. Chem. Int. Ed.* **2011**, *50*, 6766.
(84) Fabish, T. J.; Saltsburg, H. M.; Hair, M. L. *J. Appl. Phys*. **1976**, *47*, 940.
(85) Lowell, J. *J. Phys. D. Appl. Phys.* **1984**, *17*, 1859.
(86) Sow, M.; Widenor, R.; Kumar, A.; Lee, S. W.; Lacks, D. J.; Sankaran, R. M. *Angew. Chem. Int. Ed.* **2012**, *51*, 2695.
(87) Li, J.; Nagamani, C.; Moore, J. S. *Acc. Chem. Res*. **2015**, *48*, 2181.
(88) Beyer, M. K.; Clausen-Schaumann, H. *Chem. Rev*. **2005**, *105*, 2921.
(89) Giannetti, E. *J. Fluor. Chem*. **2005**, *126*, 623.
(90) Kalniņš, M. Physical Chemistry of Polymers [in Latvian]; Zvaigzne: Riga, 1988.
(91) Maeda, N.; Chen, N.; Tirrell, M.; Israelachvili, J. N. *Science* **2002**, *297*, 379.
(92) Beraldo da Silveira Balestrin, L.; Del Duque, D.; Soares da Silva, D.; Galembeck, F. **2014**, *170*, 369.
(93) Mazur, T.; Grzybowski, B. A. *Chem. Sci*. **2017**, *8*, 2025.
(94) Šutka, A.; Malnieks, K.; Lapčinskis, L.; Kaufelde, P.; Linarts, A.; Berziņa, A.; Zabels, R.; Jurķans, V.; Gorņevs, I.; Blums, J.; Knite, M. *Energy Environ. Sci.* **2019**, *12*, 2417.
(95) Lee, C. J. *Polym. Eng. Sci*. **1987**, *27*, 1015.
(96) Lamberti, A.; Di Donato, M.; Chiappone, A.; Giorgis, F.; Canavese, G. *Smart Mater. Struct.* **2014**, *23*, 105001.
(97) Yang, J.; Webb, A. R.; Ameer, G. A. *Adv. Mater*. **2004**, *16*, 511.
(98) Lapčinskis, L.; Mālnieks, K.; Blūms, J.; Knite, M.; Oras, S.; Käämbre, T.; Vlassov, S.; Antsov, M.; Timusk, M.; Šutka, A. *Macromol. Mater. Eng*. **2020**, *305*, 1.
(99) Mathúna, C. Ó.; O'Donnell, T.; Martinez-Catala, R. V.; Rohan, J.; O'Flynn, B. *Talanta* **2008**, *75*, 613.
(100) Chun, J.; Ye, B. U.; Lee, J. W.; Choi, D.; Kang, C. Y.; Kim, S. W.; Wang, Z. L.; Baik, J. M. *Nat. Commun*. **2016**, *7*, 1.
(101) He, S.; Yu, Z.; Zhou, H.; Huang, Z.; Zhang, Y.; Li, Y.; Li, J.; Wang, Y.; Li, D. *Nano Energy* **2018**, *52*, 134.
(102) Qiao, H.; Zhang, Y.; Huang, Z.; Wang, Y.; Li, D.; Zhou, H. *Nano Energy* **2018**, *50*, 126.
(103) Xu, G.; Li, X.; Xia, X.; Fu, J.; Ding, W.; Zi, Y. *Nano Energy* **2019**, *59*, 154.
(104) Yang, U. J.; Lee, J. W.; Lee, J. P.; Baik, J. M. *Nano Energy* **2019**, *57*, 293.
(105) Xie, Y.; Wang, S.; Niu, S.; Lin, L.; Jing, Q.; Yang, J.; Wu, Z.; Wang, Z. L. *Adv. Mater*. **2014**, *26*, 6599.
(106) Šutka, A.; Linarts, A.; Malnieks, K.; Stiprais, K.; Lapčinskis, L. *Mater. Horizons* **2020**, *7*, 520.
(107) Šutka, A.; Mālnieks, K.; Lapčinskis, L.; Timusk, M.; Kalniņš, K.; Kovaļovs, A.; Bitenieks, J.; Knite, M.; Stevens, D.; Grunlan, J. *Phys. Chem. Chem. Phys.* **2020**, *22*, 13299.
(108) Yi, F.; Lin, L.; Niu, S.; Yang, P. K.; Wang, Z.; Chen, J.; Zhou, Y.; Zi, Y.; Wang, J.; Liao, Q.; Zhang, Y.; Wang, Z. L. *Adv. Funct. Mater*. **2015**, *25*, 3688.

(109) Lapčinskis, L.; Linarts, A.; Mālnieks, K.; Kim, H.; Rubenis, K.; Pudzs, K.; Smits, K.; Kovaļovs, A.; Kalniņš, K.; Tamm, A.; Jeong, C. K.; Šutka, A. *J. Mater. Chem. A* **2021**, *9*, 8984.
(110) Lapčinskis, L.; Mālnieks, K.; Linarts, A.; Blūms, J.; Šmits, K.; Järvekülg, M.; Knite, M.; Šutka, A. *ACS Appl. Energy Mater*. **2019**, *2*, 4027.
(111) Li, R.; Zhao, Z.; Chen, Z.; Pei, J. *Mater. Express* **2017**, *7*, 536.
(112) Olszowy, M. *Proc. SPIE* **1997**, 3181.
(113) Chang, C.; Tran, V. H.; Wang, J.; Fuh, Y.-K.; Lin, L. *Nano Lett*. **2010**, *10*, 726.
(114) Šutka, A.; Mālnieks, K.; Lapčinskis, L.; Timusk, M.; Pudzs, K.; Rutkis, M. *iScience* **2020**, *23*, 101011.
(115) Zhang, Y.; Sun, H.; Jeong, C. K. *ACS Appl. Mater. Interfaces* **2018**, *10*, 35539.
(116) Han, J. H.; Park, K.-I.; Jeong, C. K. *Sensors* **2019**, *19*, 1444.

PIELIKUMI

Publikāciju pilnie teksti un korespondējošā autora parakstīts apliecinājums par ieguldījumu publikāciju tapšanā

APPENDICES

Full texts of publications and confirmation of contribution to preparation of papers signed by the corresponding author

1. pielikums/ Appendix I

A. Šutka, K. Malnieks, **L. Lapčinskis**, P. Kaufelde, A. Linarts, A. Berziņa, R. Zabels, V. Jurķans, I. Gorņevs, J. Blums, M. Knite, The role of intermolecular forces in contact electrification on polymer surfaces and triboelectric nanogenerators, *Energy Environ. Sci.* **2019**, *12(8)*, 2417-2421.

Energy & Environmental Science

COMMUNICATION

Check for updates

Cite this: *Energy Environ. Sci.*, 2019, **12**, 2417

Received 3rd April 2019,
Accepted 11th July 2019

DOI: 10.1039/c9ee01078e

rsc.li/ees

The role of intermolecular forces in contact electrification on polymer surfaces and triboelectric nanogenerators†

Andris Šutka, *[a] Kaspars Mālnieks, [a] Linards Lapčinskis, [b] Paula Kaufelde,[a] Artis Linarts, [b] Astrīda Bērziņa, [b] Roberts Zābels, [c] Vilnis Jurķāns,[b] Ilgvars Gorņevs,[b] Juris Blūms [b] and Māris Knite [b]

The contact electrification of polymer interfaces provides an energy harvesting function to triboelectric (nano)generators (TEG). The electron transfer between contacted-separated surfaces has been considered as the main electrification mechanism for polymers in TEG. The electron transfer mechanism widely proposed in literature requires a contact between chemically different polymer materials, as well as subsequent increase of the specific contact area, which is commonly accomplished *via* nanostructuring. Herein, we showed that contact electrification could be controlled by intramolecular forces in the polymer bulk and adhesive forces at the contact interface, and the chemical contact between different polymers was not needed for contact electrification. The results also confirm the breaking of the covalent bond as a mechanism of the contact electrification of polymer insulators.

Broader context

Triboelectric nanogenerators (TEG) that harvest ambient mechanical energy through contact electrification can be used as a power source in autonomous devices. The same phenomenon could also be applied to create local electric fields in applications such as electroactive filters. The polymeric TEG devices are currently designed based on the understanding that charging occurs through electron transfer. However, several recent studies have demonstrated that triboelectrification is instead caused by a heterolytic covalent bond breakage. In the present study, we provided a substantial proof of the occurrence of covalent bond scission to further establish the understanding of its underlying role in polymer contact electrification. We also showed, by example, how the proposed new principles could be followed in the design of superior TEG devices.

TEG devices have the potential to satisfy the increasing energy needs in portable electronics and sensors, providing a clean alternative to conventional batteries.[1] The TEG devices are produced from cheap, lightweight, flexible, widely used polymer materials and offer promise to capture the neglected and unutilized forms of mechanical energy. These devices consist of two conductive electrodes, where at least one electrode is covered with a polymer insulator film.[1] The two electrodes in TEG are connected by an outer circuit, and upon electrode oscillation, a surface charge on polymer layers and an electric potential are created that drive the electrons to flow between two electrodes to balance this electric potential difference; the TEG devices can be operated in different modes: vertical separation, sliding, rotating, single electrode *etc.*;[2] however, the key feature for high TEG efficiency is the generation of surface charge from contact electrification.[3]

Different mechanisms are responsible for contact electrification and depend on the material used. It is well demonstrated that upon metal–metal, metal–semiconductor or semiconductor–semiconductor contact, electron transfer occurs;[4,5] however, this is not very obvious for polymer insulators.[6] Moreover, three mechanisms for polymer insulator contact electrification are considered: electron transfer,[7] ionic transfer,[6] and covalent bond cleavage.[8] The electron transfer between polymers is doubtful because there are no available free electrons in insulators. The usage of the term ''effective work function'' in connection to the driving force for charge exchange between polymer insulators is also questionable even if the polymer is in contact with the metal.[6] Therefore, ion exchange between contacted polymer insulators has been considered because water under ambient conditions is adsorbed even on hydrophobic polymers.[9] The water layers on contacted surfaces fuse together upon contact, and as different polymer materials may have different affinities towards cations and anions in water, an imbalance between ions is formed during separation, thus creating the surface charge.[6] However, contact electrification is known to occur if the same polymer material is used on both sides.[10] The same material, however, should also exhibit the

[a] *Research Laboratory of Functional Materials Technologies, Faculty of Materials Science and Applied Chemistry, Riga Technical University, Paula Valdena 3/7, LV-1048, Riga, Latvia. E-mail: andris.sutka@rtu.lv*
[b] *Institute of Technical Physics, Faculty of Materials Science and Applied Chemistry, Riga Technical University, Paula Valdena 3/7, LV-1048, Riga, Latvia*
[c] *Laboratory of Materials Morphology and Structure Investigations, Institute of Solid State Physics, University of Latvia, Ķengaraga street 8, LV-1063, Riga, Latvia*

† Electronic supplementary information (ESI) available: Detailed experimental results, Fig. S1–S29, Tables S1–S4. See DOI: 10.1039/c9ee01078e

same affinity towards different ions in water, and should not lead to contact charging. In addition, it has been shown that contact electrification of polymer insulators occurs in the complete absence of water.[11]

Baytekin *et al.* have observed that nanoscopic mosaic-like structures carrying positive and negative charges are formed on polymer insulators after contacting-separating.[8] The non-equality between the positive and negative species adds up to the net surface charge. The fact that different charges may be observed on the same surface has not been reported earlier. The formation of charged species was attributed to heterolytic covalent bond cleavage. The covalent bond breaking on polymer surfaces is accompanied by reversible material transfer from one surface to another.[12]

If covalent bond cleavage is the mechanism for contact electrification, it must be higher for soft polymers with smaller cohesion energy or higher molecular weight between crosslinks because they are more prone to mechanical damage and bond breaking. In the present study, we investigated contact electrification of a large variety of polymer materials with different physicochemical properties.

Fig. 1(a) shows surface charge for various thermoplastic polymers with different elastic moduli. Polymer full names, surface charge and nanoindentation measurements are described in the (ESI†) and listed in the ESI† Table S1. Polymers with lower moduli exhibit higher surface charge values than those with higher moduli, and modulus is directly proportional to the cohesive energy of the material. The specific surface contact area-enhanced electrification can be excluded because all samples are flat (prepared with the same hot-pressing approach) and have similar surface roughness values, which have been measured by atomic force microscopy (ESI,† Table S2). The average surface roughness for the polymers shown in Fig. 1(a) was 59.76 nm with the standard deviation of 21.78 nm. Moreover, we examined the influence of roughness on the surface charge for different polymers in contact with ITO, as shown in the ESI,† Fig. S3 and Table S3. As expected, polymers with larger roughness produced over an order of magnitude higher surface charge values than their smooth counterparts. For example, upon increasing the surface roughness of polycarbonate (PC) from 70 nm to 654 nm, the surface charge value increases from 0.052 to 0.152 nC cm^{-2}, whereas the soft styrene-ethylene-butylene-styrene copolymer (SEBS) with the surface roughness of 79.40 nm exhibits the surface charge value 0.92 nC cm^{-2} after contacting ITO. SEBS, in accordance with nanoindentation measurements (Fig. 1(a) and ESI,† Table S1), shows lowest modulus. Thus, the polymer cohesion energy has a significantly stronger influence on contact electrification than the surface roughness.

We also contacted and separated chemically different polymers with the same or different hardness values (Fig. 1(b)). Although chemically different, a hard polymer (PI, polyimide) in combination with other hard polymers (PS, polystyrene) produces a small surface charge. The same was observed for soft polymers by contacting-separating low-density polyethylene (LDPE) and polytetrafluoroethylene (PTFE), which have similar

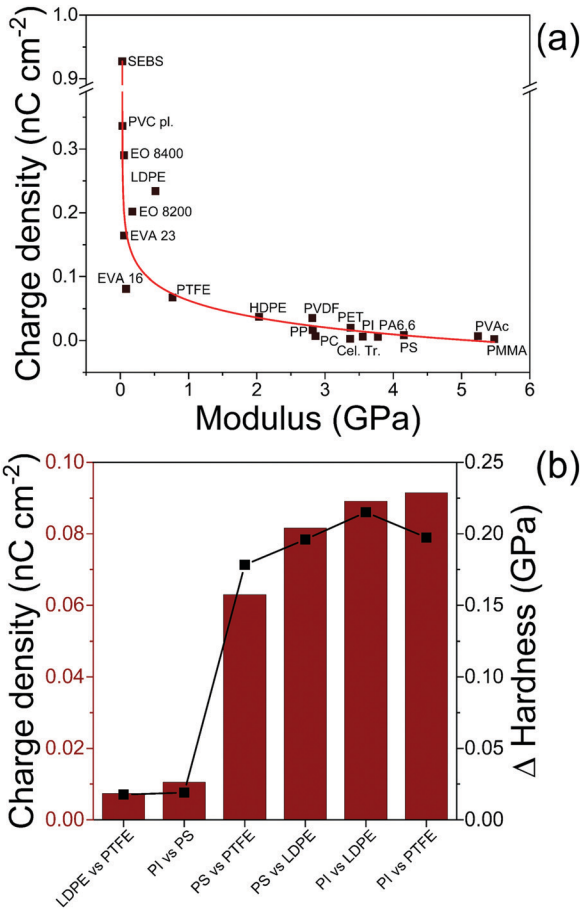

Fig. 1 Contact-electrification charge of thermoplastic polymers related to their mechanical properties. (a) Correlation between the modulus of polymer material and surface charge. (b) Contact-electrification charge density and hardness gap for different polymer combinations.

hardness values. When hard polymers were contacted with soft polymers, surface charges higher by an order of magnitude were obtained. Interestingly, the mutual contact of chemically different soft and hard polymers with the same difference between hardness produces very similar surface charge values. Open circuit voltage (V_{OC}) and short circuit current (I_{SC}) measurements for TEG devices based on polymers shown in Fig. 1 are presented in ESI,† Fig. S4–S20.

To date, there is a general understanding that to observe surface charge, the contacted materials must have different chemical compositions;[13] polymers are even empirically ordered into a so-called "triboelectric series" based on their "electron affinity"-a tendency to acquire a positive or negative charge when in contact with a distinct material.[13] These electron affinity values are commonly used to select materials for TEG. Herein, we showed that there is no need to contact chemically different polymers for electrification to occur. Fig. 2 shows the current generated by the TEG device constructed from the same polypropylene (PP) films. If the thermal history of the PP films was same, no current was observed; however, when PP films with different thermal histories were contacted-separated, the current of 35 nA and surface charge of 0.071 nC cm^{-2} were generated.

This journal is © The Royal Society of Chemistry 2019

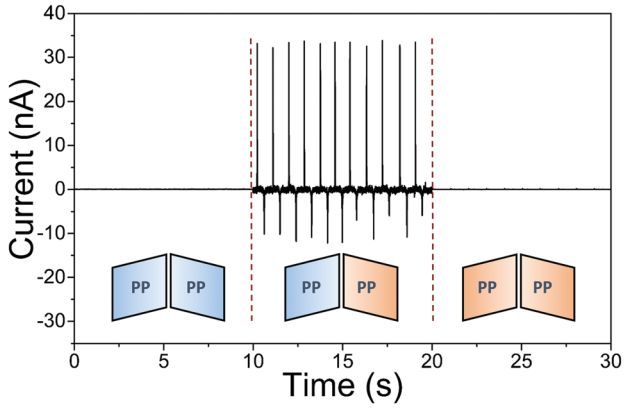

Fig. 2 Short-circuit current peaks generated by the contact-electrification of PP with similar and different thermal histories. Blue figures represent original polymer films and red figures represent polymer films subjected to thermal treatment (130 °C, 60 min).

Different thermal histories change macromolecular ordering and cohesion energy, as indicated by lower phase transition temperatures (ESI,† Fig. S21) and hardness change from 107.6 MPa to 96.2 MPa, respectively. This is in sharp contrast with the recently reported theory of contact electrification.[7,13]

Further, we studied contact electrification of polydimethylsiloxane (PDMS) with a different cross-linking degree, which was varied by changing the ratio between pre-polymer and the curing agent.[14] The surface charge increased from 0.31 to 3.39 nC cm^{-2} with an increase in the molecular weight between crosslinks (M_C, g mol^{-1}) (Fig. 3(a)). The method and measurements for the determination of M_C are described in ESI,† and the M_C values are shown in Table S4 (ESI†). The TEG device constructed from flat PDMS with the curing agent to prepolymer ratio 1 : 30 in contact with ITO generate V_{OC} 400 V (80 V cm^{-2}) (voltage and current for all PDMS based TEG devices are shown in ESI,† Fig. S22 and S23).

Further, we contacted and separated chemically identical PDMS and studied contact electrification. When the cross-linking degree between contacting PDMS films was same, almost no contact electrification was observed. The surface charge values for TEG when PDMS films in the ratio of 3 : 1 *vs.* 3 : 1 and 20 : 1 *vs.* 20 : 1 were contacted were 0.00143 nC cm^{-2} and 0.00161 nC cm^{-2}, respectively. When PDMS films with different cross-linking degrees were contacted (3 : 1 *vs.* 20 : 1), surface charge (0.0168 nC cm^{-2}), voltage, and current higher by an order of magnitude were obtained (ESI,† Fig. S24 and S25), thus confirming the above-mentioned results obtained from TEG based on thermoplastic polymers.

The increased surface charge for PDMS with a smaller cross-linking degree can also be related to higher adhesion at the contact interface. The force necessary for the separation of the two contacted films increased when the cross-linking degree was reduced. Based on our understanding, to provide high net surface charge density on the polymer, the polymer should show strong surface adhesion and low cohesion energy in bulk, such that the energy of the adhesive (physical) bonds formed between contacting surfaces is larger than the energy of the chemical or/and physical bonds in bulk. This could potentially allow enhanced covalent bond scission and material transfer between two contacting surfaces.[15]

To observe higher adhesion, we increased the contacting force as described in ESI.† With the increasing contacting force, the adhesion between contacted surfaces and force to separate them increases, and as shown in Fig. 3(b), when separation stress between two films is larger, the surface charge increases drastically.

If the reason for contact electrification is a heterolytic covalent bond break, the mass transfer should occur alongside with surface charging.[12] The mass transfer was confirmed by atomic force microscopy (AFM) and X-ray photoelectron spectroscopy (XPS) studies. As demonstrated in the ESI,† Fig. S26, the ITO surface viewed by AFM contains polymer pieces after being contacted with PDMS. The mass transfer of PDMS was also confirmed by the XPS studies, where the Si 2s (153.9 eV) and Si 2p (102.7 eV) signal peaks were observed in the photoelectron spectrum from the ITO surface after contact with PDMS (ESI,† Fig. S27).

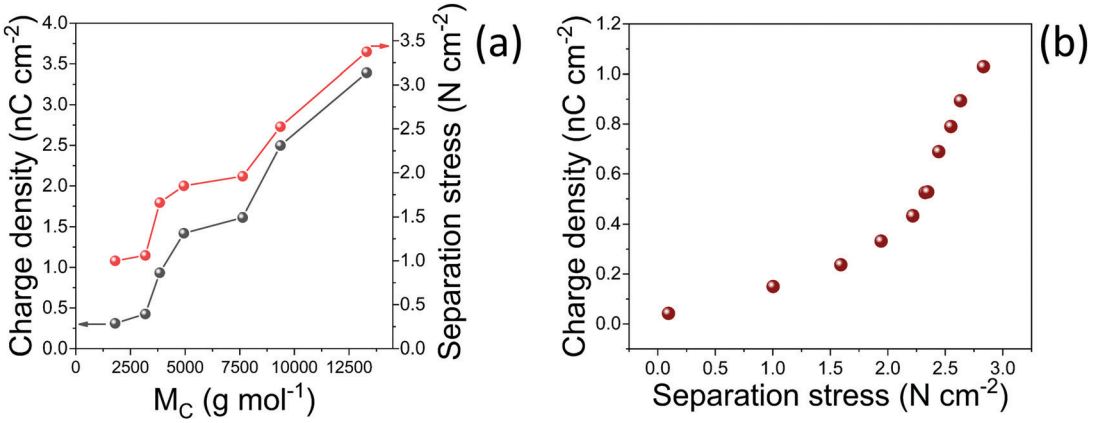

Fig. 3 Contact-electrification charge of PDMS: (a) surface charge density and adhesion force increase as we increase the molecular weight between PDMS crosslinking points. (b) Relationship between the charge and separation stress required when the contacting force before separation step is gradually increased for PDMS (10 : 1 ratio).

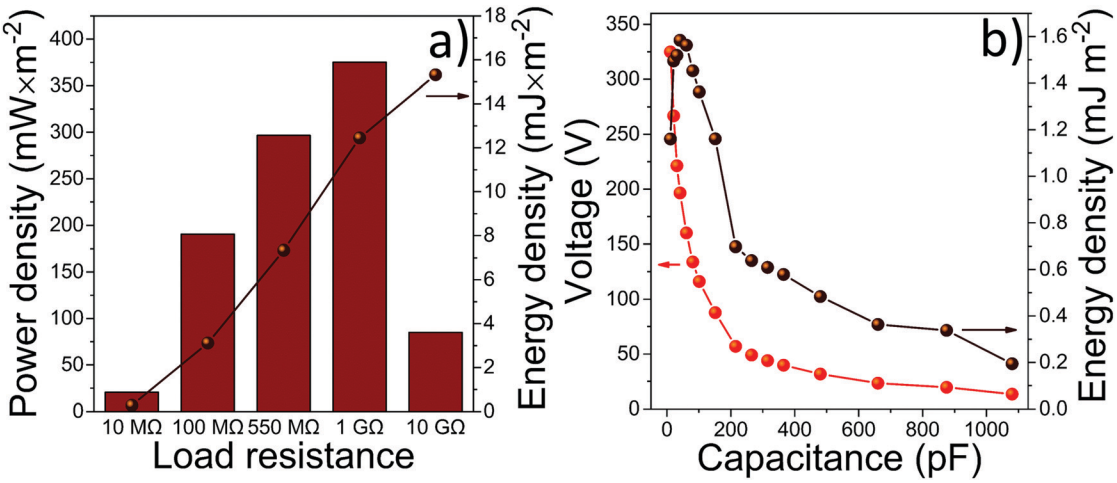

Fig. 4 Hydrogen peroxide-modified SEBS TEG energy density measurements. (a) Power and energy densities of hydrogen peroxide-treated SEBS-based TEG. (b) Energy density stored in the capacitor after contact-electrification of hydrogen peroxide-treated SEBS TEG. The corresponding voltages are shown besides the energy.

Although material transfer occurred, the TEG devices were stable because material transport could also occur in both ways. The covalent bonds could restore during contacting due to frictional heat,[16] and thus, the long-term performance had a relatively simple explanation. The long-term stability is demonstrated in the ESI,† Fig. S28 for TEG devices from three different polymers: hard (PMMA), soft (SEBS) and soft-crosslinked (PDMS). In the beginning, all the TEG devices showed smaller voltage; however, it became saturated at about 2000 cycles and did not change in the further 10 000 cycles.

Finally, we produced a TEG device using the soft thermoplastic SEBS block copolymer (ESI,† Fig. S10), which showed highest surface charging, as depicted in Fig. 1(a). We modified the surface of SEBS to make it more adhesive by treatment with a hydrogen peroxide solution, as described in ESI.† *Via* this, we observed an increase in the separation stress by 38% from 2.97 N cm^{-2} to 4.11 N cm^{-2}. The increased adhesion of the peroxide-treated SEBS surfaces can be attributed to the formation of quasi-free ends of macromolecular chains.[17] As expected, for modified SEBS, the surface charge increased 3.14 times from 0.92 nC cm^{-2} to 2.89 nC cm^{-2}, I_{SC} increased 2.4 times from 0.14 μA cm^{-2} to 0.33 μA cm^{-2} and V_{OC} increased from 60 V cm^{-2} to 156 V cm^{-2}. Further, our 5 cm^2 TEG device generated 780 V, as demonstrated in the ESI,† Fig. S29. Moreover, the hydrogen peroxide-treated SEBS reached 375.27 mW m^{-2} power density under the optimized load resistance of 1×10^9 Ω (Fig. 4(a)). The energy density was obtained by integral $E = \int P\mathrm{d}t$, which yielded 15.32 mJ m^{-2} under load resistance of 1×10^{10} Ω (Fig. 4(a)). The hydrogen peroxide-treated SEBS was also used to charge a variable capacitor circuit. The energy density stored in the capacitor after one contact–separation cycle and the corresponding voltage are shown in Fig. 4(b) for each capacitor value. The highest energy stored in the capacitor (1.58 mJ m^{-2}), calculated by $E = 0.5CU^2$, was reached when the capacitance of the capacitor circuit was set to approximately 40 pF. Note that the TEG device based on SEBS was produced for simple readily industrializable hot pressing approach. Thus, the expensive and complex nanostructuring approaches that have been considered essential for high-performance TEG devices can be excluded.

Conclusions

The surface charge for polymers can be controlled by varying their physicochemical properties, such as the strength of macromolecular interactions in bulk and the surface adhesion, and thus, our experiments confirm the covalent bond cleavage as the mechanism for the contact electrification. Higher surface charge can be expected from the polymers that show strong surface adhesion and low cohesion energy in bulk. Thus, our strategy enables the improvement in the performance of TEG, leaving aside the expensive and complex nanostructuring approaches.

Author contributions

A. Šutka and K. Mālnieks conceived the study. A. Šutka interpreted results and wrote the manuscript. K. Mālnieks, A. Linarts, L. Lapčinskis and P. Kaufelde performed sample preparation and testing. A. Bērziņa executed AFM measurements. R. Zābels performed nanoindentation measurements. Vilnis Jurķāns and Ilgvars Gorņevs conducted electrical measurements. J. Blums and M. Knite performed calculations and contributed to result interpretation.

Conflicts of interest

There are no conflicts to declare.

This journal is © The Royal Society of Chemistry 2019

Acknowledgements

This research was supported by the European Regional Development Fund within the project ''Hybrid energy harvesting systems'' 1.1.1.1./16/A/013.

References

1 Z. L. Wang, *ACS Nano*, 2013, **7**, 9533.
2 R. Hinchet, W. Seung and S.-W. Kim, *ChemSusChem*, 2015, **8**, 2327.
3 J. Wang, C. Wu, Y. Dai, Z. Zhao, A. Wang, T. Zhang and Z. L. Wang, *Nat. Commun.*, 2017, **8**, 88.
4 J. Lowell, *J. Phys. D: Appl. Phys.*, 1975, **8**, 53.
5 J. Liu, A. Goswami, K. Jiang, F. Khan, S. Kim, R. McGee, Z. Li, Z. Hu, J. Lee and T. Thundat, *Nat. Nanotechnol.*, 2018, **13**, 112.
6 L. S. McCarty and G. M. Whitesides, *Angew. Chem., Int. Ed.*, 2008, **47**, 2188.
7 M. Willatzen and Z. L. Wang, *Nano Energy*, 2018, **52**, 517.
8 H. T. Baytekin, A. Z. Patashinski, M. Branicki, B. Baytekin, S. Soh and B. A. Grzybowski, *Science*, 2011, **333**, 308.
9 A. L. Sumner, E. J. Menke, Y. Dubowski, J. T. Newberg, R. M. Penner, J. C. Hemminger, L. M. Wingen, T. Brauers and B. J. Finlayson-Pitts, *Phys. Chem. Chem. Phys.*, 2004, **6**, 604.
10 M. M. Apodaca, P. J. Wesson, K. J. M. Bishop, M. A. Ratner and B. A. Grzybowski, *Angew. Chem., Int. Ed.*, 2011, **49**, 946.
11 H. T. Baytekin, B. Baytekin, S. Soh and B. A. Grzybowski, *Angew. Chem., Int. Ed.*, 2011, **50**, 6766.
12 H. T. Baytekin, B. Baytekin, J. T. Incorvati and B. A. Grzybowski, *Angew. Chem., Int. Ed.*, 2012, **124**, 4927.
13 J. Chen and Z. L. Wang, *Joule*, 2017, **1**, 480.
14 A. Lamberti, M. D. Donato, A. Chiappone, F. Giorgis and G. Canavese, *Smart Mater. Struct.*, 2014, **23**, 105001.
15 R. K. Pandey, H. Kakehashi, H. Nakanishi and S. Soh, *J. Phys. Chem. C*, 2018, **122**, 16154.
16 M. K. Beyer and H. Clausen-Schaumann, *Chem. Rev.*, 2005, **105**, 2921.
17 N. Maeda, N. Chen, M. Tirrell and J. N. Israelachvili, *Science*, 2002, **297**, 379.

This journal is © The Royal Society of Chemistry 2019

2. pielikums/ Appendix II

L. Lapčinskis, K. Mālnieks, J. Blūms, M. Knite, S. Oras, T. Käämbre, S. Vlassov, M. Antsov, M. Timusk, A. Šutka, The Adhesion-Enhanced Contact Electrification and Efficiency of Triboelectric Nanogenerators, *Macromol. Mater. Eng.* **2020**, *305(1)*, 1900638.

Macromolecular
Materials and Engineering
www.mme-journal.de

The Adhesion-Enhanced Contact Electrification and Efficiency of Triboelectric Nanogenerators

*Linards Lapčinskis, Kaspars Mālnieks, Juris Blūms, Māris Knite, Sven Oras, Tanel Käämbre, Sergei Vlassov, Mikk Antsov, Martin Timusk, and Andris Šutka**

In the present work, the contact electrification of polymers that differ in adhesion strength is studied. Electrical current is measured along with adhesion in macroscale contacting-separation experiments. Additionally, local adhesion and roughness are studied with atomic force microscopy to get deeper insight into relations between surface properties and electrification. Measurements reveal that higher surface charge is formed on more adhesive surfaces, thus confirming covalent bond cleavage as a mechanism for contact electrification of polymers. Investigated materials possess enhanced contact electrification making them attractive candidates for the conversion of mechanical energy to electrical in triboelectric nanogenerator devices.

Energy from the motions can be converted and stored in a battery directly by using the triboelectric nanogenerator (TENG)[1,2] and piezoelectric nanogenerator (PENG) devices.[3,4] The power consumption of portable electronic devices and detectors is constantly decreasing and motion-driven charging becomes increasingly more relevant. TENG can be integrated into wearables,[5] fabrics[6] and even implanted in vivo to harvest energy from the mechanical movement of breathing to directly drive a medical device.[7] Massive TENG device networks have been also reported to harvest mechanical energy on a large scale.[8–10]

TENG consists of two connected conductive planar electrodes from which at least one is covered with polymer.[11] By vertical contacting and separating two sides, the opposite net charges are created on each surface, which then induce charges on two underlying conductive electrodes. Upon the movement of the electrode (during separation) the electric potential is varied and, in order to balance the electric potential difference, electrons are driven to flow between the two electrodes.[11]

The electron transfer is a generally accepted mechanism for contact electrification of polymer insulators in the TENG community, thus materials for devices are selected by considering their effective electron affinity in accordance with the experimentally defined triboelectric series.[12] Larger contact electrification of polymers is expected when material with high electron affinity is contacted with a material having low electron affinity. However, polymer insulators widely used in TENG devices do not contain electron-rich or electron-poor functional groups, thus the electron transfer is unlikely as there are no available free electrons. Moreover, electrons cannot be transferred from the conductive material to the insulator unless polymer has a high density of acceptors.[13]

The heterolytic covalent bond cleavage (heterolysis or heterolytic fission) alongside with material transfer has been proposed as an alternative mechanism for polymer electrification.[14–16] However, this knowledge is scarcely taken into account in the design of the TENG devices. It has been demonstrated that the performance of TENG can be enhanced by chemical surface modification, but the observed enhancement has commonly been attributed to modified electron affinity.[17–19] Here we show that materials exhibiting stronger adhesion against contacting surface also exhibit stronger contact electrification, which is direct evidence of heterolytic bond cleavage as a mechanism for contact electrification. On sticky surfaces the energy of formed adhesive (physical) bonds between contacting surfaces may be larger than the energy of chemical or/and physical bonding in the bulk. This could potentially enhance the probability of covalent bond scission and material transfer between the two contacting surfaces.

In the present study, TENG devices were constructed from polymer elastomers in combination with polyethylene terephthalate (PET) coated with indium tin oxide (ITO) as demonstrated in Figure S1, Supporting Information. Polymer elastomers were deposited on ITO-coated PET and connected with the other by an external circuit. Elastomeric materials have been widely used in TENG devices to provide flexible mechanical energy harvesters for wearables.[20–22] Upon pressing, the

L. Lapčinskis, Prof. J. Blūms, Prof. M. Knite
Institute of Technical Physics
Faculty of Materials Science and Applied Chemistry
Riga Technical University
Paula Valdena 3/7, Riga LV-1048, Latvia

Dr. K. Mālnieks, Dr. T. Käämbre, Dr. M. Timusk, A. Šutka
Research Laboratory of Functional Materials Technologies
Faculty of Materials Science and Applied Chemistry
Riga Technical University
Paula Valdena 3/7, Riga LV-1048, Latvia
E-mail: andris.sutka@rtu.lv

Dr. S. Oras, Dr. T. Käämbre, Dr. M. Antsov, Dr. M. Timusk
Institute of Physics
University of Tartu
Wilhelm Ostwald Str. 1, 50411 Tartu, Estonia

Dr. S. Vlassov
ITMO University
Kronverskiy pr., 49, 197101 Saint Petersburg, Russia

The ORCID identification number(s) for the author(s) of this article can be found under https://doi.org/10.1002/mame.201900638.

DOI: 10.1002/mame.201900638

 © 2019 WILEY-VCH Verlag GmbH & Co. KGaA, Weinheim

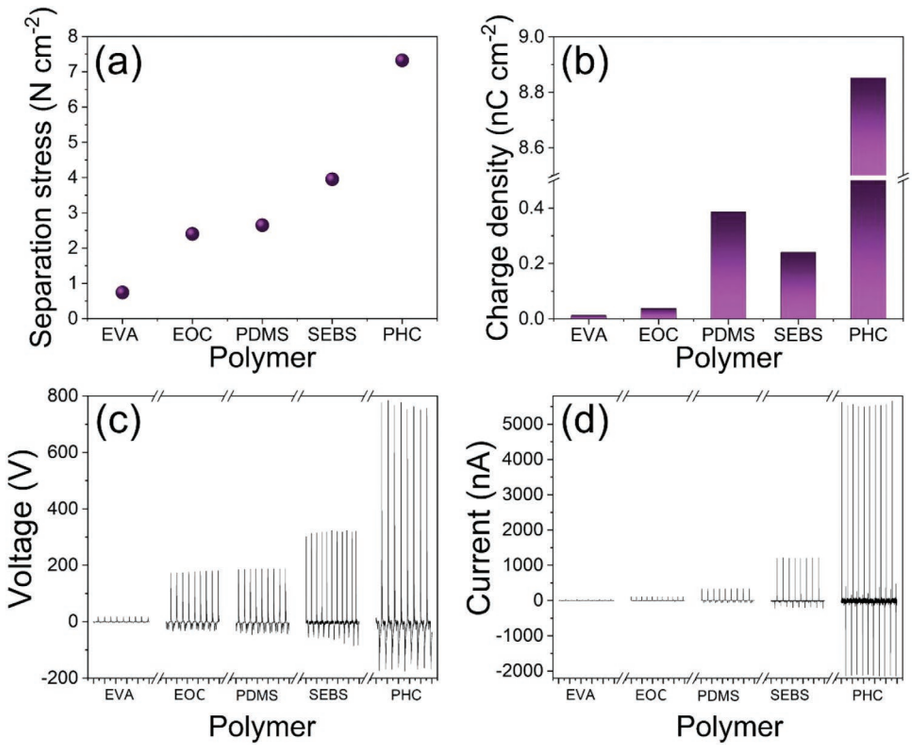

Figure 1. a) The separation stress for two contacted sides in TENG based on different polymer materials and b) corresponding charge densities for these TENG devices. c) Open-circuit voltage and d) short-circuit current peaks for TENG based on different polymers.

elastomeric polymers adapt the shape of the opposite surface more easily, thus increasing both the contact area and chance of adhesive bond formation.[23] We prepared TENG devices from polydimethylsiloxane (PDMS), ethylene–octene copolymer (EOC), styrene-ethylene-butylene–styrene copolymer (SEBS) and polyethylene–covinyl acetate copolymer (EVA). In addition, we synthesized poly(hexanediol–cocitric acid) (PHC), which is known as an elastomeric adhesive.[24] The current and voltage were measured between the two conductive plates upon separation. The surface charge was calculated as integral of current pulses measured between the two conductive plates. The force necessary for separation of contacted films was measured simultaneously with electrical measurements using Instron Test Instrument as described in Experimental Section.

Separation force values for the different elastomers are demonstrated in **Figure 1**a. The adhesion of tested materials to ITO in the TENG device increased in the order: PHC > SEBS > PDMS > EOC > EVA. Polymers that exhibit stronger adhesion against the contacted surface also show higher open-circuit voltage (V_{OC}) and short-circuit current (I_{SC}) (Figure 1c,d). The TENG device based on PHC which requires the greatest force for separation of two contacted sides (7.32 N cm^{-2}) also shows the highest V_{OC} up to 800 V from 5 cm^2 area. The surface charge density for PHC is 8.853 nC cm^{-2} (Figure 1b), which is over an order of magnitude higher than SEBS (0.241 nC cm^{-2}) and almost three orders of magnitude higher than observed for EOC (0.013 nC cm^{-2}). Note that the drastic difference observed in surface charge and adhesion cannot be directly related to different specific surface area, since most samples had comparable surface roughness as measured by atomic force microscopy (AFM) on 50 × 50 μm (Table S1, Supporting Information, last row). The single exception is PDMS, which had an order of magnitude lower surface roughness. At the same time, PDMS shows a higher surface charge than the rougher surface polymers. Currently, the nanostructured contacting surfaces in TENG devices have been considered essential for high performance.[25–30] Our work shows that these expensive and complex nanostructuring approaches can be left aside.

The observed correlation between separation force and surface charge indicates heterolysis as a potential mechanism for surface charge formation. Greater adhesion force contributes to a higher amount of covalent bond cleavage and in turn may trigger surface charge formation. To get a deeper insight into relations between surface properties and performance of the TENG device, the adhesion measurements have been performed also at the nanoscale by AFM colloidal probe technique. The results show a correlation similar to macroscopic contact-separation. Most polymers that exhibit large adhesion force at the macroscale also show large adhesion force in nanoscale. Median adhesion values for the samples are 13.4 mJ m^{-2} for EVA, 37.9 mJ m^{-2} for PDMS, 49.1 mJ m^{-2} for SEBS, and 66.9 mJ m^{-2} for EOC. The single exception here is the EOC that reveals a relatively low adhesion in the macroscopic experiment but demonstrates the highest adhesion in the AFM test. This difference between the macroscopic and the nanoscale adhesion can be explained by considering roughness at different

© 2019 WILEY-VCH Verlag GmbH & Co. KGaA, Weinheim

scales. From Table S1, Supporting Information, it is seen that on larger scale (50 × 50 µm), which is more relevant for macroscale adhesion tests, EOC has higher roughness than SEBS, while on smaller scale (3 × 3 µm), which is comparable to spherical AFM probe radius, EOC is considerably flatter than SEBS. For rough macroscopic bodies it is generally more difficult to achieve full contact over the entire surface area even in case of elastomers as the air between asperities prevents full area atomic-scale contact of two surfaces in contrast to the small AFM probe that can achieve full contact. Therefore, the macroscale adhesion correlates with the macroscopic roughness, while the results of the AFM test correlate with the local microscale roughness. Though, from the application standpoint the macroscopic values are more relevant, while the nanoscale case may require a separate study. The nanoscale adhesion value for PHC was not obtained, due to very high adhesion (impossible to get the probe out of contact within the available AFM piezo scanner range).

The heterolytic bond cleavage is further confirmed by material transfer.[14–16] The material transfer in our work was measured by AFM and X-ray photoelectron spectroscopy (XPS). The surface roughness of the ITO after 10 000 contacting-separating cycles against PDMS increases from 5.15 to 21.51 nm and contains polymer pieces as demonstrated by AFM images in **Figure 2**a. Mass transfer of PDMS is confirmed also by XPS studies where the Si 2s (153.9 eV) and Si 2p (102.7 eV) signal peaks were observed in the photoelectron spectrum from the ITO surface after contacting with PDMS (Figure 2b; Figure S2, Supporting Information). We believe that material transfer occurs with every contacting-separation event, but since the transfer happens both ways,[31] materials can be contacted repeatedly without the loss of performance.

Since PHC had shown the greatest surface charge density, the TENG device based on PHC polymer was investigated in more detail. We studied the influence of load resistance on energy and power density (**Figure 3**a). The highest energy (24.36 mJ m^{-2}) was observed at load resistance 1 GΩ, while the highest average power density (439.86 mW m^{-2}) for a contact-separation was reached when the load resistance was 100 MΩ. For comparison, charging of a typical mobile phone requires 5.45 Wh of energy. This means that for a 1 m^2 large TENG device charging of the phone would take approximately 9.3 days (223.7 h) at 1 Hz contact-separation frequency. However, the power consumption of electronic devices is tending to be reduced, thus TENG devices may take a significant role in charging or even powering of personal electronic devices in the future. For instance, TENG with a surface area of 20 cm^2 operating at 1 Hz will provide sufficient energy to a power wireless sensor node with power consumption about 100 µW.[32]

Further, we investigated the efficiency of the PHC-based TENG device by comparing the generated energy against

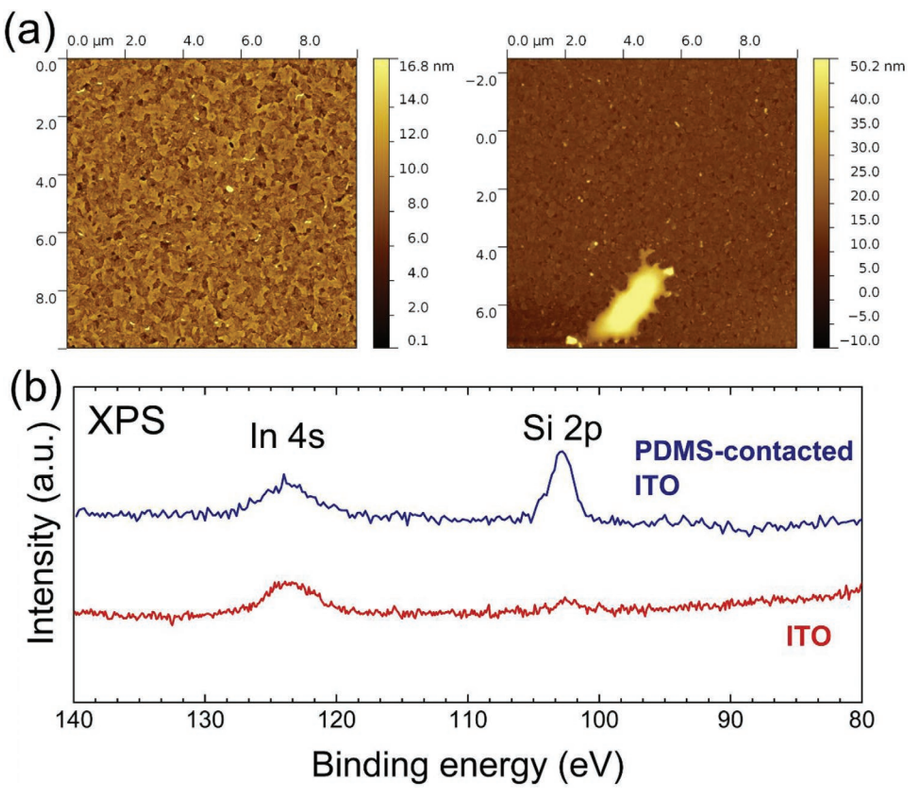

Figure 2. Material mass transfer: a) ITO surface before (left) and after (right) contacting with PDMS 10:1 for 10 000 cycles and b) XPS results comparing pristine ITO and ITO surface after contacting against PDMS 10:1 for 10 000 cycles showing Si 2p on the surface of ITO. The XPS overview spectra are demonstrated in Figure S2, Supporting Information.

© 2019 WILEY-VCH Verlag GmbH & Co. KGaA, Weinheim

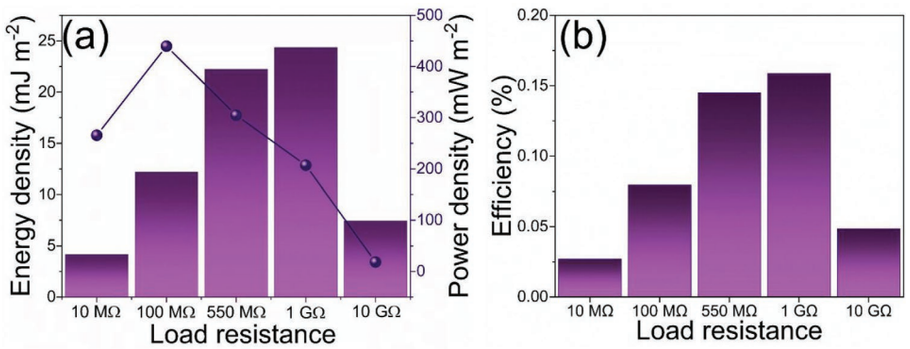

Figure 3. Characteristics of TENG device based on PHC polymer: a) energy density and power density as a function of load resistance and b) efficiency.

the mechanical work done during TENG contact-separation. Efficiency of TENGs is typically calculated by considering only the pressing force, displacement or kinetic motion energy[33–38] neglecting the influence of adhesion (separation force). Reported efficiency values are astonishing and paint an appealing picture of TENG device efficiency. However, when, for example, methodology (based on kinetic energy of motions) reported by Chun et al.[33] is applied to our PHC-based TENG, its efficiency surpasses 300%. This clearly indicates that some of the aspects have been overlooked since the law of conservation of energy still stands. When pressing force (and the corresponding polymer strain) is included in efficiency calculations, TENG based on PHC reaches 5% efficiency. However, we insist that energy required for separation also must be taken into consideration. The energy required for separation is an order of magnitude higher than energy necessary to compress, therefore the actual efficiency of the TENG device based on PHC is only 0.16% (Figure 3b) at 1 GΩ load resistance. Since load resistance does not affect the amount of spent mechanical energy, efficiency shows the same trend as energy density. Separation of the two contact sides in TENG device can be provided also by the construction elements (e.g., springs), thus there is no external work input required. Although this means that additional force must be overcome in order to contact materials. However, perhaps to achieve higher efficiency, TENG devices based on inversely polarized ferroelectric contacting layers should be considered, as they provide the energy density as high as 66 mJ m^{-2} at low separation forces.[39,40]

In conclusion, simultaneous separation force and current measurements performed for the first time on the several different TENG devices confirmed heterolysis as the mechanism for the contact electrification—polymers with higher adhesion achieve larger net surface charge upon separation. The electric energy harvested by the TENG device increases drastically when polymers with high adhesion are used as a triboelectric contacting material. Measurements did not reveal any positive correlation between surface roughness and efficiency thus we conclude that nanostructuring is not necessary for achieving high performance of the TENG device. By considering adhesion-related energy losses we have concluded that TENG devices may have smaller efficiencies than estimated previously and reported efficiency values should be reevaluated.

Experimental Section

Polymer films were prepared by hot pressing (Engage 8200 ethylene–octene copolymer—EOC, Lifoflex UV 30 GA 1030 styrene–ethylene–butylene–styrene copolymer—SEBS and Sigma-Aldrich, 12 wt% vinyl acetate containing poly(ethylene–covinyl acetate) copolymer—EVA) or spin-coating (polydimethylsiloxane—PDMS and poly(hexanediol–cocitric acid)—PHC). PDMS film (Dow Corning, Sylgard 184) was prepared by mixing base polymer and curing agent in weight ratio 10:1. After spin-coating at 3000 rpm PDMS film was cured at 70 °C for 1 h. PHC pre-polymer was synthesized similarly as described by Yang et al.[24] Briefly, 20 g of 1,6-hexanediol (99%, Aldrich) and 32.515 g of citric acid (99%, Sigma-Aldrich) were mixed and melted in a 250 mL double-neck flask under N_2 gas flow at 156 °C by using a temperature-controlled oil bath and a magnetic stirrer. Citric acid and 1,6-hexanediol melted within 10 min and subsequently temperature was decreased to 140 °C for 45 min with continued stirring under N_2 gas flow. After that, the viscous polymer mixture was left to cool at room temperature. During cooling, 50 mL of 1,4-dioxane (≥99.5%, Sigma-Aldrich) was added under mixing to dissolve the partially crosslinked polymer. PHC film was obtained by spin coating at 3000 rpm and then cured at 130 °C for 45 min.

The short circuit current and voltage pulses generated by TENG devices were measured by using a custom-made voltage divider in combination with a Keithley 6514 electrometer connected to a Picoscope 5444B PC oscilloscope to provide high time resolution. Contacting area (sample size) was 5 cm^2. Power was calculated by applying Joule's Law ($P = V2\ R–1$) to gain instantaneous power, while energy was obtained as an integral of power $E = \int Pdt$ over the duration of the pulse. The surface charge was calculated from the measured current by equation $Q = \int idt$ (where i is instantaneous current). Pressing force (10 N) and frequency (1 Hz), as well as separation speed (100 mm s^{-1}), and the gap between TENG sides (5 mm) were controlled using INSTRON E1000 All-Electric Dynamic Test Instrument, which also allows measuring the force necessary for separation of the contacted films in TENG device.

Total mechanical energy (work) was taken as a sum of kinetic energy (E_k), compression (E_c) and separation (E_s) energy. Kinetic energy of motions has been calculated using equation $E_k = 0.5\ mv2$ where m is the mass of the moving sample holder together with the sample (28 g) and v is the speed used to contact both surfaces (0.017 m s^{-1}). Separation energy to overcome the adhesive forces was obtained as integral of the mechanical power peak over time. Mechanical power was calculated as the multiplication of force measurements with the first derivative of position measurements (speed). Compression energy to compress the PHC sample was obtained as compression force multiplied by strain exerted on the PHC sample. The strain of the sample was found from the force-strain curve (INSTRON E1000 measurements) shown in Figure S3, Supporting Information. Efficiency then is determined as the percentage of generated electrical energy versus total mechanical energy.

The mean square (RMS) surface roughness among the five independently prepared samples was measured by AFM (Smena, NT-MDT) in the semi-contact mode. RMS surface roughness expresses

© 2019 WILEY-VCH Verlag GmbH & Co. KGaA, Weinheim

the square root of the mean square of height deviations of the surface, measured from the mean height of the data plane. The adhesion for the samples was measured by the AFM colloidal probe technique. A probe with a radius of 5 µm and a spring constant of 4.95 N µm^{-1} was determined with the thermal tune method.[41] Typical measurement curves are demonstrated in Figure S4, Supporting Information. The sensitivity and deflection of the cantilever were measured, and the adhesion was calculated according to Equation (1):[42]

$$\Delta\gamma = \frac{2 \cdot F_d}{3 \cdot \pi \cdot R} \quad (1)$$

Where F_d is the force applied during the cantilever deflection, R is the radius of the colloidal probe. The XPS data were measured using the electron energy hemispherical analyzer Scienta SES100 and a VG Scientific XPS/1 X-ray gun.

Supporting Information

Supporting Information is available from the Wiley Online Library or from the author.

Acknowledgements

This research was supported by the Latvian Council of Science in the framework of FLPP (Triboelectric interfaces for mechanical energy harvesting, lzp-2019/1-0182) and Russian Science Foundation project grant 18-19-00645 "Adhesion of polymer-based soft materials: from liquid to solid."

Conflict of Interest

The authors declare no conflict of interest.

Keywords

contact electrification, energy conversion, material transfer, mechanical properties, surface analyses

Received: September 24, 2019
Revised: October 11, 2019
Published online:

[1] Y. Zi, J. Wang, S. Wang, S. Li, Z. Wen, H. Guo, Z. L. Wang, *Nat. Commun.* **2016**, *7*, 10987.
[2] Y. Zheng, L. Cheng, M. Yuan, Z. Wang, L. Zhang, Y. Qin, T. Jing, *Nanoscale* **2014**, *6*, 7842.
[3] B. Moorthy, C. Baek, J. E. Wang, C. K. Jeong, S. Moon, K.-I. Park, D. K. Kim, *RSC Adv.* **2017**, *7*, 260.
[4] Y. Zhang, W. Zhu, C. K. Jeong, H. Sun, G. Yang, W. Chen, Q. Wang, *RSC Adv.* **2017**, *7*, 32502.
[5] T. Zhou, C. Zhang, C. B. Han, F. R. Fan, W. Tang, Z. L. Wang, *ACS Appl. Mater. Interfaces* **2014**, *6*, 14695.
[6] X. Pu, L. Li, M. Liu, C. Jiang, C. Du, Z. Zhao, W. Hu, Z. L. Wang, *Adv. Mater.* **2016**, *28*, 98.
[7] Q. Zheng, B. Shi, F. Fan, X. Wang, L. Yan, W. Yuan, S. Wang, H. Liu, Z. Li, Z. L. Wang, *Adv. Mater.* **2014**, *26*, 5851.
[8] J. Chen, J. Yang, Z. Li, X. Fan, Y. Zi, Q. Jing, H. Guo, Z. Wen, K. C. Pradel, S. Niu, Z. L. Wang, *ACS Nano* **2015**, *9*, 3324.
[9] L. Zhang, B. Zhang, J. Chen, L. Jin, W. Deng, J. Tang, H. Zhang, H. Pan, M. Zhu, W. Yang, Z. L. Wang, *Adv. Mater.* **2016**, *28*, 1650.
[10] L. Dhakar, S. Gudla, X. Shan, Z. Wang, F. E. H. Tay, C.-H. Heng, C. Lee, *Sci. Rep.* **2016**, *6*, 22253.
[11] Z.L. Wang, *ACS Nano* **2013**, *7*, 9533.
[12] J. Chen, Z. L. Wang, *Joule* **2017**, *1*, 480.
[13] H. S. Nalwa, in *Handbook of Organic Conductive Molecules and Polymers*, Wiley, New York **1997**.
[14] H. T. Baytekin, A. Z. Patashinski, M. Branicki, B. Baytekin, S. Soh, B. A. Grzybowski, *Science* **2011**, *333*, 308.
[15] H. T. Baytekin, B. Baytekin, J. T. Incorvati, B. A. Grzybowski, *Angew. Chem., Int. Ed.* **2012**, *51*, 4843.
[16] R. K. Pandey, H. Kakehashi, H. Nakanishi, S. Soh, *J. Phys. Chem. C* **2018**, *122*, 16154.
[17] S. Wang, Y. Zi, Y. S. Zhou, S. Li, F. Fan, L. Lina, Z. L. Wang, *J. Mater. Chem. A* **2016**, *4*, 3728.
[18] B. K. Yun, J. W. Kim, H. S. Kim, K. W. Jung, Y. Yi, M.-S. Jeong, J.-H. Ko, J. H. Jung, *Nano Energy* **2015**, *15*, 523.
[19] S.-H. Shin, Y. H. Kwon, Y.-H. Kim, J.-Y. Jung, M. H. Lee, J. Nah, *ACS Nano* **2015**, *9*, 4621.
[20] F. R. Fan, J. Luo, W. Tang, C. Li, C. Zhang, Z. Tian, Z. L. Wang, *J. Mater. Chem. A* **2014**, *2*, 13219.
[21] X. He, Y. Zi, H. Guo, H. Zheng, Y. Xi, C. Wu, J. Wang, W. Zhang, C. Lu, Z. L. Wang, *Adv. Funct. Mater.* **2017**, *27*, 1604378.
[22] G. Zhu, W. Q. Yang, T. Zhang, Q. Jing, J. Chen, Y. S. Zhou, P. Bai, Z. L. Wang, *Nano Lett.* **2014**, *14*, 3208.
[23] L. Shi, S. Dong, P. Ding, J. Chen, S. Liu, S. Huang, H. Xu, U. Farooq, S. Zhang, S. Li, J. Luo, *Nano Energy* **2019**, *55*, 548.
[24] J. Yang, A. R. Webb, G. A. Ameer, *Adv. Mater.* **2004**, *16*, 511.
[25] X. Fan, J. Chen, J. Yang, P. Bai, Z. Li, Z.L. Wang, *ACS Nano* **2015**, *9*, 4236.
[26] Z. Wen, M.-H. Yeh, H. Guo, J. Wang, Y. Zi, W. Xu, J. Deng, L. Zhu, X. Wang, C. Hu, L. Zhu, X. Sun, Z.L. Wang, *Sci. Adv.* **2016**, *2*, e1600097.
[27] G. Zhu, W.Q. Yang, T. Zhang, Q. Jing, J. Chen, Y.S. Zhou, P. Bai, Z.L. Wang, *Nano Lett.* **2014**, *14*, 3208.
[28] L. Zhang, B. Zhang, J. Chen, L. Jin, W. Deng, J. Tang, H. Zhang, H. Pan, M. Zhu, W. Yang, Z. L. Wang, *Adv. Mater.* **2016**, *28*, 1650.
[29] B. Dudem, Y. H. Ko, J. W. Leem, S. H. Lee, J. S. Yu, *ACS Appl. Mater. Interfaces* **2015**, *7*, 20520.
[30] Y. Zheng, L. Cheng, M. Yuan, Z. Wang, L. Zhang, Y. Qin, T. Jing, *Nanoscale* **2014**, *6*, 7842.
[31] H. T. Baytekin, B. Baytekin, J. T. Incorvati, B. A. Grzybowski, *Angew. Chem.* **2012**, *124*, 4927.
[32] C. ÓMathúna, T. O'Donnell, R. V. Martinez-Catala, J. Rohan, B. O'Flynn, *Talanta* **2008**, *75*, 613.
[33] J. Chun, B. U. Ye, J. W. Lee, D. Choi, C.-Y. Kang, S.-W. Kim, Z. L. Wang, J. M. Baik, *Nat. Commun.* **2016**, *7*, 12985.
[34] S. He, Z. Yu, H. Zhou, Z. Huang, Y. Zhang, Y. Li, J. Li, Y. Wang, D. Li, *Nano Energy* **2018**, *52*, 134.
[35] H. Qiao, Y. Zhang, Z. Huang, Y. Wang, D. Li, H. Zhou, *Nano Energy* **2018**, *50*, 126.
[36] G. Xu, X. Li, X. Xia, J. Fu, W. Ding, Y. Zi, *Nano Energy* **2019**, *59*, 154.
[37] U. J. Yang, J. W. Lee, J. P. Lee, J. M. Baik, *Nano Energy* **2019**, *57*, 293.
[38] Y. Xie, S. Wang, S. Niu, L. Lin, Q. Jing, J. Yang, Z. Wu, Z. L. Wang, *Adv. Mater.* **2014**, *26*, 6599.
[39] A. Šutka, K. Mālnieks, A. Linarts, M. Timusk, V. Jurķāns, I. Gorņevs, J. Blūms, A. Bērziņa, U. Joost, M. Knite, *Energy Environ. Sci.* **2018**, *11*, 1437.
[40] L. Lapčinskis, K. Mālnieks, A. Linarts, J. Blūms, K. Šmits, M. Järvekülg, M. Knite, A. Šutka, *ACS Appl. Energy Mater.* **2019**, *2*, 4027.
[41] J. L. Hutter, J. Bechhoefer, *Rev. Sci. Instrum.* **1993**, *64*, 1868.
[42] K. L. Johnson, K. Kendall, A. D. Roberts, *Proc. R. Soc. A* **1971**, *324*, 301.

© 2019 WILEY-VCH Verlag GmbH & Co. KGaA, Weinheim

3. pielikums/ Appendix III

A. Šutka, A. Linarts, K. Malnieks, K. Stiprais, **L. Lapčinskis**, Dramatic increase in polymer triboelectrification by transition from a glassy to rubbery state, *Mater. Horiz.* **2020**, *7(2)*, 520-523.

Materials Horizons

COMMUNICATION

Check for updates

Cite this: *Mater. Horiz.*, 2020, 7, 520

Received 9th September 2019, Accepted 7th October 2019

DOI: 10.1039/c9mh01425j

rsc.li/materials-horizons

Dramatic increase in polymer triboelectrification by transition from a glassy to rubbery state†

Andris Šutka, *[a] Artis Linarts, [b] Kaspars Mālnieks, [a] Klāvs Stiprais[a] and Linards Lapčinskis [b]

Here we report an order of magnitude increase of triboelectric charge density of glassy polymers such as polystyrene (PS), polycarbonate (PC) and poly(methyl methacrylate) (PMMA) when heated above the glass transition temperature. Transition is accompanied by the larger force required for separation. Undeniably, surface roughness plays a great role in contact electrification, however as we see in this work its impact is overrated when compared to the influence of physical properties.

New concepts

The triboelectrification mechanisms of polymers have been studied in different ways to find out if the mechanism is electron transfer or heterolytic covalent bond breakage. Although the experimental and theoretical observations contradict the electron transfer as a mechanism for polymer triboelectrification, several studies published recently by Zhong Lin Wang *et al.* have assumed the transfer of electrons (*Adv. Mater.*, 2018, 1706790; *ACS Nano*, 2019, **13**, 2034). The electron transfer was considered after observing faster decay of the surface charge upon heating or decreasing of triboelectrification after contacting identical materials (from which one is curved) at evaluated temperatures. In the present work, we are executing a solid experimental work and demonstrating the contact electrification of glassy polymers at different temperatures and observing a dramatic three orders of magnitude increase in surface charge when passing the transition temperature to a rubbery state. This is a first-time demonstration of such an effect, which indicates with no doubt that the triboelectrification mechanism must be a covalent bond break. Our experimental setup allows us to measure the separation force simultaneously with electric measurements and we have found that the adhesion for polymers also changes significantly when crossing the glass transition temperature. The increased adhesion, softening and deformation, with no doubt, will enhance covalent bond cleavage, material transfer, and surface charge formation. All experimental aspects are discussed in the manuscript in detail and an alternative interpretation of the experimental observations published by Wang *et al.* has been included. The results are highly important for designing triboelectric nanogenerator devices and to identify correct materials for better performance.

The mechanisms of triboelectrification in polymers have been under strong debate in the last few years as this phenomenon has a critical role in mechanical energy harvesting by triboelectric nanogenerator (TENG) devices,[1] preventing electric discharge from accumulated surface charge and protecting electric devices,[2] and to enhancing the separation in particle filters.[3] The three main mechanisms considered for polymer electrification are: (i) electron transfer,[4–6] (ii) heterolytic covalent bond break and material transfer,[7–10] and (iii) ion transfer.[11] From the aforementioned, ion transfer, where ions are separated between water adsorbate layers on contacted polymers, seems not the dominating mechanism as proven by several studies from independent groups.[5,10,12] The polymer contact electrification has been observed in the complete absence of water[12] and between identical materials[10] which should exhibit the same affinity between cationic and ionic species in water. Thus, in the past few years, the debate has concentrated on electron transfer and covalent bond breaking as possible dominating polymer triboelectrification mechanisms.

The latter, heterolytic covalent bond cleavage (heterolysis or heterolytic fission) has been gaining acceptance as a credible mechanism for polymer triboelectrification. According to this interpretation, scission and material transfer occur on contacted-separated polymers thus providing cationic and ionic species, as well as mechanoradicals on the same surface.[7–9] The charge measured in TENG devices is the net surface charge.[10] It was also demonstrated in a recent study that the surface charge increases with decreasing polymer cohesion or increasing surface adhesion. More extensive covalent bond scission and triboelectrification was recorded in case of soft and sticky polymers.[10]

Electron transfer between two contacted polymer insulators is also opposed by theoretical considerations. This process is endothermic and relocating an electron from one polymer to another would require 5–10 eV.[11] This is much higher than the

[a] *Research Laboratory of Functional Materials Technologies, Riga Technical University, Paula Valdena 3/7, Riga LV-1048, Latvia. E-mail: andris.sutka@rtu.lv*
[b] *Institute of Technical Physics, Riga Technical University, Paula Valdena 3/7, Riga LV-1048, Latvia*

† Electronic supplementary information (ESI) available: Experimental details, Fig. S1–S8 and Table S1. See DOI: 10.1039/c9mh01425j

This journal is © The Royal Society of Chemistry 2020

thermal energy at room temperature (0.026 eV). Although local frictional heating can occur during the material contacting-separating process and the polymer surface can heat up above the melting point,[13] the energy is still an order of magnitude too small to serve the electron transfer between contacted-separated polymer insulators. Polymer insulators do not contain electron-rich or electron-poor functional groups and thus the electron transfer is impossible.[11,14] In the same manner we do not expect the electron transfer between dispersed polymer species and organic solvents in suspensions. This kind of electron transfer does, however, occur in conductor–semiconductor contact where it is induced by electronic excitation under friction due to contact potential difference.[15–18]

Despite the experimental observations and theoretical considerations that appear to contradict the electron transfer as a mechanism for polymer triboelectrification, several studies published recently have assumed the transfer of electrons.[4,5] The electron transfer was considered after observing the contact electrification between two identical polymers from which one is curved and the phenomenon was attributed to the proposed charge transfer model by introducing the curvature-induced energy shift of the surface states.[5] However, this can be easily attributed to internal stresses which act in favor of covalent bond breaking and contact electrification upon contacting as it was reported already before.[19,20] Although the electron exchange is energetically costly the electron cloud overlapping the electron-cloud-potential-well model has been proposed to support electron transfer between polymer insulators.[4] To prove this experimentally, a dielectric semiconductor (SiO_2) surface was electrified by rubbing against polymer and the surface charge was measured after heating at a certain temperature. The authors observed that the surface charge decays faster at higher temperatures (especially fast at temperatures above 300 °C) and attributed this observation to electron thermionic emission.[4] However, this can be easily attributed also to thermal decomposition of transferred polymer pieces, which carry the charge.

In the present work, we are clarifying the polymer contact electrification mechanisms by testing the surface charge formation on amorphous polymers at different temperatures starting from room temperature and crossing the glass transition temperature (T_g). The experiments show with full certainty that the surface charge is drastically increased when transferring from glassy to rubbery state, thus confirming heterolytic covalent bond breakage as a mechanism for polymer triboelectrification.

Our material choice was amorphous polymers because their macromolecular structure is much simpler in comparison with crystalline polymers with the clearly observable transition from a glassy to a rubbery state. Polystyrene (PS), polycarbonate (PC) and poly(methyl methacrylate) (PMMA) films were hot-pressed on a perforated Cu electrode to ensure adherence. The film thickness was kept constant by using a 100 μm thick spacer. The processing parameters for each polymer are described in the Experimental section, ESI.† Materials were contacted with the copper counter electrode in a vertical separation TENG device as described in the Experimental section, ESI.† The pressing force, the gap between the two sides and the separation speed were controlled by an INSTRON E1000 All-Electric Dynamic Test Instrument. A specific custom-made heatable sample holder was used for the experiments (Fig. S1, ESI†). The net surface charge was calculated from the current $\left(Q = \int I \mathrm{d}t\right)$ measured between two electrodes upon contacting-separating.

The net surface charge for all polymers increases slightly when the temperature is raised from room temperature to a temperature below the polymer glass transition point. For example, by increasing the temperature from 25 °C to 110 °C in the case of PC, the surface charge increases only from 0.006 to 0.011 nC cm^{-2}. When the temperature reaches the glass transition the surface charge increases drastically by more than an order of magnitude for all polymers under study (Fig. 1(a) and (b)). The qualitative measures of performance for TENG devices such as V_{OC} and I_{SC} are also increased as demonstrated in Fig. 1(c) and (d). The glass transition temperature for each polymer was found from differential scanning calorimetry measurements (Fig. S2–S4 and Table S1, ESI†) and corresponds well to temperatures above which a drastic Q increase is observed. Also, the surface temperature was monitored by a thermal camera at each measurement temperature (Fig. S5, ESI†) to ensure the correct experiment.

Rubbery state polymers behave like elastomers – they are soft and undergo large reversible deformations. The adhesion for polymers also changes significantly when crossing T_g as observed experimentally (Fig. S6, ESI†). For example, the separation force for PS increases from 0.25 N at room temperature to 31 N at a temperature above the transition point. Our experimental setup allows us to measure the separation force simultaneously with electric measurements upon contacting-separating. All these factors *i.e.*, adhesion, softening and deformation, with no doubt, will enhance covalent bond cleavage, material transfer, and surface charge formation. Softer materials are more prone to mechanical damage, and deformation will allow achieving a larger contacting area, but adhesion will enhance the material transfer. At every step of contacting-separating, some material is transferred from one surface to another, but as the transport can occur both ways[8] a long-term performance is observed. The outputs of a PMMA TENG device operating at a temperature above the polymer T_g are stable over 5000 cycles (Fig. 2(a)). The same behaviour was observed also for other polymers.

The experimental results contradict the work by C. Xu *et al.*, where the authors measured the decrease of Q upon heating by contacting flat Kapton against chemically identical curved Kapton.[5] However, the conditions were very different in their case. First, Kapton has high temperature durability and glass transition temperature in the range of 360–400 °C, but the tests were performed at lower temperatures. Second, the contact-electrification between identical Kapton materials with different curvature may not be due to curvature-induced energy shifts of the surface states as the authors are claiming,[5] as the curvature increases the difference in cohesion energy between contacted films which, as presented in our previous work, triggers triboelectrification.[10] The strain is relaxed in polymer films by heating thus decreasing the difference in E_{coh} between

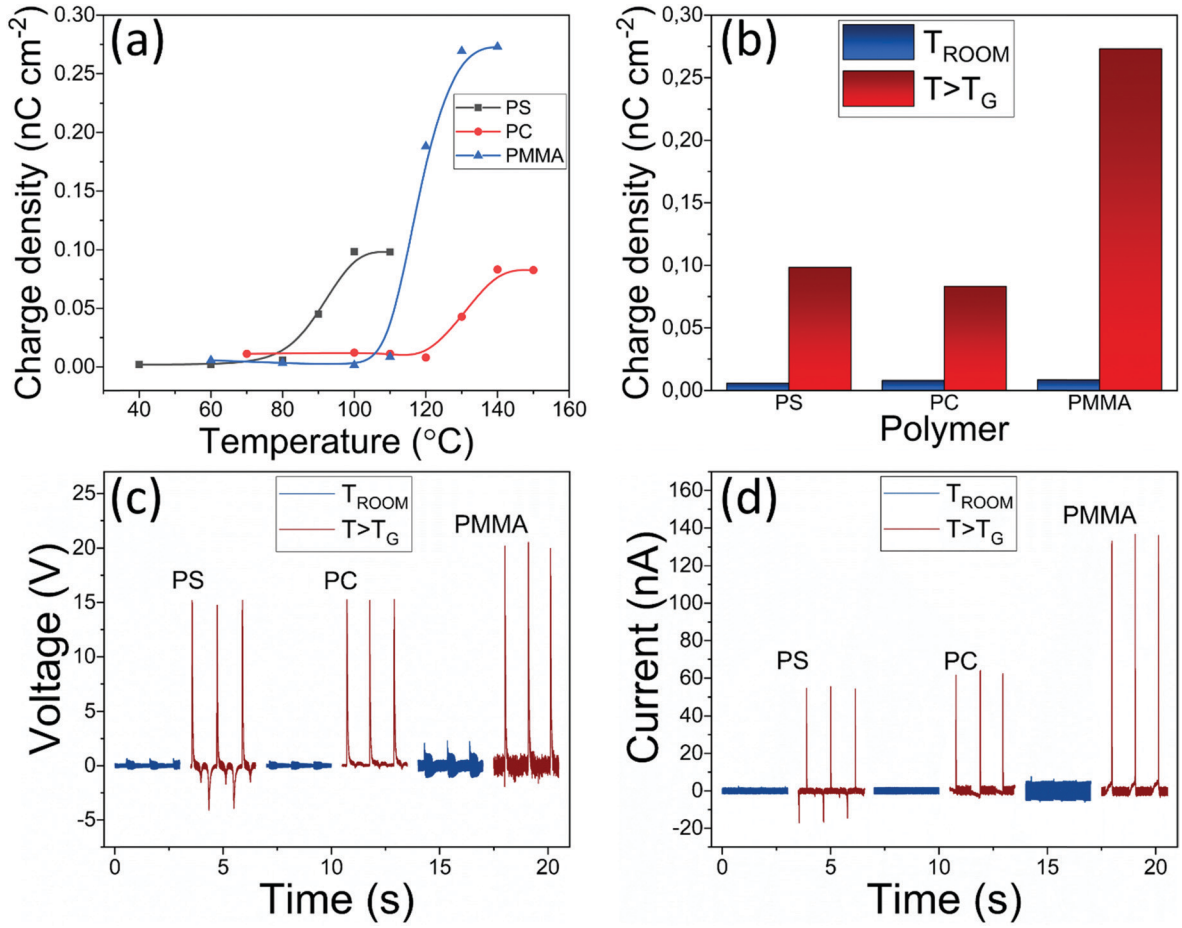

Fig. 1 (a) Charge density shows a steep rise as the temperature of the TENG device reaches the corresponding T_g of the polymer; (b) charge density at a temperature exceeding T_g differs from one at room temperature by an order of magnitude; (c) open circuit voltage and (d) short circuit current of polymers at room temperature and at temperature above T_g.

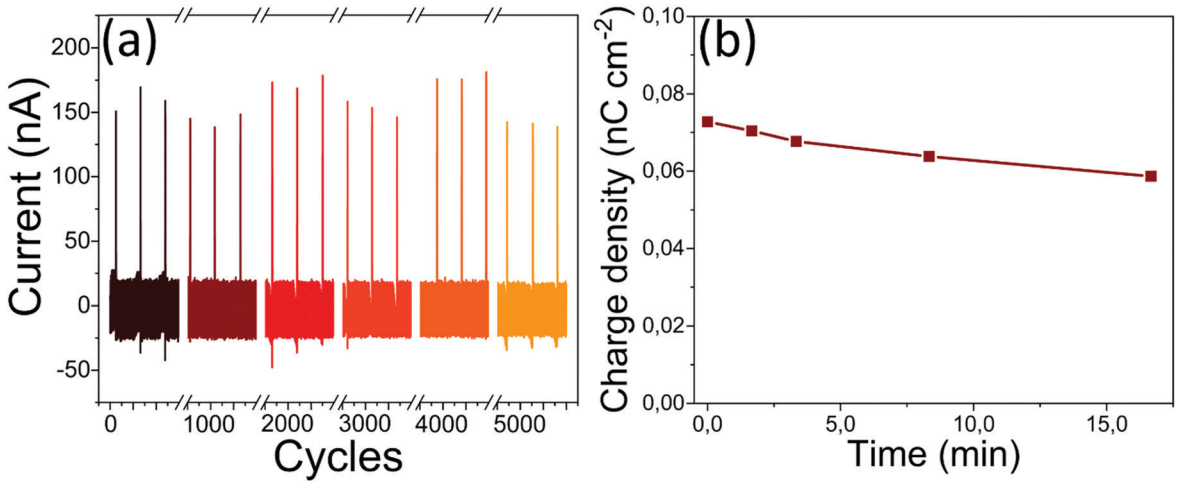

Fig. 2 (a) Current measurements of a PMMA based TENG device over 5000 contacting cycles and (b) surface charge density of a PS based TENG device in non-contact motions at temperature exceeding T_g.

flat and curved films. This is the most probable reason why charge decrease upon heating is observed by Xu *et al.*[5]

The increase in Q above T_g cannot be related to a change in surface roughness. The root mean square surface roughness was measured by atomic force microscopy as described in the Experimental section, ESI.† For PC the surface roughness remains almost the same – before: 38.4 nm, after: 33.9 nm. For PS the roughness is increased from 9.9 nm to 59.6 nm, but

 This journal is © The Royal Society of Chemistry 2020

for PMMA it is decreased from 162.0 nm to 78.1 nm. Although the surface roughness is changing for PS and PMMA, it does not influence the Q value significantly. For example, when we increase the roughness of PMMA from 0.08 μm to >1 μm, the Q changes only by a little, from 0.008 nC cm^{-2} to 0.037 nC cm^{-2} (see the ESI† experimental section for the approach to obtain rough surface, SEM images (Fig. S7, ESI†) and TENG device V_{OC} and I_{SC} measurements (Fig. S8, ESI†)), but by crossing the glass transition temperature, we observed an increase of surface charge from 0.008 nC cm^{-2} to 0.273 nC cm^{-2} in the case of PMMA. The experiments show that the role of intermolecular forces is more significant than nanostructuring, thus the expensive nanostructuring approaches for producing TENG devices can be considered unnecessary.

The stability of surface charges was studied by running the vertical separation TENG device in the non-contact regime above T_g where contacted-separated films are further oscillated without physical contact. The potential between two electrodes is changed by the oscillation and in order to balance the variable potential, the electrons are transferred between two electrodes. As can be seen from Fig. 2(b), the surface charges are relatively stable and decrease only by a little (less than 15%) in 15 minutes, thus showing that the electron transfer and thermionic emission should not be the case. The slow discharge can be attributed to the interaction of the polymer surface with the molecules, ions, and particles from the surrounding atmosphere.[7]

Conclusions

In conclusion, we have demonstrated that the polymer triboelectrification increases by more than an order of magnitude when crossing the transition temperature from glassy to rubbery state. The increase in surface charge can be attributed to material softening and an increase in stickiness. This should enhance the material transfer, thus indicating covalent bond breaking as the mechanism for polymer triboelectrification.

Conflicts of interest

There are no conflicts to declare.

Acknowledgements

This research was supported by the European Regional Development Fund within the project ''Hybrid energy harvesting systems'' 1.1.1.1./16/A/013.

Notes and references

1 B.-Y. Lee, D. H. Kim, J. Park, K.-I. Park, K. J. Lee and C. K. Jeong, *Sci. Technol. Adv. Mater.*, 2019, **20**, 758.
2 H. T. Baytekin, B. Baytekin, T. M. Hermans, B. Kowalczyk and B. A. Grzybowski, *Science*, 2013, **341**, 1368.
3 P. P. Tsai, H. Schreuder-Gibson and P. Gibson, *J. Electrost.*, 2002, **54**, 333.
4 C. Xu, Y. Zi, A. C. Wang, H. Zou, Y. Dai, X. He, P. Wang, Y.-C. Wang, P. Feng, D. Li and Z. L. Wang, *Adv. Mater.*, 2018, 1706790.
5 C. Xu, B. Zhang, A. C. Wang, H. Zou, G. Liu, W. Ding, C. Wu, M. Ma, P. Feng, Z. Lin and Z. L. Wang, *ACS Nano*, 2019, **13**, 2034.
6 J. Chen and Z. L. Wang, *Joule*, 2017, **1**, 480.
7 H. T. Baytekin, A. Z. Patashinski, M. Branicki, B. Baytekin, S. Soh and B. A. Grzybowski, *Science*, 2011, **333**, 308.
8 H. T. Baytekin, B. Baytekin, J. T. Incorvati and B. A. Grzybowski, *Angew. Chem., Int. Ed.*, 2012, **51**, 4843.
9 R. K. Pandey, H. Kakehashi, H. Nakanishi and S. Soh, *J. Phys. Chem. C*, 2018, **122**, 16154.
10 A. Šutka, K. Mālnieks, L. Lapčinskis, P. Kaufelde, A. Linarts, A. Bērziņa, R. Zābels, V. Juŗkāns, I. Gorņevs, J. Blūms and M. Knite, *Energy Environ. Sci.*, 2019, **12**, 2417.
11 L. S. McCarty and G. M. Whitesides, *Angew. Chem., Int. Ed.*, 2008, **47**, 2188.
12 H. T. Baytekin, B. Baytekin, S. Soh and B. A. Grzybowski, *Angew. Chem., Int. Ed.*, 2011, **50**, 6766.
13 P. N. Bogdanovich and D. V. Tkachuk, *Tribol. Int.*, 2006, **39**, 1355.
14 H. S. Nalwa, *Handbook of Organic Conductive Molecules and Polymers*, Wiley, New York, 1997.
15 J. Liu, A. Goswami, K. Jiang, F. Khan, S. Kim, R. McGee, Z. Li, Z. Hu, J. Lee and T. Thundat, *Nat. Nanotechnol.*, 2018, **13**, 112.
16 J. Liu, K. Jiang, L. Nguyen, Z. Lib and T. Thundat, *Mater. Horiz.*, 2019, **6**, 1020.
17 J. Liu, M. Miao, K. Jiang, F. Khan, A. Goswami, R. McGee, Z. Li, L. Nguyen, Z. Hu, J. Lee, K. Cadien and T. Thundat, *Nano Energy*, 2018, **48**, 320.
18 S. Lin, Y. Lu, S. Feng, Z. Hao and Y. Yan, *Adv. Mater.*, 2019, **31**, 1804398.
19 A. E. Wang, P. S. Gil, M. Holonga, Z. Yavuz, H. T. Baytekin, R. M. Sankaran and D. J. Lacks, *Phys. Rev. Mater.*, 2017, **1**, 035605.
20 M. Sow, R. Widenor, A. Kumar, S. W. Lee, D. J. Lacks and R. M. Sankaran, *Angew. Chem., Int. Ed.*, 2012, **51**, 2695.

4. pielikums/ Appendix IV

A. Šutka, K. Mālnieks, **L. Lapčinskis,** M. Timusk, K. Kalniņš, A. Kovaļovs, J. Bitenieks, M. Knite, D. Stevens, J. Grunlan, Contact electrification between identical polymers as the basis for triboelectric/flexoelectric materials, *Phys. Chem. Chem. Phys.* **2020**, *22(23)*, 13299-13305.

PCCP

ROYAL SOCIETY OF CHEMISTRY

PAPER

View Article Online
View Journal

Check for updates

Cite this: DOI: 10.1039/d0cp01947j

Contact electrification between identical polymers as the basis for triboelectric/flexoelectric materials†

Andris Šutka,*[a] Kaspars Mālnieks,[a] Linards Lapčinskis,[b] Martin Timusk,[c] Kaspars Kalniņš,[d] Andrejs Kovaļovs,[d] Juris Bitenieks,[e] Māris Knite,[b] Daniel Stevens[f] and Jaime Grunlan*[g]

Polymer contact electrification offers the possibility to harvest mechanical energy using lightweight, flexible and low-cost materials, but the mechanism itself is still unresolved. Several recent studies confirm heterolytic covalent bond breaking as the mechanism for surface charge formation. Here it is shown that the reason for the formation of surface charge by contacting two identical polymers results from the fluctuation in the surface irregularities, and that contacted materials with a greater porosity or surface roughness differential result in a greater generation of surface charge. Porosity and surface roughness create uneven surface length percentage changes in the lateral direction during deformation, which changes the charge density across the surface during relaxation. Multilayered membranes exhibit flexoelectric properties upon pressing and releasing by generating charge without separating individual membrane layers. This new insight deepens the understanding of polymer contact electrification and highlights better ways to prepare triboelectric or flexoelectric nanogenerator devices.

Received 10th April 2020,
Accepted 14th May 2020

DOI: 10.1039/d0cp01947j

rsc.li/pccp

Published on 08 June 2020. Downloaded by 656155 on 6/8/2020 9:09:17 AM.

Introduction

Triboelectric nanogenerator (TENG) mechanical energy harvesters, sensors, actuators, self-powered biomedical devices and flexo-electrets can be made from low-cost, flexible and soft polymers.[1–14] Most TENG devices have been designed by considering electron transfer as the primary mechanism for polymer contact electrification. The triboelectric materials in these devices are chosen by selecting two polymers with a large difference in polymer "electron affinity".[15] Despite this method for choosing materials for a TENG, it has been reported that polymer contact electrification comes from heterolytic bond cleavage that is accompanied by material transfer.[16–21] The surface charge was found to increase with decreasing polymer cohesion energy (and crosslinking degree) or increasing surface adhesion.[21] Bond scission is enhanced for soft and sticky polymers due to easier material transfer.

In the present study, the contact electrification mechanism between identical polymer materials is better clarified. The electrification between interfaces of the same material is shown to increase with larger differences in surface roughness or porosity. Surface irregularities cause uneven deformation upon contacting–separating and result in an unbalanced surface charge. Uneven deformation is a potential reason for surface charge formation on contacted–separated polymers with different cohesion energy.[21] Polymer surfaces that have different cohesion energies that undergo different extents of deformation under a fixed load results in unbalanced charges, which is a key aspect for improving the performance of TENG devices. There are several studies that report higher surface charge is generated in TENG devices where both surfaces are nanostructured,[22–24] but here it is shown that this may not be necessary to achieve high surface charge and performance.

This new insight in the contact electrification mechanism is important for the design of flexoelectric materials that could be made from neat (unfilled) polymers, but also exhibit piezo-electric-like behavior similar to ferroelectric ceramics. To observe

[a] Research Laboratory of Functional Materials Technologies, Faculty of Materials Science and Applied Chemistry, Riga Technical University, Paula Valdena 3/7, 1048 Riga, Latvia. E-mail: Andris.Sutka@rtu.lv
[b] Institute of Technical Physics, Faculty of Materials Science and Applied Chemistry, Riga Technical University, Paula Valdena 3/7, 1048 Riga, Latvia
[c] Institute of Physics, University of Tartu, W. Ostwaldi Str. 1, 50411 Tartu, Estonia
[d] Institute of Materials and Structures, Faculty of Civil Engineering, Riga Technical University, Kipsalas 6A, 1048 Riga, Latvia
[e] Institute of Polymer Materials, Faculty of Materials Science and Applied Chemistry, Riga Technical University, Paula Valdena 3/7, 1048 Riga, Latvia
[f] Department of Chemistry, Texas A&M University, College Station, TX 77843, USA
[g] Departments of Mechanical Engineering, Materials Science and Engineering, and Chemistry, Texas A&M University, College Station, TX 77843, USA. E-mail: jgrunlan@tamu.edu

† Electronic supplementary information (ESI) available: 59 figures and 4 tables. See DOI: 10.1039/d0cp01947j

Published on 08 June 2020. Downloaded by 656155 on 6/8/2020 9:09:17 AM.

flexoelectric behavior, the material should have a multilayered or porous structure, with opposite charges at the multilayer interface or on the void surface.[25] Upon deformation, the pre-existing polarization in these materials is changed and, in order to balance the potential change, current flows between conductive electrodes. To create charged interfaces, porous polymers are subjected to a high electric field that generate many tiny microplasma discharges in the voids,[25,26] or by depositing a secondary material on one side of pores,[4] resulting in positive and negative electric charges on opposite internal pore surfaces. It should be noted that the long-term stability of flexoelectric polymer foam is limited due to the discharge of the produced internal charges.[25] In this work, flexoelectric materials are produced from identical multilayered polymer films with different porosity. In this case, there is no need to apply an external electric field to generate charge. In addition, the piezoelectric-like behavior does not disappear over time. Researchers have recently demonstrated flexoelectricity for pure bone mineral with no embedded charges or piezoelectric collagen components.[27] The flexoelectricity in bone is attributed to its gradient porous structure. The literature is scarce regarding the intrinsic electrification of polymers upon deformation.

Results and discussion

Polymer films were deposited with different surface roughnesses on conductive electrodes, which were connected by an external circuit, as is common for TENG devices.[1] The schematic image of the triboelectric nanogenerator is shown in ESI,† Fig. S1. The polymer films were mutually contacted-separated with controlled force and electric current (or voltage) was measured between the conductive plates. The surface charge forms on contacted surfaces upon separation, which in turn induce the electrostatic charge on the conductive electrode in the TENG device. So as plates are separated, the potential between conductive plates is changed. To account for the change in electrical potential, electrons flow between the two plates in the external electrical circuit. When device is fully separated, equilibrium is reached. During another contact, the potential changes again and electron flow in the external circuit is induced. Fully contacting and compressing both plates allows electrostatic equilibrium to be reached once again (see ESI,† Fig. S2 for a schematic representation of the working principle). The surface charge was estimated from the current measured between the TENG electrodes under operation by using $Q = \int i\mathrm{d}t$, where i is the instantaneous current. The separation of two surfaces in the TENG device (5 mm) is much larger than the film thickness (100 μm), so the surface charge density is very close to the charge density calculated from the current.[28] More measurement details are described in the Experimental section.

Triboelectric devices prepared with the films of the same polymer with different roughness, can generate an order of magnitude larger peak voltage than devices prepared from two smooth and two porous (rough) films (Fig. 1(a)). The surface charge at smooth–smooth, porous–smooth and porous–porous contacts was measured for different polymers: polyethylene–octene copolymer (EOC), polystyrene (PS), ethyl cellulose (EC), polycarbonate (PC), poly(methyl methacrylate) (PMMA), styrene–ethylene–butylene–styrene copolymer (SEBS) and poly(vinylidene fluoride) (PVDF). PVDF did not exhibit any intrinsic piezoelectric response (ESI,† Fig. S3 and S4). For all tested devices, a significantly higher voltage, current, and charge were observed when the smooth polymer film was contacted with porous one (Fig. 1(b) and ESI† Fig. S5–S11, Table S1). The observed values are stable for at least 10 000 contact–separation cycles, as shown in ESI,† Fig. S12. The magnitude of charge density among polymers changes due to the varying differences in surface roughness between contacted films. For SEBS, there is increased adhesion between contacting layers, which contributes to charge formation.[21] The formation of a rough uniform polymer surface can be observed visually by diffusive light reflection behavior (ESI,† Fig. S13) or by increased water contact angle (ESI,† Table S2 and Fig. S14–S27). Surface roughness (RMS) of all polymer samples (both porous and smooth) is determined from atomic force microscopy (AFM) surface topography measurements (ESI,† Table S3). In addition to surface topography, tapping amplitude and tapping phase images are recorded for these samples (ESI,† Fig. S28–S41). Most of the polymers have notable differences in surface roughness when comparing smooth and rough samples. In case of PMMA and SEBS, the rough and smooth samples have the same roughness values, but the surface morphology is completely different, suggesting that the different morphology may affect surface charge formation. For example, the relatively high roughness values for smooth PMMA obviously comes from deep craters appearing in otherwise flat morphology. Tapping phase images reveal no contrast beyond obvious influences from surface topography, which can be expected in single-polymer films with no additives. In addition, no crystalline phases are also detected in these samples. For more detailed information see Discussion S1 (ESI†).

The surface charge on contacted–separated polymer films was measured as a function of the difference in surface roughness. For this purpose, PVDF films with different porosity were prepared by precipitation from solutions in dimethylformamide at different concentrations, using methanol as the non-solvent. The rationale for choosing PVDF is based on our previous experience that this methodology allows full control over PVDF film porosity. Surface roughness between samples varies from 0.2 to 1 μm (ESI,† Table S4 and Fig. S42). Electrodes made from these PVDF films were contacted–separated in a TENG device for these measurements. As expected, the surface charge density increases with increasing difference in roughness (Fig. 1(c)). Results clearly show that charges form on the interface between films of the same polymer with different porosity. Contact electrification of polymer films can be vastly improved by contacting a smooth surface with a rough one.

Surface potential studies were done using Scanning Kelvin Probe on smooth PVDF before and after contacting with another smooth or rough PVDF (ESI,† Fig. S43). By contacting–separating against another smooth sample the surface potential changed from −172 mV to −192 mV. However, after contacting

This journal is © the Owner Societies 2020

Published on 08 June 2020. Downloaded by 656155 on 6/8/2020 9:09:17 AM.

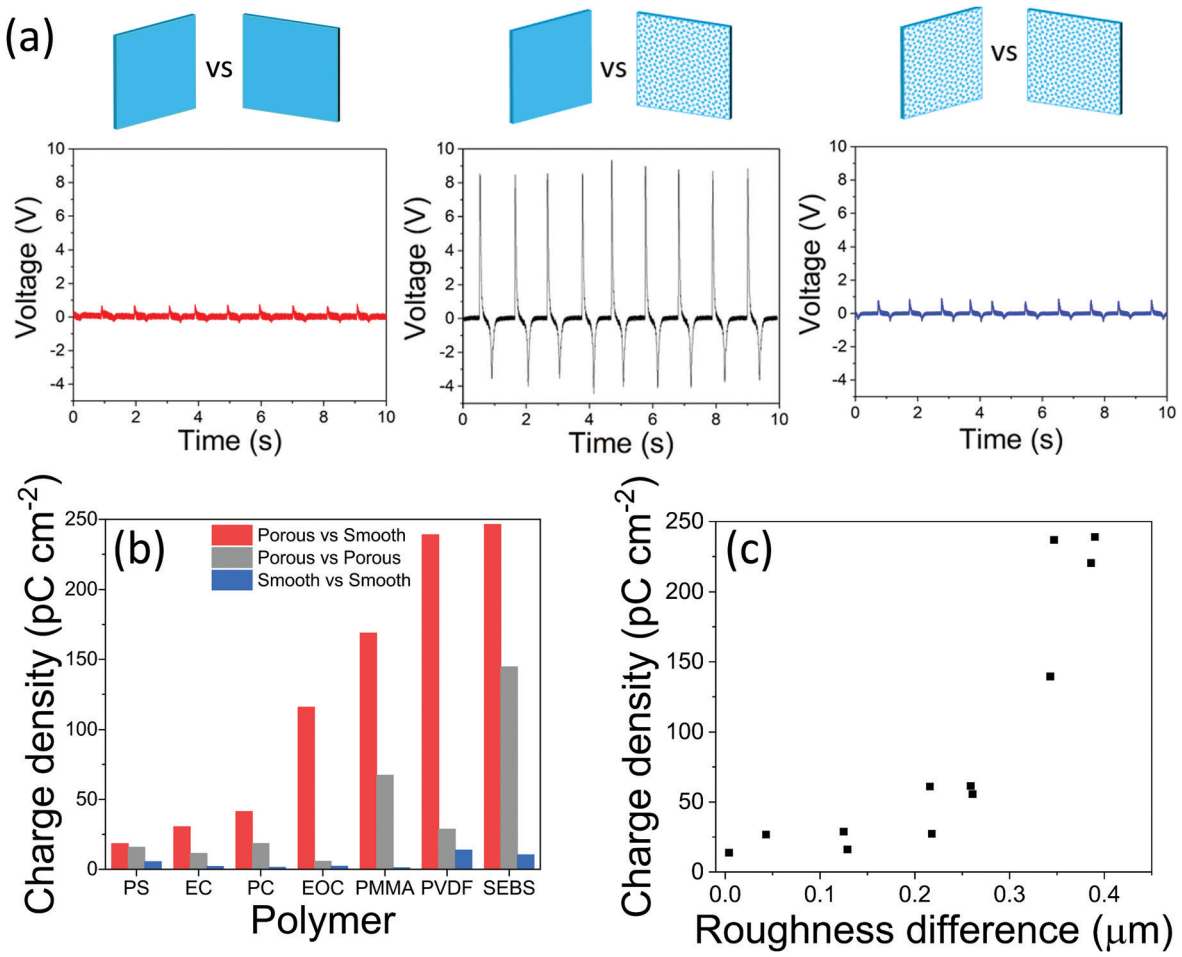

Fig. 1 (a) Open-circuit voltage (V_{OC}) generated by contacting–separating smooth–smooth, smooth–porous and porous–porous EOC film combinations (from left to right). (b) Surface charge density formed in contact–separation of two identical polymer films with different surface roughness and (c) relationship between surface charge density generated in contact–separation and surface roughness disparity of employed PVDF films.

with rough PVDF, the surface potential increased to −415 mV. Scanning Kelvin Probe measurements supports our hypothesis that contacting–separating dissimilar surfaces results in a higher charge density.

The similar trend was observed when polymers with clearly distinctive physicochemical properties are used as porous and smooth contacting materials. Higher contact-electrification is expected when hard polymer is tested in combination with a soft one.[21] For this reason, in order to obtain high performance and confirm our hypothesis, we constructed TENG device where the elastomer SEBS is contacted against the rigid PMMA – two polymers that exhibit the greatest difference in hardness among the polymers used in this study. As expected, different amounts of surface charge were dependent on surface roughness of PMMA (Fig. 2). Higher values (V_{OC} of 240 V, I_{SC} of 0.85 μA, Q of 9.6 nC cm^{-2} and E of 2.5 mJ m^{-2}) are obtained when the relatively smooth SEBS is contacted against porous PMMA. In the TENG device where smooth SEBS is combined with smooth PMMA, much smaller V_{OC} of 100 V, I_{SC} of 0.05 μA, Q of 1.2 nC cm^{-2} and E of 0.6 mJ m^{-2} values were achieved.

The observed contact electrification from contacting films containing the same polymer but with different porosity is due to uneven deformation at the contacted area, which in turn changes the charge density across the surface during relaxation.[29] Triboelectrification between interfaces induces a charge on the conductive electrodes and generates a current flow between them. This uneven deformation at the interface was confirmed by developing a 2D plane finite element model for a macro-scale simulation (described in Experimental section). The configuration of the 2D model for the rough sample was taken from AFM measurements of the PVDF surface (ESI,† Fig. S44). When the deformable rough body is pressed against a smooth deformable surface, a different surface length percentage change (Δ_f) in lateral direction for two surfaces is observed. In contrast, when two surfaces with similar roughness are contacted, the observed Δ_f on both is almost the same (Fig. 3). The difference of Δ_f between two surfaces at 140 N load is 7.4 and 1.2 times greater when rough *vs.* planar or rough *vs.* rough surfaces are contacted, respectively. These simulations are in good agreement with contact electrification measurements, supporting the assertion that uneven deformation and relaxation

Published on 08 June 2020. Downloaded by 656155 on 6/8/2020 9:09:17 AM.

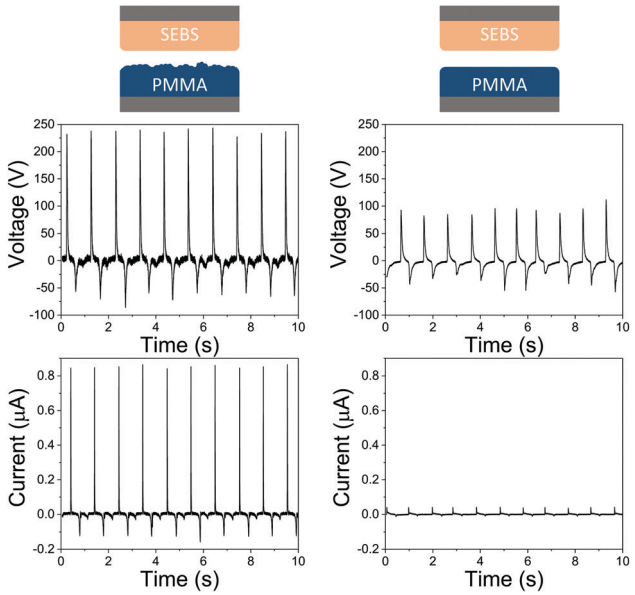

Fig. 2 Measured V_{OC} and I_{SC} values when elastomer SEBS is contacted against porous (left) and much smoother (right) PMMA film in TENG device.

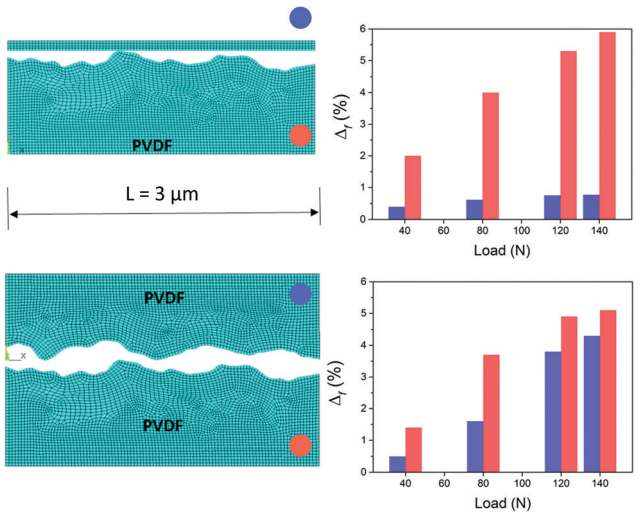

Fig. 3 Surface length percentage change (Δ_f) for each surface in rough–planar (top) or rough–rough (bottom) contacts. A larger difference in Δ_f is observed when contacting surfaces have a greater roughness disparity.

of each surface are responsible for net surface charge generation. These uneven deformations result in heterolytic bond scission that create cationic and anionic polymer chain fragments that contribute to net surface charge.

The influence of molecularly thin water adsorbate layers should also be considered as during the separation of contacted materials, ion transfer between these layers contributes to overall charge transfer.[30] This mechanism stems from the fact that different materials have different affinity towards ion adsorption from water adsorbate layers on their surface. When different polymers are contacted, the water layers fuse together, allowing ions of each layer to migrate to the opposite surface. The extent of ion migration is determined by the aforementioned adsorption affinity of different materials. When separated, a disbalance of cations and ions form in the water layers, thus providing a surface charge. However, this mechanism is improbable if chemically identical materials are contacted as both films exhibit equal adsorption affinities towards cations and anions in water adsorbate layers. Electron affinity is influenced by chemical surface properties of the polymer (crystallinity, functional groups) but it is considered to be a constant of the material. However, one may consider that the different surface roughness result in different amount of adsorbed water thus further dominating triboelectrification phenomenon. ATR-FTIR results of polymers used in this study does not show any significant changes in vibrations related to surface adsorbed water (a broad peak in wavenumber region from 3000 to 3600 cm^{-1}, ESI,† Fig. S45–S51) when smooth and porous samples are compared indicating that surface roughness has a negligible influence on the amount of the adsorbed water. All triboelectrification tests were made under constant humidity, so this effect is probably insignificant. Additionally, polymer contact electrification occurs in the absence of water.[31]

The charge transfer between two connected conductive plates can be also observed when loading and unloading contacted polymer films without separation. Layered structures prepared from commercial PVDF membranes with different porosity (0.10, 0.22 and 0.45 μm) were adhered to an electrode with double-sided carbon adhesive tape to prevent friction between film and electrode. Before testing, the films were pressed together by applying a 500 N load for 1 min. The samples were then loaded and unloaded without separation (tested in piezo-regime) with forces ranging from 5 to 100 N. As expected, the current and charge measured between two electrodes increases with increasing difference in porosity between the membranes (ESI,† Fig. S52 and S53). A charge density of 5.5 pC cm^{-2} was measured at a load of 100 N by pressing a membrane with a pore size of 0.10 μm against a membrane with 0.45 μm pores, which is an order of magnitude higher than pressing identical 0.10 μm membranes (ESI,† Fig. S53). The observed current is attributed to the flexoelectricity from the friction and uneven deformation at the interface of the two membranes with different porosity. Uneven deformation leads to unequal surface charge density at the interface of the two membranes and forms a dipole moment. Upon loading and unloading, the polarization in the membranes is changed, causing the potential change and current flow between the two electrodes.

This flexoelectric response can be further increased with multilayer films. For this purpose, three commercial PVDF membranes with different porosity were pressed together in varying order by applying a 500 N load for 1 min. The largest charge density of 26 pC cm^{-2} was measured from the multilayer with a pore size of 0.45 μm in the middle (membranes with a pore size of 0.10 and 0.22 μm on each side, respectively). The observed performance is stable for at least 10 000 compression cycles as demonstrated in ESI,† Fig. S54. This charge density is five times higher than that measured in the piezo regime at the same 100 N load from the best two-membrane

This journal is © the Owner Societies 2020

Published on 08 June 2020. Downloaded by 656155 on 6/8/2020 9:09:17 AM.

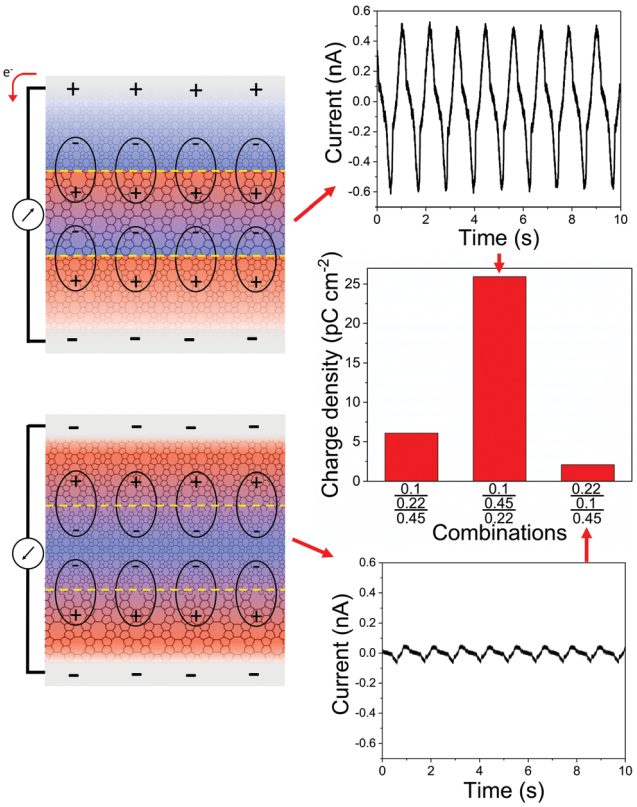

Fig. 4 Dipole and flexoelectric charge formation in multi-layered membrane samples with different membrane order. Membranes with three different pore sizes (0.10, 0.22 and 0.45 μm) were used for experiments and layered in different order as indicated on the bar graph (middle right). Higher current is measured from the layered sample with 0.45 μm pores in the middle, which is related to dipole alignment in the same direction and formation of larger intrinsic polarization. The sign of the charge formed on each membrane surface at the interface was also measured experimentally (Fig. S17 in ESI†).

sample. When the membrane with a pore size of 0.10 μm is in the middle, an order of magnitude smaller charge is measured (Fig. 4). Charge density increases with increasing pressing force (ESI,† Fig. S55). The higher performance for this three-membrane sample was also confirmed by COMSOL simulations (ESI,† Fig. S56). In the case of the three-layer sample (with a pore size of 0.45 μm in the middle), the potential difference between conductive electrodes is 7.30 mV. For the two-layer sample from membranes with pore size 0.10 μm and 0.45 μm (or 0.22 μm and 0.45 μm), the potential difference is 6.29 mV or 1.02 mV, respectively.

The formation of dipoles with opposite polarity at the interfaces explains the lower performance for the multilayered sample with a membrane pore size of 0.10 μm in the middle. For further investigation, the sign of surface charge forming on membrane films was measured after contacting with other membranes having different pore sizes (ESI,† Fig. S57). The membrane with 0.45 μm pores gains positive charge against the membrane with 0.10 μm pores, but negative charge when contacting against the membrane with 0.22 μm pores. The membranes with a pore size of 0.10 μm and 0.22 μm gain a negative and positive charge, respectively, when contacting the other membrane. This observation solidifies the better performance for the three-layer membrane film with 0.45 μm pores in the middle. In this case, dipoles are aligned in one direction, as shown in the top of Fig. 4, while in the other two cases the inverse dipoles are formed in the layered structure. As a result, electric fields are formed with an opposite direction that compensate each other and limit the charge induction on conductive plates. For the same reason, smaller electric fields are formed when making structures with more than three layers. This result is expected because every next layer will produce dipoles with the opposite polarization direction, as demonstrated in ESI,† Fig. S58.

Experimental

Materials and preparation of films

Thermoplastic polymer films were prepared by hot pressing and precipitation. Hot pressing was used to obtain smooth films of poly(methyl methacrylate) (PMMA, Sigma Aldrich), ethylene–octene copolymer (EOC; Engage 8200), styrene–ethylene–butylene–styrene copolymer (SEBS; Lifoflex UV 306A 1030) and polycarbonate (PC, recycled). These polymers were received as pellets or powders. An appropriate amount of polymer was weighed to prepare 70 × 100 mm films. Metal frames ensured that all films had a uniform thickness of 100 μm. After one minute of heating with minimal pressure, the polymer was pressed with 4–5 MPa pressure. After 3 minutes the sample was removed from the press and cooled to room temperature. To obtain porous (rough) surfaces, the pressed polymer films were immersed in solvent for 30 seconds, followed by non-solvent (*i.e.* does not dissolve the polymer phase but is miscible with the solvent). This procedure generates a porous polymer surface layer. Polymer films were studied for contact electrification and used to create triboelectric nanogenerators (TENG) by adhering to Sn-doped In_2O_3 (ITO) coated PET (sheet resistance 60 Ω sq^{-1}, Kintec) by using conductive double-sided adhesive carbon tape (Science Services).

Polyvinylidene fluoride (PVDF, Sigma Aldrich), ethyl cellulose (EC, Sigma Aldrich) and polystyrene (PS, recycled) films were prepared by spin-coating and precipitation. To prepare porous EC films, 10 wt% EC was added to ethanol (Sigma Aldrich, 99.8%) and toluene (Sigma Aldrich, 99.8%), mixed in a 1 : 4 weight ratio. This mixture was heated at 60 °C in a closed glass vial under constant stirring until its appearance became transparent. The EC solution was cooled to room temperature and then spin-coated at 3000 rpm on an ITO-coated PET substrate. The coated substrate was immediately immersed in hexane (Sigma Aldrich, 95%) non-solvent for 30 seconds to cause precipitation of EC on the substrate. These films were then removed from hexane and dried in ambient conditions. Smooth EC films were prepared by the same procedure, but without the immersion-precipitation step. The PVDF and PS films were precipitated by using a 15 wt% solution in dimethylformamide and methanol as the non-solvent. In the case of

Published on 08 June 2020. Downloaded by 656155 on 6/8/2020 9:09:17 AM.

PVDF, films were prepared from solutions with concentration ranging from 5 to 25 wt% to control the surface roughness.

Multilayer membrane samples were prepared from commercial membranes (Milipore filter, China) with pore sizes of 0.1, 0.22, and 0.45 μm. Conductive double-sided adhesive carbon tape was used between the multilayer membrane samples and ITO to prevent friction against the electrode, which provides a cleaner signal. The separate membrane layers were compressed together with a force of 500 N before testing.

Triboelectric measurements

Environmental conditions were monitored during all TENG measurements by Vernier Temperature Probe and Vernier Relative Humidity Probe connected to Vernier logger – relative humidity (RH) was in the range from 40% to 45%, while the temperature was 25 ± 1 °C. The contact area in the TENG device is 5 cm^2. The pressing force (10 N), frequency (1 Hz), separation speed (10 mm s^{-1}) and distance (5 mm) between sides were kept constant with an INSTRON E1000 All-Electric Dynamic Test Instrument (USA). To measure the flexoelectric response, the samples were tested in the piezo-regime without separating the two sides of the device and loading from 5 to 100 N. The short-circuit current (I_{SC}) and open-circuit voltage (V_{OC}) at a load resistance of 1×10^9 Ω was measured for all TENG devices by using a custom-made voltage divider in combination with a Keithley 6514 electrometer connected to a Picoscope 5444B PC oscilloscope to provide high time resolution. The surface charge was calculated from the current measured between oscillating TENG electrodes using $Q = \int i dt$, where i is the instantaneous current.

Finite element modelling

A section was selected for 2D finite element modelling using ANSYS 16.2. The model was made by PLANE182 elements. Contact between adjacent surfaces by target elements (TARGE169) was placed along the top surface of the PVDF and the contact elements (CONTA172) were used along the bottom surface of the plate. The pressure was simulated by applying displacement boundary conditions in the *y*-direction to the nodes along the upper surface of the plate. All nodes at the bottom of the material were constrained to prevent them from moving. The interaction between surfaces was defined using node-to-node contact pairs without a node penetration option. The contact algorithm was governed by Augmented Lagrangian contact. The contact problem was solved by accounting for both the geometric nonlinearity (large-displacement formulation) and the elastic-plastic material behavior. For mechanical properties, the Poisson's ratio of PVDF was held constant at 0.3 and elastic modulus at 1.428 GPa. The stress–strain curve, shown in ESI,† Fig. S59, provided the necessary information about plasticity. The smooth plate was considered rigid.

Smooth *vs.* rough and rough *vs.* rough PVDF cases were studied. The configuration of the 2D section cut through the rough sample was taken from a real PVDF 3D surface measured by AFM (ESI,† Fig. S44). The resulting surface length percentage change was calculated using the ratio between length before and after the contact (eqn (S1), ESI†):

$$\Delta_f = \left| \frac{f_0 - f_i}{f_0} \right| \times 100 \quad (1)$$

where f_0 is the length of deformable surface before contact (μm) and f_i is the length of deformable surface after contact (μm).

Atomic force microscopy

Atomic force microscopy was performed using Smena, NT-MDT AFM in the semi-contact mode. For each sample height sensor (surface topography), tapping amplitude and tapping phase images were recorded (ESI,† Fig. S28–S41, from left to right – surface topography, tapping amplitude, tapping phase). Set-point amplitude as well as PID parameters were extensively and meticulously varied to determine whether tapping phase images reveal features beyond direct correlation with surface topography images. The scan area for correct surface roughness measurement was chosen depending on the sample. For smooth and homogeneous samples with small surface roughness, small scan areas (5×5 or 10×10 μm) provide sufficient information for correct surface roughness evaluation. In general, surface roughness value increases as the scan area is increased and approaches plateau at a specific scan range. For most samples surface roughness value reaches a constant in the scan area range between 20×20 and 50×50 μm, thus requiring a scan area of 50×50 μm. The root mean squared (RMS) surface roughness was measured from at least three different areas on every film, and the RMS surface roughness uncertainty was calculated statistically at a 95% confidence level. RMS surface roughness expresses the square root of the mean square of height deviations of the surface, measured from the mean height of the data plane. Additionally, for some samples, small scan area (3×3 or 5×5 μm) was used to obtain images that would exhibit surface features at a suitable scale for tapping phase and surface topography analysis. For 50×50 μm images scan rate of 0.1 Hz was used in case of rough samples and 0.2 Hz for some smooth samples. For smaller scan areas scan rate of 0.3 Hz was used.

Scanning Kelvin probe measurements

Kelvin probe measurements were performed using a Scanning Kelvin Probe system SKP5050. The surface potential of the sample was scanned by oscillating a 2 mm gold tip in a 5-by-5 point area (total 25 points) to obtain surface potential maps. Distance between two scanned points was approximately 500 μm, therefore almost the whole area of the sample was scanned. The contact with the opposite smooth or porous PVDF sample was accomplished by placing this sample on the PVDF sample in the device and applying a load of 10 N for 1 minute. The second scan was performed right after the removal of the opposite sample.

ATR-FTIR measurements

Attenuated total reflection-Fourier transform infrared (ATR-FTIR) measurements were recorded on a Bruker Vertex 70 FTIR spectrometer in the range of 4000 to 700 cm^{-1} at a resolution of 2 cm^{-1}.

This journal is © the Owner Societies 2020

Published on 08 June 2020. Downloaded by 656155 on 6/8/2020 9:09:17 AM.

Measurements were done in constant environmental conditions at room temperature.

Conclusions

Triboelectrification by pressing together chemically identical polymers was shown to occur due to different porosity (or surface roughness), which causes uneven deformation at the contacting–separating interface that results in unequal surface charge density. An increasing disparity in porosity or roughness between the two contacting surfaces increases the magnitude of the net surface charge. The greatest triboelectric performance results when smooth and rough (nanostructured) polymer surfaces are used. The triboelectrification of the interfaces from the same material with different porosity was also observed without separation of the contacted surfaces, which caused a flexoelectric response. Multilayered membranes were shown to further increase the flexoelectric response, indicating a pathway to create multilayered polymer films with flexoelectric (piezoelectric-like) response (1.3 pC N^{-1}) comparable to solid-state piezoelectric materials, such as hydroxyapatite (2 pC N^{-1}), poly-*b*-hydroxybutyrate (1.3 pC N^{-1}) and quartz (2.3 pC N^{-1}).[32]

Conflicts of interest

There are no conflicts to declare.

Acknowledgements

Linards Lapčinskis and Andris Šutka acknowledge Riga Technical University's Doctoral Grant and Research Excellence grant programs. Kaspars Mālnieks acknowledge the European Regional Development Fund within the Activity 1.1.1.2 ''Post-doctoral Research Aid'' of the Specific Aid Objective 1.1.1 ''To increase the research and innovative capacity of scientific institutions of Latvia and the ability to attract external financing, investing in human resources and infrastructure'' of the Operational Programme ''Growth and Employment'' (Grant No. 1.1.1.2/VIAA/3/19/404).

Notes and references

1 Z. L. Wang, J. Chen and L. Lin, *Energy Environ. Sci.*, 2015, **8**, 2250.
2 L. Zheng, Y. Wu, X. Chen, A. Yu, L. Xu, Y. Liu, H. Li and Z. L. Wang, *Adv. Funct. Mater.*, 2017, **27**, 1606408.
3 C. Dagdeviren, B. D. Yang, Y. Su, P. L. Tran, P. Joe, E. Anderson, J. Xia, V. Doraiswamy, B. Dehdashti, X. Feng, B. Lu, R. Poston, Z. Khalpey, R. Ghaffari, Y. Huang, M. J. Slepian and J. A. Rogers, *Proc. Natl. Acad. Sci. U. S. A.*, 2014, **111**, 1927.
4 J. Chun, J. W. Kim, W. S. Jung, C. Y. Kang, S. W. Kim, Z. L. Wang and J. M. Baik, *Energy Environ. Sci.*, 2015, **8**, 3006.
5 B. Baytekin, H. T. Baytekin and B. A. Grzybowski, *Energy Environ. Sci.*, 2013, **6**, 3467.
6 T. Quan and Y. Yang, *Nano Res.*, 2016, **9**, 2226.
7 T. Quan, Y. Wu and Y. Yang, *Nano Res.*, 2015, **8**, 3272.
8 B. Chen, Y. Yang and Z. L. Wang, *Adv. Energy Mater.*, 2018, **8**, 1702649.
9 Y. Yang and Z. L. Wang, *Nano Energy*, 2015, **14**, 245.
10 Y. Su, Y. Yang, H. Zhang, Y. Xie, Z. Wu, Y. Jiang, N. Fukata, Y. Bando and Z. L. Wang, *Nanotechnology*, 2013, **24**, 295401.
11 Y. Wu, X. Zhong, X. Wang, Y. Yang and Z. L. Wang, *Nano Res.*, 2014, **7**, 1631.
12 X. Wang, Z. L. Wang and Y. Yang, *Nano Energy*, 2016, **26**, 164.
13 Y. Wu, X. Wang, Y. Yang and Z. L. Wang, *Nano Energy*, 2015, **11**, 162.
14 K. Zhang, S. Wang and Y. Yang, *Adv. Energy Mater.*, 2017, **7**, 1601852.
15 J. Chen and Z. L. Wang, *Joule*, 2017, **1**, 480.
16 H. T. Baytekin, A. Z. Patashinski, M. Branicki, B. Baytekin, S. Soh and B. A. Grzybowski, *Science*, 2011, **333**, 308.
17 H. T. Baytekin, B. Baytekin, J. T. Incorvati and B. A. Grzybowski, *Angew. Chem., Int. Ed.*, 2012, **51**, 4843.
18 R. K. Pandey, H. Kakehashi, H. Nakanishi and S. Soh, *J. Phys. Chem. C*, 2018, **122**, 16154.
19 M. M. Apodaca, P. J. Wesson, K. J. M. Bishop, M. A. Ratner and B. A. Grzybowski, *Angew. Chem., Int. Ed.*, 2010, **49**, 946.
20 A. E. Wang, P. S. Gil, M. Holonga, Z. Yavuz, H. T. Baytekin, R. M. Sankaran and D. J. Lacks, *Phys. Rev. Mater.*, 2017, **1**, 1.
21 A. Šutka, K. Mālnieks, L. Lapčinskis, P. Kaufelde, A. Linarts, A. Bērziņa, R. Zābels, V. Juŗkāns, I. Gorņevs, J. Blūms and M. Knite, *Energy Environ. Sci.*, 2019, **12**, 2417.
22 Y. Yang, H. Zhang, Y. Liu, Z. H. Lin, S. Lee, Z. Lin, C. P. Wong and Z. L. Wang, *ACS Nano*, 2013, **7**, 2808.
23 S. Wang, L. Lin and Z. L. Wang, *Nano Lett.*, 2012, **12**, 6339.
24 Y. Zheng, L. Cheng, M. Yuan, Z. Wang, L. Zhang, Y. Qin and T. Jing, *Nanoscale*, 2014, **6**, 7842.
25 Q. Deng, L. Liu and P. Sharma, *Phys. Rev. E: Stat., Nonlinear, Soft Matter Phys.*, 2014, **90**, 1.
26 S. Bauer, R. Gerhard-Multhaupt and G. M. Sessler, *Phys. Today*, 2004, **57**, 37.
27 F. Vasquez-Sancho, A. Abdollahi, D. Damjanovic and G. Catalan, *Adv. Mater.*, 2018, **30**, 1.
28 H. Zou, Y. Zhang, L. Guo, P. Wang, X. He, G. Dai, H. Zheng, C. Chen, A. C. Wang, C. Xu and Z. L. Wang, *Nat. Commun.*, 2019, **10**, 1.
29 F. Yi, L. Lin, S. Niu, P. K. Yang, Z. Wang, J. Chen, Y. Zhou, Y. Zi, J. Wang, Q. Liao, Y. Zhang and Z. L. Wang, *Adv. Funct. Mater.*, 2015, **25**, 3688.
30 L. McCarty and G. Whitesides, *Angew. Chem., Int. Ed.*, 2008, **47**, 2188.
31 H. T. Baytekin, B. Baytekin, S. Soh and B. A. Grzybowski, *Angew. Chem., Int. Ed.*, 2011, **50**, 6766.
32 S. Guerin, S. A. M. Tofail and D. Thompson, *NPG Asia Mater.*, 2019, **11**, 1.

5. pielikums/ Appendix V

L. Lapčinskis, A. Linarts, K. Mālnieks, H. Kim, K. Rubenis, K. Pudzs, K. Smits, A. Kovaļovs, K. Kalniņš, A. Tamm, C.K. Jeong, and A. Šutka, Triboelectrification of nanocomposites using identical polymer matrixes with different concentrations of nanoparticle fillers, *J. Mater. Chem. A* **2021**, *9(14)*, 8984-8990.

Journal of Materials Chemistry A

ROYAL SOCIETY OF CHEMISTRY

COMMUNICATION

View Article Online
View Journal | View Issue

Check for updates

Cite this: J. Mater. Chem. A, 2021, 9, 8984

Received 24th December 2020
Accepted 22nd March 2021

DOI: 10.1039/d0ta12441a

rsc.li/materials-a

Published on 25 March 2021. Downloaded by University of Tartu on 4/25/2021 6:37:17 AM.

Triboelectrification of nanocomposites using identical polymer matrixes with different concentrations of nanoparticle fillers†

Linards Lapčinskis, [ab] Artis Linarts, [b] Kaspars Mālnieks, [a] Hyunseung Kim, [cd] Kristaps Rubenis, [e] Kaspars Pudzs, [f] Krisjanis Smits, [f] Andrejs Kovaļovs, [g] Kaspars Kalniņš, [g] Aile Tamm, [h] Chang Kyu Jeong *[cd] and Andris Šutka *[a]

In this study, we investigate triboelectrification in polymer-based nanocomposites using identical polymer matrixes containing different concentrations of nanoparticles (NPs). The triboelectric surface charge density on polymer layers increased as the difference in nanoparticle filler concentration between the two triboelectric layers escalated, despite the fact that the polymer matrix was the same in both layers. This effect was observed in tests of various polymer types and filler NPs. Our mechanical experiments and finite element analysis simulations confirmed that polymeric triboelectrification is related to the surface viscoelastic deformation that occurs during mechanical contact and separation, and is not dependent on electronic or chemical properties, but rather physicochemical and mechanical properties. This supports the heterolytic scission of covalent bonds in polymer chains as an explanation for the triboelectricity. Accordingly, this study marks a significant contribution to the fundamental understanding of the mechanism of polymeric triboelectrification and will be relevant to the development of triboelectric sensors and energy harvesters.

Introduction

Achieving an improved understanding of polymeric contact electrification (*i.e.*, triboelectrification) is critical to the development of dielectric materials, high-voltage insulators, surface patterning, and triboelectric energy harvesters, as well as antistatic surfaces that improve safety.[1–3] Although several devices for triboelectric applications have recently been developed,[4–6] the principles of triboelectrification remain poorly understood. Polymeric triboelectrification is considered a particularly complex phenomenon due to the relatively complicated mechanical behaviors.[7–10] While a number of mechanisms have been proposed to explain polymer contact electrification,[11] including electron transfer,[12] bi-directional mass (material) transfer paired with heterolytic scission of bonds,[7,8,13–16] and ion transfer between water adsorbate layers.[17,18] Material transfer (*i.e.*, the transfer of minuscule pieces of polymer matter) seems to be the most likely, as a strong electron acceptor or donor groups that facilitate electron transfer are generally not present in dielectric and insulating polymers. Moreover, triboelectrification has been observed even in the complete absence of humidity and between chemically identical polymers;[7,19] accordingly, there is no obvious reason presenting imbalance between different ion species (*i.e.*, ion transfers) when the same material surfaces go through contact electrification.

Mass transfer occurs concurrently with the heterolytic scission of covalent bonds, which is a dominant contributor to polymer triboelectrification.[13] This mechanism has been confirmed through observation, by both X-ray photoelectron spectroscopy (XPS) and atomic force microscopy (AFM), of transferred polymeric pieces,[15,16] as well as by detection of very strong electrification in extremely soft and adhesive polymers.[16] Moreover, strong contact electrification is observed between polymer materials with a significant difference in mechanical hardness or porosity, regardless of their chemical composition,[7,20] as a result of the uneven surface deformation and relaxation during contact-separation.[20] Even two samples of a chemically identical polymer with a uniform surface

[a]Research Laboratory of Functional Materials Technologies, Faculty of Materials Science and Applied Chemistry, Riga Technical University, Paula Valdena 3/7, Riga, LV-1048, Latvia. E-mail: andris.sutka@rtu.lv

[b]Institute of Technical Physics, Faculty of Materials Science and Applied Chemistry, Riga Technical University, Paula Valdena 3/7, Riga, LV-1048, Latvia

[c]Division of Advanced Materials Engineering, Jeonbuk National University, Jeonju, Jeonbuk, 54896, Republic of Korea. E-mail: ckyu@jbnu.ac.kr

[d]Department of Energy Storage/Conversion Engineering of Graduate School, Hydrogen and Fuel Cell Research Center, Jeonbuk National University, Jeonju, Jeonbuk, 54896, Republic of Korea

[e]Rudolfs Cimdins Riga Biomaterials Innovations and Development Centre of RTU, Institute of General Chemical Engineering, Faculty of Materials Science, Riga Technical University, Pulka 3, Riga, LV-1007, Latvia

[f]Institute of Solid State Physics, University of Latvia, Kengaraga 8, Riga, LV-1063, Latvia

[g]Institute of Materials and Structures, Faculty of Civil Engineering, Riga Technical University, Kipsalas 6A, Riga, LV-1048, Latvia

[h]Institute of Physics, University of Tartu, W. Ostwaldi Street 1, 50411 Tartu, Estonia

† Electronic supplementary information (ESI) available. See DOI: 10.1039/d0ta12441a

This journal is © The Royal Society of Chemistry 2021

Published on 25 March 2021. Downloaded by University of Tartu on 4/25/2021 6:37:17 AM.

roughness can gain triboelectric surface charges after contact-separation if the thermal history of one of the polymers is altered to change its surface mechanical cohesive energy.[7] The thermally-enhanced mass transfer triboelectrification is maximized after glassy polymers transition to a rubbery state, undergoing a significant deformation and becoming softer and more adhesive.[8] These factors intensify and accelerate covalent bond breakage, mass transfer, and the resulting changes in the surface. Note that softer polymers are more prone to damage, as mechanical deformation in these polymers results in a larger contact area, while mass transfer increases as a result of the higher adhesion force.

Despite clear evidence of material mass transfer and covalent bond breakage as the mechanism of polymer triboelectrification, electron transfer is still considered a potential cause of polymer triboelectrification.[21–23] Moreover, devices that rely on polymer dielectrics have been developed based on polymer–inorganic composite materials, not pristine polymers.[24–29] There is, therefore, a need to investigate triboelectrification in more complex polymer-based composite systems to improve our understanding of how it operates and open the door to engineered triboelectric devices with enhanced performance.

In this paper, we confirm that mass transfer provides a better explanation for polymeric triboelectrification than electron transfer. To illustrate this, we used polymer-based composite structures with inorganic nanoparticle fillers. Identical polymer materials comprised of varying as well as identical amounts of inorganic particles were utilized to investigate the contact electrification of various polymer types. We determined that electrical output by triboelectrification increased as the difference in inorganic particle amounts increased between otherwise-identical polymer matrix-based composites. This trend was observed in numerous polymers, regardless of their chemical composition or the filler particle type of composites. The differences in the concentrations of filler particles of the composites caused uneven surface deformation during mechanical contact-separation cycles and resulted in unbalanced surface triboelectric charges even where the polymer matrix between two contacting layers was identical. These results were confirmed by our mechanical analyses and simulations. Accordingly, this study contributes to the development of improved triboelectrification mechanisms in insulating polymer-based materials.

Experimental procedure

Triboelectric device fabrication and measurement

Ethylene-vinyl acetate copolymer (EVA, vinyl acetate 40 wt%, Sigma Aldrich), polyvinyl acetate (PVAc, average M_w – 100 000, Sigma Aldrich), two-component polyurethane (PU 3544A and PU 3544B, Alchemie), and polydimethylsiloxane (PDMS, Sylgard 184 silicone elastomer, Dow) were purchased. Nanoparticles utilized for EVA-based nanocomposites were prepared as TiO_2 (Degussa P25), WO_3 (Sigma Aldrich), FeO(OH) (Sigma Aldrich), and MnO_2 (Sigma Aldrich) NPs. First, the polymer matrixes were prepared as solution status; EVA or PVAc were dissolved in $CHCl_3$, while PDMS base prepolymer was dissolved in hexane and PU-amine-containing part in acetone. NPs were dispersed in polymer solutions by ultrasonication. EVA- or PVAc-based nanocomposite slurry solution was cast in a Petri dish, dried, and cut into smaller pieces with hot pressing. The final films for testing were produced by hot pressing. PDMS- (or PU)-based nanocomposite slurry solutions were mixed until the solvent evaporated, and then the curing agent (or isocyanate-contained component) was blended for solidification, respectively, followed by casting in a Petri dish for preparing films. The thickness of each film was set as 500 μm by a separator. Next, the polymer-based film was adhered to an indium tin oxide (ITO)-coated polyethylene terephthalate (PET) substrate (PET/ITO, Sigma Aldrich) by a conductive double adhesive tape for each triboelectric generator (TEG) device with the size of 2.5 cm × 2.5 cm. The TEG testing was done at the controlled conditions – the separation distance of 5 mm, the pressing force of 10 N and the contact-separation frequency of 1 Hz. Generated voltage and current signals were measured by Keithley 6514 electrometer connected to a Picoscope 5444B PC oscilloscope system in open-circuit and short-circuit conditions, respectively. The relative humidity (RH) was maintained as 40% at the ambient atmosphere, which was known as a stable condition.[30] Surface charge was calculated from the current peak as measured from TEG devices using equation $Q = \int i dt$, where i is the instantaneous current. Contact and separation were done using Instron E1000 material testing machine to ensure repeatability.

Scanning Kelvin probe measurements

Kelvin probe measurements were performed by a Scanning Kelvin Probe system (SKP5050, KP Technology). A sample's surface potential was scanned by oscillating a 2 mm gold tip in a 5 × 5 points area (total 25 points) to obtain surface potential maps. As the distance between scanned points was about 500 μm, almost the entirety of the sample was scanned. SKP measurements of EVA/TiO_2 NPs composite were taken before and after contact with a pristine EVA layer and an identical counterpart composite layer by applying a load of 10 N for 1 min.

Finite element analysis simulation

Atomic force microscopy was used to randomly select a two-dimensional (2D) line model for finite element analysis (FEA) simulations using ANSYS R17.1 software. Five types of elastic moduli were utilized for EVA-based composite models, corresponding to different TiO_2 NP concentrations, *i.e.*, 0, 2.5, 5, 10, and 15 vol%. The Poisson's ratio of the EVA matrix was set as 0.3, and the elastic moduli of each case were set as 2.20, 3.06, 4.95, 5.92, and 7.10 MPa, respectively, as measured mechanically. The behavior of the surface roughness was considered as the reason for large surface deformation, therefore elastoplastic theory was applied for FEA and the stress–strain behavior curves of the EVA-based materials were added to the FEA models. The change in surface deformation length (Δ_f expressed as a percentage) was calculated as the ratio of original surface

Published on 25 March 2021. Downloaded by University of Tartu on 4/25/2021 6:37:17 AM.

height before contact (f_0) and deformed surface height during or after contact (f_i) using the following equation:

$$\Delta_f = \left|\frac{f_0 - f_i}{f_0}\right| \times 100$$

In ANSYS, the PLANE182 element was used in the finite element model of deformable bodies. Target elements (TARGE169) were placed along the top and bottom surfaces of the EVA-based layers and the mechanical contact elements (CONTA172) were used along the bottom and top surfaces. The pressure was simulated by applying displacement boundary conditions in the *y*-direction to the nodes along the upper surface. All bottom layer nodes were prevented from moving in the *x* and *z* directions. Interaction between surfaces was defined using the node-to-node contact pairs without penetrations. The contact algorithm was governed by the Lagrange contact. The calculation was solved, thereby accounting for the geometric nonlinearity (large-displacement formulation) and the elastic–plastic material behavior.

Results and discussion

The triboelectric polymer composite films were prepared from different polymers, *i.e.*, polyvinyl acetate (PVAc), ethylene-vinyl acetate copolymer (EVA), two-component polyurethane (PU), and polydimethylsiloxane (PDMS). Note that we did not select fluorinated polymers to exclude any artifacts of seriously different chemical components or electronegativity. To investigate the triboelectrification of various composites, we selected diverse inorganic filler particles, including TiO_2, FeO(OH), WO_3, and MnO_2 nanoparticles (NPs). Composite films were adhered to indium tin oxide (ITO) coated plastic substrates by conductive tape to fabricate a triboelectric energy generator (TEG), as illustrated in Fig. 1a.

When identical triboelectric layers contained the same particles in the same concentrations, very small current and voltage peaks were generated from the TEG (Fig. 1a, leftmost and rightmost panels). In contrast, much higher current and voltage peaks were produced where the polymer matrix was the same but the two triboelectric layers had different concentrations of filler particles (Fig. 1a, middle panel). This tendency is particularly clearly manifested in the case of pristine EVA polymer and its matrix-based composites with TiO_2 NPs filler (Fig. 1b and c). When the pristine EVA layer contacted the EVA-based composite containing 5 vol% of TiO_2 NPs filler, 24× higher current and 4×–5× higher voltage peaks were produced than the TEG resulting from two identical pristine EVA layers. The triboelectric charge density increased by an order of magnitude from 0.007 nC cm^{-2} to 0.093 nC cm^{-2}. We note that this phenomenon was consistently observed during tests of other pristine polymers and their matrix-based composites, including PVAc, PU, and PDMS matrixes with TiO_2 NPs filler (Fig. S1–S3†). The generated triboelectric charge densities of TEGs based on various polymer matrixes are presented in Fig. S4.† These results illustrate that higher surface charges are consistently induced across all types of polymers when a pristine polymer contacts a composite layer.

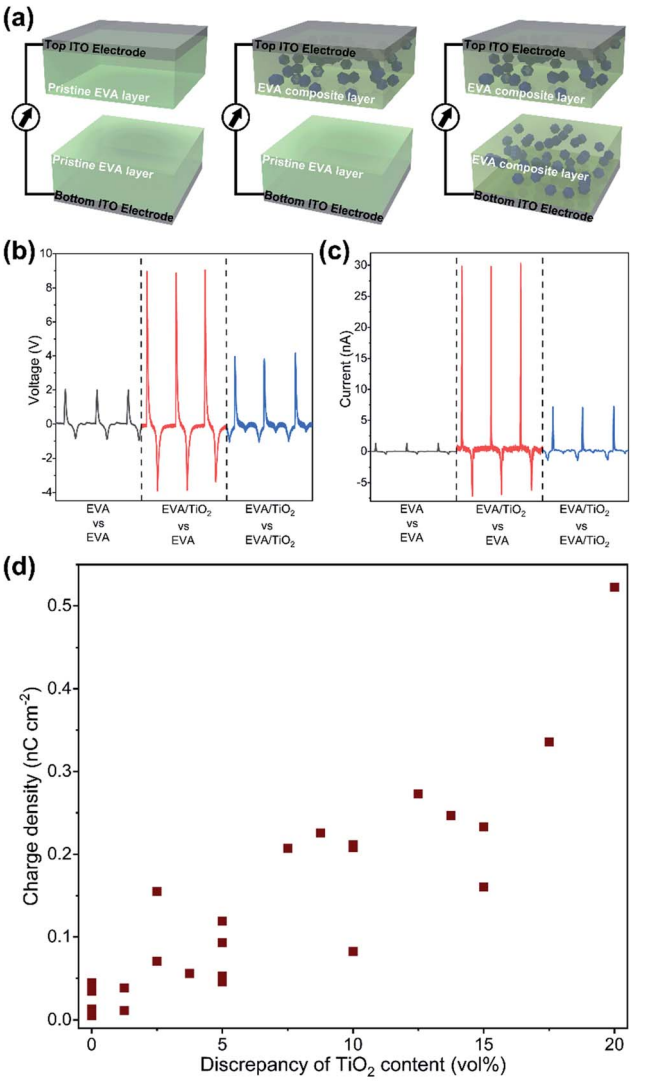

Fig. 1 (a) Schematics of three types of TEG devices using pristine EVA polymer and/or EVA-based composites. (b) Generated voltage and (c) current peaks by the three TEG devices. (d) Increasing the difference between the TiO_2 content in EVA layers used for TEG devices leads to increasing triboelectric surface charge density.

Even more interesting is the fact that surface charge increased as the difference in concentration of TiO_2 NPs in the composite increased. Fig. 1d shows the triboelectric surface charge density generated on the TEGs comprised of EVA/TiO_2 composites at different concentrations of TiO_2 NPs. Note that this data is related to only the difference in concentration, not the absolute concentration value. For example, very similar surface charges were observed from two different EVA/TiO_2 composite-based TEGs, one with TiO_2 NPs filler concentrations of 0 vol% and 5 vol%, and one with filler concentrations of 15 vol% and 20 vol%. These results strongly suggest that the difference in composite concentration determines the triboelectric charges of polymer-based composites, and not the absolute value of concentration. This in turn suggests that the

 This journal is © The Royal Society of Chemistry 2021

Published on 25 March 2021. Downloaded by University of Tartu on 4/25/2021 6:37:17 AM.

mechanical property related to the mass transfer mechanism is more important for triboelectricity than the dielectric property associated with the electronic or ionic transfer mechanisms.

In the hope of achieving deeper insights into the behavior of contact electrification, surface potential measurements of the EVA/TiO_2 composite films were taken using the scanning Kelvin probe (SKP). The area of the EVA/TiO_2 composite film with the TiO_2 NPs of 5 vol% was scanned at 25 points, resulting in a surface potential map with an average potential of 426.5 mV (Fig. 2a–c). This composite film was then contact-electrified with either another EVA/TiO_2 composite film or a pristine EVA film. The former process resulted in a slight increase in surface potential (666.0 mV, a mere 239.5 mV larger than the original surface potential). In contrast, the latter process induced a much higher surface potential (1154.7 mV), a significant amplification of 728.2 mV. In other words, triboelectric charges will vary significantly even where the same polymer matrixes undergo contact electrification, sometimes yielding strong and sometimes yielding weak triboelectric charges, depending on the quantity of filler particles.

We also determined that triboelectrification, while it is dependent on the particle filler concentration, is not a function of particle composition or shape. EVA composites based on other NPs filler types (*e.g.*, FeO(OH), WO_3, and MnO_2 NPs) were fabricated to measure triboelectric charge generation. As shown in Fig. 3a–d, particle shape, size, and composition were also different from the TiO_2 NPs. For example, WO_3 NPs are larger than TiO_2 NPs, and FeO(OH) NPs are needle-shaped rather than sphere-shaped. Water contact angle (CA) measurements for EVA composites incorporating various filler particles were determined to evaluate the effect of composites surface energy on triboelectrification (Fig. S5†). For the composites with TiO_2, MnO_2, WO_3 and FeO(OH) fillers, the CA values were measured as 96.9 ± 0.4°, 92.9 ± 1.6°, 89.2 ± 2.4° and 98.1 ± 1.0°, respectively. They are very similar. Therefore, the influence of surface energy is negligible, indicating that the filler type mainly influences the mechanical properties, not physico-chemical events. Fig. 3e shows the generated charge density of each TEG composed of different inorganic particles. Different inorganic particles-based TEG devices with the same concentration in the same polymer matrix present similar output, particularly in the case of pristine EVA polymer *versus* EVA composite with each particle type. Although the absolute values of generated triboelectric charge density may vary slightly according to filler type due to dispersion homogeneity (Fig. S6†) and other secondary effects, the trend is consistent across all cases; triboelectric charges between different composition composites were always highest.

The reason that stronger triboelectrification may be observed during mechanical contact between identical polymer matrixes containing different concentrations of filler particles might relate to the differences in the surface deformation, and the associated differences in mechanical properties.[20] The amount of filler particles affects the Young's modulus of the composite. As shown in Fig. 4, the Young's modulus of 2.20 MPa for 0 vol% TiO_2 NPs rises to 7.10 MPa for 15 vol% TiO_2 NPs. Put differently, increasing the TiO_2 content in the EVA composite

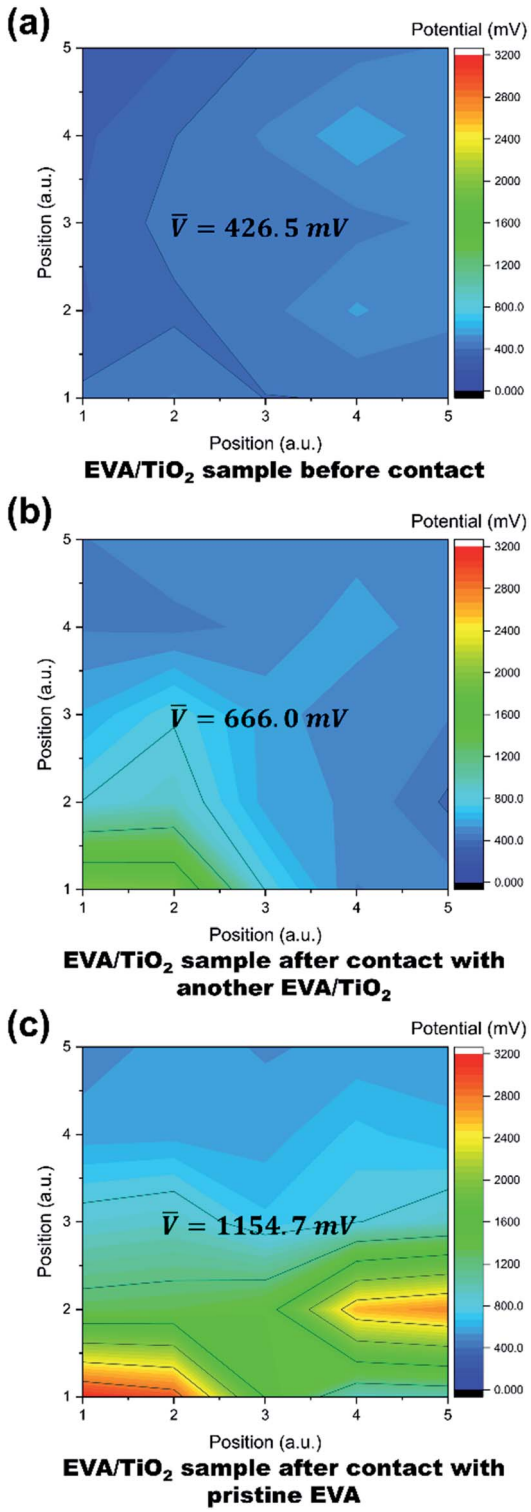

Fig. 2 Surface potentials, measured by SKP, of an EVA/TiO_2 composite sample (a) before and after contact electrification with (b) another EVA/TiO_2 composite layer and (c) a pristine EVA polymer layer.

layers results in stiffer triboelectric layers, with the mechanical contact and separation of the two polymer layers with different filler contents causing the unequal deformation of each layer. This, in turn, induces the variable stress on the triboelectric

Published on 25 March 2021. Downloaded by University of Tartu on 4/25/2021 6:37:17 AM.

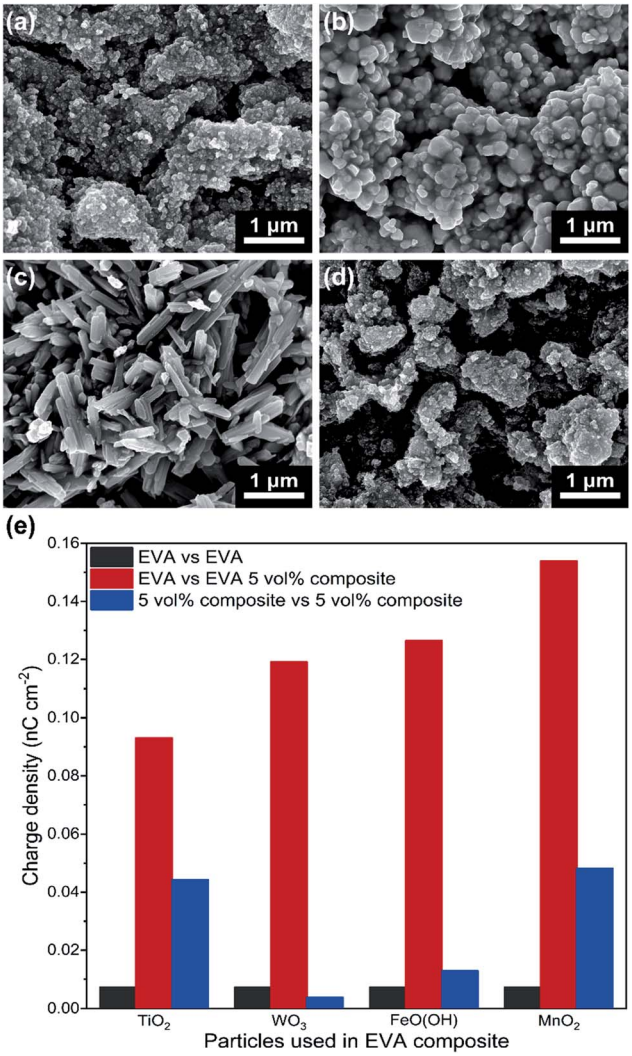

Fig. 3 SEM images of (a) TiO_2 NPs, (b) WO_3 NPs, (c) FeO(OH) NPs, (d) MnO_2 NPs. (e) The generated surface charge density of three types of TEG devices based on pristine EVA polymer and EVA/5 vol% NPs composites using various NPs as fillers.

surfaces and ultimately the different mass transfer. Where the polymers exhibit the same deformation, the bi-directional mass transfer between two surfaces would be expected to occur with the same probability, which would result in only a very small net triboelectric charge.

Raman spectroscopy was conducted to test the triboelectric principle at the identical polymer matrixes (EVA *versus* EVA/TiO_2), as shown in Fig. S7.† There is no band shift, which indicates any electrochemical events (electron or ion transfers without mass transfers) are not involved in the triboelectrification. In addition, the slight increment of intensity of TiO_2 bands after contacts is presumably due to some mass transfers of EVA matrix after mechanical contacts. Note that electron transfers are hard to occur in dielectric–dielectric structures due to high potential barriers, and the mass transfer mechanism has been also a strong candidate for the triboelectric charging of soft insulators.[13,15,17,18,31]

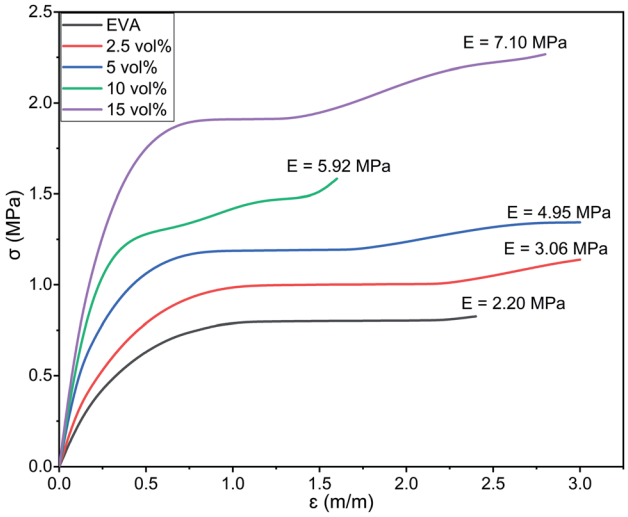

Fig. 4 Young's modulus (*E*) of pristine EVA polymer and EVA/TiO_2 NPs composite, each containing different concentrations of the TiO_2 NPs filler.

The change of dielectric property by the change of filler concentrations may also induce the change of triboelectrification.[32] However, it is mainly related to the triboelectric charging of metal-dielectrics structures because it is based on electron transfers. More importantly, the effect of dielectric property on triboelectrification is based on ferroelectric polarizations. Note that our experimental system has been established by dielectrics–dielectrics structures without ferroelectric materials.

Uneven deformation at the triboelectric surfaces was also confirmed by the finite element analysis (FEA) simulations of the pristine EVA (0 vol%) and the EVA composites (TiO_2 NPs filler concentrations of 2.5, 5, 10, and 15 vol%) using ANSYS R17.1 software (details in Experimental section). The surface configuration of the 2D models was taken from atomic force microscopy (AFM) measurements (Fig. 5a and b). Note that the pristine EVA layer and the composites were similar in terms of roughness (Fig. S8†) because all samples were finally prepared by a hot-pressing machine. The FEA simulations were performed during the process of mechanical contact and separation between the two surfaces and their mechanical properties were used to investigate the level of deformation. As presented in Fig. 5c–g, one surface was fixed as a 15 vol% composite surface while the counterpart surfaces were changed from 0 vol% to 15 vol%. Enlarged versions of Fig. 5c–g are presented in Fig. S9.† Macroscale simulations describe surface deformation during mechanical loading and after unloading. When the two surfaces contact each other (with a default average distance of 2.5 μm between the surfaces due to the maximum pressing) surface deformations appear on both surfaces. The surface deformation Δ_f of the top 15 vol% layer was smallest in the case of contact with the pristine EVA layer (Fig. 5c, top panel) and largest in the case of contact with the identical layer (Fig. 5f, top panel). This is because the pristine polymer, due to its low Young's modulus (compared to composites) was capable of absorbing the most

 This journal is © The Royal Society of Chemistry 2021

Published on 25 March 2021. Downloaded by University of Tartu on 4/25/2021 6:37:17 AM.

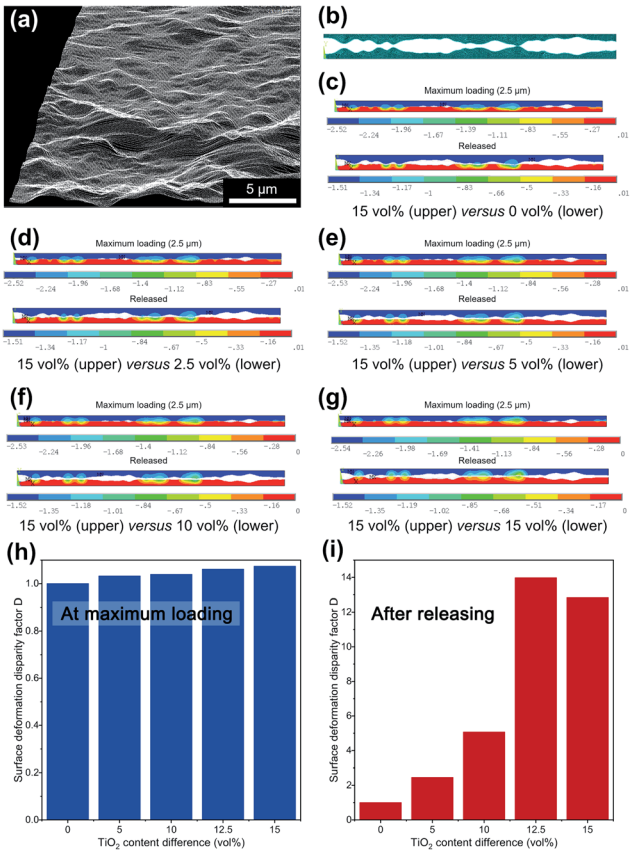

Fig. 5 (a) AFM surface topology of 15 vol% TiO_2 NPs-contained composite. (b) 2D-mesh simulation model derived from the AFM measurement for mechanical calculation of contact and separation between various TiO_2-contained EVA composites. Simulation results of deformation displacement (μm-scale, in the colour bar) of various nanocomposite counterparts: (c) the 15 vol% (upper) and 0 vol% (lower) model, (d) 15 vol% and 2.5 vol% model, (e) 15 vol% and 5 vol% model, (f) 15 vol% and 10 vol% model and (g) both 15 vol% models, during external mechanical loading (contact) and after release (separation). Surface deformation disparity factor (D) ratio as a function of differences in TiO_2 concentration in the simulations (h) during maximum loading (indentation of 2.5 μm) and (i) after release.

external mechanical stress caused by deformations. After the separation (mechanically released state), some deformations remained as a result of the viscoelastic nature of the EVA polymer matrix. These remaining deformations were particularly apparent in the pristine EVA layer and the low-concentrated composite (Fig. 5c and d, bottom panels). Even when identical polymer matrixes are being contacted and separated, a substantial difference in mechanical properties produced the large mass transfer for triboelectrification.

We assigned '1' as the surface deformation disparity in the situation where mechanical contact between two deformable bodies having the same mechanical properties resulting in the same surface deformation during contact electrification (Fig. 5h and i, respectively). When model surfaces with very different TiO_2 contents (differences of 15 vol%) contacted each other, the surface deformation disparity ratio was ~1.07 during the maximum contact loading. After the mechanical release of the triboelectric surfaces, surface deformation disparity increased as high as ~14 in the case of high concentration differences of fillers. In contrast, the triboelectric surfaces of small concentration differences continued to show low deformation disparity. Detailed results are provided in Tables S1 and S2.†

The simulation results illustrate a trend of higher differences in TiO_2 NPs content leading to elevated levels of uneven deformation and relaxation of surfaces. These results are consistent with our contact electrification measurements, and support our conclusion that uneven deformation and subsequent surface relaxation are responsible for mass transfer mechanism-based surface triboelectric charge generation, as they encourage heterolytic bond scission of polymer chains. These all results, including that the identical triboelectric layers containing the same particles with same concentrations generate a very small output, consistently present the mass (materials) transfer mechanisms of triboelectrification in the case of insulating polymers. The mass transfer mechanism of triboelectrification by heterolytic scission of polymers is simplified by the schematics in Fig. S10.† Our study can firmly support the basically reported mass and material transfer mechanism.[13,15,31]

Conclusions

In this paper, we demonstrated triboelectrification between identical polymers with different concentrations of filler NPs in their composite feature. As the difference in the filler concentrations between two triboelectric polymer layers increased, the contact triboelectrification output and generated surface charge density also increased. We experimentally and computationally determined that triboelectricity increased in strength as differences in mechanical and viscoelastic characteristics grew more extreme between the two identical polymer matrixes. This phenomenon was consistently observed in tests of numerous polymer matrixes and filler NPs, suggesting that polymer triboelectrification is mainly unrelated to chemical composition, but rather is largely a consequence of physicochemical properties. Accordingly, this study offers confirmation that the triboelectrification of polymeric materials is inextricably linked to the mass transfer mechanism. This result is reasonable and consistent with previous research into polymeric triboelectricity.[7] Our findings will assist in the development of efficient triboelectric devices or protective structures that rely on polymer materials.

Author contributions

L. L., A. L. and K. M. conducted the investigation, data curation, and formal analysis. L. L. also conducted the writing – original draft. H. K. carried out the data curation and the writing – review & editing. K. R. and K. P. conducted the validation and investigation. K. S., A. K. and K. K. carried out the formal analysis and validation. A. T. conducted validation and conceptualization. C. K. J. and A. S. carried out the conceptualization, funding acquisition, investigation, methodology, supervision, writing – original draft and writing – review & editing.

Published on 25 March 2021. Downloaded by University of Tartu on 4/25/2021 6:37:17 AM.

Conflicts of interest

There are no conflicts to declare.

Acknowledgements

L. L. and A. Š. acknowledge Riga Technical University's Doctoral Grant and Research Excellence grant programs, respectively. This work has been also supported by the European Regional Development Fund within the Activity 1.1.1.2 "Post-doctoral Research Aid" of the Specific Aid Objective 1.1.1 "To increase the research and innovative capacity of scientific institutions of Latvia and the ability to attract external financing, investing in human resources and infrastructure" of the Operational Programme "Growth and Employment" (1.1.1.2/VIAA/3/19/416). The help of Juris Bitenieks and Astrīda Bērziņa is acknowledged for water contact angle and Raman spectra measurements, respectively. This research was additionally supported by the Basic Science Research Program through the National Research Foundation of Korea funded by the Ministry of Science and ICT (NRF-2019R1C1C1002571). We would also like to express our gratitude to the editors of the Writing Center at Jeonbuk National University.

Notes and references

1 B.-Y. Lee, D. H. Kim, J. Park, K.-I. Park, K. J. Lee and C. K. Jeong, *Sci. Technol. Adv. Mater.*, 2019, **20**, 758–773.
2 H. T. Baytekin, B. Baytekin, T. M. Hermans, B. Kowalczyk and B. A. Grzybowski, *Science*, 2013, **341**, 1368–1371.
3 H. T. Baytekin, B. Baytekin, S. Huda, Z. Yavuz and B. A. Grzybowski, *J. Am. Chem. Soc.*, 2015, **137**, 1726–1729.
4 A. Ahmed, I. Hassan, A. S. Helal, V. Sencadas, A. Radhi, C. K. Jeong and M. F. El-Kady, *iScience*, 2020, **23**, 101286.
5 A. Ahmed, I. Hassan, M. F. El-Kady, A. Radhi, C. K. Jeong, P. R. Selvaganapathy, J. Zu, S. Ren, Q. Wang and R. B. Kaner, *Adv. Sci.*, 2019, **6**, 1802230.
6 S. Park, J. Park, Y. Kim, S. Bae, T.-W. Kim, K.-I. Park, B. H. Hong, C. K. Jeong and S.-K. Lee, *Nano Energy*, 2020, **78**, 105266.
7 A. Šutka, K. Mālnieks, L. Lapčinskis, P. Kaufelde, A. Linarts, A. Bērziņa, R. Zābels, V. Jurķāns, I. Gorņevs, J. Blūms and M. Knite, *Energy Environ. Sci.*, 2019, **12**, 2417–2421.
8 A. Šutka, A. Linarts, K. Mālnieks, K. Stiprais and L. Lapčinskis, *Mater. Horiz.*, 2020, **7**, 520–523.
9 A. Šutka, P. C. Sherrell, N. A. Shepelin, L. Lapčinskis, K. Mālnieks and A. V. Ellis, *Adv. Mater.*, 2020, **32**, 2002979.
10 A. Šutka, K. Mālnieks, A. Linarts, M. Timusk, V. Jurķāns, I. Gorņevs, J. Blūms, A. Bērziņa, U. Joost and M. Knite, *Energy Environ. Sci.*, 2018, **11**, 1437–1443.
11 D. J. Lacks and T. Shinbrot, *Nat. Rev. Chem.*, 2019, **3**, 465–476.
12 J. Chen and Z. L. Wang, *Joule*, 2017, **1**, 480–521.
13 H. T. Baytekin, A. Z. Patashinski, M. Branicki, B. Baytekin, S. Soh and B. A. Grzybowski, *Science*, 2011, **333**, 308–312.
14 L. Beraldo da Silveira Balestrin, D. Del Duque, D. Soares da Silva and F. Galembeck, *Faraday Discuss.*, 2014, **170**, 369–383.
15 R. K. Pandey, H. Kakehashi, H. Nakanishi and S. Soh, *J. Phys. Chem. C*, 2018, **122**, 16154–16160.
16 L. Lapčinskis, K. Mālnieks, J. Blūms, M. Knite, S. Oras, T. Käämbre, S. Vlassov, M. Antsov, M. Timusk and A. Šutka, *Macromol. Mater. Eng.*, 2020, **305**, 1900638.
17 L. S. McCarty and G. M. Whitesides, *Angew. Chem., Int. Ed.*, 2008, **47**, 2188–2207.
18 C. K. Jeong, K. M. Baek, S. Niu, T. W. Nam, Y. H. Hur, D. Y. Park, G.-T. Hwang, M. Byun, Z. L. Wang, Y. S. Jung and K. J. Lee, *Nano Lett.*, 2014, **14**, 7031–7038.
19 H. T. Baytekin, B. Baytekin, S. Soh and B. A. Grzybowski, *Angew. Chem.*, 2011, **123**, 6898–6902.
20 A. Šutka, K. Mālnieks, L. Lapčinskis, M. Timusk, K. Kalniņš, A. Kovaļovs, J. Bitenieks, M. Knite, D. Stevens and J. Grunlan, *Phys. Chem. Chem. Phys.*, 2020, **22**, 13299–13305.
21 Z. L. Wang and A. C. Wang, *Mater. Today*, 2019, **30**, 34–51.
22 C. Xu, Y. Zi, A. C. Wang, H. Zou, Y. Dai, X. He, P. Wang, Y.-C. Wang, P. Feng, D. Li and Z. L. Wang, *Adv. Mater.*, 2018, **30**, 1706790.
23 C. Xu, B. Zhang, A. C. Wang, H. Zou, G. Liu, W. Ding, C. Wu, M. Ma, P. Feng, Z. Lin and Z. L. Wang, *ACS Nano*, 2019, **13**, 2034–2041.
24 S. S. Won, M. Kawahara, C. W. Ahn, J. Lee, J. Lee, C. K. Jeong, A. I. Kingon and S. Kim, *Adv. Electron. Mater.*, 2020, **6**, 1900950.
25 L. Lapčinskis, A. Linarts, M. Knite, I. Gorņevs, J. Blūms and A. Šutka, *Appl. Surf. Sci.*, 2019, **474**, 91–96.
26 Y. Zhang, H. Kim, Q. Wang, W. Jo, A. I. Kingon, S.-H. Kim and C. K. Jeong, *Nanoscale Adv.*, 2020, **2**, 3131–3149.
27 Q. Li, L. Chen, M. R. Gadinski, S. Zhang, G. Zhang, H. U. Li, E. Iagodkine, A. Haque, L.-Q. Chen, T. N. Jackson and Q. Wang, *Nature*, 2015, **523**, 576–579.
28 C. Baek, J. E. Wang, S. Ryu, J.-H. Kim, C. K. Jeong, K.-I. Park and D. K. Kim, *RSC Adv.*, 2017, **7**, 2851–2856.
29 G.-J. Lee, M.-K. Lee, J.-J. Park, D. Y. Hyeon, C. K. Jeong and K.-I. Park, *ACS Appl. Mater. Interfaces*, 2019, **11**, 37920–37926.
30 H. T. Baytekin, B. Baytekin, S. Soh and B. A. Grzybowski, *Angew. Chem., Int. Ed.*, 2011, **50**, 6766–6770.
31 H. T. Baytekin, B. Baytekin, J. T. Incorvati and B. A. Grzybowski, *Angew. Chem., Int. Ed.*, 2012, **51**, 4843–4847.
32 W. Seung, H.-J. Yoon, T. Y. Kim, H. Ryu, J. Kim, J.-H. Lee, J. H. Lee, S. Kim, Y. K. Park, Y. J. Park and S.-W. Kim, *Adv. Energy Mater.*, 2017, **7**, 1600988.

 This journal is © The Royal Society of Chemistry 2021

6. pielikums/ Appendix VI

L. Lapčinskis, K. Mālnieks, A. Linarts, J. Blūms, K. Šmits, M. Järvekülg, M. Knite, A. Šutka, Hybrid Tribo-Piezo-Electric Nanogenerator with Unprecedented Performance Based on Ferroelectric Composite Contacting Layers, *ACS Appl. Energy Mater.* **2019**, *2(6)*, 4027-4032.

ACS APPLIED ENERGY MATERIALS
Cite This: ACS Appl. Energy Mater. 2019, 2, 4027−4032
Letter
www.acsaem.org

Hybrid Tribo-Piezo-Electric Nanogenerator with Unprecedented Performance Based on Ferroelectric Composite Contacting Layers

Linards Lapčinskis,[†] Kaspars Mālnieks,[‡] Artis Linarts,[†] Juris Blūms,[†] Krišjānis Šmits,[§] Martin Järvekülg,[∥] Māris Knite,[†] and Andris Šutka*[,‡]

[†]Institute of Technical Physics, Faculty of Materials Science and Applied Chemistry, Riga Technical University, Paula Valdena 3/7, Riga LV1048, Latvia

[‡]Research Laboratory of Functional Materials Technology, Faculty of Materials Science and Applied Chemistry, Riga Technical University, Paula Valdena 3/7, Riga LV1048, Latvia

[§]Laboratory of Solid State Radiation Physics, Institute Solid State Physics, University of Latvia, Ķengaraga 8, Riga LV1063, Latvia

[∥]Institute of Physics, University of Tartu, W. Ostwaldi 1, Tartu 50411, Estonia

Supporting Information

ABSTRACT: It was recently reported that more efficient triboelectric nanogenerator (TENG)-like devices can be prepared using inversely polarized ferroelectric films made of same material as the contacting layers. In the present work, a clear correlation between the piezoelectric response of inversely polarized ferroelectric PVDF/$BaTiO_3$ nanocomposite films and the performance of the TENG-like device based on these films is demonstrated. This observation is explained by magnified electrostatic induction that is driven by piezoelectric charges and ferroelectric properties of these films. A double capacitor model is proposed that effectively portrays the interactions between ferroelectric layers during contact−separation and subsequent charge redistributions in the external circuit. The new understanding has allowed the result of 3-fold higher open circuit voltages (2.7 kV from 5 cm^2) as compared to that of a state of the art TENG. Furthermore, findings uncover the potential for vast improvement in the field of nanogenerators for mechanical energy harvesting as a significantly better piezoelectric performance of flexible nanogenerators has been reported elsewhere.

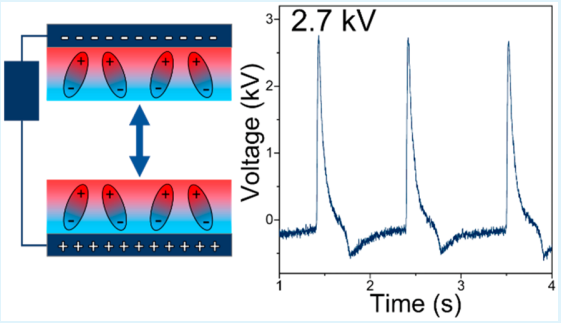

KEYWORDS: *nanogenerators, triboelectricity, piezoelectricity, ferroelectricity, poly(vinylidene fluoride)*

Triboelectric nanogenerators (TENGs) are intriguing mechanical energy-harvesting devices that could power small portable devices[1] and detectors[2] or charge batteries.[3] TENGs can also act as self-powered sensor elements for mechanical displacement, chemical or acoustic sensors, and biomedical monitors. The working principles of TENG are based on friction-related contact electrification. Most commonly, a TENG consists of two connected conductive electrode layers from which at least one is covered with a polymer insulator.[4] These two surfaces from distinct materials are then contacted and separated, creating opposite sign net charges on the surfaces, which in turn induce charges on underlying conductive electrodes. During separation the electric potential difference is established, and electrons are driven to flow between the two electrodes in order to balance the electric potential difference.[4] For surface charge formation a variety of mechanisms have been proposed. One of the widely accepted mechanisms is electron transfer between contacted materials.[4,5] However, this theory has some flaws; e.g., polymer materials generally do not contain free electrons, and therefore, other mechanisms have been put forward. Mass or ion transfer from the polymer in this context seems more credible than electron transfer.[6−10] This working mechanism involves formation of positively and negatively charged mosaic-type fragments on each surface that result in net surface charge.[9,10]

Recently, several research groups have demonstrated that the performance of TENG can be enhanced using ferroelectric films as contacting surfaces.[11−18] Polarized ferroelectric layers have been considered to have a more appropriate work function for electron transfer between polymer layers.[11,17] However, recently it has been proposed that the enhancement actually comes from piezoelectric charges, and performance can be significantly improved by contacting inversely polarized ferroelectric films from the same material due to magnified electrostatic induction.[18] It appears that the piezoelectric charges created on the ferroelectric layers during contacting (pressing) drive electrostatic induction and enhance the overall

Received: April 29, 2019
Accepted: June 12, 2019
Published: June 12, 2019

See https://pubs.acs.org/sharingguidelines for options on how to legitimately share published articles.

© 2019 American Chemical Society

DOI: 10.1021/acsaem.9b00836
ACS Appl. Energy Mater. 2019, 2, 4027−4032

performance of TENG.[18] It is also noteworthy that in case of inversely polarized ferroelectric contacting surfaces there is no need to combine distinct materials according to their position in triboelectric series, because even moderate piezoelectric charges can be sufficient for high performance.[18]

However, the complete working mechanism of TENG based on inversely polarized ferroelectric layers is not clear. Piezoelectric charges which form during contacting two ferroelectric films in a TENG device are too small to observe high current and voltage upon separation. The same situation includes a surface charge forming by contacting−separating two films from the identical material and electrostatic induction from an electric field arising from permanent dipoles. At the same time, in the present work we demonstrate an obvious correlation between the magnitude of piezoelectric charges and the performance of TENG. We are building our device from a well-established PVDF/$BaTiO_3$ nanocomposite that has been reported for usage in both piezoelectric nanogenerators (PENGs) and TENGs. PVDF is a well-known ferroelectric polymer in which the piezoelectric charge density can be increased by adding $BaTiO_3$ nanoparticles.[11−18] In the TENG setup, ferroelectric PVDF/$BaTiO_3$ nanocomposites have been contacted with other materials according to established knowledge of the triboelectric effect, but here we use identical two PVDF/$BaTiO_3$ contacting layers that are inversely polarized. As a result, we present a 3-fold higher output voltage than that from a state of the art TENG device.[19] We show that the observed high performance can be explained by introducing a double capacitor model where capacitance of the device changes twice upon contacting and separating, thus varying potential and causing current flow between two conductive plates in the TENG device.

Ferroelectric contacting electrodes for a TENG device were prepared from a PVDF solution in dimethylformamide (DMF) by spin-coating in combination with immersion−precipitation schematically demonstrated in Figure 1a. $BaTiO_3$ nanoparticles in a wide compositional range (0−35 vol %) were ultrasonically dispersed in PVDF solution and spin-coated on an indium−tin oxide (ITO) substrate. In the next step, the freshly spin-coated films were immersed in antisolvent (methanol), thus triggering the polymer precipitation and formation of porous structures. The porous PVDF structures formed in less than 1 min. All prepared sample compositions presented porous nanostructures as seen in the scanning electron microscopy (SEM) image in Figure 1b. The precipitation method is well-adopted by industry to manufacture nanoporous polymer membranes[20] and should easily facilitate large-scale production of highly porous contacting layers for TENG-like devices. This approach is apparently highly competitive with the other methods such as templating or molding,[19,21,22] electrospinning,[23] and reactive ion or chemical etching,[24,25] methods that have been applied for preparation of high specific surface area polymeric layers for TENG devices. A more detailed description of the preparation of samples, characterization, and measurement methods is presented in Supporting Information in the experimental methods details.

The homogeneity of the distribution of $BaTiO_3$ nanoparticles into the polymer matrix was studied by transmission electron microscopy (TEM) and energy-dispersive X-ray spectroscopy (EDX) analysis. As can be seen from images in Figure 1c,d, $BaTiO_3$ nanoparticles are well-dispersed throughout the PVDF matrix. It is important to achieve a higher dispersion quality, because a higher homogeneity yields a higher piezoelectric response.[26] Particles in agglomerates are not free to move, limiting the change in dipole moments.[26]

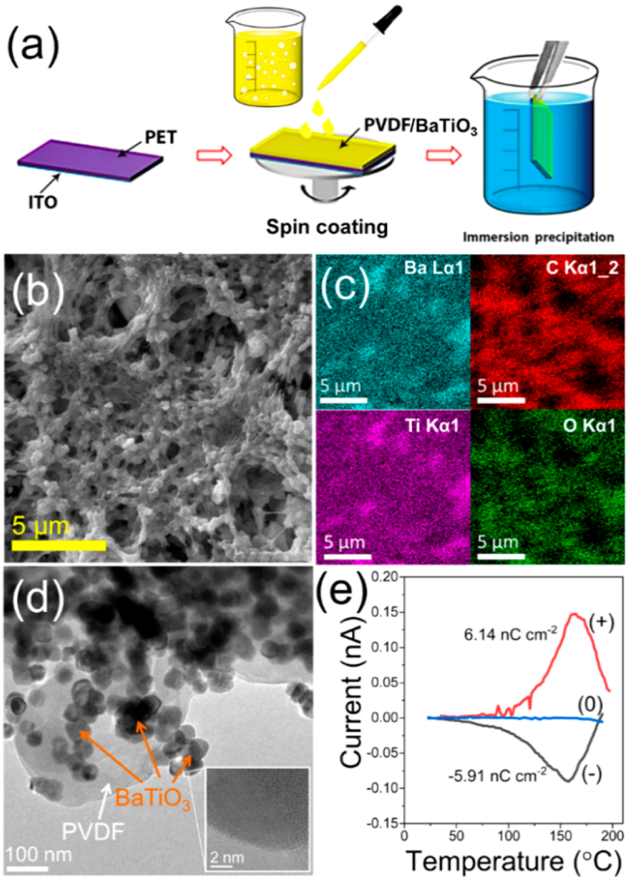

Figure 1. Schematic representation of sample film preparation by immersion−precipitation (a). Image b shows an SEM micrograph for a $BaTiO_3$/PVDF nanocomposite with $BaTiO_3$ at 25 vol % content. The same sample was analyzed by EDX (c) and TEM (d) to demonstrate homogeneous $BaTiO_3$ nanoparticle dispersion throughout the PVDF matrix. Graph e demonstrates depolarization current curves for inversely polarized (red and gray) and nonpolarized (blue) layers of the same material showing the charge stored by ferroelectric material.

Samples were prepared from both $BaTiO_3$/PVDF and neat PVDF, and identical electrical measurements were conducted on poled as well as nonpoled samples. The occurrence of ferroelectric phases of PVDF before and after poling was confirmed by attenuated total reflectance Fourier transform infrared spectroscopy (ATR-FTIR) measurements, which also revealed low crystallinity of as-prepared nonpolarized PVDF (see Supporting Information Figure S1). After heating or poling (heating in electric field) at 100 °C, the α, β, and γ phases were dominantly presented in the sample films (Supporting Information Figures S2 and S3).

Thermally stimulated depolarization current (TSDC) measurements of polarized PVDF/$BaTiO_3$ show that in the temperature range 130−180 °C ferroelectric composites undergo dipole relaxation within the crystalline phase (Figure 1e). For positively (+) and negatively (−) polarized layers, induced charge density is, respectively, 6.14 and 5.91 nC cm^{-2}. For nonpolarized PVDF/$BaTiO_3$ (0), the TSDC technique did not show charge release during heating.

DOI: 10.1021/acsaem.9b00836
ACS Appl. Energy Mater. 2019, 2, 4027−4032

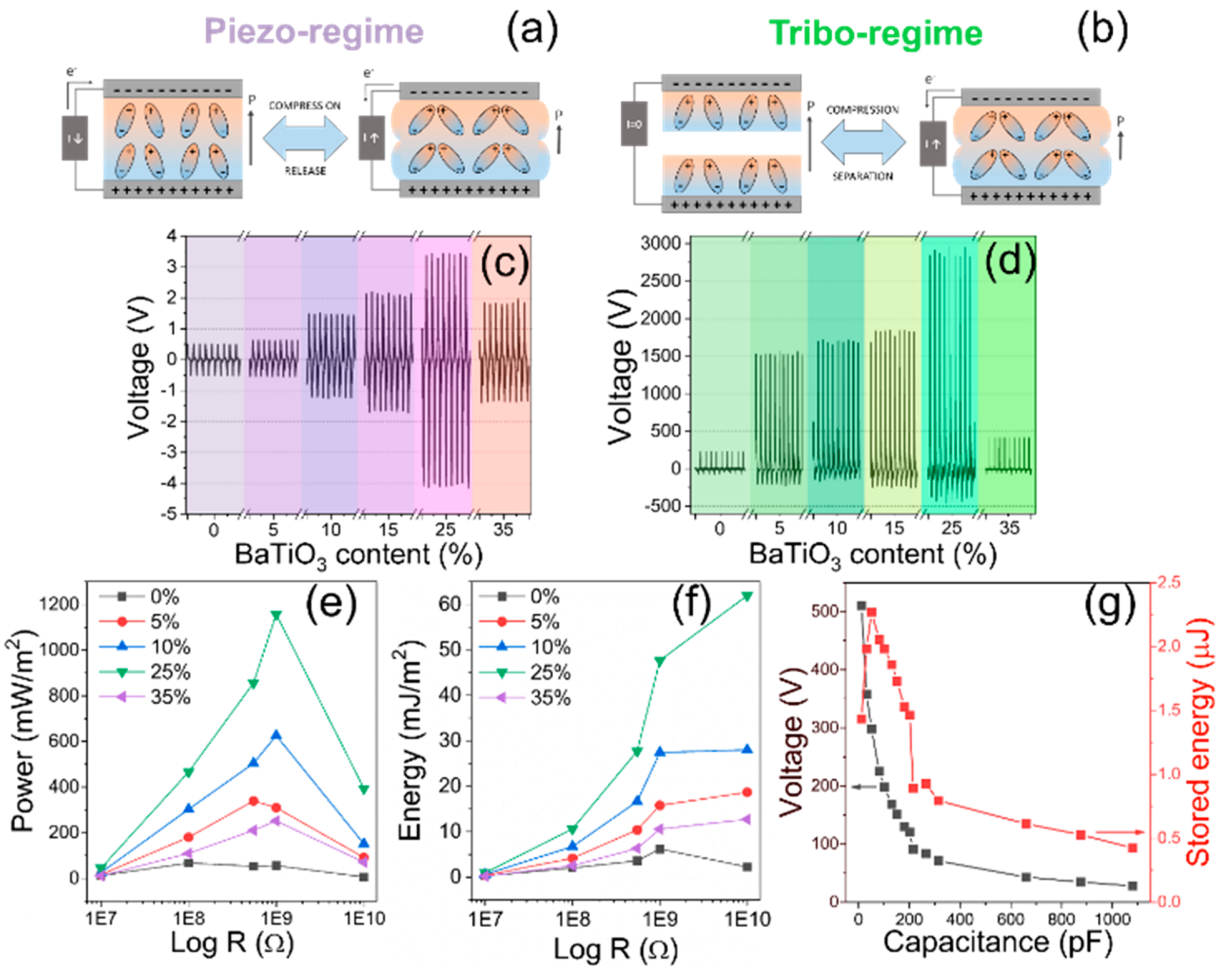

Figure 2. Schematic representation of piezo (a) and TENG (b) testing regimes. The open circuit output voltage measured at load resistance 1×10^{10} Ω in piezo (c) and TENG (d) regimes. Graphs at the bottom show power (e) and energy (f) for different compositions tested in the TENG regime. Energy stored in the capacitor (g) was determined for the nanocomposite showing the highest performance (PVDF/$BaTiO_3$ 25 vol %).

Immersion−precipitation derived poled PVDF and their composites were tested in compression mode (Figure 2a) to assess their piezoelectric response. As expected, the reference samples that were not poled generated no detectable voltage. Compositions with $BaTiO_3$ exhibited higher open circuit voltage (V_{OC}) than bare PVDF when force was applied. The higher piezoelectric response of $BaTiO_3$/PVDF nanocomposites in comparison to bare PVDF is well-described in the literature and explained by an increased number of piezoelectric dipoles in the film.[27−29] For bare polarized PVDF, a piezoelectric V_{OC} value of 0.5 V was measured. V_{OC} was found to gradually increase with $BaTiO_3$ content until saturation, followed by a decline in voltages at higher concentrations (Figure 2c). The latter can be attributed to degrading electromechanical coupling effects (i.e., deformability).[26] 25 vol % was found to be the optimal concentration of $BaTiO_3$ in PVDF, resulting in the highest V_{OC} of 4.0 V in the negative direction (Figure 2c).

Prepared inversely polarized ferroelectric films were subsequently used as contacting layers in a TENG device (Figure 2b). Identical nanocomposite films were deposited on the contacting surfaces, followed by poling to establish inverse polarization. As can be seen from Figure 2d, just like in piezoelectric measurements, compositions containing $BaTiO_3$, until certain loading, show a higher open circuit voltage in the TENG regime, clearly indicating a correlation between piezoelectric response and the corresponding performance of a nanocomposite film TENG device. For example, the generator where inversely polarized bare PVDF was used as contacting layers produced a V_{OC} value of 250 V, while the generator from the $BaTiO_3$/PVDF nanocomposite with a nanoparticle content of 25 vol % generated a V_{OC} value of 2700 V from 5 cm^2. Boosted performance of nanocomposite TENG devices relates to a higher ferroelectric polarization of layers, which is evident not only in piezoelectricity but also as an increased charge density transferred between two electrodes in a TENG device. As $BaTiO_3$ content increases to the optimal content, the net polarization of the ferroelectric layer grows. The instant power density, calculated by Joule's law ($P = V^2R^{-1}$), reached 1.157 W m^{-2} for the TENG device with the highest V_{OC} under an optimized load resistance of 1×10^9 Ω (Figure 2e), whereas the integral $E = \int P\,dt$ yielded 65.95 mJ m^{-2}. The dependence of the calculated power density and energy density on load resistance for different compositions under the TENG regime is depicted in Figure 2e,f, respectively. The results of the corresponding voltage measurements for different nanocomposites in the TENG regime under different loads are demonstrated in Supporting Information Figures S4−S9.

DOI: 10.1021/acsaem.9b00836
ACS Appl. Energy Mater. 2019, 2, 4027−4032

The composition exhibiting the best performance (25 vol % $BaTiO_3$) was used to charge a variable capacitor circuit. Figure 2g depicts energy stored in the capacitor (and the corresponding voltage of the charged state) for each capacitor value after contact between two ferroelectric layers with 5 cm^2 contact area. The highest energy stored in a capacitor after a single contact−separation step (2.27 μJ calculated by $E = 0.5CV^2$) was reached when the capacitance of the capacitor circuit was set to approximately 50 pF.

Due to their intrinsic properties, the piezoelectric performances of the ferroelectric materials applied here are rather poor compared to state of art piezoelectric nanogenerators.[26,29,30] The achieved TENG performance of the device based on the same inversely polarized ferroelectric films, however, matches the best reported values for TENGs. We also provide proof of clear correlation between the performances of the same material in these two regimes. Therefore, as state of the art PENG devices presented in the literature generate up to V_{OC} = 209 V,[30,31] significant improvement in the performance of TENG-like devices should be possible if the corresponding materials are used as inversely polarized films in the TENG regime. However, this prediction assumes that the voltage and current observed in these PENG devices have been correctly attributed to piezoelectric charges and are not exaggerated due to unaccounted friction.

However, the question arises regarding how a large voltage can be generated by a piezoelectric charge, because when we compare charges (calculated as $q = \int i_{SC}\, dt$) generated by the PVDF/$BaTiO_3$ composite based on a TENG device with optimal $BaTiO_3$ content (25 vol %) in the piezoelectric and TENG regimes in a wide applied pressure range, we see that the piezoelectric charge is 2 orders of magnitude smaller than the charge observed in the TENG regime (measured charge values in different regimes for PVDF 25 vol % $BaTiO_3$ are presented in Tables S1−S3). The increase in charge upon separation cannot be related to electrostatic effects, because charges (2.83 nC cm^{-2}) observed between oscillating electrodes in the noncontact mode (ferroelectric layers are moved toward each other similarly as in TENG measurements, but without physical contact) only partially explain the high TENG values.

The piezoelectric response allows calculation of the piezoelectric coefficient effective value d_{33} which for the 25% $BaTiO_3$ composite reaches 47.9 pC N^{-1} (calculation shown in Figure S10 and eq S1) while values reported in the literature for similar ferroelectric PVDF/$BaTiO_3$ composites range from 2.7 to 25 pC N^{-1}.[32,33] A greater piezoelectric coefficient can be related to a significantly larger deformability due to high porosity (with consideration of bulk density, weight, and thickness, the porosity was estimated to be around 70%) of the samples. Porosity provides space for local deformations in the material that are important for piezoelectric charge generation and boosts the formation of β-PVDF.[34] The piezoelectric coefficient of a dense PVDF 25% $BaTiO_3$ composite was determined to be 9.11 pC N^{-1} which is 5 times smaller than that for the porous material used in TENG devices (Figure S10 and eq S2).

For the explanation of the potential difference change between electrodes, a double capacitor model is proposed in Figure 3. Each ferroelectric layer can be considered as an individual capacitor with surface charge density σ induced during polarization. The potential difference between opposite surfaces of each layer can be described as

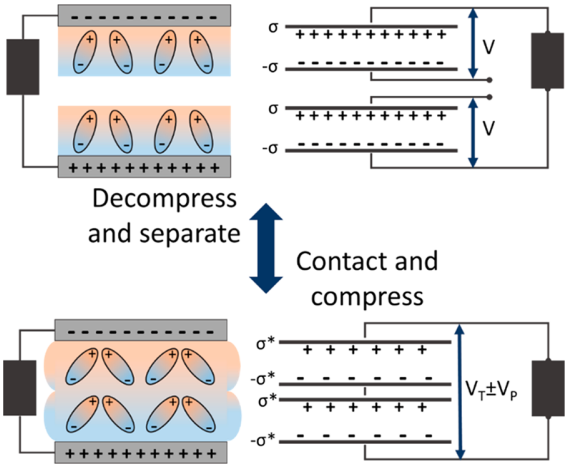

Figure 3. Double capacitor model and corresponding contact−separation stages. Dipoles in the schematic here represent both PVDF and $BaTiO_3$ dipoles in ferroelectric layers. At first, ferroelectric layers contact and form a connected capacitor, and then layers are compressed which results in a negative piezoelectric response. Next, at a much faster rate the compressed deformation is released resulting in a positive piezoelectric response which is immediately followed by separation of both surfaces, thus disconnecting the capacitors that had formed the connected circuit.

$$V = \frac{q}{C} = \frac{qd}{\varepsilon_0 \varepsilon A} = \frac{\sigma d}{\varepsilon_0 \varepsilon} \tag{1}$$

By considering two inversely polarized layers as two capacitors we can conclude that the total capacitance (and correspondingly potential difference) depends on the air gap between them. As layers come together and contact, they form a circuit of two identical capacitors in series, and the total capacitance of two layers is decreasing; however, the voltage is increasing twice in accordance with eq 2:

$$C_{TOT} = \frac{q}{V_{TOT}} = \frac{C}{2} = \frac{q}{2V} \tag{2}$$

Next, compression induces piezocharge formation as dipoles deform and the net polarization of layers drops. As a result, the surface charge density decreases to σ^*. This is followed by fast separation of compressed ferroelectric layers where net polarization quickly rises and charge density returns to σ. When ferroelectric layers are separated, the potential difference decreases in accordance with eq 2; this in turn induces additional redistribution of induced charges between electrodes in the external circuit. The charge redistributed between electrodes is registered as current peak $\int i_{SC}\, dt = 0.5(q_1 + q_2)$, where q_1 and q_2 are charge densities on polarized layer surfaces, and this allows a comparison of experimental data with the model. TENG measurement data of the PVDF 25% $BaTiO_3$ composite were used where positively and negatively polarized layers are contacted with each other and with the nonpolarized layer.

Induced charge density in the external circuit ($\int i_{SC}\, dt$) for positively and negatively polarized layers was determined by contacting them with the nonpolarized layer in the TENG mode. For positively and negatively polarized layers, $\int i_{SC}\, dt$ was determined to be 4.19 and 2.41 nC cm^{-2} while contact between two nonpolarized layers resulted in only 0.03 nC cm^{-2}, so we can assume that there is no surface charge on the nonpolarized layer. Therefore, $\int i_{SC}\, dt = 0.5(q_1 + q_2)$ gives us

DOI: 10.1021/acsaem.9b00836
ACS Appl. Energy Mater. 2019, 2, 4027−4032

that charge density q_1 on the surface of the positively polarized layer is 8.38 nC cm^{-2} while q_2 on the negatively polarized layer surface is 4.82 nC cm^{-2}.

When two capacitors with equal capacitances but with different charge density states are connected in series then the charge density on connected surfaces is $q_1 - q_2$, but on outer surfaces it is $0.5(q_1 - q_2)$ and $0.5(q_2 - q_1)$. In our case we obtain that charge density on each of the inner surfaces of two connected capacitors is 3.56 nC cm^{-2} while it is 1.78 nC cm^{-2} on outer surfaces. This means that redistributed charge density in accordance with the double capacitor model presented in Figure 3 is 8.38−1.78 = −(4.82−1.78) = 6.60 nC cm^{-2}. The induced charge density in the TENG measurement (6.55 nC cm^{-2}) when negatively and positively polarized layers are contacted is very similar to one obtained from model calculations.

In conclusion, highly porous piezoelectric nanocomposites based on $BaTiO_3$/PVDF were successfully prepared by immersion−precipitation. It was observed that the piezoelectric response rises with increasing $BaTiO_3$ loading until 25 vol % content is reached. Sample films were further used in TENG devices as contacting layers on electrodes, and a clear correlation was observed between piezoelectric response and TENG performance. The PVDF/$BaTiO_3$ nanocomposite with optimal composition shows 47.9 pC N^{-1} as the piezoelectric coefficient, higher than that usually reported for such composites, and in TENG mode a record high 2.7 kV V_{OC} value is achieved. However, our results also indicate that piezoelectric charges cannot be solely responsible for great TENG performance; thus, a "double capacitor model" has been introduced. The mechanism involves interaction between two charged ferroelectric layers during contact−separation, and contacted inversely polarized layers can be considered as capacitors connected in series. Air gap formation during separation rapidly decreases the total capacitance while the potential difference increases. The induced charge redistribution in the external circuit is registered as a current. Predictions of our model also hold true when experimentally obtained charge density (6.55 nC cm^{-2}) values are compared with ones obtained from model calculations (6.60 nC cm^{-2}). As triboelectric research continues to thrive and expand, we anticipate that our work will help the TENG community to further improve the performance of ferroelectric-based triboelectric devices.

■ ASSOCIATED CONTENT

Supporting Information

Experimental details, Figure S1−S10, Table S1−S3, Equations S1 and S2. The Supporting Information is available on the ACS Publications Web site. The Supporting Information is available free of charge on the ACS Publications website at DOI: 10.1021/acsaem.9b00836.

Experimental details and additional device characterization information (PDF)

■ AUTHOR INFORMATION

Corresponding Author

*E-mail: Andris.Sutka@rtu.lv.

ORCID

Linards Lapčinskis: 0000-0002-5048-2429

Andris Šutka: 0000-0002-5739-0164

Notes

The authors declare no competing financial interest.

■ ACKNOWLEDGMENTS

This research was supported by the European Regional Development Fund within the project "Hybrid energy harvesting systems" 1.1.1.1./16/A/013.

■ REFERENCES

(1) Kim, W. G.; Kim, D.; Jeon, S. B.; Park, S. J.; Tcho, I. W.; Jin, I. K.; Han, J. K.; Choi, Y. K. Multidirection and Multiamplitude Triboelectric Nanogenerator Composed of Porous Conductive Polymer with Prolonged Time of Current Generation. *Adv. Energy Mater.* **2018**, *8*, 1800654.

(2) Wen, Z.; Chen, J.; Yeh, M.; Guo, H.; Li, Z.; Fan, X.; Zhang, T.; Zhu, L.; Wang, Z. L. Blow-driven triboelectric nanogenerator as an active alcohol breath analyzer. *Nano Energy* **2015**, *16*, 38−46.

(3) Pu, X.; Li, L.; Song, H.; Du, C.; Zhao, Z.; Jiang, C.; Cao, G.; Hu, W.; Wang, Z. L. A Self-Charging Power Unit by Integration of a Textile Triboelectric Nanogenerator and a Flexible Lithium-Ion Battery for Wearable Electronics. *Adv. Mater.* **2015**, *27*, 2472−2478.

(4) Wang, Z. L. Triboelectric Nanogenerators as New Energy Technology for Self-Powered Systems and as Active Mechanical and Chemical Sensors. *ACS Nano* **2013**, *7*, 9533−9557.

(5) Lin, S.; Xu, L.; Xu, C.; Chen, X.; Wang, A. C.; Zhang, B.; Lin, P.; Yang, Y.; Zhao, H.; Wang, Z. L. Electron Transfer in Nanoscale Contact Electrification: Effect of Temperature in the Metal−Dielectric Case. *Adv. Mater.* **2019**, *31*, 1808197.

(6) Horn, R. G.; Smith, D. T. Contact Electrification and Adhesion Between Dissimilar Materials. *Science* **1992**, *256*, 362−364.

(7) Baytekin, H. T.; Baytekin, B.; Incorvati, J. T.; Grzybowski, B. A. Material Transfer and Polarity Reversal in Contact Charging. *Angew. Chem., Int. Ed.* **2012**, *51*, 4843−4847.

(8) Baytekin, H. T.; Baytekin, B.; Hermans, T. M.; Kowalczyk, B.; Grzybowski, B. A. Control of Surface Charges by Radicals as a Principle of Antistatic Polymers Protecting Electronic Circuitry. *Science* **2013**, *341*, 1368−1371.

(9) Baytekin, H. T.; Patashinski, A. Z.; Branicki, M.; Baytekin, B.; Soh, S.; Grzybowski, B. A. The Mosaic of Surface Charge in Contact Electrification. *Science* **2011**, *333*, 308−312.

(10) Apodaca, M.; Wesson, P.; Bishop, K.; Ratner, M.; Grzybowski, B. Contact Electrification between Identical Materials. *Angew. Chem., Int. Ed.* **2010**, *49*, 946−949.

(11) Bai, P.; Zhu, G.; Zhou, Y. S.; Wang, S.; Ma, J.; Zhang, G.; Wang, Z. L. Dipole-moment-induced effect on contact electrification for triboelectric nanogenerators. *Nano Res.* **2014**, *7* (7), 990−997.

(12) Seung, W.; Yoon, H.-J.; Kim, T. Y.; Ryu, H.; Kim, J.; Lee, J.-H.; Lee, J. H.; Kim, S.; Park, Y. K.; Park, Y. J.; Kim, S.-W. Boosting Power-Generating Performance of Triboelectric Nanogenerators via Artificial Control of Ferroelectric Polarization and Dielectric Properties. *Adv. Energy Mater.* **2017**, *7*, 1600988.

(13) Suo, G.; Yu, Y.; Zhang, Z.; Wang, S.; Zhao, P.; Li, J.; Wang, X. Piezoelectric and Triboelectric Dual Effects in Mechanical-Energy Harvesting Using $BaTiO_3$/Polydimethylsiloxane Composite Film. *ACS Appl. Mater. Interfaces* **2016**, *8*, 34335−34341.

(14) Chun, J.; Kim, J. W.; Jung, W. S.; Kang, C. Y.; Kim, S. W.; Wang, Z. L.; Baik, J. M. Mesoporous pores impregnated with Au nanoparticles as effective dielectrics for enhancing triboelectric nanogenerator performance in harsh environments. *Energy Environ. Sci.* **2015**, *8*, 3006−3012.

(15) Yang, X.; Daoud, W. A. Synergetic effects in composite-based flexible hybrid mechanical energy harvesting generator. *J. Mater. Chem. A* **2017**, *5*, 9113−9121.

(16) Choi, Y. S.; Jing, Q.; Datta, A.; Boughey, C.; Kar-Narayan, S. A triboelectric generator based on self-poled Nylon-11 nanowires fabricated by gas-flow assisted template wetting. *Energy Environ. Sci.* **2017**, *10*, 2180−2189.

DOI: 10.1021/acsaem.9b00836
ACS Appl. Energy Mater. 2019, 2, 4027−4032

(17) Lee, K. Y.; Kim, S. K.; Lee, J.-H.; Seol, D.; Gupta, M. K.; Kim, Y.; Kim, S.-W. Controllable Charge Transfer by Ferroelectric Polarization Mediated Triboelectricity. *Adv. Funct. Mater.* **2016**, *26*, 3067−3073.
(18) Šutka, A.; Mālnieks, K.; Linarts, A.; Timusk, M.; Jurķāns, V.; Gorņevs, I.; Blūms, J.; Bērziņa, A.; Joost, U.; Knite, M. Inversely polarised ferroelectric polymer contact electrodes for triboelectric-like generators from identical materials. *Energy Environ. Sci.* **2018**, *11*, 1437−1443.
(19) Chun, J.; Ye, B. U.; Lee, J. W.; Choi, D.; Kang, C. Y.; Kim, S. W.; Wang, Z. L.; Baik, J. M. Boosted output performance of triboelectric nanogenerator via electric double layer effect. *Nat. Commun.* **2016**, *7*, 12985.
(20) van de Witte, P.; Dijkstra, P. J.; van den Berg, J. W. A.; Feijen, J. Phase separation processes in polymer solutions in relation to membrane formation. *J. Membr. Sci.* **1996**, *117*, 1−31.
(21) Fan, F. R.; Lin, L.; Zhu, G.; Wu, W.; Zhang, R.; Wang, Z. L. Transparent Triboelectric Nanogenerators and Self-Powered Pressure Sensors Based on Micropatterned Plastic Films. *Nano Lett.* **2012**, *12*, 3109−3114.
(22) Han, M.; Zhang, X. S.; Meng, B.; Liu, W.; Tang, W.; Sun, X.; Wang, W.; Zhang, H. r-Shaped Hybrid Nanogenerator with Enhanced Piezoelectricity. *ACS Nano* **2013**, *7*, 8554−8560.
(23) Zheng, Y.; Cheng, L.; Yuan, M.; Wang, Z.; Zhang, L.; Qin, Y.; Jing, T. An electrospun nanowire-based triboelectric nanogenerator and its application in a fully self-powered UV detector. *Nanoscale* **2014**, *6*, 7842−7846.
(24) Fan, X.; Chen, J.; Yang, J.; Bai, P.; Li, Z.; Wang, Z. L. Ultrathin, Rollable, Paper-Based Triboelectric Nanogenerator for Acoustic Energy Harvesting and Self-Powered Sound Recording. *ACS Nano* **2015**, *9*, 4236−4243.
(25) Lin, Z. H.; Cheng, G.; Li, X.; Yang, P. K.; Wen, X.; Wang, Z. L. A multi-layered interdigitative-electrodes-based triboelectric nanogenerator for harvesting hydropower. *Nano Energy* **2015**, *15*, 256−265.
(26) Lee, E. J.; Kim, T. Y.; Kim, S.-W.; Jeong, S.; Choi, Y.; Lee, S. Y. High-performance piezoelectric nanogenerators based on chemically-reinforced composites. *Energy Environ. Sci.* **2018**, *11*, 1425−1430.
(27) Zhao, Y.; Liao, Q.; Zhang, G.; Zhang, Z.; Liang, Q.; Liao, X.; Zhang, Y. High output piezoelectric nanocomposite generators composed of oriented $BaTiO_3$ NPs@PVDF. *Nano Energy* **2015**, *11*, 719−727.
(28) Siddiqui, S.; Kim, D.-I.; Duy, L. T.; Nguyen, M. T.; Muhammad, S.; Yoon, W.-S.; Lee, N.-E. High-performance flexible lead-free nanocomposite piezoelectric nanogenerator for biomechanical energy harvesting and storage. *Nano Energy* **2015**, *15*, 177−185.
(29) Shin, S.-H.; Kim, Y.-H.; Lee, M. H.; Jung, J.-Y.; Nah, J. Hemispherically Aggregated $BaTiO_3$ Nanoparticle Composite Thin Film for High-Performance Flexible Piezoelectric Nanogenerator. *ACS Nano* **2014**, *8*, 2766−2773.
(30) Gu, L.; Cui, N.; Cheng, L.; Xu, Q.; Bai, S.; Yuan, M.; Wu, W.; Liu, J.; Zhao, Y.; Ma, F.; Qin, Y.; Wang, Z. L. Flexible Fiber Nanogenerator with 209 V Output Voltage Directly Powers a Light-Emitting Diode. *Nano Lett.* **2013**, *13*, 91−94.
(31) Yi, F.; Lin, L.; Niu, S.; Yang, P. K.; Wang, Z.; Chen, J.; Zhou, Y.; Zi, Y.; Wang, J.; Liao, Q.; Zhang, Y.; Wang, Z. L. Stretchable-Rubber-Based Triboelectric Nanogenerator and Its Application as Self-Powered Body Motion Sensors. *Adv. Funct. Mater.* **2015**, *25*, 3688−3696.
(32) Li, R.; Zhao, Z.; Chen, Z.; Pei. Novel BaTiO3/PVDF composites with enhanced electrical properties modified by calcined $BaTiO_3$ ceramic powders. *Mater. Express* **2017**, *7*, 536−540.
(33) Olszowy, M. Piezoelectricity and dielectric properties of PVDF/$BaTiO_3$ composites. *Proc. SPIE* **1996**, *3181*, 69−72.
(34) Chang, C.; Tran, V. H.; Wang, J.; Fuh, Y. K.; Lin, L. Direct-Write Piezoelectric Polymeric Nanogenerator with High Energy Conversion Efficiency. *Nano Lett.* **2010**, *10*, 726−731.

DOI: 10.1021/acsaem.9b00836
ACS Appl. Energy Mater. 2019, 2, 4027−4032

7. pielikums/ Appendix VII

A. Šutka, K. Mālnieks, **L. Lapčinskis**, M. Timusk, K. Pudzs, M. Rutkis, Matching the Directions of Electric Fields from Triboelectric and Ferroelectric Charges in Nanogenerator Devices for Boosted Performance, *iScience* **2020**, *23(4)*, 101011.

iScience

CellPress
OPEN ACCESS

Article

Matching the Directions of Electric Fields from Triboelectric and Ferroelectric Charges in Nanogenerator Devices for Boosted Performance

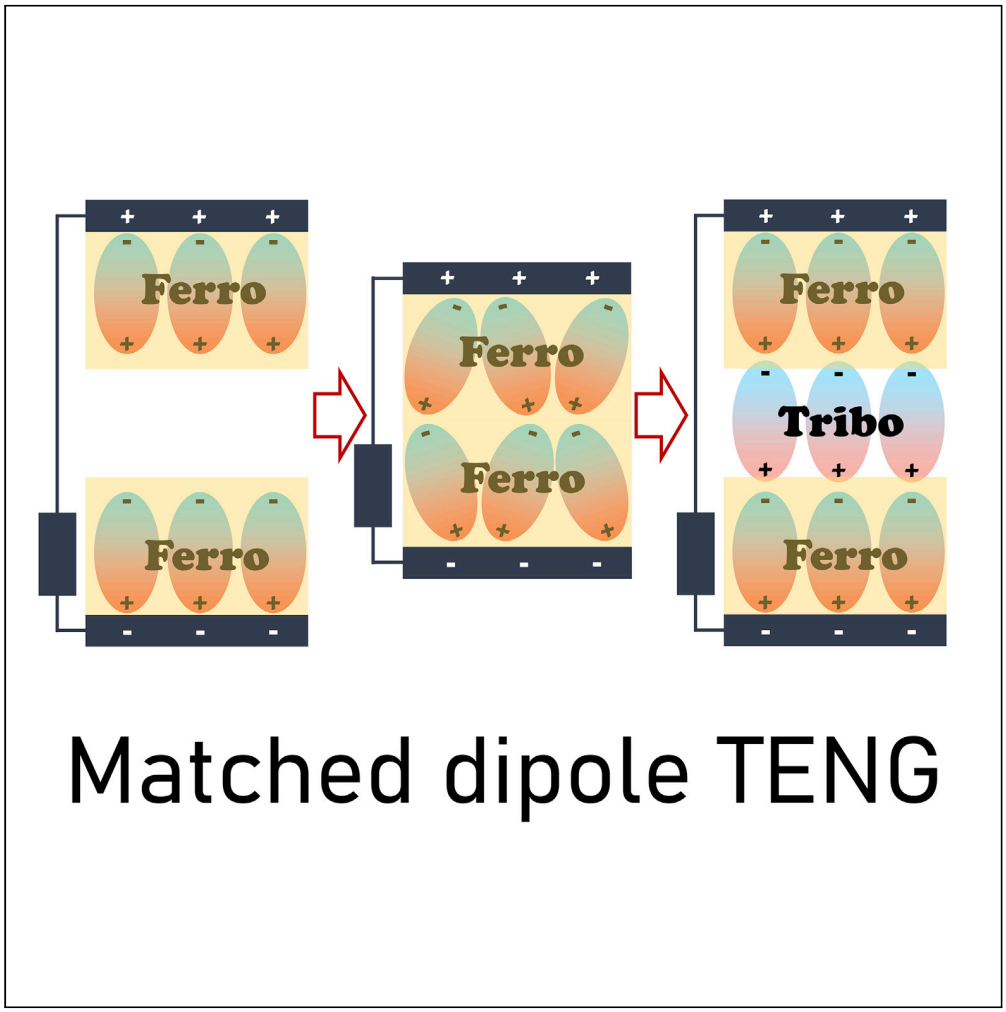

Andris Šutka,
Kaspars Mālnieks,
Linards Lapčinskis,
Martin Timusk,
Kaspars Pudzs,
Martins Rutkis

andris.sutka@rtu.lv

HIGHLIGHTS

TENG devices based on ferroelectric polymer/ $BaTiO_3$ composites were prepared

$\vec{E}$ from ferroelectric dipoles and triboelectric charges drive electrostatic induction

Matching $\vec{E}$ directions in TENG device lead to up to four times higher performance

$\vec{E}$ from different sources are summing up and provide a stronger induction

Šutka et al., iScience 23, 101011
April 24, 2020 © 2020 The Author(s).
https://doi.org/10.1016/j.isci.2020.101011

iScience

CellPress
OPEN ACCESS

Article

Matching the Directions of Electric Fields from Triboelectric and Ferroelectric Charges in Nanogenerator Devices for Boosted Performance

Andris Šutka,[1,5,*] Kaspars Mālnieks,[1] Linards Lapčinskis,[2] Martin Timusk,[3] Kaspars Pudzs,[4] and Martins Rutkis[4]

SUMMARY

Embedding additional ferroelectric dipoles in contacting polymer layers is known to enhance the performance of triboelectricnanogenerator (TENG) devices. However, the influence of dipoles formed between the triboelectric surface charges on two contacting ferroelectric films has been ignored in all relevant studies. We demonstrate that proper attention to the alignment of the distinct dipoles present between two contacting surfaces and in composite polymer/$BaTiO_3$ ferroelectric films can lead to up to four times higher energy and power density output compared with cases when dipole arrangement is mismatched. For example, TENG device based on PVAc/$BaTiO_3$ shows energy density increase from 32.4 $\mu J\ m^{-2}$ to 132.9 $\mu J\ m^{-2}$ when comparing devices with matched and mismatched dipoles. The presented strategy and understanding of resulting stronger electrostatic induction in the contacting layers enable the development of TENG devices with greatly enhanced properties.

INTRODUCTION

The field related to triboelectricnanogenerator (TENG) devices is emerging rapidly. Many original and creative TENG concepts have been presented in the literature for harvesting mechanical energy and converting it into electricity (Lee et al., 2019). The working principle of TENG devices is straightforward. The triboelectric materials (most commonly polymer insulators) are deposited on two conductive electrodes connected by an external circuit. Upon contacting-separating or sliding, surface charges are formed on the triboelectric materials, which induce an electrostatic charge on the conductive electrodes. Due to electrode oscillation or movement, a potential difference is created, which causes a current flow in the external electric circuit. TENG devices can be integrated into fabrics (Zhou et al., 2014), wearables (Kanik et al., 2015), interior objects (Dhakar et al., 2016), membranes (to harvest energy from sound) (Fan et al., 2015), and even implantable devices (Yao et al., 2018).

To enhance the performance of TENG, different approaches have been used. The most obvious way is to increase the specific contact area via nanostructuring (Zhang et al., 2015; Dudem et al., 2015; Zheng et al., 2014). Another possibility is the modification of surface or physicochemical properties of the triboelectric material (Šutka et al., 2019; Šutka et al., 2019; Lapčinskis et al., 2019; Fan et al., 2014; Yun et al., 2015; Wang et al., 2016). The performance can be also enhanced by using ferroelectric polymer or composite films as the contacting surfaces (Bai et al., 2014; Seung et al., 2017; Suo et al., 2016; Chun et al., 2015; Yang and Daoud, 2017; Choi et al., 2017; Lee et al., 2016; Šutka et al., 2018; Lapčinskis et al., 2019; Kim et al., 2019; Huang et al., 2020). State-of-the-art performance of ferroelectric material-based TENG devices can be expected when the ferroelectric material layers on contacting sides of the device are inversely polarized (Šutka et al., 2018; Lapčinskis et al., 2019). The contacted inversely polarized layers then act similarly to a series of connected capacitors (Lapčinskis et al., 2019). The total capacitance of the system decreases dramatically, whereas the potential difference increases as the air gap is created during separation. The induced charge redistribution in the external circuit manifests itself as current.

However, previous works related to TENG devices based on ferroelectric materials overlook the dipole that forms between the triboelectric surface charges on contacting surfaces. As soon as we consider this additional factor, it follows that the electric field direction from ferroelectric dipoles should match the direction of the electric field from triboelectric surface charge to achieve maximum electric field strength and

[1]Research Laboratory of Functional Materials Technologies, Faculty of Materials Science and Applied Chemistry, Riga Technical University, Paula Valdena 3/7, 1048 Riga, Latvia

[2]Institute of Technical Physics, Faculty of Materials Science and Applied Chemistry, Riga Technical University, Paula Valdena 3/7, 1048 Riga, Latvia

[3]Institute of Physics, University of Tartu, W. Ostwaldi Str. 1, 50411 Tartu, Estonia

[4]Laboratory of Organic Materials, Institute of Solid State Physics, Kengaraga 8, 1063 Riga, Latvia

[5]Lead Contact

*Correspondence: andris.sutka@rtu.lv

https://doi.org/10.1016/j.isci.2020.101011

This is an open access article under the CC BY license (http://creativecommons.org/licenses/by/4.0/).

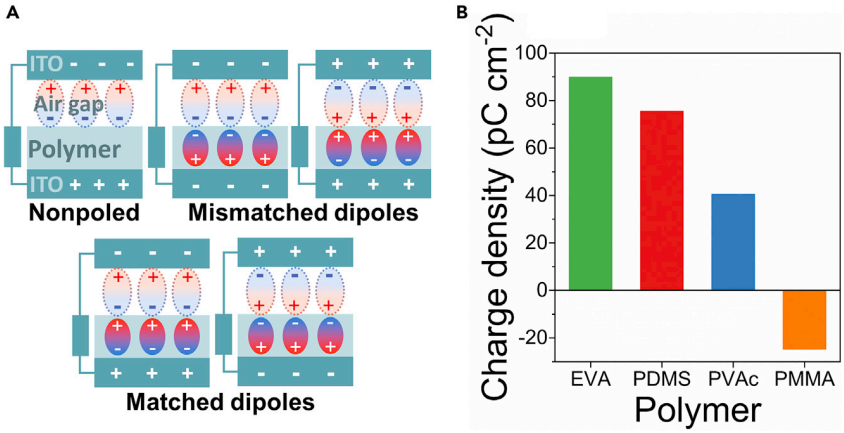

Figure 1. Dipole Formed between Polymer and ITO Can Be Matched with Ferroelectric Dipole

Schematic representation of possible interactions between surface charge dipoles in the air gap and ferroelectric dipoles in TENG device (A). The calculated surface charge density of non-ferroelectric polymers indicates the magnitude and direction of the formed dipole in contact-separation cycle (B) (See also Figures S7 and S8).

electrostatic induction. In other words, the alignment direction of ferroelectric dipoles has to coincide with the dipoles forming between the opposite charges on contacting surfaces as demonstrated in Figure 1A. In the present paper, we examine the performance of TENG devices when the electric field direction from surface charges and ferroelectric dipoles are matched or mismatched. To impart the ferroelectric properties for non-ferroelectric polymers used as triboelectric contacting layers, we added $BaTiO_3$ nanoparticles. $BaTiO_3$ were chosen as a feasible filler to allow preparation of ferroelectric polymer composite films so that contributions from contact-charging and ferroelectric dipoles could be compared. We demonstrate that matching the distinct kinds of dipoles present in TENG device leads to a significant increase in the power and energy density.

RESULTS AND DISCUSSION

Polydimethylsiloxane (PDMS), ethylene-vinyl acetate copolymer (EVA), poly(vinyl acetate) (PVAc), and poly(methyl methacrylate) (PMMA) were used in our studies to prepare TENG devices. The polymer films were spin coated on indium tin oxide (ITO) conductive electrode and contacted against another ITO (see Figure S1 for schematic TENG device representation). The polymer films were given ferroelectric properties by adding 7.5 vol% $BaTiO_3$ nanoparticles <100 nm in size (see Figure S2 for scanning electron microscopy (SEM) image). Particles were well dispersed throughout the polymer matrix in the prepared composites (the SEM images of cross-sections for different composites are demonstrated inFigures S3–S6). The experimental details for sample preparation are provided in SI.

The sign of triboelectric surface charges formed on pure polymers after contacting against ITO was determined by measuring the current between the underlying electrode and the ground in Faraday cup mode Figure 1B (see also Figure S7). Polymers PDMS, PVAc, and EVA obtain a negative charge on their surface, whereas for PMMA a positive charge is observed when contacted ITO. The sign of the net triboelectric charge did not change when $BaTiO_3$ nanoparticles were incorporated into the polymers (Figure S8).

All poled $BaTiO_3$/polymer composites exhibit piezoelectric properties (Figure S9). The poling procedure is described in Supplemental Information. The piezoelectric charges of 2.9 pC cm^{-2}, 10.9 pC cm^{-2}, 3.7 pC cm^{-2}, and 2.4 pC cm^{-2} were measured for $BaTiO_3$/EVA, $BaTiO_3$/PDMS, $BaTiO_3$/PVAc, and $BaTiO_3$/PMMA composites, respectively. The higher piezoelectric response of $BaTiO_3$/PDMS could be attributed to its larger deformability under the constant loading force. The elastic modulus values of the four polymers are 5.48 GPa for PMMA, 5.24 GPa for PVAc, 44.3 MPa for EVA, and 2.9 MPa for PDMS (Šutka et al., 2019).

Figure 2 shows time-resolved current (I_{SC}) and voltage measurements (V_{OC} at 1 GΩ) for TENG devices based on polymer composite layers and ITO. Composite layer in each of these TENG devices was tested as non-poled and also positively and negatively poled, so that ferroelectric dipole is matched and

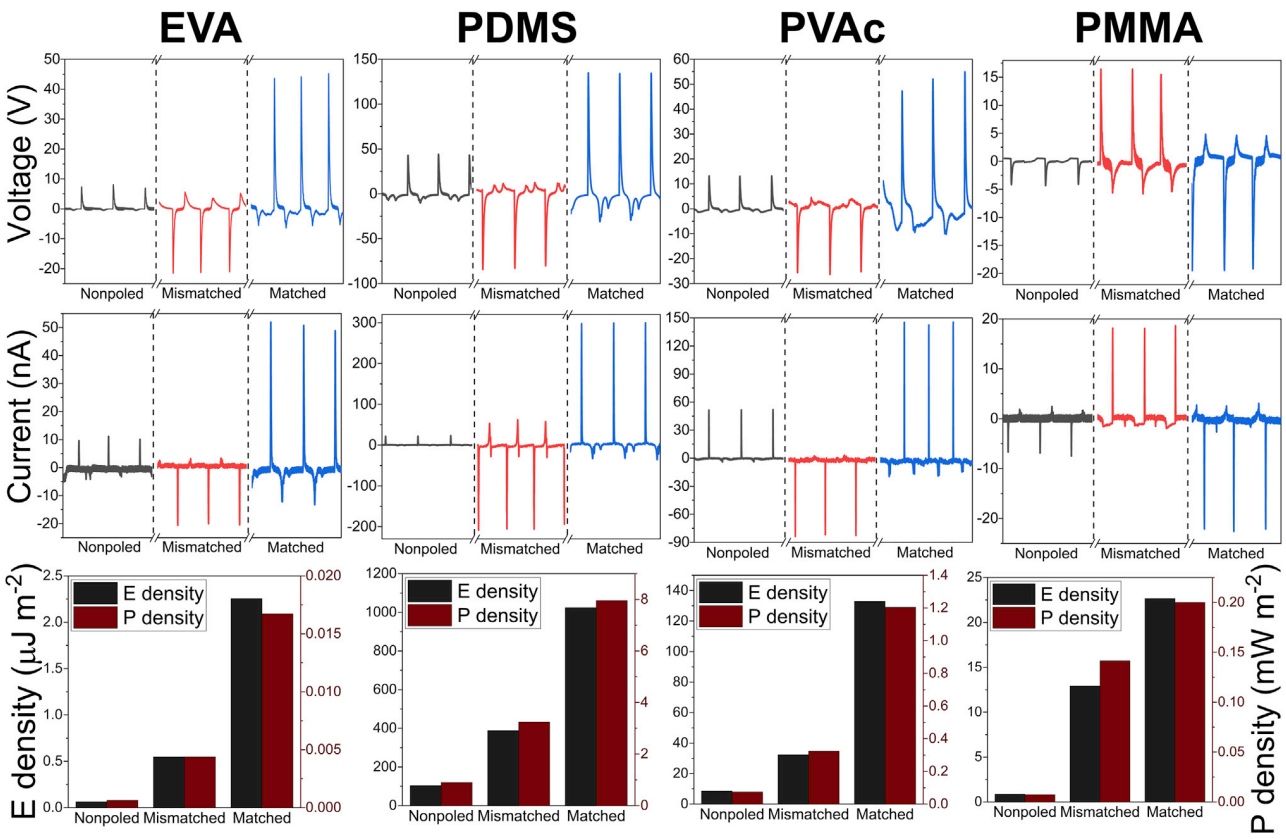

Figure 2. Comparison of Three Possible Dipole Alignment Configurations

Ferroelectric dipoles are not present (non-poled), they are mismatched to dipoles formed by contact electrification (mismatched), and they are matched in the same direction as contact-electrification generated dipoles (matched). These states are shown to influence open-circuit voltage, short-circuit current, energy density, and power density for each $BaTiO_3$/polymer composite studied in this work.

mismatched with the previously determined surface charge. The performance of a TENG device is very different depending on whether a positive or negative voltage is applied for poling (Figure 2), regardless of the polymer used. This phenomenon of one polarization direction resulting in a larger impact than the other is widely reported before (Bai et al., 2014; Suo et al., 2016; Lee et al., 2016; Šutka et al., 2018; Lapčinskis et al., 2019; Kim et al., 2019; Huang et al., 2020); however, the explanation provided for that has been inaccurate. We argue that the observed difference can be explained by elementary match and mismatch between the directions of the electric field from the ferroelectric dipole moment and the dipole moment created by triboelectric charges. As we can see from Figure 2, for PVAc, EVA, and PDMS, which obtain a negative triboelectric surface charge after contacting ITO, better performance is observed when the positive pole of the ferroelectric dipole is facing away from the underlying ITO electrode. In the case of PMMA, which has a positive triboelectric surface charge after contacting ITO, better performance is observed when the negative pole of the ferroelectric dipole is facing away from the substrate ITO electrode. Net dipole direction between surface triboelectric charges was confirmed by COMSOL finite element simulation (Figure S10). The experiments show that the TENG device has higher performance when the direction of dipole between triboelectric surface charge and ferroelectric dipoles are matching.

To provide even more evidence, we constructed a TENG device where both ITO electrodes are covered with a $BaTiO_3$/polymer composite film. For the highest performance, the dipoles in the two films are polarized inversely (Šutka et al., 2018; Lapčinskis et al., 2019), whereas the polymer matrix material for each side is chosen so that the dipole moment direction of triboelectric and ferroelectric charges are matched. The surface charges on the contacted polymers used in the study were determined experimentally by measuring current in Faraday cup mode (Figure S11). A TENG device was constructed from PMMA and PDMS as

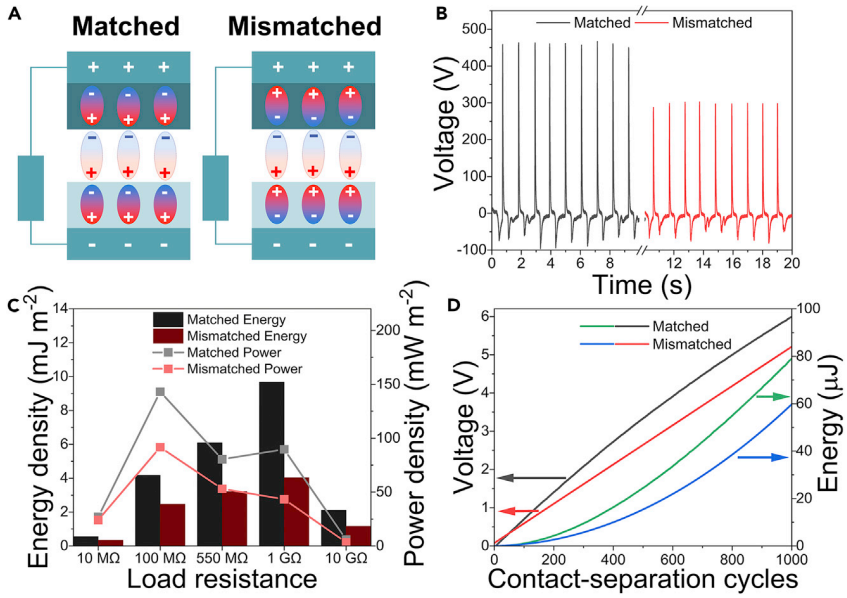

Figure 3. Comparison of TENG Devices Using Matched and Mismatched Dipole Configurations

Inversely polarized $BaTiO_3$/PDMS (top layer) and $BaTiO_3$/PMMA (bottom layer) TENG device constructed in a way that ferroelectric polarization direction is matched (left) and mismatched (right) with contact-electrification-generated surface charge dipole direction (A). Graphs for matched and mismatched configuration show V_{OC} (at 1 GΩ) (B), energy, and power density during one contact-separation cycle (C) and the voltage across 4.4 μF capacitor during charging with the corresponding stored energy (D) (see also Figures S11–S13).

PMMA charges positively and PDMS negatively. The poling direction in composite $BaTiO_3$/PMMA was chosen so that the negative pole of the ferroelectric dipole was facing away from the substrate, whereas $BaTiO_3$/PDMS was polarized so that the positive pole of ferroelectric dipole is facing away from the substrate. A schematic representation of the device is shown in Figure 3A. As expected, this particular TENG device performed excellently, and the output was superior to any other presented in this study. The peak open-circuit voltage (V_{OC}) of device with matched dipoles reached 460 V as shown in voltage-time plot in Figure 3B. The instant energy and power densities of this TENG device reached 9.7 mJ m^{-2} and 143.2 mW m^{-2}, respectively (black bars and gray line in Figure 3C). For comparison, a TENG device from the same polymers without $BaTiO_3$ NPs shows V_{OC} as small as 16 V and three orders of magnitude smaller energy and power densities of 0.012 mJ m^{-2} and 0.104 mW m^{-2} (Figure S12). Also, the TENG device from the same inversely polarized composite films but with mismatched dipoles exhibited significantly lower output—V_{OC} of 300 V (red line in Figure 3B) and instant energy and power densities of 4.0 mJ m^{-2} and 91.6 mW m^{-2} from the same contacting area (red bars and red line in Figure 3C).

We also performed a macroscale scanning Kelvin Probe measurements (detailed description given in Transparent Methodssection). The average surface potential for nonpolarized $BaTiO_3$/PDMS was determined to be 0.06 V. The average potential after contacting with PMMA was measured to be 146.4 V (surface potential maps of a nonpolarized sample before and after contacting PMMA are shown in Figure 4). Surface potential scanning was also performed on both positively and negatively polarized $BaTiO_3$/PDMS samples before and after contacting with PMMA. Average potential values at first were measured to be 24.3 V and −70.5 V, respectively. A quasi-permanent surface potential is created by ferroelectric dipoles in PDMS/$BaTiO_3$ composite layer. Just like in the case of a nonpolarized sample, contacting PMMA caused both samples to obtain an additional positive charge. Therefore, the average potential value grew to 107.2 V for the positively polarized sample and to −1.1 V in the case of the negatively polarized sample after they were contact separated. Full-surface potential maps for both polarized samples before and after the contact with PMMA are shown in Figure 4. Experimental results confirm the proposed mechanism for better performance of TENG devices where two sources of the electric field are present—triboelectric charges and ferroelectric dipoles. In the case of the matched direction of electric fields arising from triboelectric and ferroelectric dipoles, the electric field strength summarizes and amplifies the electrostatic induction

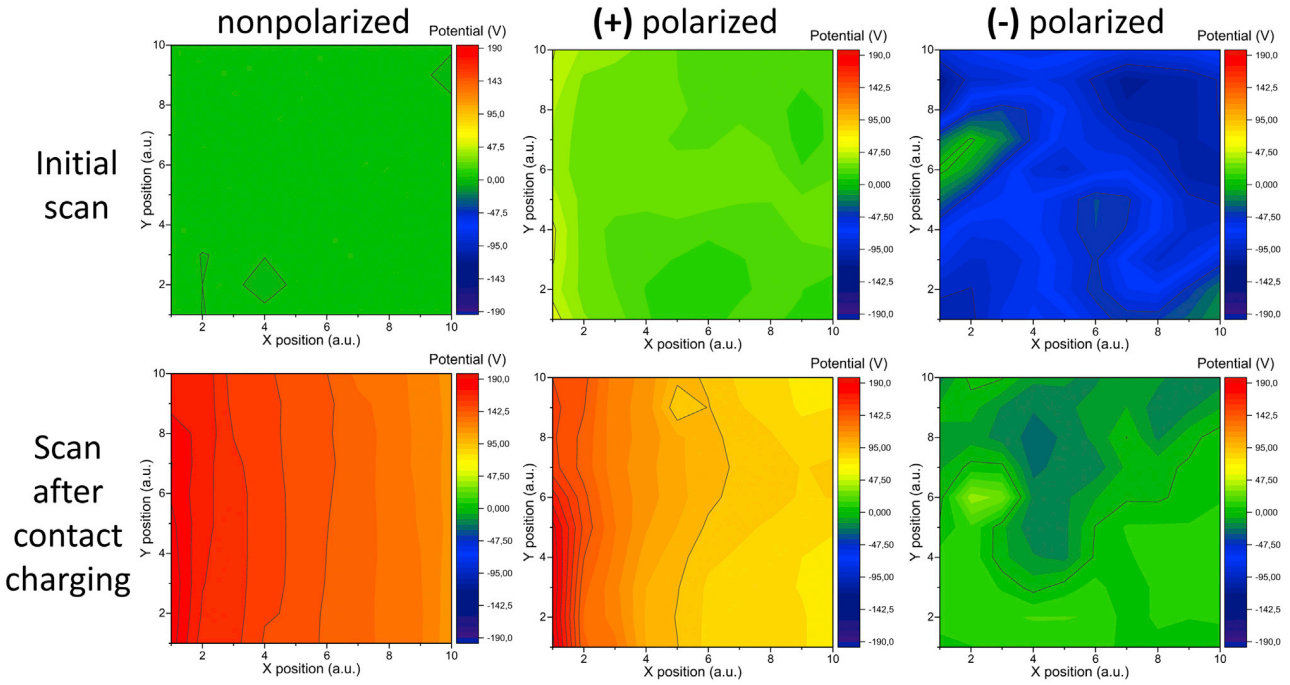

Figure 4. Surface Potential Maps of Three $BaTiO_3$/PDMS Composites (Nonpolarized, Positively and Negatively Polarized)

Top maps show respectively neutral, positive, and negative surface potential at initial scan. All surfaces show tendency to charge positively after contact with PMMA as evidenced by more positive surface potential (bottom). A gradual decrease of potential in the direction from left to right is observed because the triboelectric charge decreases as the surface is being scanned in this direction.

on TENG electrodes. Due to the potential difference between positive and negative induced charge, the stronger current flow between two TENG electrodes is measured. As shown in Figure S11B, a PDMS contact layer induces a positive current peak on the underlying electrode when contacted against PMMA. Therefore, surface potential of positively polarized PDMS layer (positive pole of ferroelectric dipole facing away from underlying electrode) after contact with PMMA corresponds to a matched dipole case, whereas the negatively polarized corresponds to mismatched dipoles.

The TENG device that was constructed from inversely polarized $BaTiO_3$/PDMS and $BaTiO_3$/PMMA composite films with matched dipoles was used to charge a 4.4 μF capacitor (Figure S13). This experiment is beneficial to understanding the practicality of the developed device because charged capacitors can be further used to charge batteries or power small sensors, and voltage across the capacitor also conveniently shows the amount of stored energy. By performing 1,000 contact-separation cycles the voltage across the capacitor increased by 6.0 V that corresponds to the stored energy of 79 μJ, as demonstrated in Figure 3D. In the meantime, TENG device constructed from equivalent contact layers, but with intentionally mismatched dipoles, increased the voltage across the capacitor only by 5.2 V and accumulated 60 μJ energy under the same operating conditions and number of contact-separating cycles.

The proof-of-concept demonstrated here can be further used to construct TENG devices with record performance. Polymers with a superior tendency for triboelectrification (Lapčinskis et al., 2019) and polymer composite materials with high intrinsic piezoelectric responses have been reported in literature widely (Zhang et al., 2018; Jeong et al., 2019; Han et al., 2019). A combination of methodology shown in this paper with high-performance ferroelectric materials could bring the TENG research community closer to new cutting-edge discoveries.

Conclusions

Results presented here shine a light upon the path to improvements in the construction of advanced TENG devices. The energy and power density of a TENG device can be increased up to four times by matching the

directions of electric fields arising from ferroelectric dipoles and triboelectric surface charges when compared with mismatched case. Matching of the dipoles magnifies the electric field strength and electrostatic induction on a conductive electrode that in turn leads to a higher voltage output.

Limitations of the Study

Performance values (V_{OC}, I_{SC}, Energy, and power density) in this work do not reach state-of-the-art level reported in the latest works. However, this study shows proof of concept that would allow to supersede all reported TENG devices. This could be done by more elaborate choice of polymer materials with superior contact-charging capabilities and by choosing ferroelectric materials with much higher piezoelectric constant d_{33}.

METHODS

All methods can be found in the accompanying Transparent Methods supplemental file.

DATA AND CODE AVAILABILITY

Supplemental Information can be found online.

SUPPLEMENTAL INFORMATION

Supplemental Information can be found online at https://doi.org/10.1016/j.isci.2020.101011.

ACKNOWLEDGMENTS

This research was supported by Riga Technical University's Doctoral Grant program. This research was also supported by the European Regional Development Fund within the project ''Hybrid energy harvesting systems'' 1.1.1.1./16/A/013.

AUTHOR CONTRIBUTIONS

K.M. and L.L. prepared the samples and conducted the experiments; K.P. performed Kelvin Probe measurements; M.R. contributed to interpretation of results; M.T. prepared COMSOL finite element simulation; A.Š. generated the main idea presented in the paper, designed the experiments, and wrote the paper with contributions from K.M. and L.L.

DECLARATION OF INTERESTS

The authors declare no competing interests.

Received: February 11, 2020
Revised: March 7, 2020
Accepted: March 19, 2020
Published: April 24, 2020

REFERENCES

Bai, P., Zhu, G., Zhou, Y.S., Wang, S., Ma, J., Zhang, G., and Wang, Z.L. (2014). Dipole-moment-induced effect on contact electrification for triboelectricnanogenerators. Nano Res. *7*, 990–997.

Choi, Y.S., Jing, Q., Datta, A., Boughey, C., and Kar-Narayan, S.A. (2017). A triboelectric generator based on self-poled Nylon-11 nanowires fabricated by gas-flow assisted template wetting. Energy Environ. Sci. *10*, 2180–2189.

Chun, J., Kim, J.W., Jung, W.S., Kang, C.Y., Kim, S.W., Wang, Z.L., and Baik, J.M. (2015). Mesoporous pores impregnated with Au nanoparticles as effective dielectrics for enhancing triboelectricnanogenerator performance in harsh environments. Energy Environ. Sci. *8*, 3006–3012.

Dhakar, L., Gudla, S., Shan, X., Wang, Z., Tay, F.E.H., Heng, C.-H., and Lee, C. (2016). Large scale triboelectricnanogenerator and self-powered pressure sensor array using low cost roll-to-roll UV embossing. Sci. Rep. *6*, 22253.

Dudem, B., Ko, Y.H., Leem, J.W., Lee, S.H., and Yu, J.S. (2015). Highly transparent and flexible triboelectricnanogenerators with subwavelength-architecturedpolydimethylsiloxane by a nanoporousanodic aluminum oxide template. ACS Appl. Mater. Interfaces *7*, 20520–20529.

Fan, F.R., Luo, J., Tang, W., Li, C., Zhang, C., Tian, Z., and Wang, Z.L. (2014). Highly transparent and flexible triboelectricnanogenerators: performance improvements and fundamental mechanisms. J. Mater. Chem. A *2*, 13219–13225.

Fan, X., Chen, J., Yang, J., Bai, P., Li, Z., and Wang, Z.L. (2015). Ultrathin, rollable, paper-based triboelectricnanogenerator for acoustic energy harvesting and self-powered sound recording. ACS Nano *9*, 4236–4243.

Han, J.H., Park, K.-I., and Jeong, C.K. (2019). Dual-structured flexible piezoelectric film energy harvesters for effectively integrated performance. Sensors *19*, 1444–1457.

Huang, T., Zhang, Y., He, P., Wang, G., Xia, X., Ding, G.Q., and Tao, T.H. (2020). "Self-Matched"tribo/piezoelectric

nanogenerators using vapor-induced phase-separated poly(vinylidene fluoride) and recombinant spider silk. Adv. Mater. *32*, 1907336.

Jeong, C.K., Hyeon, D.Y., Hwang, G.-T., Lee, G.-J., Lee, M.-K., Park, J.-J., and Park, K.-I. (2019). Nanowire-percolated piezoelectric copolymer-based highly transparent and flexible self-powered sensors. Mater. Chem. A *7*, 25481–25489.

Kanik, M., Say, M.G., Daglar, B., Yavuz, A.F., Dolas, M.H., El-Ashry, M.M., and Bayindir, M. (2015). A motion- and sound-activated, 3D-printed, chalcogenide-based triboelectricnanogenerator. Adv. Mater. *27*, 2367–2376.

Kim, H.S., Kim, D.Y., Kim, J.-E., Kim, J.H., Kong, D.S., Murillo, G., Lee, G.-H., Park, J.Y., and Jung, J.H. (2019). Ferroelectric-polymer-enabled contactless electric power generation in triboelectricnanogenerators. Adv. Funct. Mater. *29*, 1905816.

Lapčinskis, L., Mālnieks, K., Blūms, J., Knite, M., Oras, S., Käämbre, T., Vlassov, S., Antsov, M., Timusk, M., and Šutka, A. (2019). The adhesion-enhanced contact electrification and efficiency of triboelectricnanogenerators. Macromol.Mater.Eng. *305*, 1900638.

Lapčinskis, L., Mālnieks, K., Linarts, A., Blūms, J., Šmits, K., Järvekülg, M., Knite, M., and Sutka, A. (2019). Hybrid tribo-piezo-electric nanogenerator with unprecedented performance based on ferroelectric composite contacting layers. ACS Appl. Energy Mater. *2*, 4027–4032.

Lee, K.Y., Kim, S.K., Lee, J.-H., Seol, D., Gupta, M.K., Kim, Y., and Kim, S.W. (2016). Controllable charge transfer by ferroelectric polarization mediated triboelectricity. Adv. Funct. Mater. *26*, 3067–3073.

Lee, B.-Y., Kim, D.H., Park, J., Park, K.-I., Lee, K.J., and Jeong, C.K. (2019). Modulation of surface physics and chemistry in triboelectric energy harvesting technologies. Sci. Technol. Adv. Mater. *20*, 758–773.

Seung, W., Yoon, H.-J., Kim, T.Y., Ryu, H., Kim, J., Lee, J.-H., Kim, S., Park, Y.K., Park, Y.J., and Kim, S.-W. (2017). Boosting power-generating performance of triboelectricnanogenerators via artificial control of ferroelectric polarization and dielectric properties. Adv. Energy Mater. *7*, 1600988.

Suo, G., Yu, Y., Zhang, Z., Wang, S., Zhao, P., Li, J., and Wang, X. (2016). Piezoelectric and triboelectric dual effects in mechanical-energy harvesting using $BaTiO_3$/polydimethylsiloxane composite film. ACS Appl. Mater. Interfaces *8*, 34335–34341.

Šutka, A., Mālnieks, K., Linarts, A., Timusk, M., Jurķāns, V., Gorņevs, I., Blūms, J., Bērziņa, A., Joost, U., and Knite, M. (2018). Inversely polarised ferroelectric polymer contact electrodes for triboelectric-like generators from identical materials. Energy Environ. Sci. *11*, 1437–1443.

Šutka, A., Linarts, A., Mālnieks, K., Stiprais, K., and Lapčinskis, L. (2019). Dramatic increase in polymer triboelectrification by transition from a glassy to rubbery state. Mater.Horiz. https://doi.org/10.1039/C9MH01425J.

Šutka, A., Malnieks, K., Lapčinskis, L., Kaufelde, P., Linarts, A., Berziņa, A., Zabels, R., Jurķans, V., Gorņevs, I., Blums, J., and Knite, M. (2019). The role of intermolecular forces in contact electrification on polymer surfaces and triboelectricnanogenerators. Energy Environ. Sci. *12*, 2417–2421.

Wang, S., Zi, Y., Zhou, Y.S., Li, S., Fan, F., Lin, L., and Wang, Z.L. (2016). Molecular surface functionalization to enhance the power output of triboelectricnanogenerators. J. Mater. Chem. A *4*, 3728–3734.

Yang, X., and Daoud, W.A. (2017). Synergetic effects in composite-based flexible hybrid mechanical energy harvesting generator. J. Mater. Chem. A *5*, 9113–9121.

Yao, G., Kang, L., Li, J., Long, Y., Wei, H., Ferreira, C.A., Jeffery, J.J., Lin, Y., Cai, W., and Wang, X. (2018). Effective weight control via an implanted self-powered vagus nerve stimulation device. Nat. Commun. *9*, 5349.

Yun, B.K., Kim, J.W., Kim, H.S., Jung, K.W., Yi, Y., Jeong, M.-S., Ko, J.-H., and Jung, J.H. (2015). Base-treated polydimethylsiloxane surfaces as enhanced triboelectricnanogenerators. Nano Energy *15*, 523–529.

Zhang, L., Zhang, B., Chen, J., Jin, L., Deng, W., Tang, J., Zhang, H., Pan, H., Zhu, M., Yang, W., and Wang, Z.L. (2015). Lawn structured triboelectricnanogenerators for scavenging sweeping wind energy on rooftops. Adv. Mater. *28*, 1650–1656.

Zhang, Y., Sun, H., and Jeong, C.K. (2018). Biomimetic Poriferaskeletal structure of lead-free piezocomposite energy harvesters. ACS Appl. Mater. Interfaces *10*, 35539–35546.

Zheng, Y., Cheng, L., Yuan, M., Wang, Z., Zhang, L., Qin, Y., and Jing, T. (2014). An electrospun nanowire-based triboelectricnanogenerator and its application in a fully self-powered UV detector. Nanoscale *6*, 7842–7846.

Zhou, T., Zhang, C., Han, C.B., Fan, F.R., Tang, W., and Wang, Z.L. (2014). Woven structured triboelectricnanogenerator for wearable devices. ACS Appl. Mater. Interfaces *6*, 14695–14701.

8. pielikums/ Appendix VIII

Korespondējošā autora parakstīts apliecinājums par ieguldījumu publikāciju tapšanā.
Confirmation of contribution to preparation of papers signed by the corresponding author.

Rīgā, 2021. gada 22. novembrī

Asoc. Profesors, Dr. sc. ing. Andris Šutka
Materiālu un virsmas tehnoloģiju institūts
Materiālzinātnes un lietišķās ķīmijas fakultāte
Rīgas Tehniskā universitāte
Paula Valdena iela 7 – 204. kab., Rīga, LV-1048
Telefons: 26138155
E-pasts: andris.sutka@rtu.lv

Prof. J. Ločam
RTU Promocijas padomes
RTU P-02 priekšsēdētājam

Apliecinājums par doktora grāda pretendenta Linarda Lapčinska personisko ieguldījumu publikāciju sagatavošanā

Linarda Lapčinska promocijas darbs ir tematiski vienota publikāciju kopa, kurā apvienotas 7 oriģinālpublikācijas. Tabulā apkopots mans kā promocijas darba vadītāja apliecinājums par doktora grāda pretendenta personisko ieguldījumu publikāciju sagatavošanā:

N.p.k.	Publikācijas dati	Korespondējošais autors	L. Lapčinska ieguldījuma novērtējums
1.	A. Šutka, K. Malnieks, L. Lapčinskis, P. Kaufelde, A. Linarts, A. Berziņa, R. Zabels, V. Jurķans, I. Gorņevs, J. Blums, M. Knite, The role of intermolecular forces in contact electrification on polymer surfaces and triboelectric nanogenerators, *Energy Environ. Sci.* **2019**, *12(8)*, 2417-2421.	A. Šutka	Polimēra kontaktējamo kārtiņu izgatavošana izmantojot uzklāšanu ar rotāciju un presēšanu paaugstinātā temperatūrā. Polimēru triboelektrisko īpašību mērījumi. PDMS cietības mērījumi un šķērssaistīšanās pakāpes aprēķini. Datu vizuālais attēlojums. Procentuālais ieguldījums – 50 %.
2.	L. Lapčinskis, K. Mālnieks, J. Blūms, M. Knite, S. Oras, T. Käämbre, S. Vlassov, M. Antsov, M. Timusk, A. Šutka, The Adhesion-Enhanced Contact Electrification and Efficiency of Triboelectric Nanogenerators, *Macromol. Mater. Eng.* **2020**, *305(1)*, 1900638.	A. Šutka	Polimēra kārtiņu izgatavošana izmantojot uzklāšanu ar rotāciju un triboelektrisko īpašību testēšana. Datu vizuālais attēlojums. TEĢ efektivitātes aprēķini un ieguldījums manuskripta rakstīšanā. Procentuālais ieguldījums – 75 %.
3.	A. Šutka, A. Linarts, K. Malnieks, K. Stiprais, L. Lapčinskis, Dramatic increase in polymer triboelectrification by transition from a glassy to rubbery state, *Mater. Horiz.* **2020**, *7(2)*, 520-523.	A. Šutka	Paraugu izgatavošana un triboelektrisko īpašību testēšana. Triboelektriskā efekta un lādiņa noturības paaugstinātā temperatūrā ilgtermiņa stabilitātes mērījumi. Procentuālais ieguldījums – 50 %.
4.	A. Šutka, K. Mālnieks, L. Lapčinskis, M. Timusk, K. Kalniņš, A. Kovaļovs, J. Bitenieks, M. Knite, D. Stevens, J. Grunlan, Contact electrification between identical polymers as the basis for triboelectric/flexoelectric materials, *Phys. Chem. Chem. Phys.* **2020**, *22(23)*, 13299-13305.	A. Šutka J. Grunlan	Paraugu izgatavošana un triboelektrisko īpašību testēšana. Skenējošās Kelvina zondes (SKZ) mērījumu analīze. Ieguldījums manuskripta rakstīšanā un datu vizualizācija. Procentuālais ieguldījums – 60 %.

5.	L. Lapčinskis, A. Linarts, K. Mālnieks, H. Kim, K. Rubenis, K. Pudzs, K. Smits, A. Kovaļovs, K. Kalniņš, A. Tamm, C.K. Jeong, and A. Šutka, Triboelectrification of nanocomposites using identical polymer matrixes with different concentrations of nanoparticle fillers, *J. Mater. Chem. A* **2021**, *9(14)*, 8984-8990.	A. Šutka C.K. Jeong	Paraugu izgatavošana izmantojot presēšanu paaugstinātā temperatūrā. Triboelektrisko īpašību izpēte. Skenējošās Kelvina zondes (SKZ) mērījumu analīze. Datu vizuālais attēlojums. Manuskripta sākotnējās versijas rakstīšana. Procentuālais ieguldījums – 80 %.
6.	L. Lapčinskis, K. Mālnieks, A. Linarts, J. Blūms, K. Šmits, M. Järvekülg, M. Knite, A. Šutka, Hybrid Tribo-Piezo-Electric Nanogenerator with Unprecedented Performance Based on Ferroelectric Composite Contacting Layers, *ACS Appl. Energy Mater.* **2019**, *2(6)*, 4027-4032.	A. Šutka	Polimēru nanokompozītu izgatavošana un polarizācija. Triboelektrisko un pjezoelektrisko īpašību testēšana. Ieguldījums manuskripta rakstīšanā. Procentuālais ieguldījums – 75 %.
7.	A. Šutka, K. Mālnieks, L. Lapčinskis, M. Timusk, K. Pudzs, M. Rutkis, Matching the Directions of Electric Fields from Triboelectric and Ferroelectric Charges in Nanogenerator Devices for Boosted Performance, *iScience* **2020**, *23(4)*, 101011.	A. Šutka	Polimēru nanokompozītu izgatavošana un polarizācija. Triboelektrisko un pjezoelektrisko īpašību testēšana. Skenējošās Kelvina zondes (SKZ) mērījumu analīze. Ieguldījums manuskripta rakstīšanā. Procentuālais ieguldījums – 70 %.

Kā Linarda Lapčinska promocijas darba vadītājs un visu uzskaitīto zinātnisko oriģinālpublikāciju korespondējošais autors, piekrītu šo darbu izmantošanai Linarda Lapčinska promocijā.

/A. Šutka/ 22.11.2021.